HYDROGENOLYSIS OF HYDROCARBONS

ON

SUPPORTED METAL CATALYSTS

To Harleen

To my parents

HYDROGENOLYSIS OF SOME PARAFFINIC

HYDROCARBONS ON SUPPORTED CATALYSTS

OF RUTHENIUM, NICKEL, COBALT, AND IRON

By

CHRISTIAAN JOSEPHUS MACHIELS, ir.

A Thesis

Submitted to the Faculty of Graduate Studies

in Partial Fulfilment of the Requirements

for the Degree

Doctor of Philosophy

McMaster University

November, 1977

DOCTOR OF PHILOSOPHY (1977)   McMASTER UNIVERSITY
(Chemical Engineering)   Hamilton, Ontario

TITLE: Hydrogenolysis of Some Paraffinic
              Hydrocarbons on Supported Catalysts
              of Ruthenium, Nickel, Cobalt, and Iron

AUTHOR: Christiaan Josephus Machiels,

                 B.Eng. (Eindhoven University of Technology)

                 ir. (Eindhoven University of Technology)

SUPERVISOR: Professor R.B. Anderson

NUMBER OF PAGES: 319, xviii

ABSTRACT

The hydrogenolysis of propane, n-hexane, 2,3-dime-
thylbutane, and 2,2-dimethylbutane was studied over supported
catalysts of ruthenium, nickel, cobalt, and iron, some con-
taining structural promoters. The catalysts were prepared by
impregnation of several supports, and were characterized
using mainly atomic absorption and chemisorption techniques.
A differential reactor system was used, consisting of a
fixed-bed reactor and an external recycle pump. The data from
propane hydrogenolysis were fitted to a power rate equation
and a selectivity equation. The results are in general agree-
ment with those of similar experiments with ethane. The pro-
ducts from the hydrogenolysis of the hexanes were fitted to
selectivity equations that were based on reaction networks
derived for reversible, adsorption-desorption of the hydro-
carbons and irreversible rupture of the carbon-carbon bonds
of the surface species. The product distributions were
measured over a wide range of conversion (10 to 80%), but in
most cases only at one temperature. In the sequence -ectheni-
um, nickel, cobalt, iron - the distribution shifts toward
smaller hydrocarbons. Ruthenium tends to split the carbon-
carbon bonds in a straight chain with equal probability,

while nickel preferably splits terminal bonds. Structural
promoters increase the activity of the nickel and cobalt
catalysts, and stabilize the iron catalysts. Because of this
the catalysts on low area supports had activities very simi-
lar to those on high area supports; the amount of metal,
however, was higher on the low area supports.

ACKNOWLEDGEMENTS

TABLE OF CONTENTS

LIST OF FIGURES

x

LIST OF TABLES

Chapter 1

INTRODUCTION

1.1 General

The catalytic hydrogenolysis of hydrocarbons usually refers to reactions involving the rupture of carbon-carbon bonds by interaction of the hydrocarbon with hydrogen. Other bond types that can be considered in hydrogenolysis are carbon-oxygen, carbon-nitrogen, and carbon-halogen (1). The hydrogenolysis reactions of higher hydrocarbons to lower ones are always thermodynamically favourable (116).

Hydrogenolysis of hydrocarbons is closely related to hydrocracking, which is one of the important hydroprocesses and is used in the petroleum industry. The hydroprocesses are carried out under hydrogen atmosphere and on a bi-functional catalyst, combining the features of metal and acid catalysis. They also include hydrorefining, hydroisomerisation, and hydrodealkylation. The main reactions are cracking of hydrocarbons, removal of sulphur and nitrogen, isomerisation of paraffinic hydrocarbons and removal of alkylgroups from alkylaromatics. The hydrogen is needed to saturate bonds that are broken and to keep the catalyst active and free of carbonaceous deposits.

Besides rupture of carbon-carbon bonds, the hydrogen-olysis reactions also involve the rupture and the formation

1

of carbon-hydrogen bonds. The ultimate product of the reactions is methane, but selective rupture can take place with paraffins and cycloalkanes using the right catalyst and under moderate conditions. The catalysts used in the hydrogenolysis reactions are usually transition metals, and most of the investigations were done with supported metal catalysts; these are of interest because of their commercial importance. At higher temperatures hydrogenolysis can also occur on acidic oxides such as alumina or silica-alumina (2); in this case the reactions are commonly considered in terms of carbonium-ion mechanisms.

The simplest example is the hydrogenolysis of ethane, which has been investigated by many researchers over a wide range of catalysts and experimental conditions.

$$C_2H_6 \quad + \quad H_2 \rightleftharpoons \quad 2 \ CH_4 \qquad (1-1)$$

Many reactions, like hydrogenolysis and isotopic exchange, are best explained by radical-type, neutral intermediate species bonded to the surface (3). Variations in activity between catalysts can then be related to the adsorption properties of the reactants. If the adsorption bond is too strong, the catalyst may be fully covered with a surface spe-

cies which are too stable to react (in hydrogenolysis and exchange reactions this is the case on metals of group V A and VI A, such as vanadium, molybdenum, chromium and tungsten). If chemisorption of the reactant is weak (group I B metals, copper, silver, gold), the reaction may be limited by the adsorption step. Maximum activity therefore results when chemisorption of the reactant is fast, but not very strong, as in the case of group VIII transition metals with their incomplete d-shell available for coordinate-type bond formation (4).

The purpose of the present investigation is to obtain information on the kinetics and mechanisms of hydrogenolysis of several hydrocarbons (propane, n-hexane, 2,2-dimethylbutane and 2,3-dimethylbutane) using supported catalysts of iron, cobalt, nickel and ruthenium, and examining both the rate of reaction and the distribution of products. A gas recycle system was used to obtain differential reactor conditions, the system acting as a completely mixed reactor, so that data were obtained at one level of concentration and temperature. The catalytic behaviour of the different metals was investigated.

1.2 Hydrogenolysis of Hydrocarbons over Transition Metals

The kinetics of the hydrogenolysis of ethane were first investigated on nickel (5), cobalt (6) and iron (7). In the reaction over nickel, dissociative adsorption took place. The apparent activation energy was 180. kJ/mol (43. kcal/mol),

and the rate was a strong inverse function of the hydrogen
pressure. Later experiments showed an increase of activation
energy with increasing hydrogen pressure (8,9). The reaction
on cobalt was also inhibited by hydrogen, but to a smaller
extent than on nickel. This inverse dependence of the rate on
the hydrogen pressure has been found to be typical for a num-
ber of metals, including all the metals of the platinum group
i.e. Pt, Pd, Ru, Os, Rh, Ir (10-20,177). The magnitude of the
inverse dependence varies with the metal, and in some cases a
positive dependence of the rate on the hydrogen pressure has
been found: on iron (12) and on rhenium (20). Table 1-1 shows
a summary of the kinetic results of the hydrogenolysis of
ethane on a number of silica supported metals as obtained by
Sinfelt et. al., where the rate data were fitted to the sim-
ple power rate expression

$$r = k_0 \ exp \ (-E_a/RT) \ P_{H_2}^m \ P_{C_2H_6}^n \qquad (1-2)$$

The activities for Ag and Au were very low, and no data were
available on Tc, but the group VI A metal, molybdenum, has a
very much lower activity than the group VIII metals (21); the
reaction proceeds only at temperatures high enough to cause
carbiding of the molybdenum (400°C), and the rate increases
with carbiding.

A compensation effect is observed, but this effect
seems to be smaller for the metals in the platinum group than
for the metals of the iron group (Fe, Co, Ni, Cu). In the
platinum group, an increase in activity is always accompanied

TABLE 1-1

Kinetic Parameters for Ethane Hydrogenolysis

over Silica Supported Metals

Metal	Reaction Orders n[a]	m[b]	T[c] (°C)	E[d] (kJ/mol)	(kcal/mol)	a[e]	a[f]	Ref.
Fe	0.6	0.5	270	-	-	1	-	(12)
Co	1.0	-0.8	219	126.	30.0	2	1	(10)
Ni	1.0	-2.4	177	170.	40.0	3	2	(10)
Cu	1.0	-0.4	330	90.	21.4	1	-	(10)
Ru	0.8	-1.3	188	134.	32.0	3	2	(11)
Rh	0.8	-2.2	214	176.	42.0	3	3	(11)
Pd	0.9	-2.5	354	243.	58.0	3	3	(11)
Re	0.5	0.3	250	130.	31.0	1	-	(20)
Os	0.6	-1.2	152	147.	35.0	3	2	(12)
Ir	0.7	-1.6	210	151.	36.0	3	2	(11)
Pt	0.9	-2.5	357	226.	54.0	3	3	(10)

a. Power of the ethane pressure.

b. Power of the hydrogen pressure.

c. Temperature at which n and m are determined.

d. Apparent activation energy.

e. Degree of unsaturation of the species C_2H_x , $a = (6-x)/2$

$$\text{from } r = kP_{HC}^n P_{H_2}^{(1-na)}$$

f. Degree of unsaturation of C_2H_x using $r = kP_{HC}^n P_{H_2}^{(-na)}$

a decrease in activation enery. Maximum activity in the three transition series occurs for Os, Ru, and Ni. The different behaviour between the metals of the iron-group (1[e] transition series) and those of the platinum-group (2[e] and 3[e] series) reflects known chemical differences (22). Within given transition series, a similar pattern exists for hydrogenolysis activity as a function of percentage d-character of the metals (24, 136); the latter represents the extent of participation of d-orbitals in the bonding between atoms in the metal lattice (4, 23). It has been suggested that except for this electronic factor, an additional geometrical factor is involved (24, 25),which might explain the different behaviour of the metals in the iron-group; the lattice spacings of these metals are relatively smaller. At $205^{\circ}C$, the sequence of activity for ethane hydrogenolysis is

Os > Ru > Ni > Rh > Ir > Re > Co > Fe > Cu > Pt ∿ Pd

A kinetic interpretation of the hydrogenolysis of ethane was first given by Cimino, Boudart and Taylor (7). As a first step it was assumed that ethane chemisorbs dissociatively to give an unsaturated surface species C_2H_x which is then attacked by hydrogen resulting in the rupture of the carbon-carbon bond. The monocarbon fragments hydrogenate off the surface to form methane.

$$C_2H_6 \quad \rightleftarrows \quad C_2H_x(ads) \quad + \quad aH_2 \quad a=(6-x)/2 \quad (1\text{-}3)$$

$$C_2H_x(ads) \quad + \quad H_2 \rightarrow CH_z(ads) \quad + \quad CH_y(ads) \quad (1\text{-}4)$$

$$CH_y \text{ (ads)} \quad + \quad CH_z \text{ (ads)} \quad \overset{+H_2}{\rightleftharpoons} \quad 2CH_4 \qquad (1\text{-}5)$$
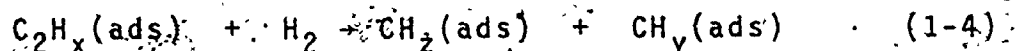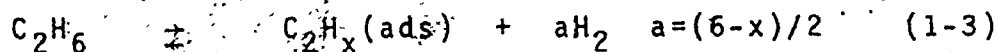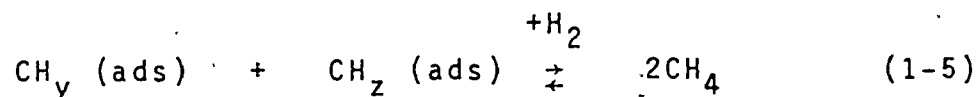
Reaction (1-4) is assumed to be irreversible, i.e. no chain growth occurs. Deuterium exchange experiments showed that the rate determining step in the sequence is the rupture of the carbon-carbon bond (5,26). If reaction (1-3) is in equilibrium, the Langmuir adsorption isotherm is given by

$$\theta = \frac{b \, (P_{C_2H_6} / P_{H_2}^{\,a})}{1 + b \, (P_{C_2H_6} / P_{H_2}^{\,a})} \qquad (1\text{-}6)$$

where $\quad \theta \; = \;$ fraction of surface covered by C_2H_x

$\qquad b \; = \;$ adsorption equilibrium constant

Over a limited range of pressures, (1-6) can be approximated by

$$\theta = b^n \, (P_{C_2H_6} / P_{H_2}^{\,a})^{\,n} \qquad (1\text{-}7)$$

with $\qquad 0 < n < 1$

The reaction rate is determined by the slow step (1-4)

$$r = kP_{H_2} \cdot \theta = k' \, P_{C_2H_6}^{\,n} \, P_{H_2}^{\,(1-na)} \qquad (1\text{-}8)$$

where $\qquad k' = kb^n$

This scheme does not apply in cases where the adsorption and desorption reactions are not in equilibrium, as has been claimed for iron and cobalt (12, 27, 102). A reasonable assumption is that "a" can have the values 1, 2, or 3, corresponding to ethylene, acetylene, and acetylenic residues

on the surface. Values for "a", the degree of unsaturation of the surface complex, can be calculated from equation (1-8) and the experimental exponents of ethane. These values are given in table 1-1 in column e. For rhenium and iron, the positive hydrogen exponents suggest that equilibrium in the initial dehydrogenative adsorption step is not established. Methane-deuterium exchange experiments suggested that the desorption of adsorbed C_1 fragments as methane may be rate controlling on several other metals as well. Apparent activation energies in table 1-1 increase as the degree of unsaturation of C_2H_x increases. The apparent activation energy is composed of the true activation energy for the C-C bond rupture plus the heat of adsorption, if coverages are low. This kinetic analysis does not take into account competition for active sites by hydrogen and the reaction products; it is possible that part of the inverse dependence on the hydrogen pressure is due to this effect (28).

Recently, the kinetic scheme was slightly modified by Sinfelt (29); this new scheme yielded a much improved fit of the kinetic data:

$$C_2H_6 \underset{k_1'}{\overset{k_1}{\rightleftarrows}} C_2H_5 \text{ (ads)} + H \text{ (ads)} \quad (1-9)$$

$$C_2H_5 \text{ (ads)} + H \text{ (ads)} \rightleftarrows C_2H_x \text{ (ads)} + aH_2 \quad (1-10)$$

$$C_2H_x \text{ (ads)} \overset{k_3}{\rightarrow} \text{ adsorbed } C_1 \text{ fragments} \quad (1-11)$$
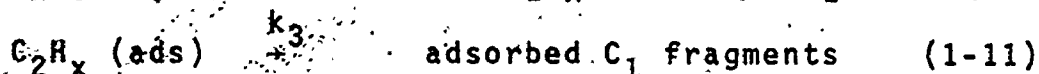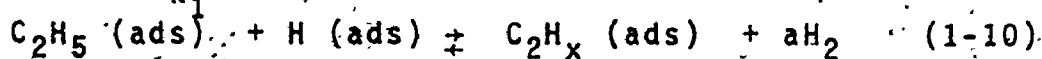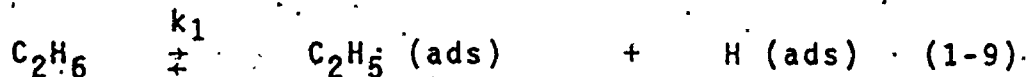
The reaction scheme differs from the previous one in that the C_2H_x -scission step does not involve hydrogen interaction, so that the reaction rate now is

$$r = k\, P_{C_2H_6}^n\, P_{H_2}^{-na} \tag{1-12}$$

The values of "a" calculated according to this scheme are in table 1-1, column f.

At high temperatures, the assumption of adsorption equilibrium between C_2H_6 and C_2H_x, on which equation (1-12) is based, breaks down; the rate of deuterium exchange becomes small compared to the rate of hydrogenolysis (30). In order to account for the kinetics over a wide range of temperature, a steady state treatment can be used in which the net rate of chemisorption of ethane is balanced by the rate of disappearance of C_2H_x (136).

$$k_1\, P_{C_2H_6} \quad - \quad k_1'\, \theta_{C_2H_5}\, \theta_H \;=\; k_3\, \theta_{C_2H_x} \tag{1-13}$$

If an effective equilibrium is assumed between C_2H_5 (ads) and C_2H_x (ads),

$$K_2\, \theta_{C_2H_5}\, \theta_H \;=\; \theta_{C_2H_x}\, P_{H_2}^a \tag{1-14}$$

$$\dot{r} = k\, \theta_{C_2H_x} \;=\; \frac{k_1\, P_{C_2H_6}}{(1 + b\, P_{H_2}^a)} \tag{1-15}$$

where $b = k_1' / (k_3 K_2)$

Since b is temperature dependent, so is the dependence of the rate on the hydrogen pressure.

For cobalt (24,27), b decreases with increasing temperature,
so that at sufficiently high temperatures the rate becomes
independent of the hydrogen pressure, $r = k_1 \; P_{C2H6}$, cor-
responding to the situation where ethane chemisorption is
completely irreversible. This was also observed in hydroge-
nolysis and exchange reactions of ethane on nickel powders
(30); at high temperature the reaction was independent of
the hydrogen pressure.

An alternate scheme was proposed by Boudart (97);
the reaction is considered to be a two-step irreversible se-
quence on a catalytically non-uniform surface. For nickel,
platinum, and copper-nickel catalysts, this model predicts
the same composition for the surface intermediates as the
Sinfelt model (100).

The most recent studies of ethane hydrogenolysis
have been on bimetallic catalysts, often consisting of a
group VIII metal and a group IB metal. For nickel-copper al-
loy powders, the catalytic activity decreased markedly and
continuously as copper was added, although most of the de-
cline was observed on addition of the first few percent of
Cu (61, 136); 5 at% of copper causes a decrease of three or-
ders of magnitude. On the same alloys, reactions with cyclo-
propane and methylcyclopropane (62, 63) showed that alloying
influences the reactions of carbon-hydrogen bonds less than
reactions of carbon-carbon bonds, i.e. alloying favours
isomerisation reactions but suppresses the hydrogenolysis

reaction; in other words, alloying can markedly shift selectivities. Experiments with n-hexane supported these results (154). The effect of copper was explained by the decreasing percentage d-character as copper is added. The very sharp initial decrease in activity suggests that the surface region has a much higher copper content than the bulk; hydrogen chemisorption studies support this: copper does not chemisorb hydrogen strongly (61, 64). It has been concluded that highly dispersed bimetallic clusters exist on the surface of the support. Similar phenomena were observed on ruthenium - copper and osmium-copper systems (64), and an increased catalytic performance was found for platinum-molybdenum catalysts compared to the platinum catalyst (118); the activity was higher, the catalyst more stable, and the inhibiting effect of hydrogen was decreased. Shifts of selectivity from hydrogenolysis to isomerisation reactions were also reported for films of gold with platinum or iridium (72), and for nickel-copper on zeolite Y (73).

Some work has been done to study the effect of the support and state of dispersion on the properties of the metal. The order of effectiveness of different supports for ethane hydrogenolysis on cobalt and nickel was

$$SiO_2 \; > \; Al_2O_3 \; >> \; SiO_2 \; - \; Al_2O_3 \; \sim C \; (15,17,24).$$
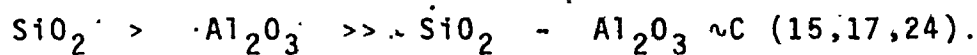
All the oxide carriers had about the same activation energy, but on carbon it was much lower.

Selectivities also were influenced by the support used (56).
The support effects are not yet fully understood. On a nickel
on silica catalyst, the rate of ethane hydrogenolysis was
proportional to the nickel surface (16), and the reaction
orders and apparent activation energies were unchanged. The
effect of metal dispersion has been investigated for Ni (19)
and Rh (18); the crystallite sizes were varied by sintering
the catalysts in hydrogen at different temperatures. The
specific catalytic activity of the metals (i.e. per unit met-
al area) decreased as the degree of sintering and the crys-
tallite size increased. The study suggested that ultimately
the catalytic activity decreases as the metal dispersion is
increased to a very high degree; highest catalytic activity.
was associated with an intermediate range of dispersion,
about 3.0 nm crystallites. These observations suggest that
metal atoms may be more active if they have a low coordina-
tion, like corner or edge atoms or lattice imperfections
(123,124). In terms of the characterisation introduced by
Boudart (96), hydrogenolysis reactions are therefore demand-
ing or structure sensitive. Metal particle size may also.
influence the selectivity towards skeletal reactions as report-
ed for supported platinum (127) and platinum films with a
range of crystallite sizes (123, 125).

    Considerably less work has been done on hydrogenoly-
sis reactions of hydrocarbons larger than ethane.

The hydrogenolysis of propane on supported nickel (9) and ruthenium (31, 101) and on films of nickel, rhodium, and platinum (32) occurs more readily than that of ethane, parallel with a higher rate of deuterium exchange. At higher temperatures and low pressures, the amount of methane in the products increases.. The pressure dependence of propane hydrogenolysis was studied over supported ruthenium (33). Using calculations similar to those for ethane, the activated surface species was found to be C_3H_3, indicating an 1,2-diadsorbed species. The reaction rate decreased with increasing pressure and the hydrogenative desorption of C_1 and C_2 species was much faster than the cracking reaction. The rate of hydrogenolysis increases with the number of carbon atoms in normal hydrocarbons, while branching decreases the rate. The activation energies for the hydrogenolysis of higher hydrocarbons are usually much lower than for ethane; the reaction orders with respect to the hydrocarbons are again unity or slightly smaller, while the hydrogen exponents are large and negative on most metals, similar to ethane. Reaction schemes similar to those for ethane seem to apply. The increased rate could in part result from lower average dissociation energies of carbon-carbon bonds in larger molecules (34). Another reason may be that 1,3-diadsorbed species can be formed as has been suggested by Anderson and Avery (35, 36) for some metals, notably platinum. Ethane can only form 1,2-diadsorbed intermediates.

On platinum and sometimes on palladium, isomerisation and
dehydrocyclisation reactions can take place in addition to
hydrogenolysis (35, 37-41, 53, 54, 135). The hydrogenolysis
reactions on platinum are so slow that much higher tempera-
tures are required than for the other noble group VIII me-
tals, so that isomerisation could also occur on these other
metals at similar temperatures, but can not be observed
since the hydrogenolysis is too fast. On platinum three dif-
ferent mechanisms have been proposed for various hydrocar-
bons (123): a) 1-2 adsorbed intermediates, b) 1-3 adsorbed
intermediates, c) π- adsorbed intermediates.

Interesting results can be obtained from the product
distributions from hydrogenolysis reactions of hydrocarbons
with several non-identical carbon-carbon bonds; there may be
different rates of rupture of bonds at different locations
in the molecule. Kempling used n- and isobutane and iso- and
neopentane over supported ruthenium (44-47). He found the
following relative reactivities of hydrocarbons: C_2 0.02;
C_3 1.0; n-C_4 10.0; i-C_4 0.8; i-C_5 9.5; neo C_5 0.04. The
number of hydrogen atoms dissociated to form the surface in-
termediate was 5-6 for normal hydrocarbons (and i-C_5)and 4
for neo-C_5 and i-C_4. This again suggests 1,2 type intermedi-
ates, completely stripped of the hydrogen at the adsorbed
carbon atoms. In n-butane, all the bonds had an equal change
of breaking, for isopentane the probabilities were 82% type I,

$$C \xrightarrow{\text{I}} C \xrightarrow{\text{II}} \underset{\underset{C}{\overset{\displaystyle |}{C}}}{C} \xrightarrow{\text{III}} C \qquad \text{10\% type II, 8\% type III.}$$
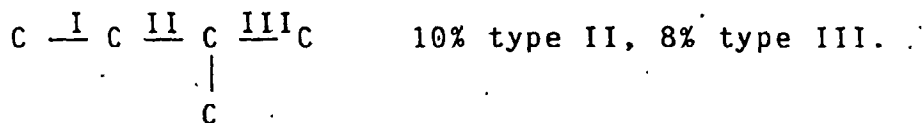
Desorption of the products was much faster than the cracking reactions, justifying the original mechanism. Splitting factors of this type are also given for other molecules (3, 135). The product distributions very much depend on the metal used, the hydrocarbon and the temperature. In all cases more extensive cracking occurs at higher temperatures, so that more smaller products are obtained.

A classical example of catalytic specificity is the highly selective attack of nickel catalysts on the terminal carbon atoms in contrast to for instance platinum where the rupture of different bonds is non-selective (48-50). Ruthenium also cracks the different carbon-carbon bonds in normal alkanes with equal probability, but in branched paraffins splitting occurs preferentially in the straight chain portion of the molecule. At low conversion, hydrogenolysis of n-hexane on nickel yielded only methane and n-pentane in equal amounts (51, 82). On platinum, where the carbon-carbon bonds crack almost statistically, a carbonium-ion mechanism has been proposed to interpret both the initial product distribution and the skeletal isomerisation (25, 32, 82). According to this theory, splitting of a carbon-hydrogen bond yields a carbonium-ion, which is easily isomerised and thereafter splitting of carbon-carbon bonds occurs by

β-scission. Similar examples of specificity were found with several other hexane isomers (51, 52, 82) and n-pentane (53, 54, 130). In these experiments it was again noticed that on cobalt and iron the traditional mechanism does not apply because the desorption steps are rate determining; this is shown by the large yields of small paraffins on these metals. Octanes and decanes over nickel showed a similar pattern of successive demethylation as the predominant reaction (55). In case of branched molecules, only methyl groups bonded to secondary and tertiary carbon atoms were attacked; the reaction stopped at quaternary carbon atoms. Experiments with n-heptane over a series of noble metal catalysts in powder form (Pd, Rh, Ru, Ir, Pt), showed that skeletal rearrangements took place on platinum only. Again the activity of platinum and palladium was much lower than that of the other metals. Palladium and rhodium behaved like nickel in cracking almost exclusively the terminal carbon-carbon bond, the other metals were non-selective.

Hydrogenolysis of cycloalkanes over several group VIII metals in the form of films and supported catalysts has covered cyclopropane and methylcyclopropane (1, 56, 57), cyclo-butanes, -pentanes, and -hexanes (55, 58, 60, 148). Pi-bonded species, involving partially delocalized electrons of the ring and unfilled d-orbitals of the metals, are suggested as the adsorbed intermediates for the noble metals,

where mainly ring opening occurred. Over nickel and cobalt
fragmentation reactions are also observed, and in these
cases the intermediates may be dissociatively chemisorbed.
On platinum and palladium, the cleavage of the cyclic bonds
was non-selective, while on nickel only disecondary cyclic
bonds were broken. Alkylcyclohexanes over nickel (55, 60)
showed a successive demethylation of the alkyl group, while
the cyclohexane ring was not cleaved under these conditions;
this in contrast to pentane- and heptane rings, where ring -
opening was observed.

Interesting results were obtained by using hydrocar-
bons with tagged carbon atoms, C^{13} or C^{14} (135).

1.3 Reactor

The goal of a kinetic study is to develop a fundamen-
tal rate equation that fits the kinetic data and is consis-
tent with observations about the reaction mechanism. The fol-
lowing steps can be distinguished in catalytic processes (77):

1. bulk diffusion to the external surface of the catalyst
2. diffusion in pores
3. adsorption of reactants
4. reactions at the catalyst surface
5. desorption of products
6. diffusion out of pores
7. bulk diffusion from external surface

The catalyst bed should be isothermal, and intra- and inter-

particle mass and heat transfer should be rapid compared to
the reaction rate and the rate of heat generation. Concentration and temperature gradients should be eliminated. Criteria expressed in terms of several dimensionless groups
were derived to assess the relative importance of transport effects in heterogeneous catalysis (23, 74-76). The
most critical consideration in the design of fixed-bed reactors is maintaining isothermal operation (74). The way to
achieve this is to reduce the reactor radius, but this can
be done only to an extent, because wall effects may become important, i.e. the more open packing near the wall causes larger fluid velocities (69). Experiments have shown that the
best compromise is a value of 5-10 for the ratio R_o/r_p,
radii of the reactor tube and an average particle, respectively. Another method of achieving isothermal conditions is by
diluting the catalyst bed with inert particles to reduce the
heat generated per unit volume. The reactor should have a
simple flow pattern, either plug flow (fixed bed reactor) or
complete mixing (continuous flow stirred tank reactor). The
equations determining reaction rates in these systems can be
derived from a mass balance around the reactor.

Differential-type reactors have the practical advantage of obtaining data at one level of concentration and
temperature; no integrations of rate equations are necessary.
In addition differential selectivities are obtained.

The reaction rate can be determined directly from the efflu-
ent flow rate and concentration (69):

$$r_i = \lim_{X_i \to 0} \frac{dX_i}{d(W/Q_i)} = \frac{X_i\, Q_i}{W}$$

(1-16)

where   W = weight of the catalyst

X_i = fractional conversion

Q_i = molar feed rate

r_i = reaction rate

Empirical or theoretically derived rate equations can be
examined by direct application of the data.

Several types of differential reactors are possible:
a fixed-bed reactor and very low conversions; a fixed-bed
with recycling where the conversion per pass is maintained
sufficiently low as to meet the requirements of equation
(1-16), while the total conversion can be higher so as not
to cause analytical problems; and finally a continuous
stirred reactor can be used (31, 45). For an isothermal con-
secutive reaction system, mixing favours formation of the
ultimate product, the yield of intermediate is lower than
in the absence of mixing at the same conversion. For isother-
mal simultaneous reactions, mixing favours the reaction of
lowest order and if all reactions are of the same order, the
product ratio is unaffected by mixing (99, 109).

1.4 Analysis of Data

An adequate theory of heterogeneous catalytic reactions should provide:

1. a kinetic description of the detailed path along which reactants are converted to products.

2. a conceptional foundation by which, at least in principle, the fundamental parameters (rate constants, activation energies and heats of adsorption) may be computed from the physicochemical properties of the system.

The basic assumptions are:

1. uniform surface.

2. the number of active sites is constant and proportional to the mass of catalyst.

3. no interactions between adsorbed species.

4. the concentration of intermediates is constant.

Basically, two types of equations or mathematical models can be used to correlate kinetic data.

The power rate functions are empirical:

$$r = kP_A^a \; P_B^b \qquad \text{where} \quad k = k(T) \qquad (1\text{-}17)$$

The power rate law rests upon a nonideal real-surface premise, characterized by the Freundlich isotherm, $\theta = kA^{1/n}$, which is an approximation of the Langmuir isotherm,

$$\theta = \frac{KA}{1 + KA}$$, on which the Hougen - Watson type models

are based.

θ = fraction of surface covered by adsorbed species

A = concentration of adsorbed species in gas phase

The Hougen - Watson type models are based on Langmuir - Hinshelwood kinetics and possess the form (77, 99),

$$r = \frac{k \, P_A \, P_B}{(1 + K_A P_A + K_B P_B)^n} \qquad (1\text{-}18)$$

where k = B exp (-E/RT) is a rate constant

and K = A exp (Q/RT) is an adsorption constant

A plot of lnK vs $1/T$ reveals a slope q_0, the lowest value of the heat of adsorption, q, corresponding to high coverage. (The heat of adsorption usually decreases with increasing coverage(132)). This type of rate equation is derived from a specific reaction mechanism, often assuming a single rate determining step. An attempt should be made to select a model with a minimum number of parameters.

Kinetic·data for heterogeneous systems often contain so much error that the use of mathematical expressions like (1-18) or even more complicated equations is unwarranted, and an improved fit to these equations often arises solely by the greater flexibility of the equations due to the abundance of parameters. It has also been pointed out that the assumptions in deriving these equations are seldom met, and that it would be better to use simple empirical forms like (1-17) whenever possible (131, 133).

A discrimination technique, like minimum sum of squares between observed and predicted rates is usually used to obtain the best equation (78), the assumptions being that the errors are independent and normally distributed with constant variance (99). Obtaining parameter estimates usually involves the use of linear or non-linear regression techniques (80, 81). Model rejection criteria may be based on:

a. lack of fit

b. unacceptable characteristics of estimated parameters, such as negative rate constants.

Negative adsorption constants are usually also rejected, but they may result from enhanced adsorption and should not necessarily be rejected (99, 131, 133). Many rate equations can be linearized, and relevant plots will enable the rejection of inadequate models. The procedures in model discrimination and parameter estimation are discussed in appendix B.

1.5 Thermodynamic considerations

Hydrogenolysis reactions are thermodynamically favourable, there have been no reports of chain growth over the metal catalysts used in these reactions. Equilibrium constants were calculated using free energy function data from Pitzer (121) and from Stull (137); tabulated free energy function values make it much easier to calculate ΔG^0 for a reaction at various temperatures than it would be by using an analytical equation for ΔG^0.

Free energy functions are given for individual compounds, and are handled like free energies of formation. Free energy functions are defined as $\{ (-G^0 - H_x^0)/T \}$, where G^0 is the standard Gibbs free energy and H_x^0 the standard enthalpy at "x"K; in general they are based on 0 or 298 K. The functions are derived from the properties of a single substance, they are not very sensitive to temperature, so that it is convenient and accurate to interpolate free energy fuctions. Some results at 500 K are tabulated in table 1-2. The equilibrium constants show the hydrogenolysis reactions are very favourable whereas the isomerisation reactions given, of normal to branched paraffins, are also favourable. Ring forming reactions of n-hexane to benzene, cyclohexane or methylcyclopentane are thermodynamically unfavourable at the temperatures used in these experiments. During the experiments, no isomerisation products, heptane, benzene or cyclohexane were observed in the products. The gaschromatographic system was able to separate the C_5 and C_6 isomers, methylcyclopentane and cyclohexane (appendix A). The separation of benzene and cyclohexane would require different column conditions.

There have been reports that some of the metals used in these experiments are hard to reduce, especially iron oxides, and to a lesser extent those of cobalt and nickel (12, 91, 129, 150). Promoters appeared to slow the reduction of iron, while an increased temperature or space velocity

TABLE 1-2

Equilibrium Constants at 500 K, Calculated from Free Energy Function Data

reaction	$\log_{10} K_{eq}$
$C_3H_8 + H_2 \rightleftarrows C_2H_6 + CH_4$	6.5
$C_3H_8 + 2H_2 \rightleftarrows 3CH_4$	14.0
$C_2H_6 + H_2 \rightleftarrows 2CH_4$	7.5
$n\text{-}C_6H_{14} \rightleftarrows C_6H_6 + 4H_2$ (benzene)	-4.8
$n\text{-}C_6H_{14} \rightleftarrows c\text{-}C_6H_{12} + H_2$ (cyclohexane)	-2.5
$n\text{-}C_6H_{14} \rightleftarrows c\text{-}C_6H_{12} + H_2$ (methylcyclopentane)	-2.1
$n\text{-}C_6H_{14} \rightleftarrows$ 2-Methylpentane	1.1
$n\text{-}C_5H_{12} \rightleftarrows i\text{-}C_5H_{12}$	2.3
C (graphite) + $2H_2 \rightleftarrows CH_4$	3.4 3.0 (650 K)
$3Fe + CH_4 \rightleftarrows Fe_3C + 2H_2$	-4.8 -3.1 (700 K)
$3Fe + C_3H_8 \rightleftarrows Fe_3C + 2CH_4$	18.2 16.9 (700 K)
$9Fe + C_3H_8 \rightleftarrows 3Fe_3C + 4H_2$	8.6 10.7 (700 K)

increased it; on the other hand, promoters also stabilized the α-Fe structure (150). Equilibrium constants for the reduction of oxides of nickel, cobalt, and iron are given (66), and they confirm that the reduction becomes more difficult in this sequence.

Silica-supported metals are in general much easier to reduce than those supported on alumina where the metal reacts with the support more readily (124, 128). But silica-supported metals are harder to reduce than bulk metals (132, 150), and the reducibility decreases greatly with increasing degree of dispersion. For iron it has been shown that even though thermodynamic considerations suggest that bulk iron oxides can be reduced to the metallic state by hydrogen at 400°C, more severe conditions are needed if the metal is on a support (129, 150).

In the case of iron catalysts, problems may also arise because the iron may form carbides easily, as is the case in a H_2-CO atmosphere (66). This has been reported to occur at 327°C with paraffins of carbon numbers greater than 2, and from methane at 500°C. Cobalt also can carburize, but is more readily reduced in a hydrogen atmosphere. A final problem that may arise in these reactions is the deposition of elemental carbon, especially if the hydrocarbon to hydrogen ratio is high (91). In the present experiments this ratio is kept low to avoid this problem.

Chapter 2

PREPARATION AND CHARACTERIZATION OF THE CATALYSTS

2.1 Introduction

All the catalysts used in this work were supported
metal catalysts. They are of special interest because metal
can be dispersed as very small crystallites on the surface of
the carrier which is commonly a porous, inert oxide such as
alumina or silica. In this form the metal has a high surface
area and is more resistant to sintering than unsupported me-
tal powders or films (24, 135). There are different ways of
preparing supported metal catalysts (124, 132, 134); in this
work the most common method, impregnation, has been used. The
support is contacted with a solution of ions of the metal in
question, and the metal ions are deposited onto the carrier
surface. If available, nitrates of the metals are used, since
they decompose readily upon heating.

To compare activities of different catalysts, it is
important to determine their physical properties also. The
following sections summarize the preparations and the inves-
tigations performed to characterize the catalysts. The high
state of dispersion of supported metals makes them very dif-
ferent from bulk metals in some of their properties (24).
There may be differences in magnetic properties, and the X-ray

diffraction patterns may show very broad and weak lines in contrast to the strong, sharp lines observed for large metal crystals. Since there usually is a metal particle size distribution, the average crystallite size obtained by different methods (magnetic, chemisorption, X- ray line broadening, transmission electron microscopy (T.E.M.), Mössbauer spectroscopy), are usually not directly comparable. Magnetic properties of dispersed metals have been described (65, 67, 68, 88, 122).

Low area supports and high area supports can be used in the preparation of the catalysts. The high area supports usually require a lower metal loading, because the metal is more highly dispersed than on low area supports. Low area supports have the advantage that the pores are larger, thereby making it less likely that diffusion effects will be a slow step in the reactions. For the same reason, larger particles can be used, which is of advantage, especially in a differential recycle reactor, where the pressure drop over the catalyst bed should be rather low. If low area supports are used, it will often be advantageous to add a structural promoter to the catalyst, such as magnesium oxide or calcium oxide, to increase the metal surface area and avoid sintering of the metal crystallites. Low area supports are also less likely to react with the metals they support.

2.2 Preparation of the Catalysts

Several types of supports have been used to prepare catalysts containing nickel, cobalt, and iron. The ruthenium catalyst and one of the iron catalysts used were commercial preparations; their properties are discussed in section 2.4.

A high area silica gel from Grace (57-08-5x-1950) was used to prepare the high area catalysts. This silica gel was crushed, sieved into fractions of 14-28 mesh and 28-48 mesh, and dried at $400^{o}C$ for 24 h. The properties of this support are given in section 2.3.

Several low area supports were used in the preparation of the low area catalysts: siliconcarbide, sintered aluminiumoxide, silica and zircon. These supports were furnished by The Carborundum Company. They were sieved to a size of 10-12 mesh, and their strength properties and thermal conductivities are better than those of the high area support, siliconcarbide being the best. Some of the properties of these supports, as given by the manufacturer are listed in table 2-1. The supports were dried at $400^{o}C$ for 24 h before being used in the catalyst preparations.

The chemicals used in the impregnations were: Co $(NO_3)_2$ · $6H_2O$ (A.C.S.) and Ni$(NO_3)_2$ · $6H_2O$ (purified), both from Fisher Scientific Co., Fe $(NO_3)_3$ · $9H_2O$ (Analyzed Reagent) and Mg $(NO_3)_2$ · $6H_2O$ (Analyzed Reagent), both from J.T. Baker Chemical Co.. The metal nitrates were dissolved

TABLE 2-1

Summary of some Properties of the low Area Supports (Carborundum)

Chemical Analysis	Physical Properties			
	% pore volume	surface area m^2/g	solid bulk density g/cm^3	average pore size μm
Sintered Aluminum Oxide 96.0% Al_2O_3 2.4% SiO_2 0.6% Fe_2O_3 0.5% MgO	60.0	0.74	1.5	0.4
Siliconcarbide 77.0% SiC 5.6% Al_2O_3 15.5% SiO_2 0.4% Fe_2O_3 0.5% Na_2O	45.0	0.27	1.64	25.0

TABLE 2-1 (continued)

	Chemical Analysis	% pore volume	surface area m^2/g	solid bulk density g/cm^3	average pore size μm
		Physical Properties			
Silica	93.1% SiO_2 5.8% Al_2O_3 0.1% Fe_2O_3 0.3% MgO	60.0	0.45	1.02	5.0
Zircon	53.6% ZrO_2 38.% SiO_2 6.6% Al_2O_3 0.2% Fe_2O_3 0.6% CaO	37.0	0.31	2.48	6.0

in the appropriate amount in distilled water; for promoted
catalysts, the metal and promoter ions were in the same so-
lution. The amount of solution used in each impregnation was
1.5 - 2.0 times the pore volume of the support sample.

It turned out that the catalyst was more uniformly
impregnated if twice the pore volume was used, as opposed to
the standard one times the pore volume. The support and the
solution were mixed well, dried overnight at 105°C in air,
and calcined at 450°C for 2 h in air to decompose the nitra-
tes to metal oxides. Visual and microscopic inspection sho-
wed that after calcining the metal oxide seems to be distri-
buted throughout the support particles in both the high area
and the low area catalysts. For the low area catalysts, three
consecutive impregnations were performed, each one followed
by a drying and calcining step. This was done because the
metal loading in these catalysts must be higher, to obtain a
reasonable activity, and also because the pore volume of
these supports is rather small.

High area catalysts were prepared for iron, cobalt
and nickel on high area silica (28-48 mesh); cobalt and
nickel catalysts were also prepared on larger particles (14-
28 mesh) with approximately equal metal loadings. Low area
catalysts were prepared in the following combinations:
nickel on siliconcarbide, and iron on silica, siliconcarbide,
alumina and zircon.

Promoted catalysts were prepared only on the low area supports, using magnesium as a promoter: nickel-magnesium on siliconcarbide, cobalt-magnesium on siliconcarbide, and iron- magnesium on silica.

2.3 Characterization of the Catalysts

2.3.1 Chemical Analysis

The catalyst samples were treated with a mixture of nitric acid and hydrochloric acid to dissolve all of the metals. The solutions were filtered and diluted, and atomic absorption spectroscopy was used to determine the metal loading on each of the catalysts. The results of these analyses are shown in table 2-2. The amount of metal on the catalyst was usually slightly lower than that calculated from the amount and the concentration of the impregnation solution.

No iron was detected in the solutions prepared from the catalysts supported on siliconcarbide, even though the chemical composition of this support shows 0.42% iron. This result indicates that this iron is in the bulk of the support and should have no effect on the catalytic activity. The unpromoted iron catalysts on the low area supports were made to contain approximately 20% iron; they were not analysed since they were inactive for hydrogenolysis.

2.3.2 Physical Adsorption

Physical adsorption of nitrogen at its boiling point can be used to determine the total surface area and the pore

Table 2-2

Properties of the Catalysts prepared in this research

Catalyst	Chemical Composition (a) wt %	Total Surface Area (b) m^2/g	Metal Surface Area (c) m^2/g	-1 (d) nm	Metal Dispersion (e)
high area					
nickel on silica (14-28 mesh)	-	235.	7.7	7.0	-
nickel on silica (28-48 mesh)	4.1 Ni	253.	8.3	2.8	0.28
cobalt on silica (14-28 mesh)	7.0 Co	248.	3.2	12.3	0.06
cobalt on silica (28-48 mesh)	6.3 Co	-	2.1	16.9	0.05
iron on silica (28-48 mesh)	8.1 Fe	-	0.35	150.	0.01
low area (10-12 mesh)					
nickel on siliconcarbide	16.7 Ni	0.2	0.12	780.	0.001
nickel-magnesium on siliconcarbide	{ 14.9 Ni 1.0 Mg	2.6	2.0	42.	0.02
cobalt-magnesium on siliconcarbide	{ 17.3 Co 0.7 Mg	3.0	-	-	-
iron-magnesium on silica	{ 14.5 Fe 0.9 Mg	-	-	-	-

(a) by atomic absorption spectroscopy

(b) by nitrogen adsorption at 77 K

(c) by chemisorption of hydrogen at room temperature

(d) average crystallite size using equation(2-7)

(e) defined as the ratio of the number of hydrogen atoms adsorbed and the number of metal atoms present

volume of the catalysts and the supports. A conventional volumetric technique was used to measure adsorption and desorption isotherms of high area silica and the high area catalysts (69). A sample cell fitted with two stopcocks permitted flowing hydrogen over the samples during reduction. The dead volume of the cell was minimized by using glass beads and glass rods. The catalysts were reduced under approximately the same conditions as used for the hydrogenolysis experiments, usually 24 h at 450°C. The samples were then evacuated at this temperature for one hour, and cooled to room temperature under vacuum. The nitrogen adsorption isotherms of the high area catalysts were determined at 77K over a range of relative pressures of 0.05 to 0.99. The isotherm, as expected, is a type IV isotherm (95), and the surface area can be determined by using the linearized BET equation (66, 70), and plotting $x/(V(1-x))$ against the relative pressure:

$$\frac{x}{V(1-x)} = \frac{1}{V_m c} + \frac{x(c-1)}{V_m c} \qquad (2-1)$$

where:

x = relative pressure = p/p_0

V = volume adsorbed

V_m = volume corresponding to a monolayer

c = constant

In the calculations it is assumed that each molecule of adsorbate covers .163 nm^2 of surface, based on the density of the physically adsorbed layer being equal to that of the

liquid phase. The surface area is then equal to

$$S = 4.37 \ V_m \qquad\qquad (2-2)$$

The pore volume V_p is calculated from the total amount adsorbed at saturation (relative pressure 1.0), and an average pore radius can be determined from:

$$\bar{r} = 2V_p \ / \ S \qquad\qquad (2-3)$$

with the assumptions that the pores are uniform and cylindrical (69).

The adsorption isotherm of the high area silica gave a pore volume of 1.0 cm^3/g and a surface area of 265 m^2/g; the average pore radius is 7.5 nm. The isotherms of the nickel and cobalt catalysts, including an isotherm of the nickel catalyst after using it for one month in hydrogenolysis experiments, gave slightly lower areas and pore volumes, but the results were very similar, areas varied from 240 - 255 m^2/g, pore volumes from 0.92 - 0.96 cm^3/g, and the average pore radius was between 7.0 and 7.6 nm (table 2-2).

An example of a complete isotherm is given in fig. 2-1 for the nickel on silica catalyst. Fig. 2-2 shows that the plot of $^x/(V(1-x)$ versus x is linear in the region x is 0.1 - 0.3. For this catalyst the area was 253 m^2/g, pore volume 0.96 cm^3/g and average pore radius 7.6 nm.

The areas of the low area supports and catalysts, could not be determined by the volumetric technique, since too much of the catalyst would be needed.
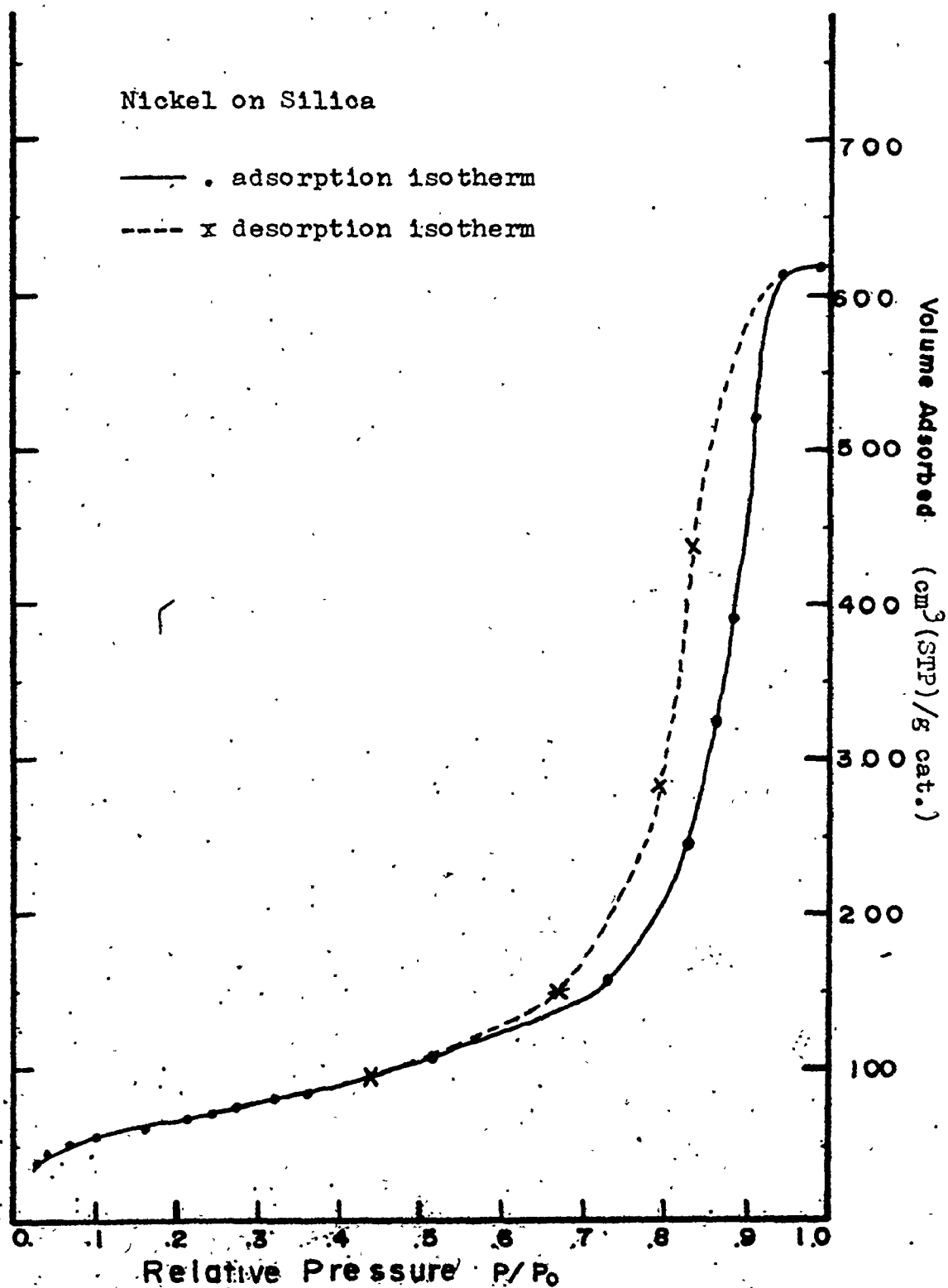
Figure 2-1: Nitrogen Adsorption Isotherm at 78 K

Nickel on Silica

$(P/Po) / (Vads(1-P/Po)) \times 10^3$ (g cat./cm^3 (STP))

$$\frac{P/Po}{Vads\ (1-P/Po)} = \frac{1}{V_m c} + \frac{P}{Po}\left[\frac{c-1}{V_m c}\right]$$

Relative Pressure $\left[P/Po\right]$
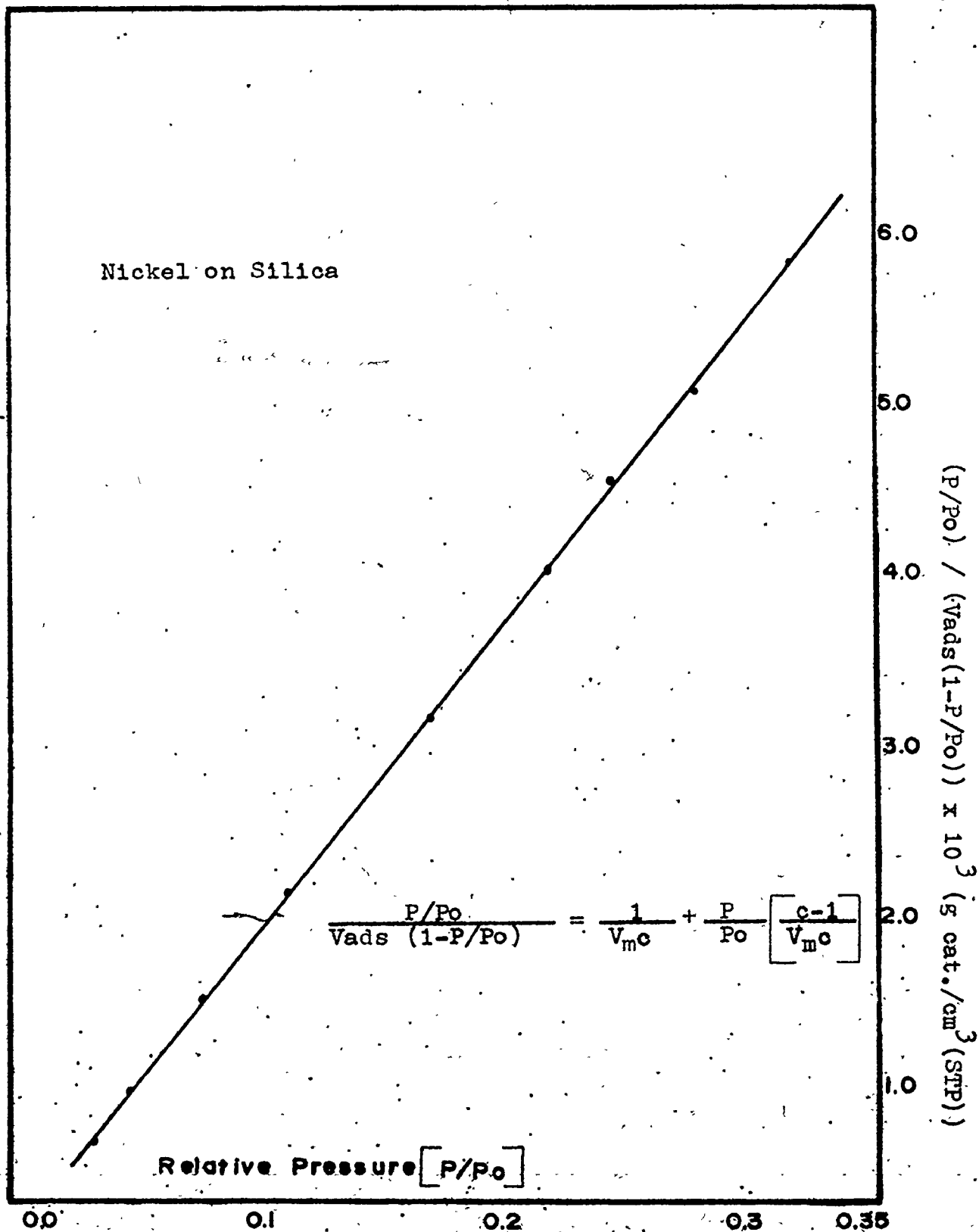
Figure 2-2: Linearised B.E.T. equation

Instead a sorptomat was used for these catalysts, a diagram of which is shown in fig. 2-3 (89, 90). Only two points of the isotherm are obtained, both in the linear region of the isotherm: P/p_0 approximately 0.1 and 0.2. The total surface area can now be calculated as before, but the pore volume is not obtained. Nitrogen is adsorbed by the sample at liquid nitrogen temperature from a gas stream of nitrogen and helium, and eluted upon warming up the sample. The nitrogen liberated is measured by means of a thermal conductivity cell. There are several advantages of this method over the conventional volumetric BET method: no vacuum techniques are involved, it is faster and simpler for routine applications, and it is more sensitive to low area samples because of the high sensitivity of the thermal conductivity cell. Calibrations were made using pure nitrogen and calibrated sample loops. The results are tabulated in table 2-2. To check the method, the area of high area silica was determined and found to be 240 m^2/g. The total area of the nickel on siliconcarbide catalyst is of the same order as that of the support, while the promoted catalyst has an area of about a factor ten higher; i.e., most of the area of the promoted catalyst must be metal.

2.3.3 Pore Distribution

The pore distribution of the high area silica was measured with a mercury porosimeter (Micrometrics Instrument

39

Figure 2-3: Determination of surface area by continuous flow method
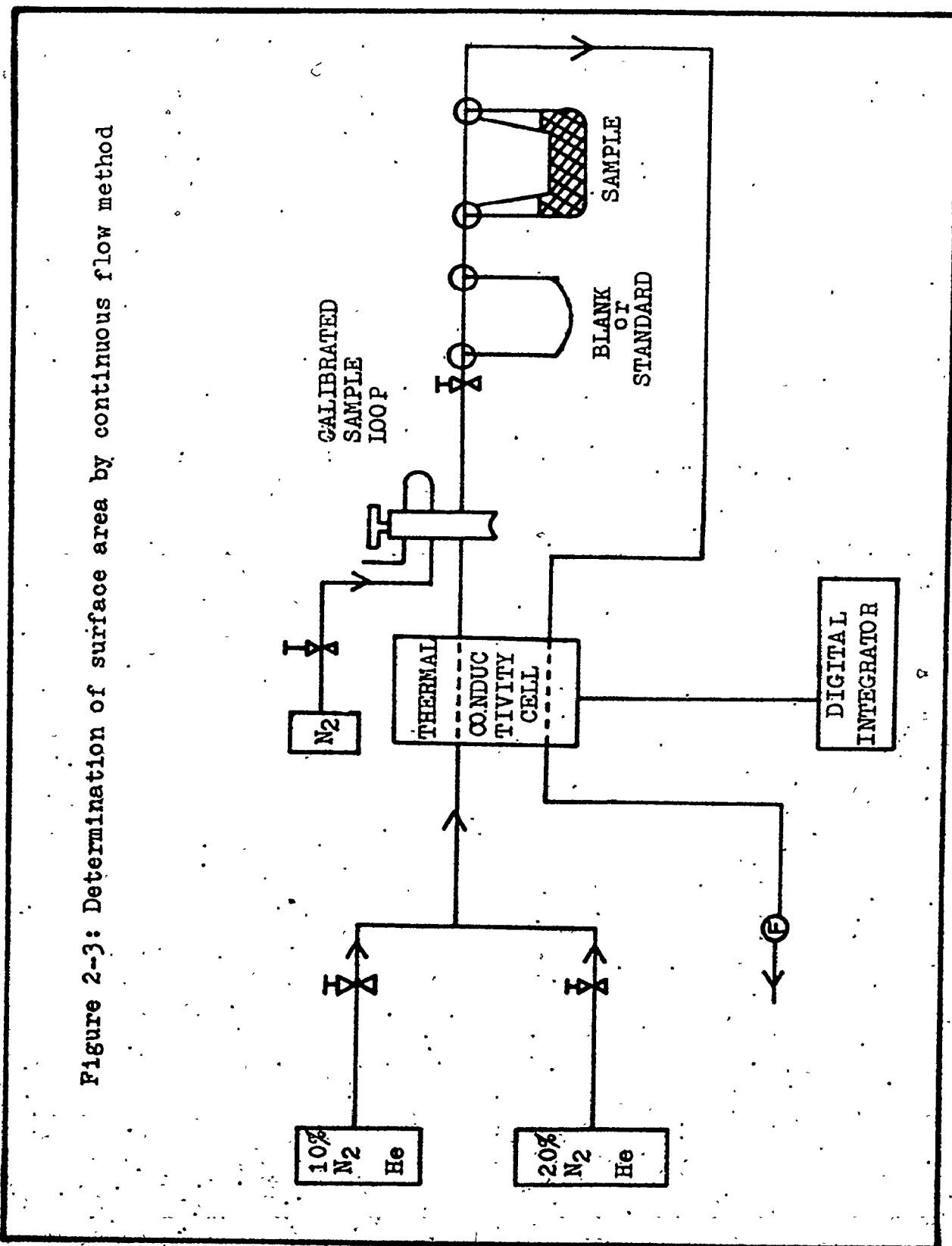
Corporation), and the average pore diameter compared with the one obtained from the nitrogen adsorption experiments. Mercury, unlike most other liquids, has a positive contact angle with most solid materials; hence pressure must be exerted for mercury to penetrate the pores; the smaller the pore radius, the higher the pressure required to force the mercury into the pores. The catalyst sample is evacuated and the sample holder is filled with mercury. The amount of mercury entering the pores is then measured as a function of pressure. The equation relating the pressure and the pore radius is (23, 33, 66, 71):

$$P = -2\sigma \cos \theta / r \qquad (2\text{-}4)$$

where: r = cylindrical pore radius

θ = contact angle of mercury (taken to be 130^{0})

σ = surface tension of mercury

$(0.474 \ ^{N}/m \ at \ 25^{0}C)$.

This yields:

$$r = .61 / P \qquad (2\text{-}5)$$

where the pressure is in pascals and r in meters.

The pore size distribution D(r) for cylindrical pores can be represented as (23):

$$D(r) = -\frac{P}{r} \frac{dV}{dP} \qquad (2\text{-}6)$$

A plot of D(r) versus r can easily be obtained, and is shown in fig. 2-4 for the silica sample. The pore distribution is rather narrow, with a peak at r = 7.0 nm, which is in good agreement with the results of the nitrogen adsorption experiments. The pore volume is estimated from the total amount of mercury penetrated and it is found to be 1.0 cm^3/g, which also agrees with the previous results. The surface area can be obtained by graphical integration (23) and this gives a value of 225 m^2/g.

2.3.4 Chemisorption

An important problem in studies of supported metal catalysts is the determination of the surface area and the size of the metal crystallites. The most effective method of obtaining the metal surface areas is chemisorption of a gas that adsorbs selectively on the metal rather than on the support (11, 65, 96). Hydrogen and carbonmonoxide at room temperature have been used for several metal catalysts (10-12, 15-20, 44, 83, 132). To correct for the amount of adsorbate that may be weakly adsorbed on the support, a second isotherm is usually obtained after a brief evacuation period, and the difference between the two isotherms is considered to be the amount which is strongly chemisorbed (18, 44, 62).

Hydrogen was used as an adsorbate on most of the catalysts prepared in this research at room temperature. It is generally assumed hydrogen adsorbs dissociatively (88) on
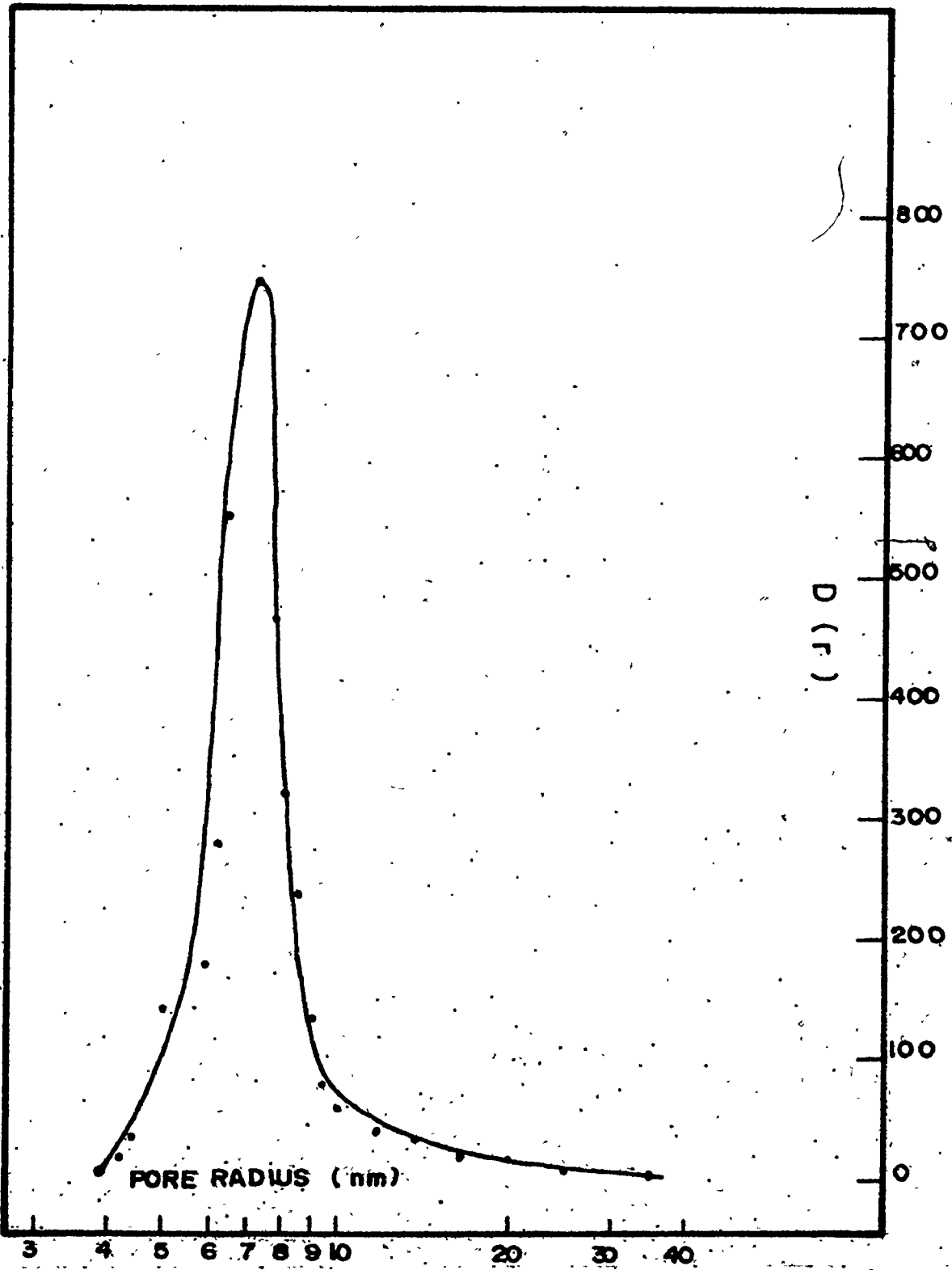
Figure 2-4: Pore Distribution of high area Silica

these metals, with one hydrogen atom adsorbed per surface metal atom. From the amount adsorbed at saturation, the specific surface area of the metal can be calculated, using an appropriate value for the area associated with a single metal atom on the surface (10, 11, 65). The average area equivalent for nickel is 0.065 nm^2/nickel surface atom, and this value is the same for cobalt and iron (10, 12, 15, 16). An average crystallite size can be calculated, assuming cubic crystallites of length 1 with five exposed faces (65):

$$1 = 5 /(Sd) \tag{2-7}$$

where   S =   surface area per gram of metal

d =   density of the metal

Before the chemisorption experiments, the catalysts are reduced and evacuated at the reduction temperature. The adsorption experiments were performed at room temperature and hydrogen pressures up to 0.40 atm. The time required for equilibration was approximately 45 min. The evacuation step between the two isotherms was 20 min, but is was observed that the results did not change even if the evacuation would last as long as one week. The results, expressed as metal surface area in m^2/g are given in table 2-2, the results are based on the difference of two hydrogen adsorption isotherms. The average crystallite diameters are also given, based on equation (2-7), with appropriate values for the bulk metal densities: 8.9 g/cm^3 for cobalt and nickel, 7.86 g/cm^3 for iron.

Finally, values of the metal dispersion, defined as the ra-
tio of the number of chemisorbed hydrogen atoms and the num-
ber of metal atoms, are given

The results for cobalt on silica and the nickel on
silica catalysts indicated that the metal area was not influ-
enced by the sintering step in the catalyst preparation, i.e.
if the catalyst is reduced directly after drying, the metal
area is the same as for the catalyst sintered before reduc-
tion. A blank experiment was performed with the high area
silica. After treatment in hydrogen at 400°C no adsorption
took place on this sample.

On the supported iron catalyst there appeared to be
only weakly adsorbed hydrogen, and the amount adsorbed in-
creased with temperature, whereas on the nickel catalyst the
amount adsorbed decreased when the temperature was raised
from 20°C to 200°C. The results compared favourably with ad-
sorption isobars of hydrogen on an iron ammonia synthesis
catalyst (91, fig. 16) and a nickel on kieselguhr catalyst
(94). The iron catalyst was reduced at 520°C since it had
been reported (12, 91, 93) that these catalysts are hard to
reduce, if structural promoters are present (150). Hydrogen
isotherms are shown in fig. 2-5 for cobalt on silica (14-28
mesh) and nickel on silica (28-48 mesh).

2.3.5 X-ray Line Broadening

Another method for obtaining an average metal parti-
cle size is X-ray line broadening.
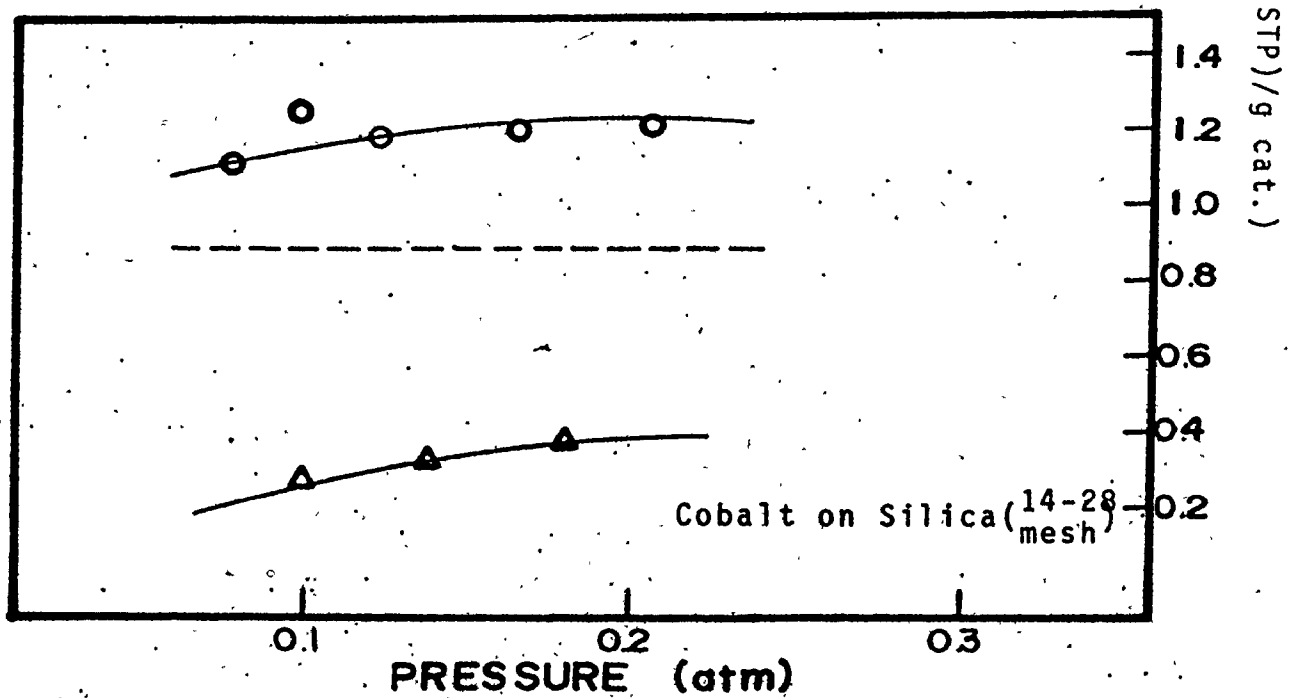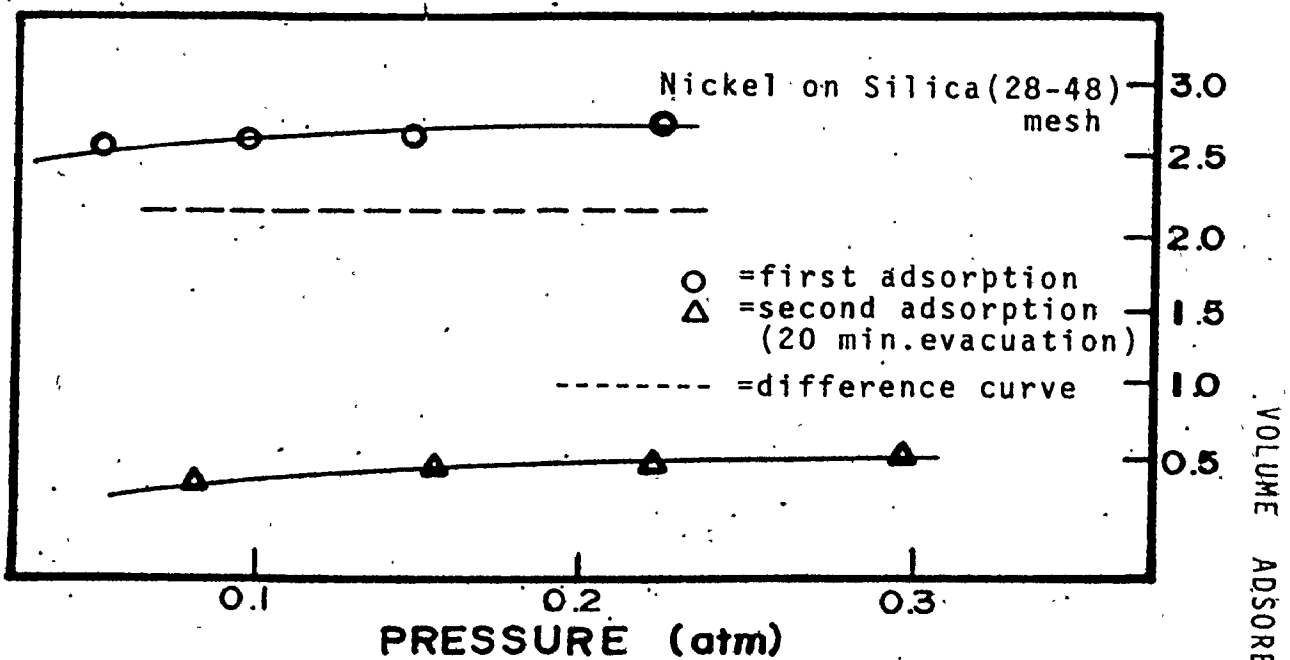
Figure 2-5   Hydrogen Chemisorption at Room Temp.

The mean diameter, D, of crystallites is related to the pure X- ray diffraction broadening β, as (65, 87):

$$D = k\lambda / (\beta \cos \theta) \qquad (2\text{-}8)$$

where: k = constant and approximately unity

λ = radiation wavelength

θ = Bragg angle

The reflected X- rays are recorded with a proportional counter, which has a linear response.

The line broadening due to crystallite size effects must be corrected for the effects of instrument broadening by:

$$\beta = (B^2 - b^2)^{\frac{1}{2}} \qquad (2\text{-}9)$$

where: B = observed diffraction line width

b = width of a line under similar conditions of a material with a crystallite size well in excess of 100 nm.

The reference used here to determine the instrument broadening is a quartz powder.

High area nickel and cobalt on silica were studied using this technique. The reduced catalyst is kept under ethanol, crushed to a fine powder, mixed with quartz powder and collodion, mounted on a microscopic slide, and dried under vacuum. Samples were scanned from $2\theta = 7^{\circ}$ to 70° at 1°/min; a Cu tube was used (16mA, 100kV).

In the nickel sample no oxide peaks were observed, indicating that the preparation of the sample prevented

extensive oxidation. The main nickel peaks are at 44.5^O and 51.8^O, the (111) and (200) peaks, respectively. The (111) peak gave a value for the average crystallite size of $L =$ 13.5 nm. An oxidized nickel sample showed no nickel peaks, and from the oxide peak (100) at 43.6^O, a crystallite size was obtained of 12.0 nm. The cobalt samples gave very weak peaks, and a thick layer of finely crushed powder was needed. The crystallite size was estimated to be 8.0 nm, but the accuracy was low.

In all the samples, a very broad signal was observed at $21-22^O$. A spectrum of pure silica again showed this peak; two silica samples, heated at $150^O C$ and at $500^O C$, gave the same results. It is therefore safe to assume that this peak is due to the support, and the phase it appears to indicate is α-cristobalite, which has a strong signal in this region. Cristobalites have been detected in some kieselguhrs before (92). The temperatures of transformation of the different silica phases are as follows:

$$\beta \text{ quartz} \underset{575^O C}{\overset{870^O C}{\rightleftharpoons}} \gamma \text{ tridymite} \underset{220^O C}{\overset{1470^O C}{\rightleftharpoons}} \beta \text{ cristobalite}$$

$$\alpha \text{ quartz} \qquad\qquad\qquad\qquad \alpha \text{ cristobalite}$$
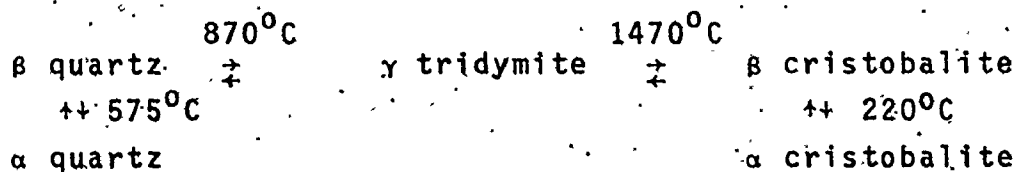
β cristobalite can be formed in kieselguhrs at lower temperatures if alkali are present in the samples. Detecting cristobalite in the silicagel is an unexpected result. The width of the cristobalite peak corresponds to a crystal-

lite size of 2.5 nm. An example of parts of a spectrum is
shown in fig. 2-6 for a nickel on silica sample.

2.3.6 Electron Microscopy

The nickel on silica catalyst has also been exam-
ined using transmission electron microscopy. This technique
has the advantage that information can be obtained on both
the shape and the size of the particles. A distribution of
particle size can be obtained, as well as, sometimes, infor-
mation on the interaction of the metal particles with the
support. Improved electron microscope designs have decreased
the routine resolution limit to less than 1.0 nm (9, 65, 85,
86, 126). Average particle sizes can be calculated, and it
can be determined whether the metal particles are randomly
distributed or concentrated in clusters. If the particles
are large enough, their crystalline form may also be deter-
mined. Because of these advantages, electron microscopy is
capable of revealing more information about the samples, if
compared to X- ray diffraction and chemisorption.

A Phillips E.M. 300 transmission electron microscope
(100 kv) was used to investigate the nickel on silica cata-
lyst. The catalyst was reduced, ground and stored under etha-
nol. The suspension was then mixed with collodion, and made
into a very thin film by pressing between two microscope slides.

The film was coated with a thin layer of carbon, to im-
prove its strength, cut into pieces, and floated on dis-
tilled water.
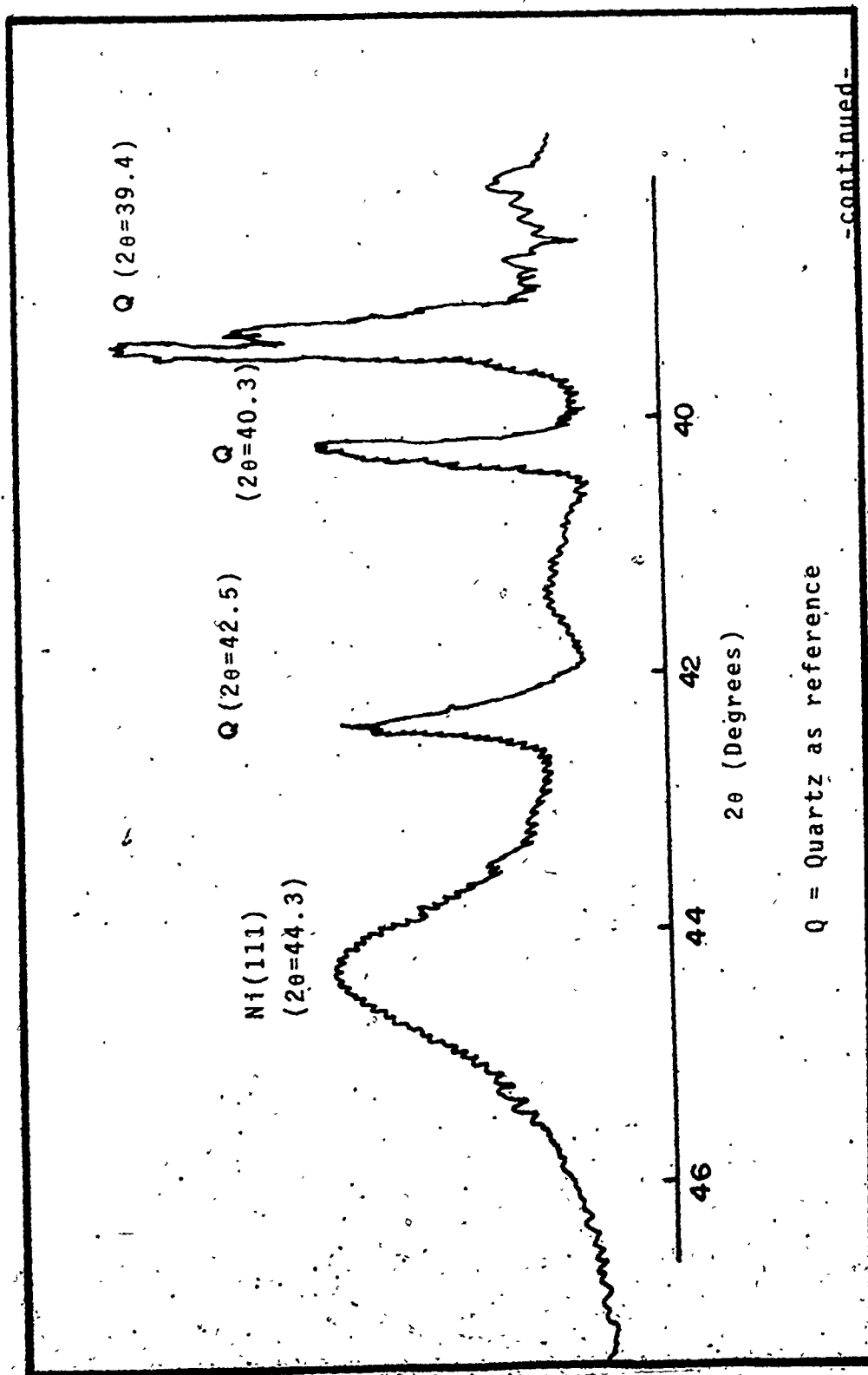
Figure 2-6 X-ray Line Broadening Spectrum of a Reduced Nickel on Silica Catalyst.

-continued-
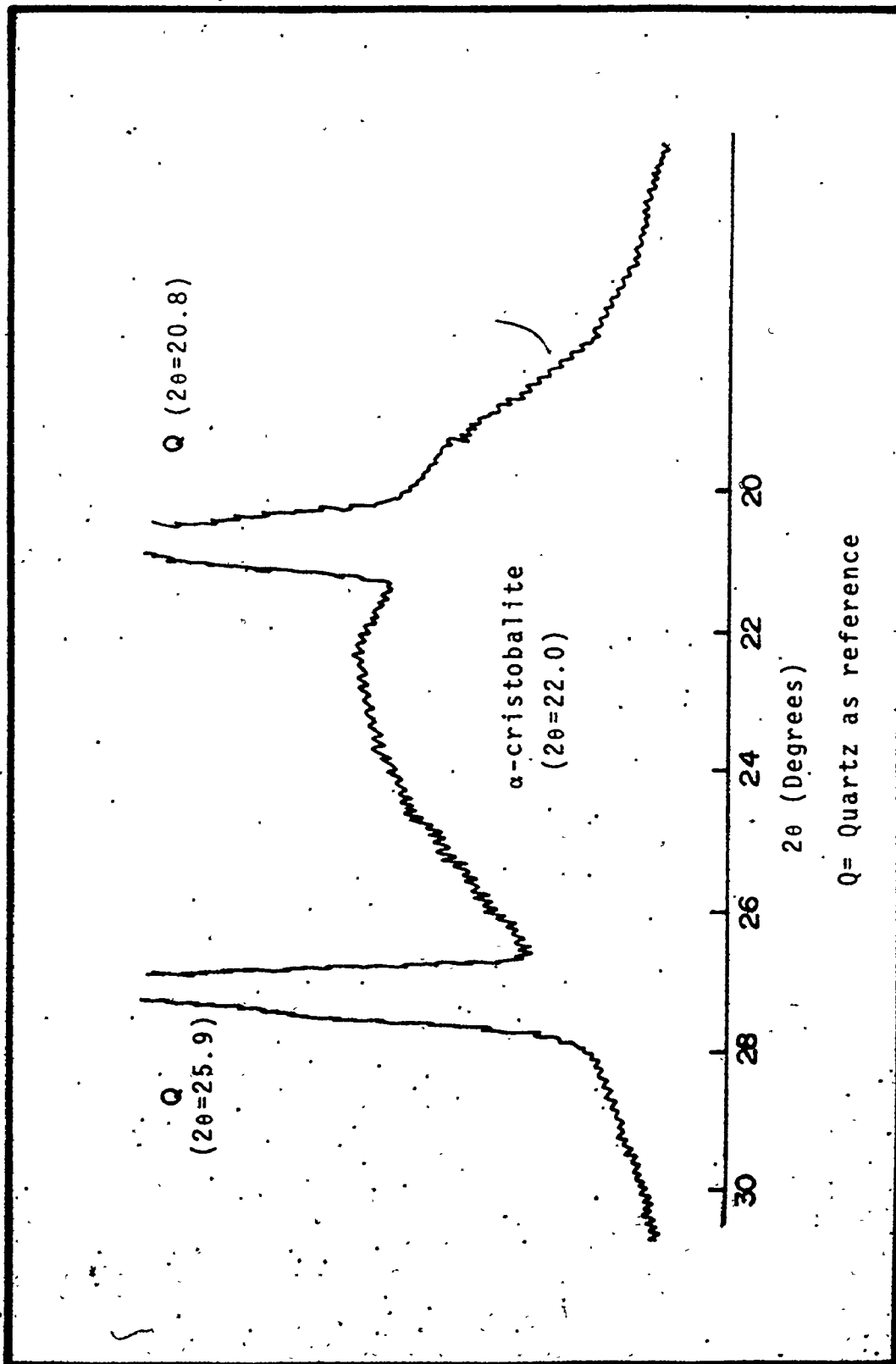
Figure 2-6. X-ray Line Broadening Spectrum of a Reduced Nickel on Silica Catalyst.

Pieces of the film were then picked up by fine copper grids
(200 mesh) and dried. Magnifications were up to 120.000 *.
Several samples were prepared, and photographs were taken of
a number of areas at each sample. For comparison, also some
photographs were made of the silica gel. The negatives were
projected on a screen, and the particles were counted and
measured. 27 Photographs were used in this counting process,
and a total of 300 particles were measured; this number
should be sufficient, since the particle size distribution
was rather narrow. Most of the particles had a rather regu-
lar, round shape, and they could only be observed near the
edge of the silica particles, and on very small silica par-
ticles. A histogram is shown in fig. 2-7, and some of the
photographs are in fig. 2-8. The maximum of the histogram
is in the region 8.0-9.5 nm.

A number-average diameter can be obtained from:

$$d_n = \Sigma n_i d_i / \Sigma n_i = 9.3 \text{ nm}$$

Similarly, a surface-average and a volume-average diameter
can be calculated (134):

$$d_s = \Sigma n_i d_i^3 / \Sigma n_i d_i^2 = 13.0 \text{ nm}$$

$$d_v = \Sigma n_i d_i^4 / \Sigma n_i d_i^3 = 14.9 \text{ nm}$$

The volume-average diameter is what one would expect to ob-
tain from X-ray line broadening experiments, and the agree-
ment is satisfactory. The surface-average diameter should
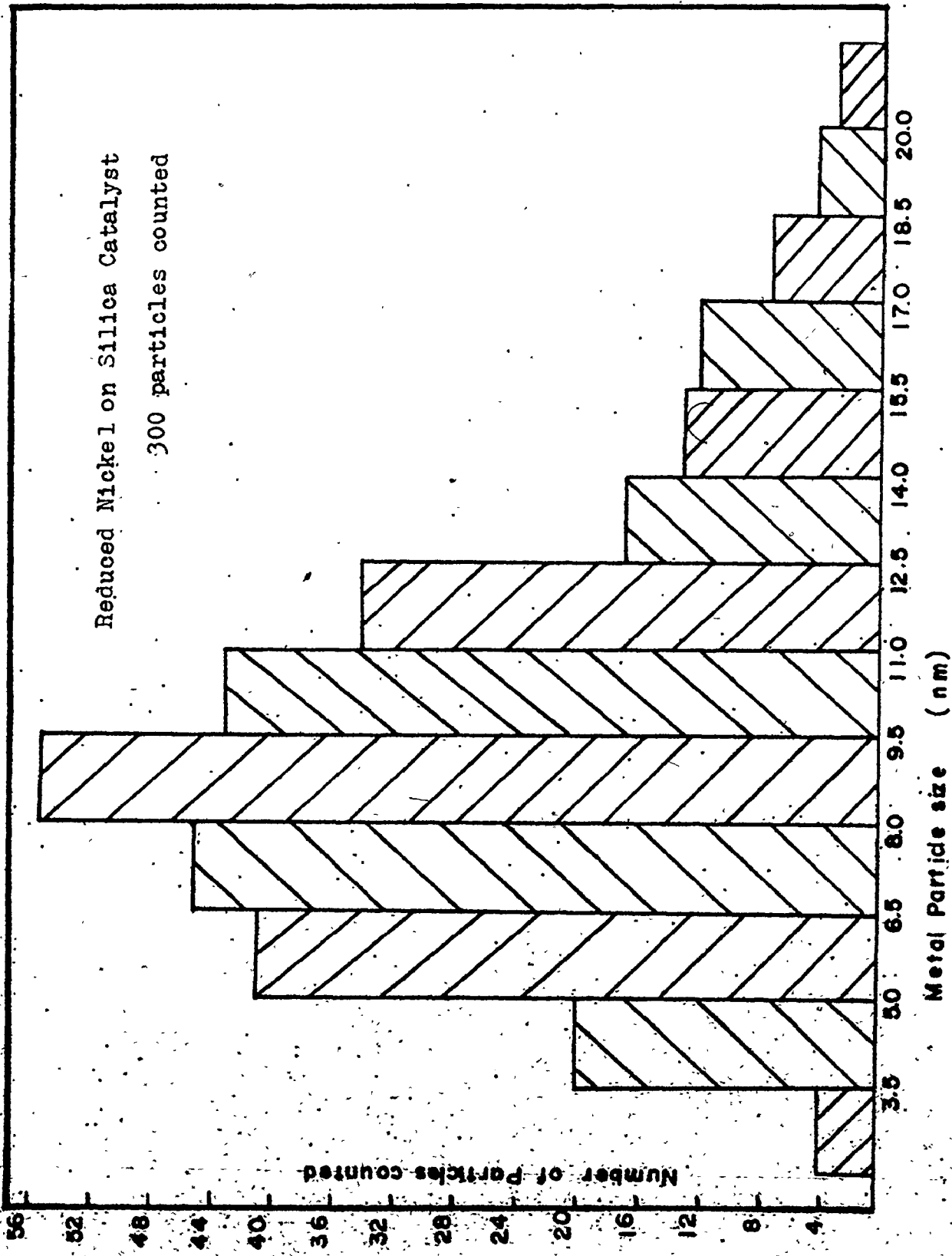
Figure 2-7: Metal particle size Distribution from T.F.M.

001836

Magnification

34,000 *

300 nm

Magnification

64,000 *

200 nm

Figure 2-8: Transmission Electron Micrographs of a Reduced
Nickel on Silica Catalyst

correspond to the results of the chemisorption experiments; the agreement is not good here.

2.4 Industrial Catalysts

Experiments have also been performed with two industrially prepared catalysts.

A 0.5 weight percent ruthenium on γ-alumina catalyst was used (Engelhard Industries, Inc.). This catalyst was in the form of 3.2 by 3.2 mm cylindrical pellets, that had to be cut in half in order to be used in the reactor. Kempling (44) studied this catalyst using adsorption studies and an electron probe microanalyser. He found that the ruthenium is deposited near the periphery of the pellets, in a shell of about 200 μm thickness. The total area of the catalyst was about 90 m^2/g, with an average pore radius of 5.0 nm. The ruthenium area as determined by hydrogen chemisorption was .82 m^2/g of catalyst, corresponding to an average crystallite size of about 2.5 nm.

The other industrially prepared catalyst was an ammonia synthesis catalyst (D 3001), crushed and sieved to 14-28 mesh. The properties of this catalyst have been described (93): after reduction the surface area is 10 m^2/g; the composition of the catalyst is:

67.4% total Fe, 4.6% MgO, 0.5% K_2O, 0.7% SiO_2, 0.6% Cr_2O_3.

This catalyst was also extracted with hot distilled water in a soxhlet unit for 20 days to remove some of the promoters,

which may have an effect on the catalytic properties (7).
After the extraction it was found by atomic absorption spec-
troscopy that the concentration of MgO had dropped from 4.6%
to 0.9%. Most of the alkali should have been removed in this
treatment.

Chapter 3

EXPERIMENTAL

3.1 Materials

The catalysts used have been described in the previous chapter. The carrier gases of the gas chromatographs were hydrogen (Matheson, prepurified), helium (Matheson, high purity), and argon (Linde, high purity); all of these were dried over 4 A molecular sieves (activated at 400°C).

Propane and hydrogen were from the Matheson Co., as well as ethane (CP grade), methane (UHP), isobutane (CP grade), n-butane (CP grade), and neopentane (CP grade), which were used only to calibrate the gas chromatographs. The hydrogen was ultra high purity (99.999%) and it was passed over a deoxo unit (Engelhard, Ind, Inc.) and dried over 4 A molecular sieves (activated at 400°C). The propane, CP grade, only showed traces of impurities and was used directly.

2,3-Dimethylbutane (di-isopropyl) was from Aldrich Chemical Company Inc. (97[+]%) and gas chromatography showed only traces of impurities. n-Hexane was from Fisher Scientific Co. (certified, 99[+]%), no impurities were found by gas chromatography. 2,2-Dimethylbutane (neohexane) was from Phillips Petroleum Co. (pure grade, 99[+]%). An impurity of approximately 0.25% was present, but it could not be identified.

In order to check for impurities in the liquid hydrocarbons, large samples of 1-5 μl were injected and the column temperature was increased from 166°C, where all the smaller components can be separated, to 190°C, to check for higher boiling impurities. Isopentane was used in one experiment and for calibrations, and was from Aldrich (99⁺%), n-pentane for calibration was from Fisher (certified, 99⁺%).

The liquid hydrocarbons were used directly, but purification of 2,3-dimethylbutane was attempted after it was found to deactivate the ruthenium catalyst. (This study will be described in chapter 5).

3.2 Equipment

3.2.1 Introduction

The differential reactor used in these studies consisted of a recycle pump and a fixed-bed reactor. The reasons for using a differential reactor were described in section 1.3. The flow system consisted of four parts: the feed system, the recycle system, the reactor, and the effluent system. A schematic of the flow system is shown in fig. 3-1, and the different parts are described in the following sections.

3.2.2 Feed System

During the propane experiments, hydrogen and propane were mixed and fed to the reactor at the appropriate flow rate.
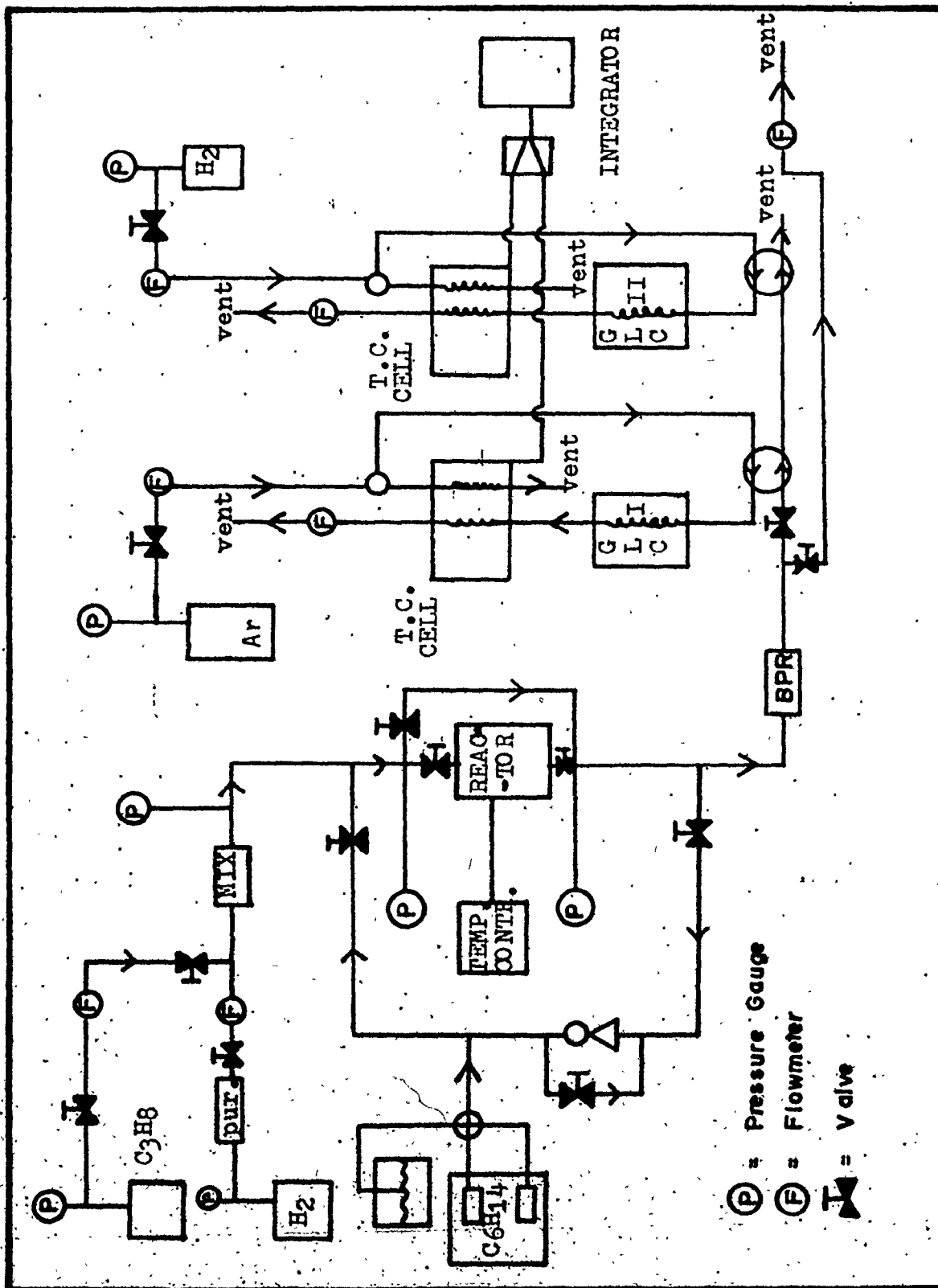
Figure 3-1: Flow diagram of the experimental set up

A 15 cm section of 1.20 cm i.d. copper tubing was filled
with 3 mm solid glass beads and placed before the entrance
to the reactor system to ensure mixing of propane and hydro-
gen. The lines in the reactor system were always 0.64 cm o.d.
copper tubing, but in the feed and effluent systems, 0.32 cm
o.d. tubing was used wherever possible to minimize the
volumes. Both the hydrogen and hydrocarbon flow rates were
controlled by fine metering valves, and an estimate of these
flow rates was obtained by monitoring calibrated capillary-
type manometers.

The liquid hydrocarbons were introduced using a
multispeed transmission pump (Harvard Apparatus Co.) and two
50 cc gastight syringes (Hamilton 1050), moving in opposite
directions, so that one syringe could be filled while the
other was being emptied. A brass four-way ball valve (Whitey
Company) connected the two syringes to a vessel containing
the feed hydrocarbon, and to the recycle part of the reactor
system where the feed entered into the centre of the tube
via a hypodermic needle soldered into the tube. When a li-
quid feed was used, all the lines of the reactor system as
well as the effluent system were heated with heating tape
to 70-80°C. The multispeed transmission pump had 12 discrete
settings and could accomodate syringes of 2-50 cc capacity.
Only 50 cc syringes were used, with the lowest six settings,
the minimum flow rate with a 50 cc syringe was 0.00764 cc/
min of liquid, corresponding to about 0.0035 mol/h of hexane.

The pump was calibrated with water and n-hexane, pumping against pressures of up to 2 atm. At pressures above 1.5 atm leaks occurred when hexane was used, otherwise the flow rates were constant and independent of small changes in pressure. Since the hypodermic needle ends just downstream from the recycle pump, where the gas flow is large, the liquid evaporated in the gasstream easily. Over an eight hour period, the concentration of n-hexane in the reactor system, as measured by gas chromatography, was constant within 5%.

3.2.3 Recycle System

A metal bellows pump (MB 41, Metal Bellows Corporation) was used to recirculate the gases. This type of pump has several advantages:

- no leakage
- contaminant free, stainless steel and teflon are the only materials in contact with the gas
- consistent pump performance, unaffected by continuous operation
- maintenance free
- the volume of the pump is very small (less than 4 cm^3) and the speed is high (3000 rpm), so that pulsations in the flow are not important

The maximum flow rate of the pump is 11.2 l/min at zero pressure drop, and the capacity decreases linearly with pressure drop to 5.6 l/min at a pressure drop of 0.55 atm between the

inlet and outlet of the pump. The maximum pressure at which
the pump could operate was 2.4 atm; to work at higher
pressures, the pump should be enclosed in a pressurizing
system. A bypass around the pump with a needle valve was
used to control the recycle flow rate. During the experiments,
the recycle to feed ratio was kept high (> 20).

3.2.4 Reactor

The reactor was a 39 cm long stainless steel tube,
0.75 cm i.d., surrounded by a 20 cm long aluminium cylinder
of 10 cm diameter. Six holes were drilled in the top of the
cylinder, equally spaced between the reactor tube and the
outside of the cylinder. The holes accomodated six 15 cm -
250 watt (100 Ω) cartridge heaters.

The catalyst was placed at the centre of the reactor,
resting on a retention device of 200 mesh stainless steel
gauze. A trap of the same gauze was used at the end of the
reactor tube to collect any particles that fell through the
retention device and might contaminate the recycle pump or
the valves. The only times particles were found on this
gauze was with the 28-48 mesh catalysts, and they amounted
to 2-3% of the catalyst charge.

A chromel-alumel thermocouple was placed in the cen-
tre of the catalyst bed, and was connected to a proportional
temperature controller (Electronic Control System, Inc.).
The temperature of the bed could be held constant to within
$0.2^{\circ}C$.

Three heating elements, in parallel, were placed in an asbestos plate in series with the furnace, to decrease the voltage to the reactor heaters. A switch allowed these resistances to be bypassed if desired.

Another thermocouple was placed in the centre of the aluminium block, between two heaters. Both thermocouples were connected to a digital multimeter (3465 A, Hewlett Packard) and a portable DC potentiometer type P.3(Croydon Precision Instr. Co.). The reference junctions were in an ice-bath. The temperature difference between the catalyst bed and the furnace never exceeded $2^{\circ}C$.

The amount of catalyst in the reactor varied from 1 to 3 g, the depth of the bed from 1.5 to 4 cm. The thermocouple was positioned 0.8 cm above the retention device. The reactor space above the catalyst bed, about 12 cm in length, was filled with 3 mm glass beads, which served as a preheating zone for the gasstream. The direction of gasflow in the reactor was down, and the reactor could be bypassed if desired.

3.2.5 Effluent System

The purpose of the effluent system was to regulate the pressure in the reactor, to measure the flow rate of effluent and to analyze the composition of the effluent stream. A back-pressure regulator (Fairchild-Hiller) with a range of 1.1-5.2 atm was used directly downstream from the reactor. The effluent was then passed through two sampling

of the system is described in appendix A. Just before taking
the samples, the effluent stream was switched to bypass the
sample valves so that samples were always taken at atmosphe-
ric pressure, and the flow rate through the valves did not
affect the size of the samples. The effluent stream then
went to a 50 cm^3 soap flow meter where the total flow rate
of the effluent was measured. Since all the hydrogenolysis
reactions are equimolar, this flow rate equals the feed rate.

3.3 Operating Procedure

After the catalyst and the glass beads were introdu-
ced, the reactor was flushed with hydrogen and leak tested
at 2.0 atm. The catalyst was then reduced with UHP hydrogen,
the reactor being operated as a single pass unit with the
recycle part of the system closed. The hydrogen flow during
reduction was 40-60 cc/min, depending on the amount of cata-
lyst present, and the temperature and period of reduction
depended on the type of catalyst: for ruthenium 16 h at
350°C, for nickel and cobalt catalysts the reduction was at
430°C for 24-36 h, and for iron 40-48 h at 460°C.

To begin an experiment, the gas was passed through
the bypass around the reactor, the flow rates of hydrogen
and hydrocarbon were set at the desired level, and the recy-
cle pump was started. The reactor temperature and pressure
were also set at the desired values. The recycle flow was
then switched from the bypass to the reactor and the reactor

temperature was allowed to stabilize. The flow rate, feed composition, temperature, and pressure were maintained constant for a time equal to at least five reactor residence times plus the residence time of the feed and effluent lines. Steady state was then assumed to have been attained. The effluent flow rate was measured with a soap film flowmeter, the final reactor temperature and pressure were recorded, and a set of samples taken and analyzed. One or more of the experimental conditions was then changed and a new experiment was started. The pressure was taken as the average between the pressures recorded at the top and the bottom of the bed; the pressure drop was usually very low: about 0.04 atm with the large particles of the low area catalysts, and 0.1 atm with the high area catalysts. The pressure drop across the catalyst bed also depended on the composition of the gas (more hydrogen, lower drop) and on the recycle flow rate. The pressure gauges were calibrated with a mercury manometer.

The composition of the feed was calculated from the composition of the effluent stream by means of a carbon balance and the knowledge that all hydrogenolysis reactions are equimolar. Carbonaceous deposits were never observed on the catalyst samples, the presence of an excess hydrogen at all times makes such deposits unlikely. During one of the propane experiments, the compositions of the feed obtained

in this way were compared with the compositions obtained by
taking the sample directly from the feed stream and analy-
sing it by gas chromatography. The results agreed very well
and are shown in table 3-1.

Overnight the hydrocarbon flow was usually shut off
and the recycling system closed; hydrogen was passed over
the catalyst at about 30 cc/min, usually at the temperature
of the previous experiment. If the catalyst showed signs of
deactivation, the temperature was increased to 400°C over-
night. In some of the propane experiments, the hydrogen-pro-
pane mixture and the recycle were maintained overnight, this
procedure did not seem to deactivate the catalyst more ra-
pidly.

A cylinder with a prepared mixture of 10% propane in
hydrogen (Matheson) was used once a day at a standard set of
conditions to check the activity of the catalyst. If the ac-
tivity changed substantially, corrections were made to the
reaction rates; this happened very rarely, usually only if
experiments were carried out over periods of several weeks.

3.4 Investigations of the Reactor System

3.4.1 Recycle Flow

The flow rate in the recycle part of the reactor was
not measured directly. To obtain differential conditions,
the recycle flow had to be at least twenty times larger than
that of the fresh feed.

Table 3-1

Composition of the Feed

% propane from feed (a)	% propane from effluent (b)
12.3	12.1
14.9	14.9
11.5	11.6
12.0	12.2
18.2	18.7
11.9	11.7
5.0	5.6

(a)   sample from feed, analysed by GLC
(b)   sample from effluent, using carbon balance
       to calculate feed composition

An excessively high recycle to feed ratio does not improve
the differential conditions, and is undesirable because the
pressure drop across the catalyst bed increases and the high
flow may cool the catalyst. Since the feed flow rate never
exceeded 250 cc/ min (and usually was less than 100 cc/min),
and the capacity of the recycle pump was 11 l/min, a bypass
with a needle valve was made around the pump to allow the
recycle flow rate through the reactor to be regulated. When
the bypass valve was completely open, most of the gas recy-
cled by the pump flowed in the bypass loop, when the valve
was completely closed, all the gas was forced through the
reactor. Complete mixing of the different components in the
gas was ensured by the glass beads and the catalyst bed. The
recycle bypass was set at an intermediate value, except at
very high feed rates, when it was almost closed.

Two observations could be made as to obtain an esti-
mate of the recycle flow rate.

1. The tubes immediately downstream of the reactor became
   quite hot, indicating a high gas flow through the reactor;
   the toggle valve behind the reactor had to be air cooled
   to prevent it from melting. To estimate the recycle flow,
   a very high feed of hydrogen and propane was led through
   the reactor at the same temperature and with the recycle
   pump off. The lines began to feel warm only at flow rates
   above 2 l/min.

2. The pressure drop across the catalyst bed is a function of the recycle flow (as well as of the composition of the gas and the catalyst particle size). If the pressure drop is measured with the recycle bypass closed, the corresponding flow rate can be obtained from the pump specifications, assuming all of the pressure drop is caused by the bed. Using the same gas composition and at different positions of the bypass valve, the gas flow can now be determined from the new pressure drop and the relation that the pressure drop varies with the gas flow to the power 1.9 (106, 107). The flow rates calculated in this way satisfied the requirements. Another, similar method to calculate the flow rate through a porous bed when given the pressure drop and the conditions of the bed and the gas was given elsewhere (108).

3.4.2   C.S.T.R. Behaviour

In the analysis of the data, differential reactor conditions were assumed, meaning that the composition of the effluent gas was taken to represent the composition of the gas in the reactor (69, 99, 109, 111). This condition simplifies the calculations of rates and selectivities considerably. A Plug Flow Tubular Reactor (PFTR) operating at large recycle ratio, R, behaves as a single well-stirred perfectly mixed vessel. Mixing behaviour intermediate between plug flow an perfect mixin an   riz   At vi s of R

of 10-20, C.S.T.R. behaviour is approached closely (99, 110).
The composition of the fluid contacting the catalyst is near-
ly the same throughout the bed under these conditions. The
recycle ratio is defined as $R = q/Q$ in fig. 3-2 (99).

Figure 3-2

Recycle Reactor
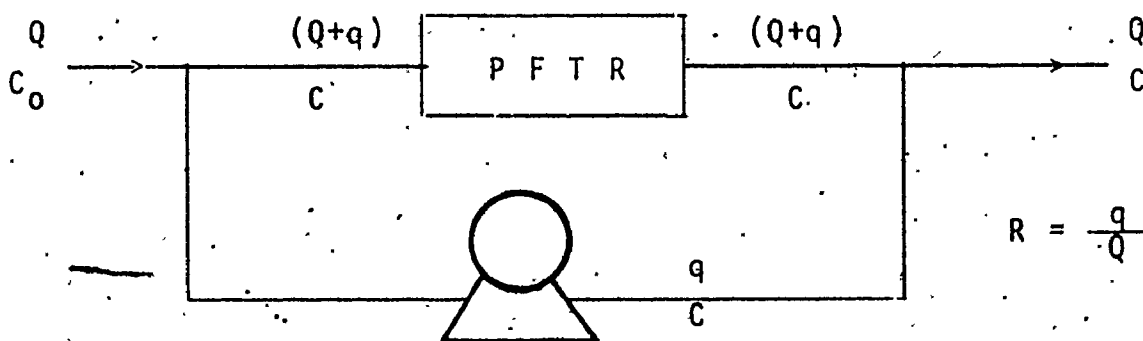
To check whether the recycle system worked as a
C.S.T.R., it was subjected to pulse and step inputs of an
inert tracer, and the response was registered. If a pulse
of inert tracer is added to a C.S.T.R. reactor, the response
of tracer concentration is given by (109, 111)

$$C = C^* \quad \exp \ (- t/\tau) \qquad (3-1)$$

where   C   = concentration of tracer at t

     C^* = concentration of tracer at t=0 (maximum)

     τ = reactor residence time = V/Q

A plot of log C/C* versus t should then be a straight line
with slope $-1/\tau$. A pulse of tracer injected to a plug flow
reactor, i.e. the system with the recycle part closed,
should cause a delta response function. Similarly, if at
t < 0 the concentration of tracer is C* in the reactor and
the feed, and at t = 0 the tracer concentration in the feed
is set at C = 0, the response of tracer concentration in the
reactor and the effluent can be found to be, by a simple
mass balance, C/C* = exp (- t/τ), identical to (3-1), but
C* is defined differently, if the change in total flow rate
can be neglected (i.e. tracer concentration was small to
start with): The latter test can be considered as a "negative
step input".

Both these tests have been performed at different
recycle ratios, to check for C.S.T.R. behaviour. The reactor
was filled with a nickel catalyst and a preheating zone, and
was at operating conditions. The tracer was nitrogen, propa-
ne or ethane in a helium stream that was led directly to a
thermal conductivity cell, and was monitored continuously
on a recorder. In this way, the response was obtained direct-
ly as a function of time, though a delay occurred, equal to
the time needed for the disturbance to reach the TC cell.
Some of the results are shown in figures 3-3 and 3-4. The
plots of ln C*/C versus time show that the reactor indeed
behaves as a C.S.T.R., only at very small times are there

	recycle bypass	tracer	flowrate cm³/min	calculated reactor volume, cm³
A	open	Propane	51.7	155
B	almost closed	N_2	44.1	138
C	open	N_2	141.5	148
D	closed	N_2	115.4	154

He carrier

$\ln (C^*/C)$

t (minutes)
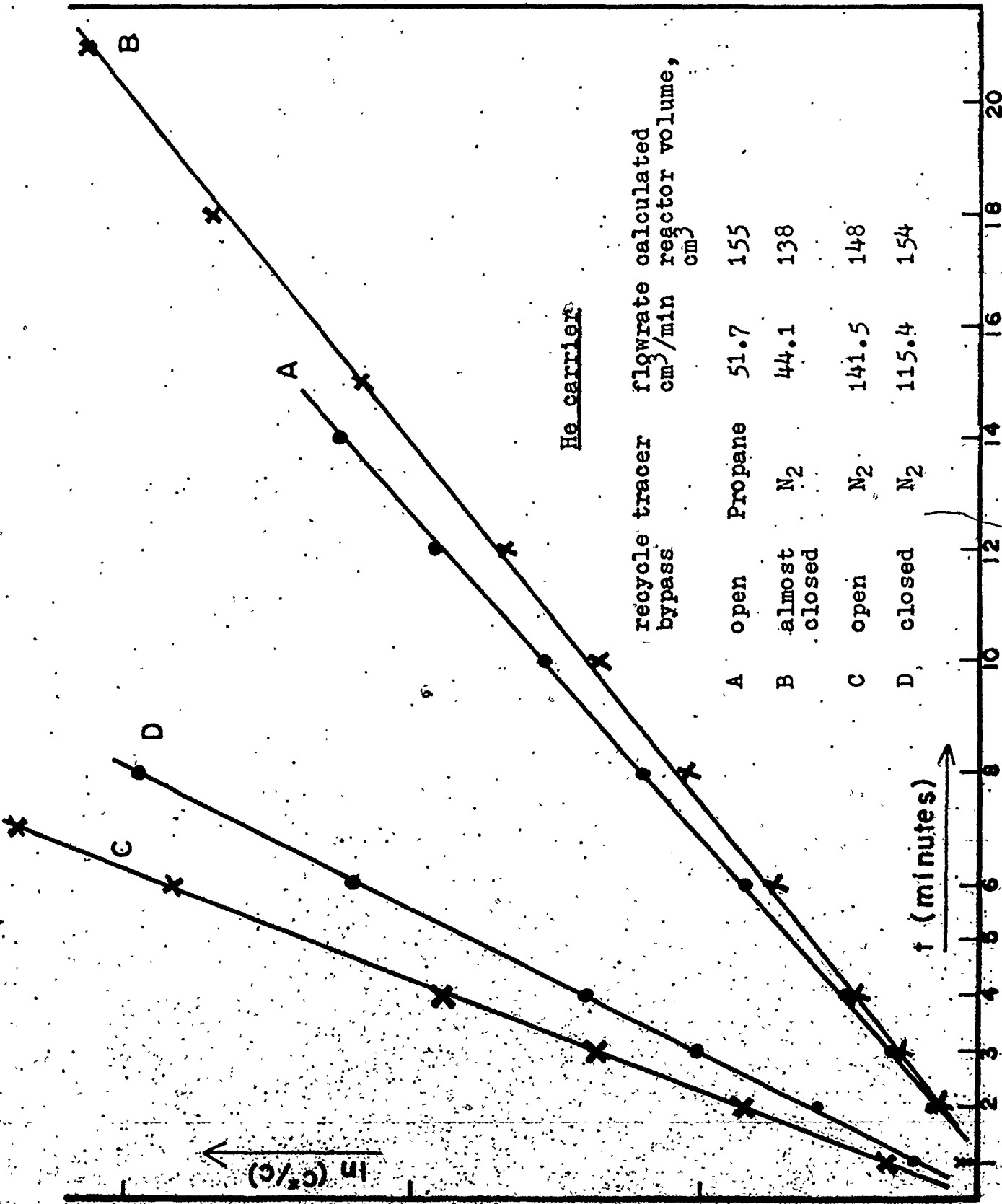
Figure 3-3: Response to step changes in tracer concentration in recycle system
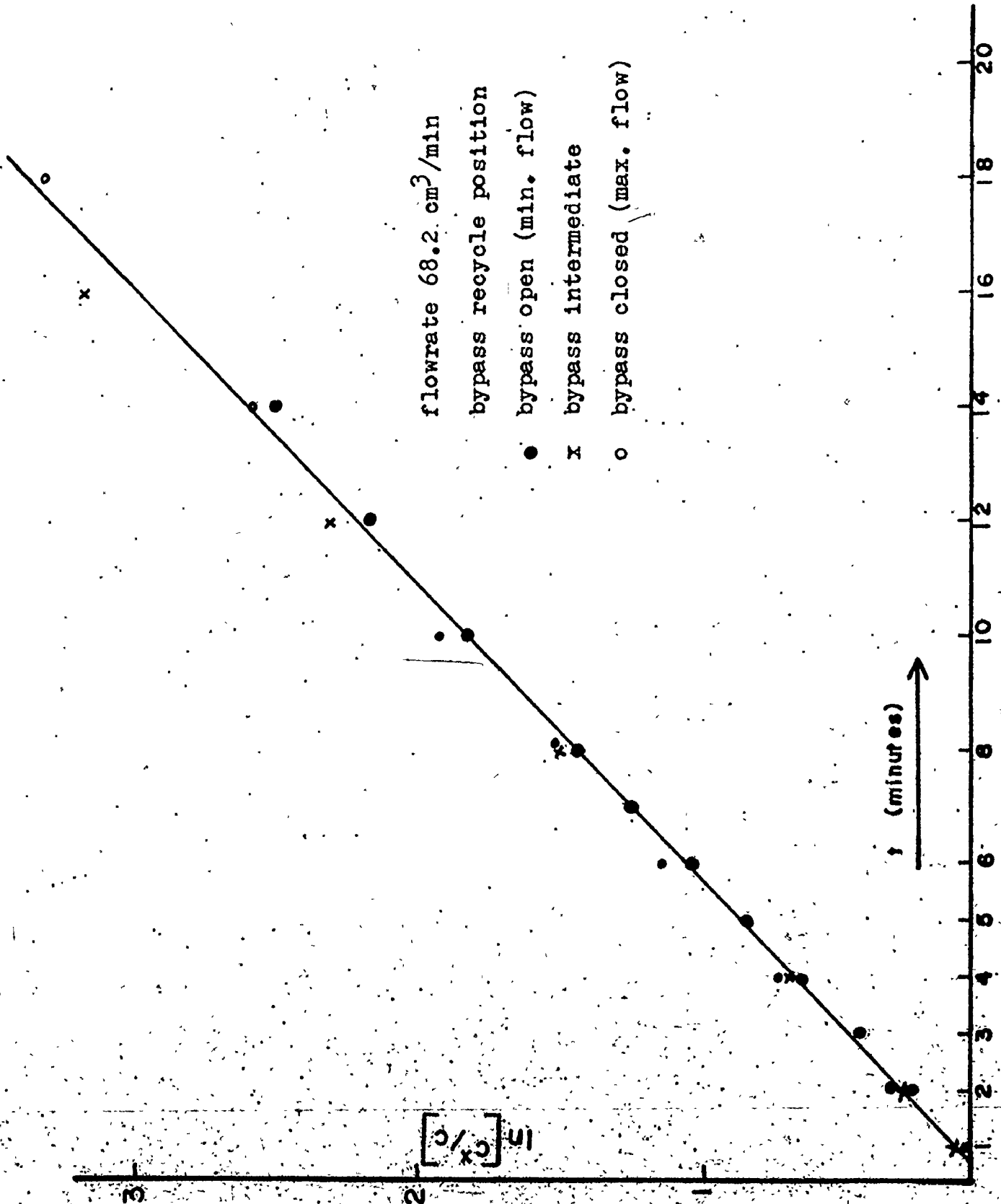
Figure 3-4: Response to a pulse input of Ethane in the Recycle System (He carrier)

flowrate 68.2 cm³/min
bypass recycle position

● bypass open (min. flow)
x bypass intermediate
o bypass closed (max. flow)

ln [c*/c]

↑ (minutes)

At all but very high flow rates (> 200 cm^3/min) can the re-
cycle bypass be opened completely and still maintain good
mixing. There was no difference between the use of nitrogen
or a hydrocarbon as the tracer, the amount of catalyst is
clearly too small to cause differences due to the hydrocar-
bon adsorption. If the recycle flow was led through the by-
pass, the results were identical as if it were through the
reactor. Without recycle the responses were those expected
for a plug flow reactor.

The values for V, the reactor volume, are shown in
fig. 3-3, and are obtained from the slopes and the correspon-
ding flow rates. The volume of the reactor and other parts
of the system were also measured by collecting and measuring
the amount of gas escaped after depressurizing several sec-
tions of the system. The volume of the reactor measured in
this way, including the bypass and the recycle system was
145 cc, in good agreement with the values in fig. 3-3. The
total volume of feed and effluent lines was about 200 cc.

When a reaction takes place in the reactor, it has
been shown that steady state conditions will be reached af-
ter about five residence times (44). Since it would take too
long to check for steady state each time (analyses last al-
most 30 minutes), the sample was taken after steady state
should have been reached. Since the volume of the feed and
effluent lines has to be accounted for too, the minimum time

assumed to be needed to reach steady state was 1000/F minutes, where F is the flow rate in cc/min at the pressure of the reactor (5 * 150 (= V reactor) + 200 (feed+effluent) = 950 cc). This was checked and justified periodically by taking replicate samples.

The influence of the recycle flow rate on the reaction rates was also checked for several catalysts during the experiments with propane. Differences were always found to be within experimental errors when the recycle bypass was varied from completely open to completely closed with other conditions about equal (the pressure drop changed during this procedure). Some results are shown in table 3-2.

3.4.3 Mass and Heat Transfer Effects

Catalytic reactions can be considered as a sequence of four steps: bulk diffusion to and from the external surface of the catalyst, diffusion in and out of the pores, adsorption of reactants and products, and reactions at the catalyst surface. To ensure that kinetic data obtained in an experimental reactor reflect only chemical events, the first two steps must be fast compared to the last two, so that inter- and intraparticle mass and heat effects, respectively, are negligible.

Several methods have been reported to measure and control these effects and to do calculations as to their importance (44, 74, 75, 76, 112). In general, interparticle

Table 3-2

Effects of Recycle Flow on

Reaction Rates in Propane Hydrogenolysis

A $Co/S \cdot O_2$, T=287 $^{\circ}$C, P=2.2atm ,flowrate 55 cm^3/min

	(a)	(b)	(c)	(d)
	min.	0.75	2.47	2.89
(recycle	-	0.75	2.42	2.89
flow	-	0.75	2.35	2.89
increases)	-	0.74	2.37	2.88
	max.	0.74	2.36	2.88

B   same,with flowrate 320 cm^3/min

	(a)	(b)	(c)	(d)
	min.	0.31	5.75	2.81
	-	0.31	5.80	2.81
	-	0.32	5.59	2.80
	-	0.31	5.74	2.82
	max.	0.32	5.62	2.82

C   Ni/SiC; T=305°C, flowrate 50 cm^3/min

	(a)	(b)	(c)	(d)
	min.	0.66	2.54	2.62
	-	0.64	2.49	2.61
	max.	0.63	2.47	2.60

D   D 3001, T=316°C, flowrate 52 cm^3/min

	(a)	(b)	(c)	(d)
	min.	0.14	0.19	2.96
	-	0.14	0.19	2.96
	max.	0.15	0.20	2.95

(a) recycle flow as regulated with bypass recycle pump.

(b) conversion of propane

(c) rate of reaction (μmol/s.g cat.)

(d) selectivi for n

effects are minimized by using high flow rates, and intra-particle effects by using small catalyst particles. Empirical tests for intra- and interparticle limitations, respectively, include the use of progressively smaller particle sizes, and the effect of flow rate on conversion at constant space velocity. If transport effects are absent, these tests do not affect the reaction rate per unit particle volume or the conversion. This type of tests has not been done, though experiments with cobalt catalysts of different sizes (14-28 mesh and 28-48 mesh respectively) and approximately equal metal content indicate that transport limitations are small.

Sample calculations are made to check for transport limitations. Interparticle effects are due to the boundary layer around the particles. The transport mechanism across this film varies from molecular diffusion near the surface to turbulent mixing in the bulk fluid phase. Mass and heat transfer rate can be expressed as

$$N_m = k_G^o \, a \, (P_o - P_s) \tag{3-2}$$

$$N_H = h \, a \, (T_o - T_s) \tag{3-3}$$

where N_m, N_H = mass and heat transfer rate

$\qquad$ a = area available for transfer

$\qquad$ k_G, h = mass and heat transfer coefficients

$\qquad$ P_o, P_s = partial pressure of component in bulk and at surface

$\qquad \qquad$ at surface

$\qquad$ T_o, T_s = temperature in bulk and at surface

The transfer coefficients can be obtained from correlations by De Acetis and Thodos (113); Reynolds, Schmidt and Prandtl numbers need to be computed first.

$$Re = \frac{d_p G}{\mu} \qquad (3-4)$$

$$Sc = \frac{\mu}{\rho D} \qquad (3-5)$$

$$Pr = \frac{\mu C_p}{k} \qquad (3-6)$$

where d_p =   diameter of particle

   G =   mass flow rate

   μ =   viscosity of fluid

   ρ =   density of fluid

   D =   bulk diffusivity of fluid

   C_p =   heat capacity of fluid

   k =   thermal conductivity of fluid

Values used in the calculations were: d_p = 0.6 mm, maximum diameter in 28-48 mesh fraction; $\rho = 3.0 \times 10^{-4}$ g/cm^3, density of a 5:1 mixture of hydrogen and propane at 275°C and 1.5 atm; $\mu = 1.9 \times 10^{-4}$ g/s, cm, for the same mixture at 550 K, using the Chapman-Enskog kinetic theory for viscosity (114); $G = 9 \times 10^{-2}$ g/s, cm^2, for the same conditions and a flow of 3.0 1/min; D = 0.88 cm^2/sec, using the Chapman-Enskog theory for diffusivity (114) and the appropriate Lennard-Jones

potentials; $k = 2.5 * 10^{-3}$ J/s, cm, ^{o}C. using the same theory for thermal conductivity (114); $C_p = 5.0$ J/g, ^{o}C, using parameters from Smith & Van Ness (115); heat of reaction $(-\Delta H) = 59$ kJ/mol, again at these conditions (550K), and using the C_p parameters (115); $a = 75$ cm^2/g catalyst for 0.6 mm spherical particles.

This gives the following values for the dimensionless numbers: $\quad$ Re = 28 $\qquad$ Sc = 0.72 $\qquad$ Pr = 0.38

Using the correlations from De Acetis and Thodos, this gives

$$k_G = 3.2 * 10^{-3} \quad \text{mol/s, cm}^2, \text{atm}$$

$$h = 0.39 \qquad \text{J/s, cm}^2, ^{o}\text{C}$$

Negligible driving forces of concentration and temperature differential between bulk and surface gas are considered 10^{-3}atm and 0.1 ^{o}C, so that substitution into (3-2) and (3-3) gives: $\quad N_H = 5 * 10^{-5} \quad$ mol/s,g cat.

$$N_m = 2.4 * 10^{-4} \quad \text{mol/s,g cat.}$$

According to these calculations, no interparticle heat transfer limitations will occur as long as the reaction rates do not exceed 50 μ mol/s,g cat., and no mass transfer limitations until the reaction rates exceed 240 μ mol/s,g cat. The experimental reaction rates seldom exceed 5.0, and are usually smaller than 1.0, so it seems appropriate to rule out interparticle limitations in these experiments. The results of table 3-2, with different recycle flow rates, support this assumption.

The calculations were made for a typical set of conditions, using the high area catalyst; for the low area catalysts, values of a and d_p are smaller and larger, respectively, but this is offset by larger flow rates used here, so that the conditions are still easily satisfied.

Intraparticle calculations are done for the high area catalyst; the low area catalysts will certainly not exhibit any diffusion problems in the pores, because the pore radii are about 3000 times larger than those of high area catalysts. Most likely bulk diffusion will occur in these pores as opposed to Knudsen diffusion in the smaller pores of the high area catalysts (75). The calculations are performed for propane only; the other main component, hydrogen, diffuses much faster and no concentration gradients are expected for it. In kinetic studies, it is advantageous if the effectiveness factor, η, is close to unity. η is defined as the ratio of the actual rate to that which would occur if the temperature and concentration were constant throughout the particle. If diffusion of reactants and/or products is rate limiting, temperature and/or concentrations gradients will exist in the catalyst particles. The maximum rate at which the effectiveness factor is near unity is calculated as follows, where the system is treated as isothermal and the reaction is assumed to be first order in hydrocarbon. For chemical reactions in a spherical catalyst particle, the effectiveness factor is (114):

$$\eta = 3 \left(\frac{1}{\phi \tanh \phi} - \frac{1}{\phi^2} \right) \quad (3\text{-}7)$$

where ϕ is the Thiele modulus, defined as

$$\phi = R (k/D)^{\frac{1}{2}} \quad (3\text{-}8)$$

where   R = radius of catalyst particle

D = effective diffusion coefficient

k = first order reaction rate constant

In pores of this size, Knudsen diffusion will be operative,
and the effective diffusion coefficient can be calculated
using the following equation (75, 76):

$$D_K = 9700 \, r \left(\frac{T}{M} \right)^{\frac{1}{2}} \left(\frac{\theta}{\tau} \right) \quad (3\text{-}9)$$

where   T = temperature (K)

M = molecular weight

θ = porosity of the catalyst

τ = tortuosity factor

r = average pore radius

substitution of 0.6 and 2.0 for θ and τ, 550 for T, 44 for M
and 7.5 nm for the average radius, gives

$$D_K = 7.7 * 10^{-3} \ cm^2/sec$$

By plotting η versus ϕ (equation (3-7)),the maximum value for
ϕ can be obtained for which $\eta > 0.95$: $\phi < 0.9$
Equation (3-8),with these values for ϕ and D, and R equal to
0.29 mm, gives the maximum value for the first order rate

constant,k,while diffusion is still fast compared to reacti-
on: k < 7.42 sec^{-1}. This corresponds to a rate of 90 μ mol/
s,g cat. at typical experimental conditions (10% propane
and 1.5 atm). This again is much larger than the experimen-
tal rates are.

To check the assumption of an isothermal catalyst
particle, the following relationship is used (44), which is
based on the fact that at steady state, the diffusion of re-
actants across a boundary equals the rate of reaction within
that boundary, and the heat released must all be transferred
across the same boundary.

$$\Delta T = \frac{(-\Delta H)\ D_K}{k}\ (\ C_s - C\ ) \qquad (3\text{-}10)$$

where ΔT = temperature change

   $(-\Delta H)$ = heat of reaction

   k = thermal conductivity

   C_s, C = concentration of reactant at surface and
           within the particle

The maximum temperature difference between catalyst surface
and centre occurs when all of the reactant is consumed, and
this gives $\Delta T = 1.0°C$. The assumption of isothermal parti-
cles seems justified, especially considering that the con-
centration gradients within the particle were shown to be
small.

Chapter 4

HYDROGENOLYSIS OF PROPANE

4.1 Introduction

The rates of hydrogenolysis of propane were examined over the different catalysts as a function of temperature and partial pressures; the total pressure was also varied, but only over a limited range: 1.1 - 2.1 atm. The experiments were always performed in an excess hydrogen (ratios of hydrogen to propane in the feed varied from 4:1 to 100:1), and at appropriate temperatures, such that the rates were measurable but not so large that they could cause diffusion effects. Blank experiments were made with 20% propane in hydrogen over the high area silica and the low area siliconcarbide using plugflow conditions. In both cases no reactions were observed up to 450°C; the results indicate that the stainless steel reactor was inert and that the metallic impurities in the siliconcarbide are in the bulk, and do not contribute to the catalytic activity. The differential rate and selectivity data could be applied directly to proposed rate- and selectivity equations. Calculation procedures are described in appendix B.1. A wide range of conversions was covered.

Catalyst activities were checked as a function of time using a premixed 10% propane in hydrogen mixture at constant flow rate and reactor pressure and temperature.

This test was usually done once a day. In most cases the catalyst activity was essentially constant throughout the experiments with a particular catalyst; if the activity was not constant the reaction rates were corrected, extrapolated to the activity of the fresh catalyst, using the activity at the standard conditions as a measure of the extent of deactivation.

Deactivation of a catalyst can have three different causes (99).

a) poisoning: chemisorption of reactants, products or impurities.

b) fouling: solid deposits on the surface, like coke in cracking reactions.

c) sintering or phase transformations.

The remedies against causes a) and b) are elimination of impurities and increasing the hydrogen pressure. Adding promoters to the catalyst may also help. Against cause c), addition of promoters may help as well as temperature control of the catalyst bed.

The kinetic data on all catalysts were fitted to a power rate expression to obtain the best parameter estimates, using a linear or nonlinear regression program to minimize the sum of squares of the differences between the experimental and calculated rates. The assumptions and procedures in using the regression programs are discussed in appendix B.2.

$$r = A \exp(-E_a/RT) \; P_{H_2}^m \; P_{C_3H_8}^n \qquad\qquad (4\text{-}1)$$

where
r = rate of hydrogenolysis of propane

P_{H_2}, $P_{C_3H_8}$ = partial pressures of hydrogen and propane

m, n = reaction orders with respect to hydrogen and propane

$A \exp(-E_a/RT)$ = rate constant

E_a = apparent activation energy

A = preexponential factor

Data at constant temperature were fitted to the same equation with only three parameters. The reaction orders were used to calculate the degree of unsaturation of the adsorbed hydrocarbon species according to equations (1-8) and (1-12).

The premixed gas could also be used to obtain an estimate of the activation energies; if the flow rate is adjusted to keep the conversion very low (less than 10%), the composition of the gas in the reactor can be considered constant, and by covering a range of temperatures the apparent activation energy can be obtained from the slope of a plot of ln r versus 1/T.

In most cases the data were also fitted to a number of mechanistic rate equations based on Langmuir-Hinshelwood reaction mechanisms.

A number of these equations are described in appendix B.3. Experimental errors in the rate data are estimated to be 10-12%.

The propane molecule has two identical carbon-carbon bonds, no splitting factors are therefore necessary. The only possible products are ethane and methane; the ethane can crack further to form more methane. The maximum selectivities for ethane and methane are 1.0 and 3.0 respectively. The selectivities for ethane and methane were plotted as a function of conversion, and the ethane selectivities were fitted to a selectivity equation. The derivation of the equation and the assumptions on which it is based are shown in appendix C.1 and C.2. The reaction network for propane involved reversible adsorption-desorption of each hydrocarbon and irreversible cracking of carbon-carbon bonds of the adsorbed surface species. The network and the analytical solution are shown in fig. 4-1. The selectivity data were fitted to this equation using nonlinear regression (appendix B.2) or simply by linearizing the equation and plotting $1/S_2$ versus the function $X/(1-X)$. The parameters obtained are k_2'' / k_3'' and k_2^* / k_2', respectively the ratio of overall rates of hydrogenolysis of ethane and propane, and the ratio of cracking and desorption of adsorbed C_2 species. If the rate of carbon-carbon splitting is the rate determining step, k_2^* / k_2' will be very small. The data used in the selectivity equation were from the same experimental runs as those used in the rate equations.

$$C_3 \quad \overset{k_3}{\underset{k_3'}{\rightleftarrows}} \quad A_3$$

$$C_2 \quad \overset{k_2}{\underset{k_2'}{\rightleftarrows}} \quad A_2$$

$$C_i \quad \overset{k_1}{\underset{k_1'}{\rightleftarrows}} \quad A_1$$

$$A_3 \quad \overset{k_3^*}{\longrightarrow} \quad A_2 + A_1$$

$$A_2 \quad \overset{k_2^*}{\longrightarrow} \quad 2A_1$$
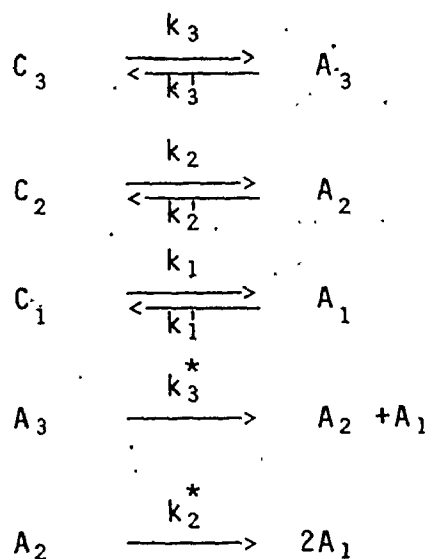
Selectivity for Ethane: $\quad S_2 = \dfrac{k_2'/(k_2' + k_2^*)}{1 + \dfrac{k_2''}{k_3''} \dfrac{X_3}{1-X_3}}$

where

X_3 = fractional conversion of propane

$k_X'' = k_X \, k_X^* \, / (k_X' + k_X^*)$

C_X = gaseous hydrocarbons

A_X = adsorbed hydrocarbon species

k_X = adsorption rate constant

k_X' = desorption rate constant

k_X^* = surface cracking rate constant

Figure 4-1. <u>Reaction Network for Hydrogenolysis of Propane</u>

Experimental errors in the selectivity data are estimated to be 6-8%. In the following sections the four different metals are examined individually, and the results will then be summarized in the final section.

4.2 Propane over Nickel Catalysts

Propane hydrogenolysis experiments were performed on three nickel catalysts, supported on: high area silica (28-48 mesh), low area siliconcarbide (10-12 mesh), and low area siliconcarbide with magnesiumoxide as a structural promoter. Their compositions are described in section 2.3. The experimental conditions and the kinetic results are shown in tables D-2, D-3, and D-4 respectively. The data were fitted to equation (4-1) using nonlinear least squares techniques, and the results of this analysis are shown in table 4-1. The 95% confidence intervals are given in the table, and the average deviation between the calculated and experimental rate in the table is defined as

$$\frac{(RSS/n)^{\frac{1}{2}}}{average\ rate} \quad * \quad 100\% \quad\quad (4-2)$$

where RSS = residual sum of squares, minimized in the program

   n = number of observations

Different initial guesses yielded the same parameter values, but the number of iterations differed widely. The confidence limits of the parameters are only very approximate in these experiments (appendix B.2).

Table 4-1

Data for the Hydrogenolysis of Propane over Nickel, fitted to Equation (4-1)[a]

Catalyst	number of observations	temperature range (^{o}C)	$\log_{10}A$ [c]	E_a kJ/mol	E_a kcal/mol	m	n	average deviation %[b]
Ni/SiO$_2$	120	254-303	18.0	175.	41.8±0.1	-1.57±0.07	0.73±0.03	12
Ni/SiC	72	277-305	20.8	217.	51.8±0.1	-2.41±0.06	0.86±0.02	10
Ni-Mg/SiC	72	250-281	19.5	193.	46.2±0.2	-2.29±0.13	0.67±0.07	28

(a) $r = A \exp(-E_a/RT) \, P_{H_2}^{m} \, P_{C_3H_8}^{n}$

(b) $\% = (RSS/n)^{1/2}/(\text{average rate}) * 100\%$

(c) units of A are based on r in (μmol/s,g cat.) with partial pressures in atm.

The data were also reparameterized around 550 K, but the results were almost identical, the correlations being slightly smaller. A plot of the calculated versus the experimental rates based on the data of table 4-1 is shown in fig. 4-2 for the Ni/SiC catalyst.

The activities did not change significantly during the two to four weeks of experiments with these catalysts. Only for the promoted catalyst on siliconcarbide were slight corrections necessary since the activity dropped about 10% in two weeks of experiments. Since data were taken at several constant temperatures, they were also fitted to the power rate law at constant temperature, with only three parameters. The fit of the data usually improved and an interesting result was obtained: the exponent of the hydrogen pressure increased (became less negative) as the temperature increased for all nickel catalysts. Similar results were obtained by Sinfelt (27) and Guczi (30) for ethane over cobalt and nickel, and by Sheppard (9) and Guczi (138) for propane over nickel on alumina and over unsupported nickel respectively. The propane exponent remained nearly constant. The results are shown in table 4.-2. The rate constants obtained in this way can not be applied to the Arrhenius equation since the hydrogen exponents are different at each temperature. Under the conditions used, the promoted nickel catalyst is about ten times more active than the unpromoted one on the
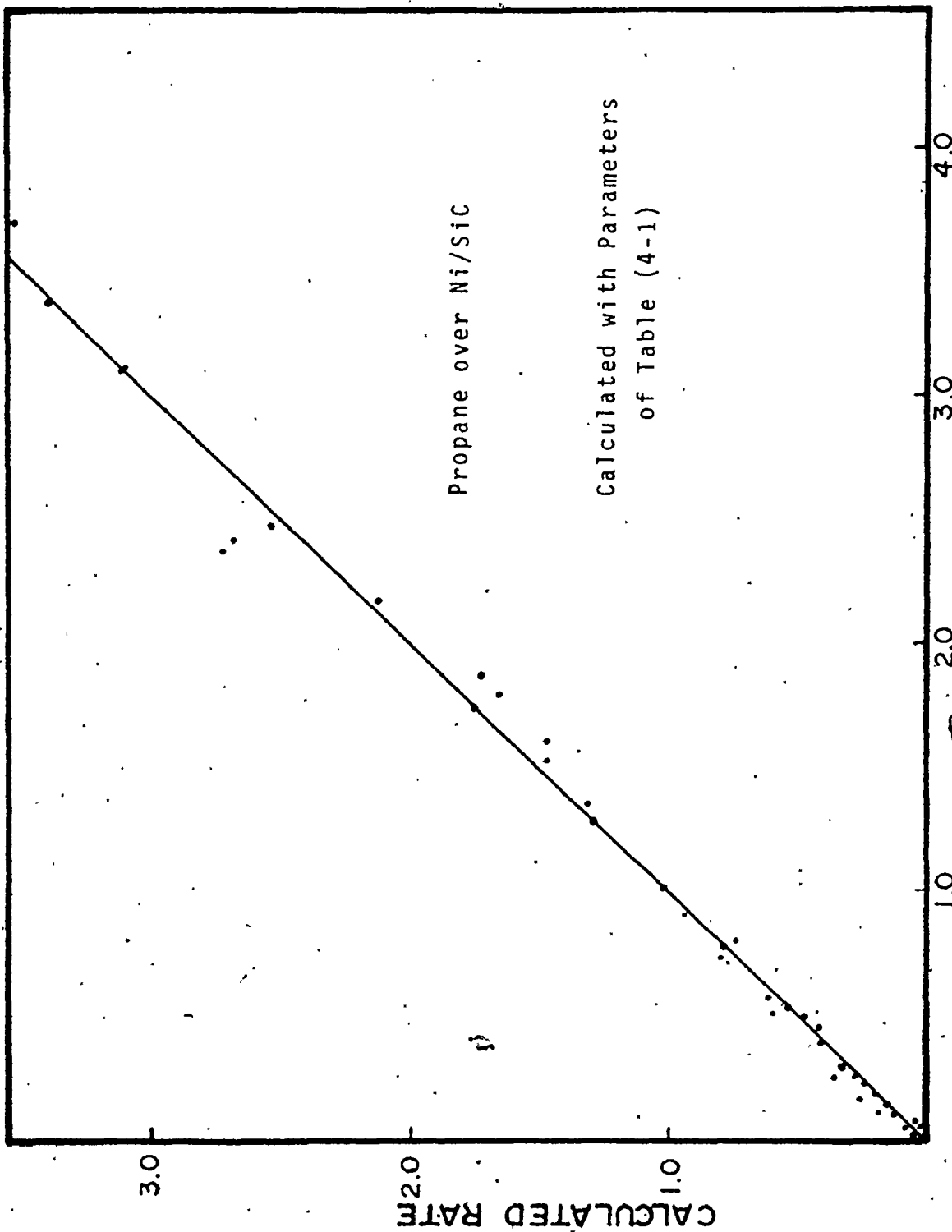
Figure 4-2 (Calculated versus Experimental Rates.)

Table 4-2

Propane Hydrogenolysis over Nickel at constant Temperature[a]

Catalyst	Temp. (^{o}C)	k [b]	m	n	average deviation %
	254	8.5±1.1	-2.37±0.15	1.00±0.08	9
Ni/SiO$_2$	278	30. ±5.	-2.04±0.11	0.76±0.07	10
	303	149. ±27.	-1.43±0.10	0.73±0.06	7
	277	1.5±0.2	-2.98±0.12	0.77±0.07	7
Ni/SiC	291.5	5.4±0.4	-2.50±0.08	0.80±0.05	8
	305	17.9±3.	-2.33±0.14	0.85±0.07	8
	250.5	2.2±0.2	-2.77±0.13	0.89±0.06	6
Ni-Mg/SiC	266.5	6.5±2.	-2.56±0.26	0.75±0.15	20
	281.	14. ±6.	-2.15±0.28	0.57±0.17	23

(a) $r = k \, P_{H_2}^m \, P_{C_3H_8}^n$

(b) units of k are based on rate in (μmol/s,g cat.)
     with partial pressures in atm.

same support, while the kinetic parameters are not very different.

Values for "a", the degree of unsaturation of the surface complex were calculated using Sinfelt's theory and equation (1-12). The values for "a" are 2.5 and 3.0, corresponding to adsorbed surface species of composition C_3H_3 and C_3H_2 respectively (table 4-3). C_3H_3 can be visualized as an 1,2-diadsorbed species losing all the hydrogen atoms of the adsorbed carbon atoms; C_3H_2 could be a similar 1,3-diadsorbed species. The fact that all the hydrogen atoms are lost does not conflict with known facts (122, 136). The power rate law was also extended, adding the partial pressures of the reaction products raised to some power. The fit did not improve significantly and these exponents always were small. The data were also fitted to equation (4-1) at constant levels of total pressure, although the range of total pressures covered was very limited, 1.1 - 2.1 atm. The fits improved slightly and the exponents for hydrogen were more negative at high pressures. The propane exponent was constant, and the activation energy fluctuated irregularly. This is in accordance with observations by Tsjeng (33) and Kempling(44) that the power rate law may in some cases not be able to provide a good fit to data over a wide range of pressures.

The kinetic data were fitted to most of the mechanistic rate equations described in appendix B.3; this was

Table 4-3

Analysis of power rate law in Propane Hydrogenolysis over Nickel

Catalyst	$x^{(a)}$	exponent for hydrogen pressure	
		observed m	calculated $(-na)^{(b)}$
Ni/SiO$_2$	3	-1.6	-1.7
Ni/SiC	3	-2.4	-2.3
Ni-Mg/SiC	2	-2.3	-2.1

(a)   number of hydrogen atoms in chemisorbed intermediate, C_3H_x

(b)   using equation(1-12) and $a = (8-x)/2$

done at constant temperatures to keep the number of parameters small. None of these models fit the data better than the power rate law, in many cases the agreement was much worse. In the models that fitted the data as well as the power rate law, the parameters varied erratically with temperature.

The selectivities for ethane were fitted to the selectivity equation of fig. 4-1. Plotting $1/S_2$ versus $\{X/(1-X)\}$ yielded values for the groups of parameters k_2''/k_3'', the ratio of overall rates of hydrogenolysis of ethane and propane, and k_2^*/k_2', the ratio of the rates of cracking and desorption of the adsorbed C_2 species. The linear plots were not always well defined, but they were sufficient to obtain reasonable estimates of the parameters. Some examples for Ni/SiO_2 are given in fig. 4-3, and a summary of all the results is given in table 4-4. The rate of desorption of the C_2 species is not rapid compared to the rate of cracking, especially at higher temperatures. The rate of hydrogenolysis of ethane is lower than that of propane, but the ratio depends very much on the temperature.

4.3 Propane over Cobalt Catalysts

Three cobalt catalysts were used in the hydrogenolysis of propane: cobalt on high area silica, with particle sizes in the range 14-28 mesh and 28-48 mesh, and cobalt promoted with magnesium on low area siliconcarbide.
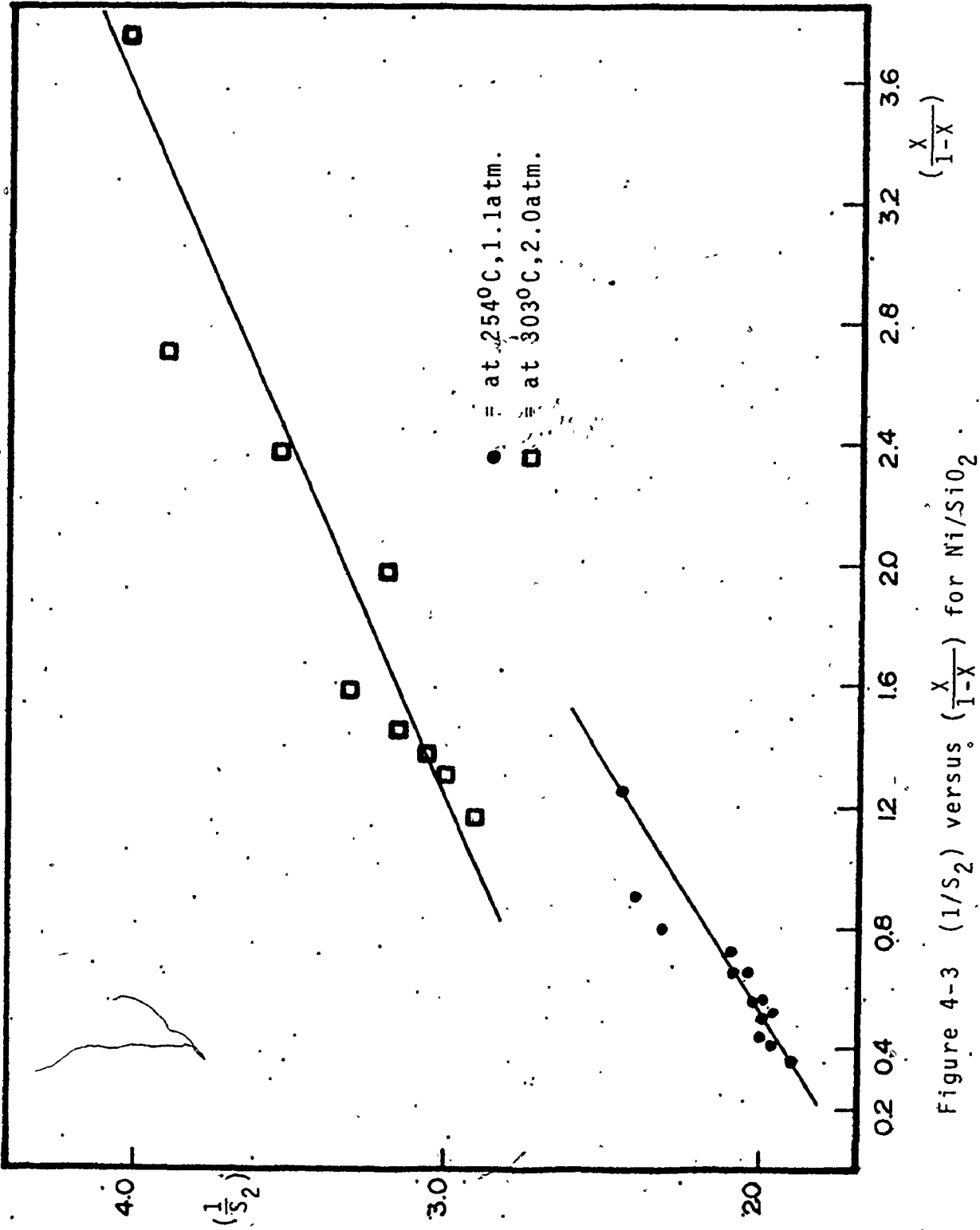
Figure 4-3 $(1/S_2)$ versus $(\frac{X}{1-X})$ for Ni/SiO$_2$

● = at 254°C, 1.1 atm.
□ = at 303°C, 2.0 atm.

Table 4-4

Propane Hydrogenolysis over Nickel,

fit to Selectivity Equation[a]

Catalyst	Temp. (^{o}C)	Pressure (atm.)	k_2^*/k_2'	k_2''/k_3''
Ni/SiO$_2$	254	1.1	0.6	0.5
	254	2.0	0.4	0.6
	278	1.1	1.6	0.2
	278	2.0	0.9	0.2
	303	1.1	3.0	0.1
	303	2.0	1.6	0.2
Ni/SiC	277	1.1	-	-
	277	2.0	0.4	1.4
	292	1.1	1.4	0.2
	292	2.0	0.8	0.3
	305	1.1	2.2	0.2
	305	2.0	1.2	0.2
Ni-Mg/SiC	250	1.1	0.8	0.3
	250	2.0	0.3	0.1
	266	1.1	-	-
	266	2.0	0.5	0.6
	281	1.1	1.1	0.5
	281	2.0	1.0	0.3

(a)   figure 4-1

The composition of these catalysts is described in section 2.3. The kinetic results and experimental conditions are shown in table D-5 for Co/SiO_2 (28-48 mesh) and D-6 for CoMg/SiC. The kinetic data were fitted to equation (4-1) by methods similar to those for nickel in section 4.2; the results are shown in tables 4-5 and 4-6. A plot of the experimental rates versus the calculated ones, based on the parameters of table 4-5 is shown in fig. 4-4 for CoMg/SiC. The activity of the Co/SiO_2 (28-48) catalyst dropped about 25% in three weeks; the rate data were corrected. The activation energy of this catalyst was very low, but this is compensated by a small value of the preexponential factor (see also section 4.6).

Activation energies obtained from low conversion runs with the 10% propane in hydrogen mixture gave values of 34.-36. kcal/mol, which agrees much better with previously obtained values over cobalt. The exponents for propane and hydrogen and the reaction rates are similar for the two high area catalysts of different particle size, indicating that diffusion control was not an important problem, in agreement with the calculations in section 3.4.3. The fit of the experimental data was improved substantially again if data at constant temperature were used. The exponent for hydrogen increased with increasing temperature on Co/SiO_2 just like in the case of nickel, but this was not so clear on CoMg/SiC.

Table 4-5

Data for the Hydrogenolysis of Propane over Cobalt, fitted to Equation (4-1)[a]

Catalyst	number of observations	temperature range (°C)	$\log_{10}A$ [c]	E_a kJ/mol	E_a kcal/mol	m	n	average deviation %[b]
Co/SiO$_2$ (14-28mesh)	263	233-268	15.95	140.	33.3	-0.95	0.70	21
Co/SiO$_2$ (28-48)	59	228-268	9.96	93.	22.2±3.	-0.72±0.14	0.79±0.12	25
Co-Mg/SiC	46	245-266	20.99	204.	48.6±0.1	-0.78±0.03	1.03±0.03	6

(a) $r = A \exp(-E_a/RT) P_{H_2}^m \, P_{C_3H_8}^n$

(b) $\% = (RSS/n)^{\frac{1}{2}}/(\text{average rate}) * 100\%$

(c)   units as in table 4-1

Table 4-6

Propane Hydrogenolysis over Cobalt at constant Temperature[a]

Catalyst	Temp. ($^{\circ}$C)	k[b]	m	n	average deviation %
	228	1.38±0.14	-1.89±0.11	0.75±0.06	6
Co/SiO$_2$	248	7.4 ±1.3	-1.25±0.13	0.90±0.10	10
(28-48)	268	9.3 ±1.8	-0.61±0.16	0.78±0.13	13
	245	2.2 ±0.3	-0.85±0.04	0.80±0.10	7
Co-Mg/SiC	256	6.1 ±0.3	-1.00±0.3	0.90±0.12	9
	266	19.4 ±0.3	-0.71±0.06	1.05±0.05	4

(a) $r = k \, P_{H_2}^{m} \, P_{C_3H_8}^{n}$

(b) units as in table 4-2
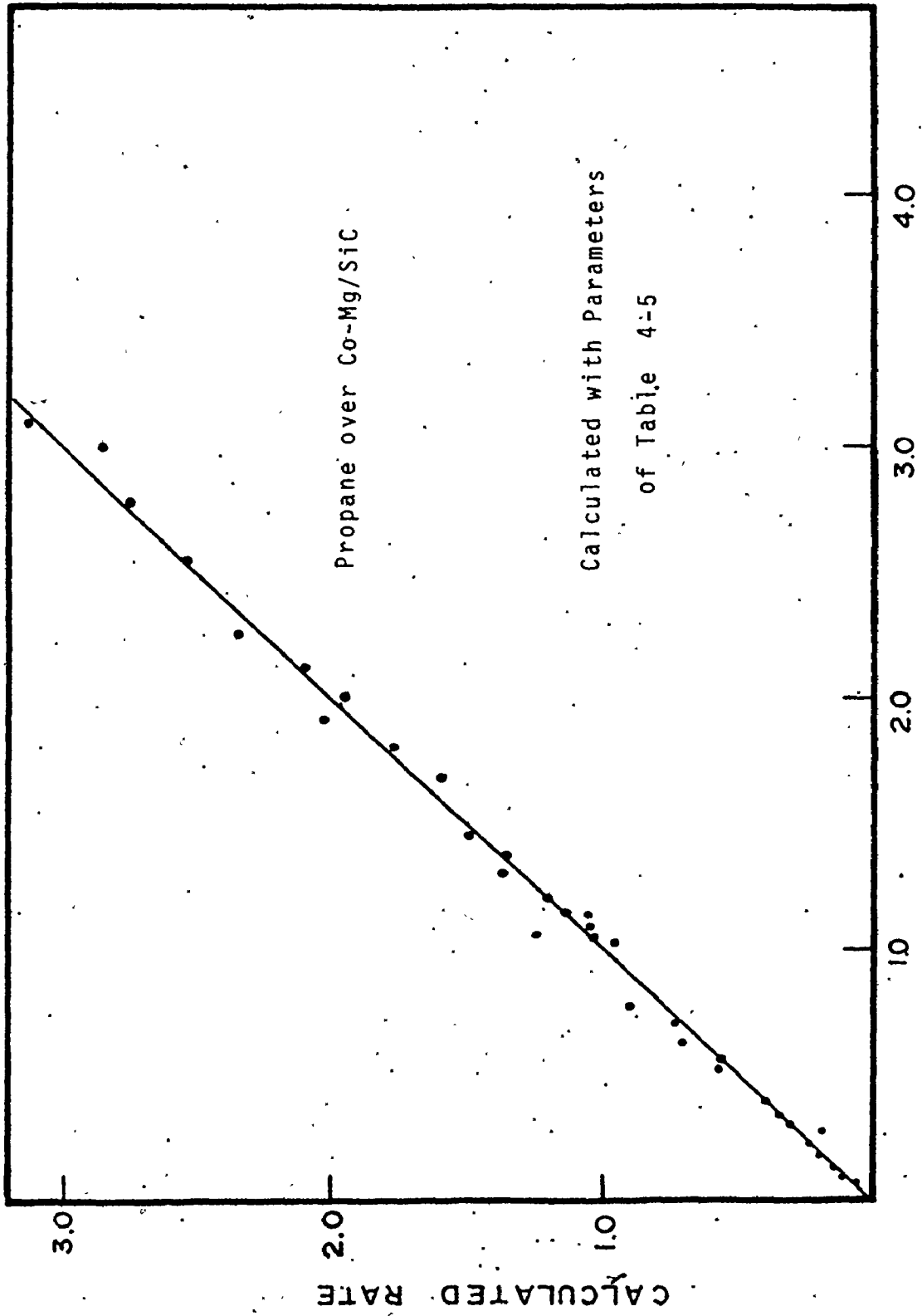
EXPERIMENTAL RATE $(\mu mol/s;g\ cat.)$

Figure 4-4   Calculated versus Experimental Rates.

The values of "a" calculated are close to unity, which means that the composition of the adsorbed surface species is C_3H_6. The much less dehydrogenated surface species for cobalt as compared to nickel agrees with the results of other workers (24, 136). Mechanistic rate equations (appendix B.3) were used with these kinetic data, but none of the models fit the data better than the power rate law, and parameter values obtained were erratic. The extended power rate law, including terms for the reaction products, improved the fit only slightly, and the exponents for ethane and methane were rather small.

The selectivities for ethane were fitted to the selectivity equation using nonlinear least squares; the initial values for the parameters were obtained from plots of $1/S_2$ versus $X/(1-X)$. The parameters k_2'' / k_3'' and k_2^* / k_2' are shown in table 4-7. The selectivities for ethane over cobalt are very small, which causes some erratic results, especially at low temperature, where the range of conversion covered is not large. According to the k_2^* / k_2' values, the rate of cracking of adsorbed C_2 species is larger than the rate of desorption.

4.4 Propane over Iron Catalysts

Supported iron catalysts were prepared without promoters on several supports: high area silica(28-48 mesh), and low area silica, alumina, siliconcarbide and zircon.

Table 4-7

Propane Hydrogenolysis over Cobalt,

fit to Selectivity Equation[a]

Catalyst	Temp. (^{o}C)	Pressure (atm.)	k_2^*/k_2'	k_2''/k_3''
	228	1.2	2.7	1.4
	228	2.2	0.9	3.6
Co/SiO$_2$ (28-48)	248	1.2	5.5	0.4
	248	2.2	2.6	0.5
	268	1.2	7.2	0.6
	268	2.2	4.2	0.5
	245	1.2	4.0	0.7
Co-Mg/SiC	255	1.2	4.3	0.3
	265	1.2	4.3	0.6

(a) figure 4-1

(10-12 mesh). These catalysts were used for propane hydro-genolysis after reduction at 450°C, but none of them were active catalysts. The observations were identical with the five catalysts: initially they had a low activity, and the temperatures had to be at least 300°C. The activity decreased steadily during the test to become hardly measurable after one day (temperature 350-400°C). The catalyst could not be reactivated by treatment with hydrogen at temperatures as high as 500°C. During the short active period, almost all of the product was methane. The initial activity was approximately equal on all supports. Iron is known to form carbides and deposit elemental carbon, but in both cases one might expect the catalyst to be reactivated in hydrogen (section 1.5). Another possibility is that iron reacts with the support (150), but this seems unlikely with for instance silicon-carbide. The impurities in the low area supports (Ca, Mg, K, Ba, Na) appear to be located in the bulk since they do not seem to serve as promoters for the iron catalysts.

The iron catalysts used in the propane hydrogenolysis kinetics were iron promoted with magnesiumoxide on low area silica, an ammonia synthesis catalyst (D3001) and the same catalyst that was extracted for 20 days with water to remove most of the alkali. The composition of these catalysts is described in section 2.3, and the reaction conditions and kinetic results are in tables D-7, D-8, D-9 respectively.

These catalysts had a rather constant activity,though it de-
creased somewhat after several weeks. It is especially re-
markable that the magnesium promoted catalyst on silica
shows such a marked improvement in stability compared to the
unpromoted catalysts. It has been suggested (139) that mag-
nesium actively interacts with the iron to form stabilized
metallic particles.

The kinetic data were fitted to equation (4-1), and
the results are tabulated in tables 4-8 and 4-9. A plot of
experimental versus calculated rates for $FeMg/SiO_2$ is shown
in fig. 4-5. The data of the ammonia synthesis catalysts,
gave a much worse fit than any of the other catalysts. It is
not fruitful to calculate "a" values in these cases, since
different mechanisms appear to be operative for iron cata-
lysts (7, 12, 24),which is indicated by the positive expo-
nents for the hydrogen pressure.

The extracted ammonia synthesis catalyst is about
five times more active as the promoted one, which agrees
with results by Boudart et.al. (7) on similar systems, where
it was also noticed that the exponent for hydrogen was nega-
tive for catalysts without promoters and positive for those
with promoters. This also agrees with the results of table
4-9. Increasing temperature again shows, an increase in the
exponent for the hydrogen pressure, as observed for nickel
and cobalt.

Table 4-8

Data for the Hydrogenolysis of Propane over Iron, fit to Equation(4-1)(a)

Catalyst	number of observations	temperature range (°C)	$\log_{10}A$(c)	E_a kJ/mol	E_a kcal/mol	m	n	average deviation %(b)
Fe-Mg/SiO$_2$	72	314-353	12.59	149.	35.6±0.2	0.67±0.13	0.65±0.13	20
D3001 (promoted)	76	288-330	11.06	129.	30.8±0.2	2.00±0.53	1.17±0.20	53
D3001 (extracted)	97	270-338	11.01	124.	29.5±0.2	-0.06±0.10	0.80±0.11	38

(a) $r = A \exp(-E_a/RT) P_{H_2}^m P_{C_3H_8}^n$

(b) $\% = (RSS/n)^{\frac{1}{2}}/(\text{average rate}) * 100\%$

(c) units as in table 4-1

Table 4-9

Propane Hydrogenolysis over Iron at constant Temperature[a]

Catalyst	Temp. (^{o}C)	k[b]	m	n	average deviation %
	314	0.21±0.04	-0.53±0.25	0.45±0.10	16
Fe-Mg/SiO$_2$	334	0.74±0.08	0.23±0.12	0.63±0.07	8
	353	1.58±0.41	0.78±0.20	0.69±0.15	15
	288	0.14±0.04	0.03±0.32	0.96±0.22	13
D3001 (promoted)	311	0.71±0.38	0.86±1.40	1.15±0.50	22
	330	0.98±0.16	3.47±0.82	1.47±0.26	18
	270	0.08±0.01	0.12±0.39	0.60±0.27	15
D3001 (extracted)	297	0.52±0.16	-0.03±0.46	0.71±0.17	20
	318	2.22±0.39	0.20±0.27	1.10±0.17	16
	338	1.76±0.80	-0.22±0.17	0.39±0.25	23

(a) $r = k \, P_{H_2}^{\bar{m}} \, P_{C_3H_8}^{n}$

(b) units as in table 4-2
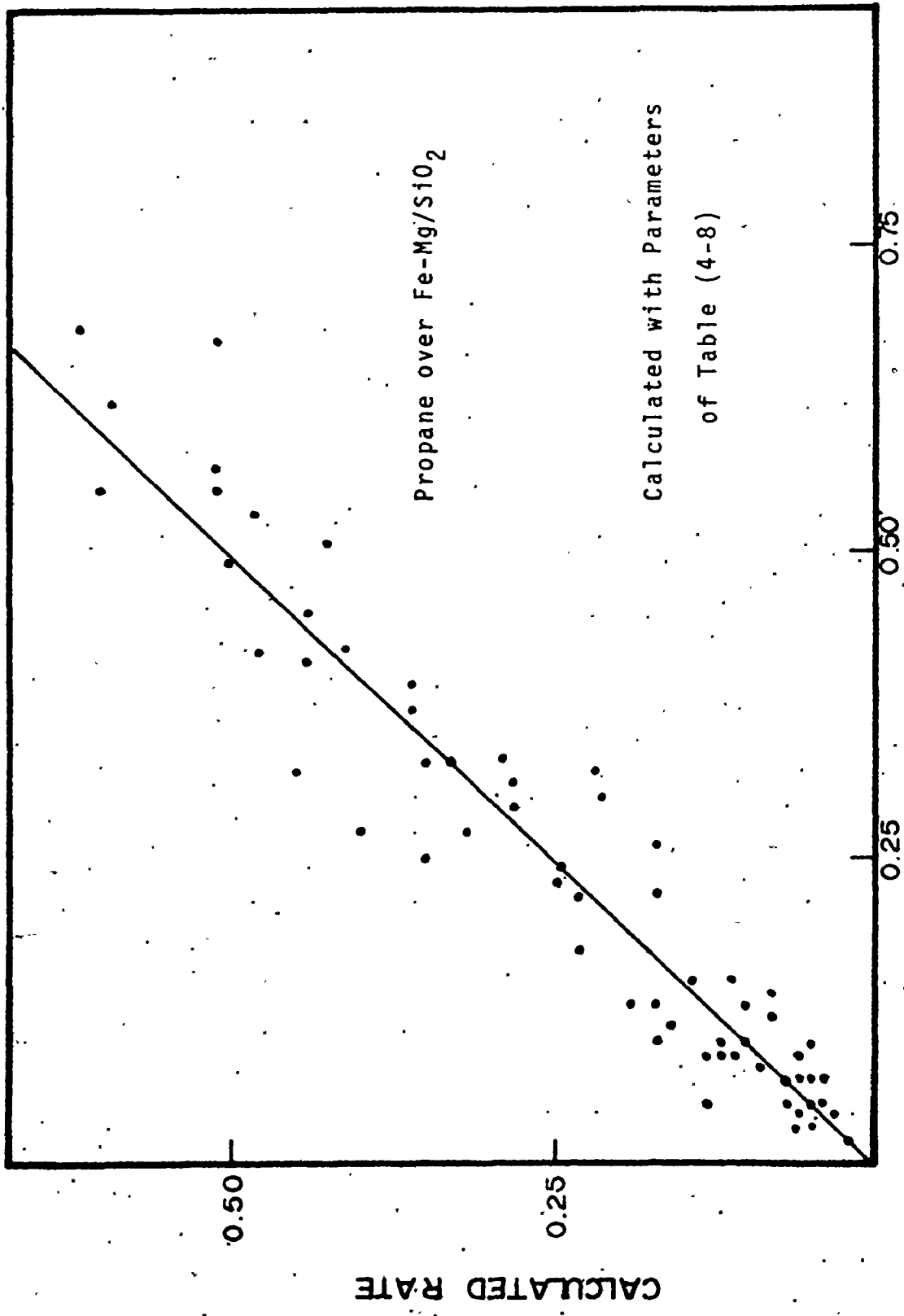
Figure 4-5   Calculated versus Experimental Rates.

Mechanistic rate equations did not fit the data better; the extended power rate law improved the results slightly, but the exponents for ethane and methane were always small. The selectivities for ethane using iron catalysts were very small, so that no satisfactory results were obtained by applying the selectivity equation. Selectivities for ethane rarely exceed 0.05 and often are too small to be measured; especially at low conversions they can not be determined with accuracy. If the proposed network is valid, this can only mean that the values of k_2' / k_2^* are very small for iron.

4.5 Propane over Ruthenium

Only one ruthenium catalyst was used; it is described in section 2.4. The experimental conditions and kinetic results are shown in table D-1. The amount of ethane in the products is largest over this catalyst compared with all the catalysts described in previous sections. The results of the fit to equation(4-1) are shown in table 4-10 and the plot of calculated versus experimental rates is shown in fig. 4-6. The hydrogen exponent again increases with the temperature; ruthenium behaves in the same way as the other catalysts in this respect. The value of "a", derived using equation (1-12), is 2.5; this corrsponds to an adsorbed surface species C_3H_3, which could be an 1,2-diadsorbed species devoid of hydrogen at the adsorbed carbon atoms. This agrees with intermediates suggested for propane and other hydrocarbons on ruthenium (31, 47, 101).

Table 4-10

Propane Hydrogenolysis over Ruthenium[a], fit to Equation(4-1)[b]

number of observations	Temp. range (°C)	$\log_{10}A$[c]	E_a kJ/mol kcal/mol	m	n	average deviation %
29	150-179	19.15	155. 36.9±0.1	-1.98±0.14	0.80±0.06	10

(a) Ru/Al$_2$O$_3$

(b) $r = A \exp(-E_a/RT) P_{H_2}^m P_{C_3H_8}^n$ (c) units as in table 4-1

at Constant Temperature[d]

Temp. (°C)	k[e]	m	n	%
150	1.28±0.22	-2.81±0.23	0.61±0.12	7
179	18.3 ±0.1	-2.00±0.13	0.75±0.06	6

(d) $r = k P_{H_2}^m P_{C_3H_8}^n$ (e) units as in table 4-2

110

Propane over Ru/Al$_2$O$_3$

Calculated with Parameters

of Table (4-10)

EXPERIMENTAL RATE (μmol/s,g cat.)
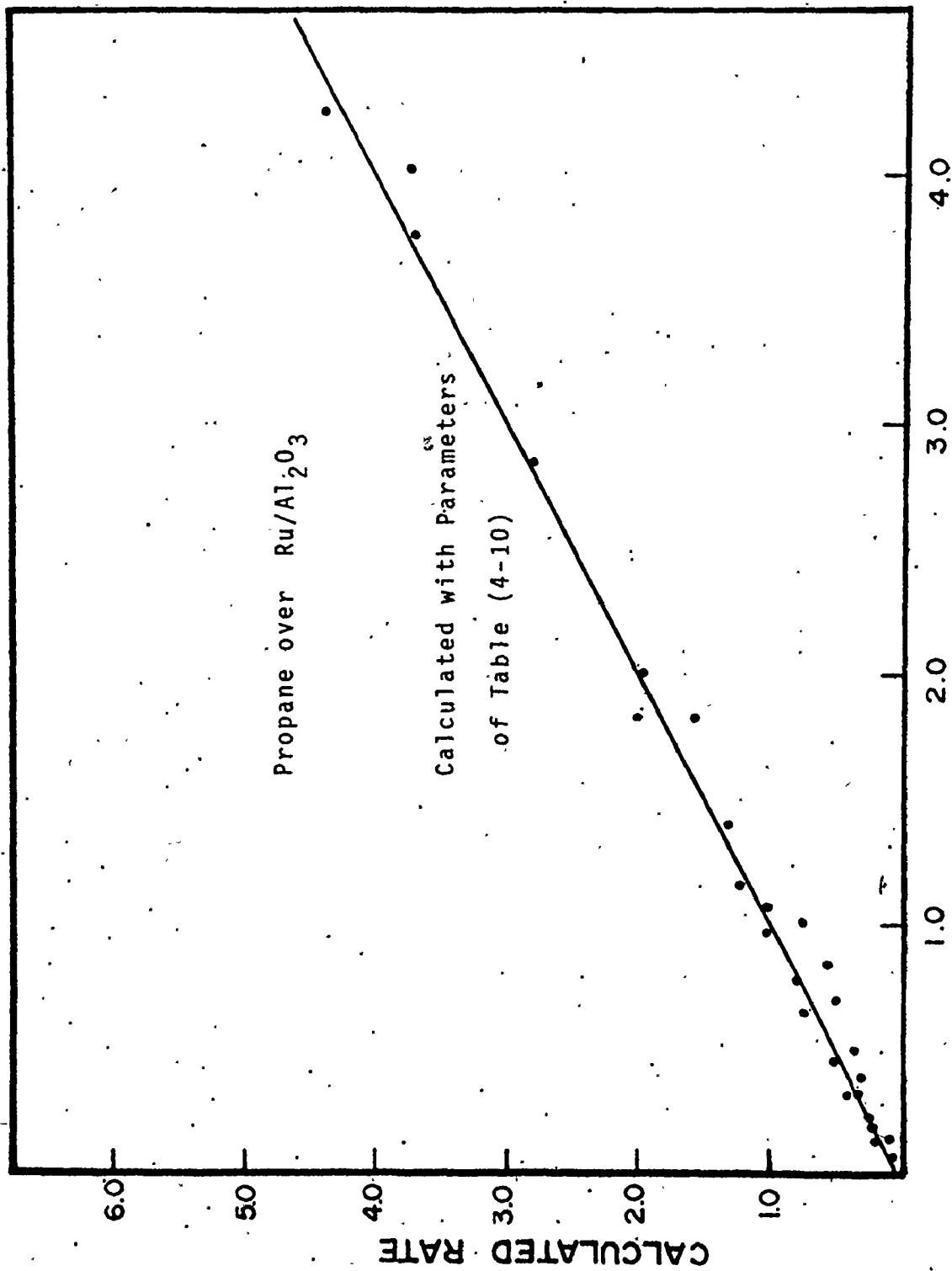
Figure 4-6   Calculated versus Experimental Rates.

CALCULATED RATE

The ethane selectivity equation was applied to the selectivity data for ethane, the results are in table 4-11, and show that the rate of cracking of an adsorbed C_2 species is much lower than the rate of desorption. This is one of the assumptions of the Cimino and Sinfelt models, and it only appears to hold for ruthenium in these experiments. It is in agreement with data of other hydrocarbons over ruthenium (44, 47, 101). A possible reason for this phenomenum is that the temperatures used in the reactions with ruthenium were much lower than for the other metals...

4.6 Discussion

Some values of kinetic parameters from the literature are shown in table 4-12. Table 4-13 shows the results of the experiments described in the previous sections. The exponents for hydrogen and propane appear to agree quite well with those of table 4-12, and they seem to be rather independent of the support for a given metal and whether or not a promoter is present. The values near unity for the exponent of propane suggest a low surface coverage by the adsorbed hydrocarbon species, the negative hydrogen exponent is due to dissociative adsorption of the hydrocarbons. Increased hydrogen pressure causes the adsorption equilibrium to shift and decreases the number of reactive species on the surface. The compositions of the surface intermediates, calculated from the exponents, suggest 1,2-diadsorption on ruthenium (surface species C_3H_3),

Table 4-11

Propane Hydrogenolysis over Ruthenium, fit to Selectivity Equation[a]

Temperature (^{o}C)	Pressure (atm)	k_2^{*}/k_2'	k_3''/k_3''
150	1.3	0.01	0.03
150	2.0	0.01	0.03
179	1.3	0.03	0.02
179	2.0	0.02	0.01

(a)　figure 4-1

Table 4-12

Hydrogenolysis of Propane and Ethane, some

values from the literature

Propane				
catalyst	E_a kcal/mol	m	n	reference
Ru/Al$_2$O$_3$	35.8	-1.5	1.0	(31)
Ni/Al$_2$O$_3$	50.	variable (-1.0→-2.4)	variable (0.6→1.0)	(9)
Ni/SiO$_2$	34.	-2.6	0.9	(124)
Ni SiO$_2$	33.	variable (0.0→-0.6)	0.9	(138)

Ethane				
catalyst	E_a kcal/mol	m	n	reference
Ru Al$_2$O$_3$	36.	-1.5	1.0	(117)
Ni/SiO$_2$	40.6	-2.4	1.0	(10)
Co/SiO$_2$	30.	-0.8	1.0	(10)
Co/kieselguhr	30.-34.	variable (-0.7→-1.2)	–	(6)

Table 4-13

Summary of results of Propane Hydrogenolysis, power rate law[a]

Catalyst	temperature range($^{\circ}$C)	$\log_{10}A$	E_a kJ/mol	kcal/mol	m	n
Ru/Al$_2$O$_3$	150-180	19.1	155.	36.9	-1.98	0.80
Ni/SiO$_2$	254-303	18.	175.	41.8	-1.57	0.73
Ni/SiC	277-305	20.8	217.	51.8	-2.41	0.86
Ni-Mg/SiC	250-281	19.5	193.	46.1	-2.29	0.67
Co/SiO$_2$ (14-28mesh)	233-268	15.95	140.	33.3	-0.95	0.70
Co/SiO$_2$ (28-48mesh)	228-268	10.0	93.	22.2	-0.72	0.79
Co-Mg/SiC	245-266	21.0	204.	48.6	-0.78	1.03
Fe-Mg/SiO$_2$	314-353	12.6	149.	35.6	0.67	0.65
D3001	288-330	11.0	129.	30.8	2.00	1.17
D3001 (extracted)	270-238	11.0	124.	29.5	-0.06	0.80

(a) $r = A \exp(-E_a/RT) \, P_{H_2}^m \, P_{C_3H_8}^n$

and 1,2- or 1,3-diadsorption on nickel (C_3H_3 or C_3H_2), all completely devoid of hydrogen at the adsorbing carbon atoms. For cobalt C_3H_6 is found to be the surface species, no conclusion can be made about the type of adsorption. The apparent activation energies are much higher on the low area catalysts than on those on high area supports. This poses the question whether a compensation effect may be observed, as was the case for ethane hydrogenolysis over group VIII metals (24). Fig. 4-7, where $\log_{10}A$ is plotted versus the apparent activation energy for all the catalysts, shows that a compensation effect is indeed operative: higher values of E_a are compensated by higher values of A. The correlation is satisfactory for all catalysts, except for the ruthenium catalyst. This agrees with results by Sinfelt (24), who suggested separate compensation lines existed for the noble and the non-noble metals of group VIII. Comparable patterns of kinetic behaviour have been described for many surface reactions, a number of examples and several possible explanations are discussed in reference (151).

To compare the activities of the different catalysts, reaction rates were calculated at a set of conditions: at 240°C, 1.0 atm hydrogen pressure and 0.2 atm propane pressure. These values are shown in table 4-14 together with values of T_r for all the catalysts. T_r is defined as the temperature at which the rate of reaction is equal to a cer-
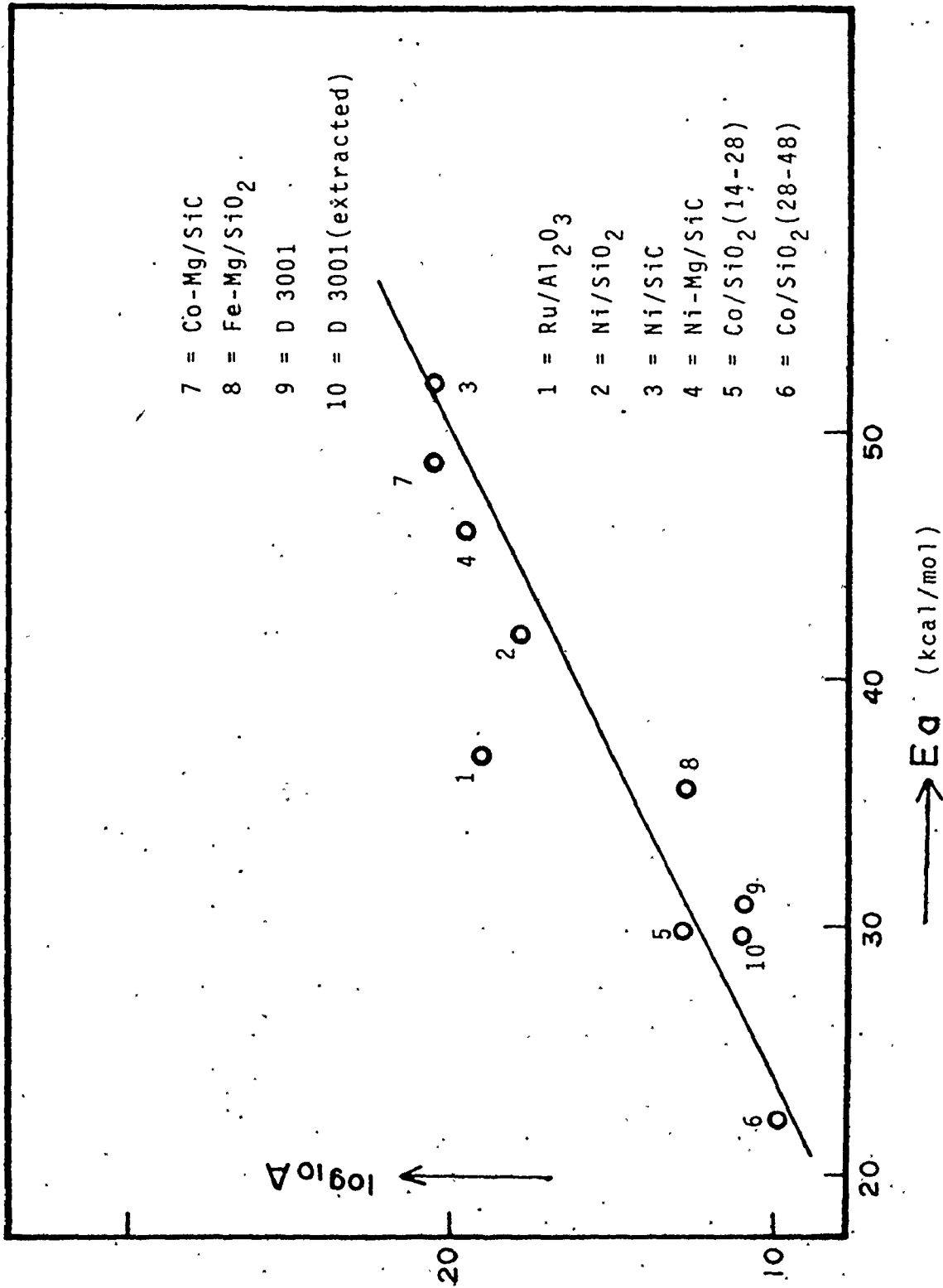
Figure 4-7 Compensation Effect in Propane Hydrogenolysis.

Table 4-14

Comparison of Activity of the Catalysts

Catalyst	T_R[a] ($^{\circ}C$)	R[b] $\mu mol/s,g$ cat.	Metal surface area[c]
Ru/Al$_2$O$_3$	167	733.	0.8
Ni/SiO$_2$	255	0.50	8.3
Ni/SiC	297	0.01	0.1
Ni-Mg/SiC	268	0.21	2.0
Co/SiO$_2$ (14-28)	252	0.61	3.2
Co/SiO$_2$ (28-48)	244	0.97	2.1
Co-Mg/SiC	252	0.38	
Fe-Mg/SiO$_2$	360	0.001	
D3001	353	0.002	13.8
D3001 (extracted)	341	0.01	

(a) · temperature at which the rate of reaction is
1.0 $\mu mol/s,g$ cat.

(b) rate at 240$^{\circ}C$,1.0 atm. hydrogen pressure,0.2 atm.
propane pressure

(c) (m^2 metal)/(g catalyst)

tain value, in this case 1 μmol/s,g cat.. This concept was
introduced by Boudart (98), it avoids extrapolation and is
therefore a more useful parameter to compare activities. The
hydrogen and propane partial pressures used to calculate T_r
were 1.5 and 0.25 atm respectively. The ruthenium catalyst
is the most active, the iron catalysts are the least active;
this agrees with the results for ethane hydrogenolysis (24,
136). The promoted nickel catalyst is much more active than
the corresponding unpromoted one, as was expected from the
surface area measurements. The activity per unit metal area
is almost the same for all three nickel catalysts. The activ-
ities of the nickel and cobalt catalysts are almost equal,
cobalt being slightly more active. With ethane, nickel was
more active than cobalt. The most interesting fact observed
is., that both for nickel and cobalt, the catalysts on the
low area supports have similar activities as those on the
high area supports, albeit that they contain 2-3 times as
much metal. Low area supports have several practical advan-
tages as explained in section 2.1.

Various mechanistic rate equations, derived from
Langmuir-Hinshelwood type mechanisms (appendix B.3) were test-
ed but none of these gave an improved fit of the data and
the parameters obtained were erratic.

A summary of the values of k_2^*/k_2' and k_2''/k_3'' is given
in table 4-15 for the high pressure region (2.0-2.2 atm
total pressure). k_2''/k_3'' values behave erratically with

Table 4-15

Summary of results for Ethane Selectivities.(2.0-2.2 atm.)

Catalyst	Temperature (^{o}C)	k_2^*/k_2' (a)	k_2''/k_3'' (a)
Ru/Al$_2$O$_3$	150	0.01	0.03
	180	0.02	0.01
Ni/SiO$_2$	255	0.4	0.6
	278	0.9	0.2
	304	1.6	0.2
Ni/SiC	277	0.4	1.4
	292	0.8	0.3
	305	1.2	0.2
Ni-Mg/SiC	251	0.3	0.1
	266	0.5	0.6
	281	1.0	0.3
Co/SiO$_2$	228	0.9	3.6
	248	2.6	0.5
	268	4.2	0.5
Co-Mg/SiC	245	4.0	0.7
	255	4.2	0.3
	265	4.3	0.6

(a) $\qquad S_2 = \dfrac{k_2'/(k_2'+k_2^*)}{1 + k_2''/k_3'' \dfrac{X}{1-X}}$

temperature, k_2^* / k_2' values always increase with increasing temperature. This suggests the cracking step has a higher activation energy than the desorption step. The values for k_2^* / k_2' indicate that only for ruthenium is the rate of desorption of the adsorbed C_2 species fast compared to the rate of cracking; for nickel these rates are roughly equal and for cobalt the cracking is faster than the desorption. This parallels a decrease in the amount of ethane in the products. This fact and the previous suggestion that the surface species on both ruthenium and nickel is C_3H_3 indicates that the modes of adsorption may be different on these metals. In both cases multiple bonds are present, but most likely these are in the adsorbed hydrocarbon in the case of ruthenium and between the metal and the hydrocarbon in the case of nickel. The overall rate of ethane hydrogenolysis is always lower than that of propane hydrogenolysis, but the difference is largest on ruthenium and smallest on cobalt. At lower pressure the values for k_2^* / k_2' are always somewhat lower, but the values of k_2'' / k_3'' are not affected by the pressure. This agrees with observations by Tsjeng (33).

The values of table 4-15 were used to calculate ethane selectivities at several levels of conversion, the results are in table 4-16. The data for iron are estimated from the experimental selectivities and are not very accurate. At lower total pressures the amount of ethane is slightly smaller.

Table 4-16

Selectivity for Ethane at various levels of

Conversion,using parameters of table 4-15

Catalyst	Temperature (^0C)	S_2 at conversion X		
		X= 0.0	0.4	0.8
Ru/Al$_2$O$_3$	150	0.99	0.97	0.88
	180	0.98	0.97	0.94
Ni/SiO$_2$	255	0.71	0.51	0.21
	278	0.53	0.46	0.29
	304	0.38	0.34	0.21
Ni/SiC	277	0.71	0.37	0.11
	292	0.56	0.46	0.25
	305	0.45	0.40	0.25
Ni-Mg/SiC	251	0.77	0.72	0.55
	266	0.67	0.48	0.20
	281	0.50	0.42	0.23
Co/SiO$_2$	228	0.53	0.15	0.03
	248	0.28	0.21	0.09
	268	0.19	0.14	0.06
Co-Mg/SiC	245	0.20	0.14	0.05
	255	0.19	0.16	0.09
	265	0.19	0.13	0.06
Fe-Mg/SiO$_2$	330	0.05	0.02	0.01
D3001	310	0.06	0.01	0.00
D3001(extr.)	300	0.07	0.04	0.02

The selectivity for ethane decreases in the sequence - ruthenium, nickel, cobalt, iron-; data for iron were not analysed because the amount of ethane in the product was always very low. The amount of ethane decreases with increasing temperature and increasing conversion, but selectivity over a given metal appears not to be very dependent on the support, and is about equal for promoted and unpromoted catalysts. Fig. 4-8 shows the ethane selectivities at zero conversion as a function of temperature (values are from table 4-16).

123
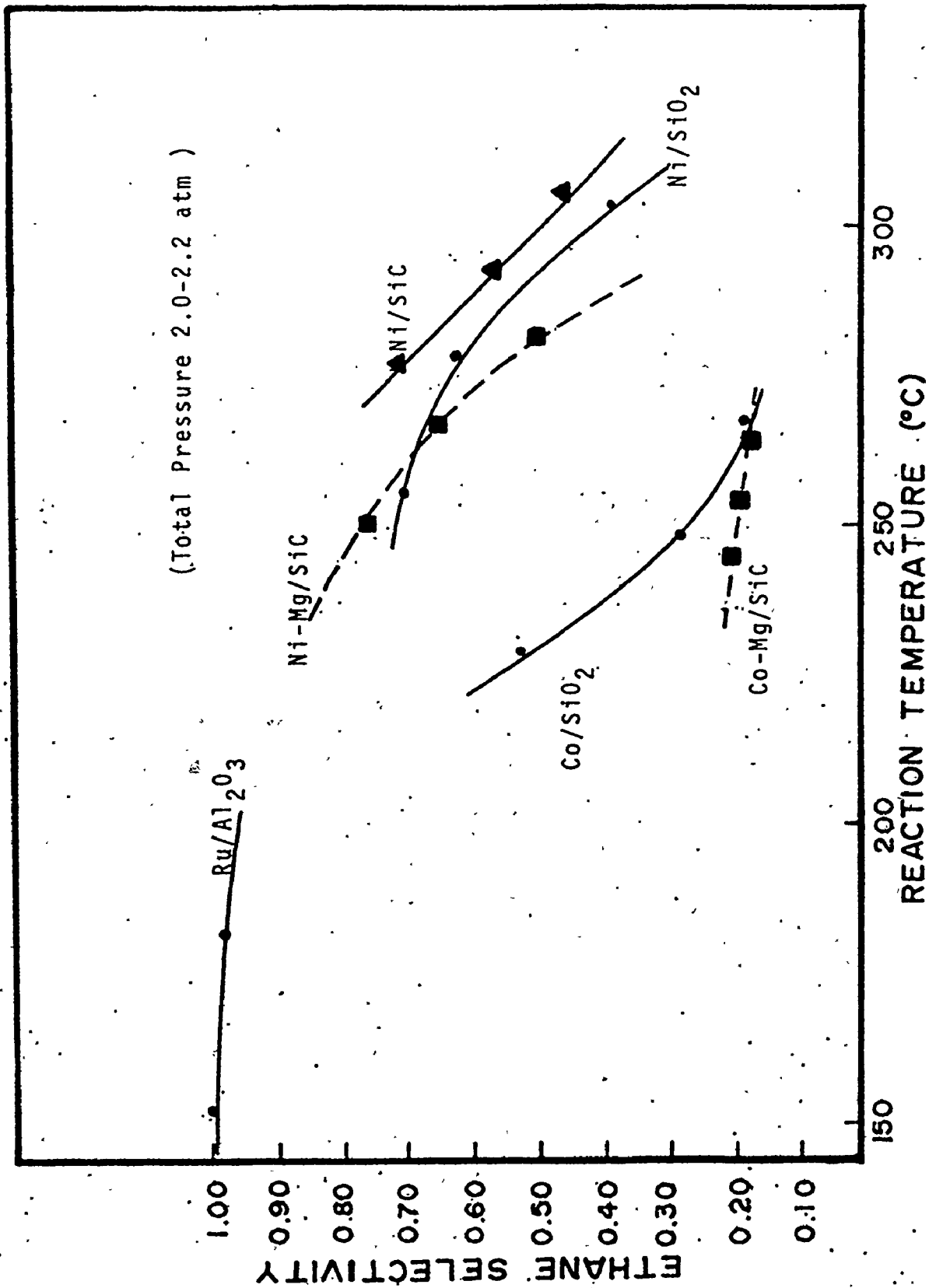
Figure 4-8   Ethane Selectivity at Zero Conversion as a Function of Temperature.

Chapter 5

HYDROGENOLYSIS OF HEXANES

5.1 Introduction

The hydrogenolysis of higher hydrocarbons, in this case three hexanes (n-hexane, 2,2-dimethylbutane, 2,3-dimethylbutane), yields a number of alkanes because there are several nonidentical carbon-carbon bonds, and because the initial products can react further to yield more smaller molecules. The products from a given hexane are functions of the catalyst, the temperature and the extent of reaction. The selectivities are related to the reaction mechanism, and the compositions are not equilibrium compositions (except in the case of iron), so that studying the product distributions should provide more insight into the reaction mechanisms.

The effluent concentrations were measured (appendix A) and the data were reported in terms of selectivities; the selectivity for a particular product is defined as the ratio of the moles of the product formed to the moles of feed hydrocarbon reacted. The calculation procedures are in appendix B.1. The extent of the reaction is expressed in terms of conversion of the feed hydrocarbon. All the experiments were performed at one operating pressure, 1.20 atm and over as wide a range of conversion as possible. Higher pressures could not be used because of leakage in the feed system.

124

The formation of smaller products is favoured by high con-
version, high temperature and low hydrogen pressure (44). The
product distribution at very low conversion is representative
of the hydrogenolysis of the feed hydrocarbon alone. In appen-
dix C, reaction networks are proposed with consecutive and
parallel reaction paths and including the reversible adsorp-
tion and desorption of all hydrocarbons and the irreversible
splitting of the carbon-carbon bonds of the adsorbed species.

Equations relating the selectivities of all products
and the conversion of the feed hydrocarbon were derived from
these networks; no rate determining step was assumed in this
process, all steps were coupled. Simultaneous multiple bond
breaking was not considered, since this can not be distin-
guished from the case where an initial product will crack be-
fore desorption from the surface. Other simplifying assump-
tions in the derivations are given in appendix C. The selec-
tivity data were fitted to the appropriate selectivity equati-
ons using nonlinear least squares analysis, to obtain the
parameters. Splitting factors are some of these; they are
defined as the probability that a particular carbon-carbon
bond will break in molecules with several nonidentical bonds;
for a given metal they are assumed to be independent of con-
version, but may change with temperature.

In the following sections each of the hydrocarbons
is examined individually over each of the catalysts, the re-

sults are then summarized in the final section. The catalysts used in these experiments were Ru/ Al_2O_3, Ni/ SiC, NiMg/ SiC, CoMg/ SiC, and FeMg/ SiO_2. The nickel and cobalt catalysts on high area silica were not used since they increase experimental problems and did not differ significantly from the catalysts on the low area supports during the hydrogenolysis of propane. The modifications of the reactor system were described in section 3.2.2; the liquid feeds are introduced with a calibrated syringe pump, and the tubing in the reactor and effluent systems are heated to about 70°C (boiling points of the hexanes vary from 50-68°C). The molfraction of hexane in the feed is kept below 10% to avoid condensation and because much more hydrogen can be consumed in these reactions compared to those of propane. If the hydrogen to hydrocarbon ratio becomes too low, carbon deposits may foul the catalyst.

During these experiments the activity of the catalysts decreased much more rapidly than was the case for propane. This deactivation was observed for all three hexanes and on all catalysts, but was especially severe for 2,3-dimethylbutane on ruthenium. The deactivation was slower with nickel and cobalt, possibly because the reaction temperatures were higher. On ruthenium the rate decreased by a factor 20 after 3 days of operation with 2,3-dimethylbutane at 180°C; at higher temperature the decrease was slower. Treatment with hydrogen overnight at temperatures slightly higher than those of the reacti-

ons reactivated the catalysts to their original activity. The

10% propane-in-hydrogen mixture was used again to determine

the activity. It was thought at first that impurities in the

hexanes might be responsible for the deactivation, and puri-

fication of 2,3-dimethylbutane was attempted. First, the

hexane was stored over a mixture of Raney nickel and 3A and

5A molecular sieves. The Raney nickel should remove sulphur

components, and the molecular sieves should adsorb traces of

water and straight hydrocarbons. This treatment did not

change the rapid aging of the catalyst. Peroxides are another

possible cause of aging. In cumene cracking, peroxides have

been shown to be precursors in the coke formation (152, 153).

The hydrocarbon was treated with 50-200 mesh silica that was

heated at 400°C; a method used to remove peroxides from cu-

mene. The silica should also remove other polar impurities.

After this treatment of the feed, deactivation still occurred

Due to the rapid deactivation, kinetic analyses, like the

ones for propane, could not be made; moreover the range of

partial pressures covered was very narrow so that orders of

reaction could not be determined with much accuracy. However,

the selectivity data were not affected by the deactivation:

selectivities determined at constant temperature over a

period of four days all fitted the same curves, even though

the activity of the catalyst decreased substantially over

this period. The aging apparently did not involve selective

poisoning of particular active sites.

It was decided that product distributions would be determined at one level of temperature for all combinations of catalysts and hydrocarbons; if necessary the catalyst could be reduced to recover the activity. The temperature was chosen for each system such that as wide a range of conversion as possible could be covered.

5.2 2,2-Dimethylbutane

5.2.1 Introduction

2,2-Dimethylbutane contains three different types of carbon-carbon bonds:

$$C \xrightarrow{\text{III}} \overset{\displaystyle \overset{C}{|}}{\underset{\displaystyle \underset{C}{|}}{C}} \xrightarrow{\text{II}} C \xrightarrow{\text{I}} C$$
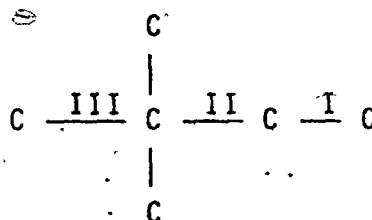
Cracking of bond I yields methane and neopentane which can crack further to isobutane, propane, ethane and methane. Breaking of bond II gives ethane and isobutane which can crack further in a similar way. Cracking of bond type III gives methane and isopentane, which in itself has three different bond types and can yield all the above mentioned products plus n-butane. 1,2-diadsorption at bond I will yield neopentane, while 1,3-diadsorption is expected to yield isopentane initially. On ruthenium, isopentane was shown to react for 82% to form isobutane and only for 8% to form n-butane (47).

On nickel, 2,2-dimethylbutane yielded almost only methane and neopentane in almost equimolar amounts at low conversion (51, 55), indicating that demethylation takes place, but this stops at quaternary carbon atoms. This result agrees with other data on nickel; α- scission occurs along the longest alkyl chain at secondary or tertiary carbon atoms (48, 53, 54, 125). On platinum a carbonium ion mechanism is operable, isomerisation takes place as well as hydrogenolysis. No neopentane was produced and the product contained mainly i-butane and ethane plus some i-pentane and methane (51). Thus, methyl groups at quaternary carbon atoms are not always the most stable (50). Isomerisation of neopentane was observed on Au and Ir as well as on Pt (41).

The proposed reaction scheme for 2,2-dimethylbutane and the pertinent rate constants and splitting factors are shown in fig. 5-1, the assumptions and the derivations of the selectivity equations are discussed in appendix C.4.

The analytical solutions are:

$$S_{ne5} = \frac{k'_{ne5}\ell \; / \; (k'_{ne5} + k^*_{ne5})}{1 + (k''_{ne5} \; / \; k''_6)\{x/(1-x)\}} \qquad (5-1)$$

$$S_{i5} = \frac{k'_{i5}\ell' \; / \; (k'_{i5} + k^*_{i5})}{1 + (k''_{i5} \; / \; k''_6)\{x/(1-x)\}} \qquad (5-2)$$

$$C_6 \xrightarrow[<\overline{k_6'}]{k_6} A_6 \quad neC_5 \xrightarrow[<\overline{k_{ne5}'}]{k_{ne5}} neA_5 \quad i\text{-}C_5 \xrightarrow[<\overline{k_{i5}'}]{k_{i5}} i\text{-}A_5 \quad i\text{-}C_4 \xrightarrow[<\overline{k_{i4}'}]{k_{i4}} i\text{-}A_4$$

$$C_1 \xrightarrow[<\overline{k_1'}]{k_1} A_1 \quad C_2 \xrightarrow[<\overline{k_2'}]{k_2} A_2 \quad C_3 \xrightarrow[<\overline{k_3'}]{k_3} A_3 \quad n\text{-}C_4 \xrightarrow[<\overline{k_{n4}'}]{k_{n4}} n\text{-}A_4$$

$$A_6 \xrightarrow{k_6^*} \begin{cases} \xrightarrow{\ell} ne\text{-}A_5 + A_1 \\ \xrightarrow{\ell'} i\text{-}A_5 + A_1 \\ \xrightarrow{(1-\ell-\ell')} i\text{-}A_4 + A_2 \end{cases}$$

$$i\text{-}A_5 \xrightarrow{k_{i5}^*} \begin{cases} \xrightarrow{f} i\text{-}A_4 + A_1 \\ \xrightarrow{f'} n\text{-}A_4 + A_1 \\ \xrightarrow{(1-f-f')} A_3 + A_2 \end{cases}$$

$$ne\text{-}A_5 \xrightarrow{k_{ne5}^*} i\text{-}A_4 + A_1$$

$$i\text{-}A_4 \xrightarrow{k_{i4}^*} A_3 + A_1$$

$$n\text{-}A_4 \xrightarrow{k_{n4}^*} \begin{cases} \xrightarrow{m} 2A_2 \\ \xrightarrow{(1-m)} A_3 + A_1 \end{cases}$$

$$A_3 \xrightarrow{k_3^*} A_2 + A_1$$

$$A_2 \xrightarrow{k_2^*} 2A_1$$

C_x = gaseous hydrocarbon, carbon number x

A_x = adsorbed hydrocarbon species

k_x = adsorption rate constant k_x' = desorption rate constant

k_x^* = surface cracking rate constant $k_x'' = k_x^* k_x / (k_x' + k_x^*)$

Figure 5-1   Reaction Network for Hydrogenolysis of 2,2-DMB

$$S_{i4} = \frac{\{k'_{i4} / (k'_{i4} + k^*_{i4})\} \{1 - \ell'(1-f) - S_{ne5} - fS_{i5}\}}{1 + (k''_{i4}/ k''_6) \{x/(1-x)\}} \qquad (5\text{-}3)$$

$$S_{n4} = \frac{\{k'_{n4} / (k'_{n4} + k^*_{n4})\} \{f'(\ell' - S_{i5})\}}{1 + (k''_{n4}/ k''_6) \{x/(1-x)\}} \qquad (5\text{-}4)$$

$$S_3 = \frac{\frac{k'_3}{(k'_3 + k^*_3)} \{1 - mf'\ell' - S_{n4}(1-m) - S_{ne5} - S_{i5}(1-mf') - S_{i4}\}}{1 + (k''_3/ k''_6) \{x/(1-x)\}} \qquad (5\text{-}5)$$

$$S_2 = \frac{\frac{k'_2}{(k'_2 + k^*_2)} \{2 - \ell - f\ell' - f'\ell' + mf'\ell' - S_3 - S_{n4}(1+m) - S_{i4} - S_{ne5} - S_{i5}(2-f-f'+mf')\}}{1 + (k''_2/ k''_6) \{x/(1-x)\}} \qquad (5\text{-}6)$$

$$S_1 + 2S_2 + 3S_3 + 4(S_{n4}+S_{i4}) + 5(S_{ne5}+S_{i5}) = 6 \qquad (5\text{-}7)$$

where x = fractional conversion of 2,2-dimethylbutane

S_x = selectivity for product x

k = rate constants as defined in fig. 5-1

Maximum selectivities are 1.0 for the pentanes, the butanes and propane, 2.0 for ethane, and 6.0 for methane. Isomerisation products and hydrocarbons larger than hexanes were not observed in any of the experiments with 2,2-dimethylbutane.

The reaction of 2,2-dimethylbutane over the iron catalyst (FeMg/SiO$_2$), yielded mainly methane, and some neopentane (selectivity 0.11 to 0.27) and isobutane (selectivity 0.06 to 0.20). Only traces of the other products were present. The methane selectivity varied from 4.0 to 5.3. Temperatures of at least 300°C were required for this catalyst, and this may be part of the reason for the high methane yield. No analyses were made on the data of iron, because the yield of products other than methane was too small. The activity of the iron catalyst was quite constant, albeit low.

5.2.2 2,2-Dimethylbutane over Ruthenium

The experimental data, expressed in terms of selectivities of the products, and the conversion of 2,2-dimethylbutane are tabulated in tables D-11 and D-12. All the experiments were performed at a total pressure of 1.20 atm, and at 185°C and 200°C respectively. The selectivities are plotted as a function of the conversion of 2,2-dimethylbutane in fig. 5-2 and fig. 5-3 at 185°C and 200°C. The experimental selectivities are indicated by the points. Isopentane and n-butane were never detected, neopentane and methane were the main products, with small amounts of ethane and i-butane and traces of propane.
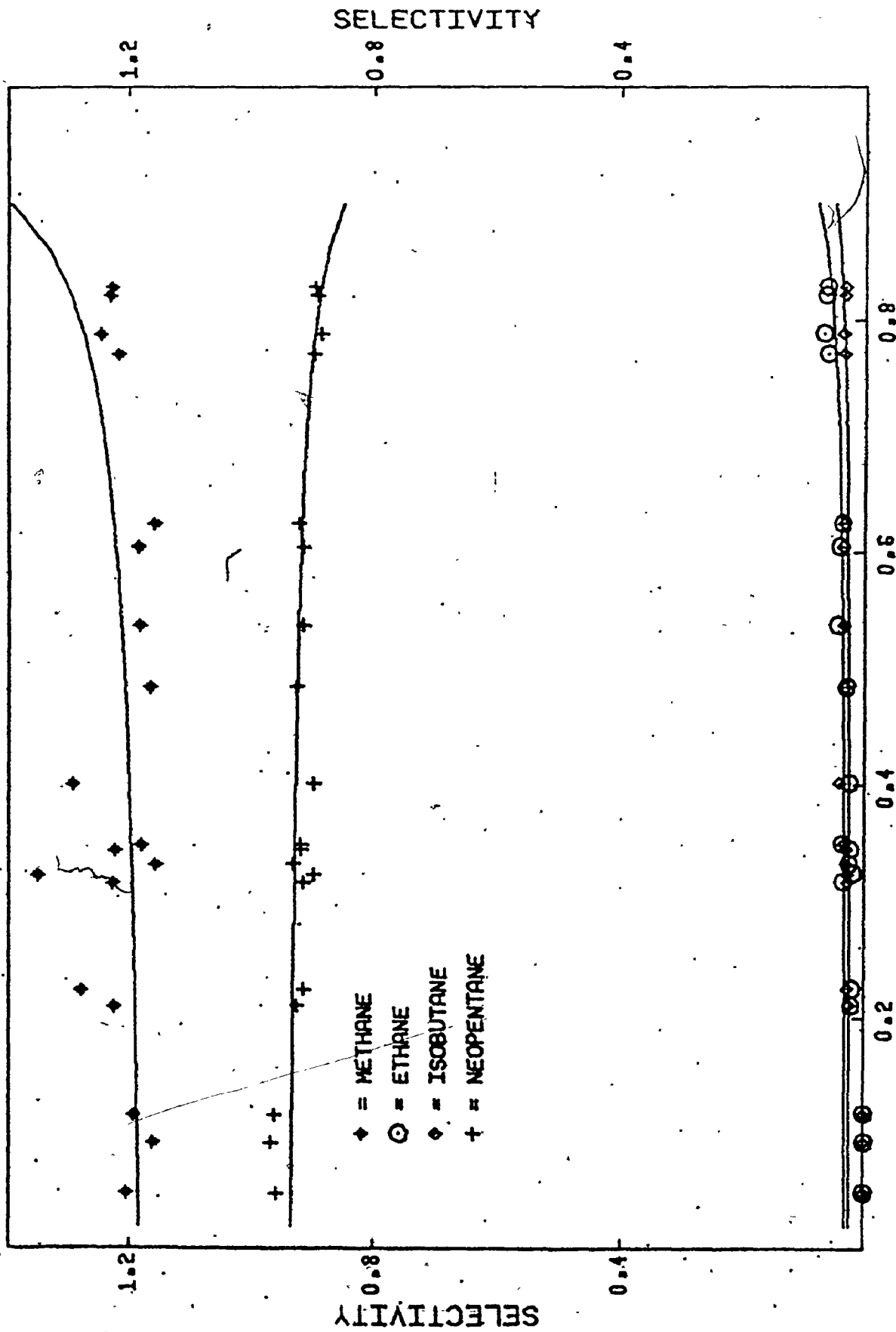
Figure 5-2 Product Distribution of Hydrogenolysis of 2,2-Dimethylbutane over Ru/Al$_2$O$_3$ at 185°C and 1.2 atm.

134
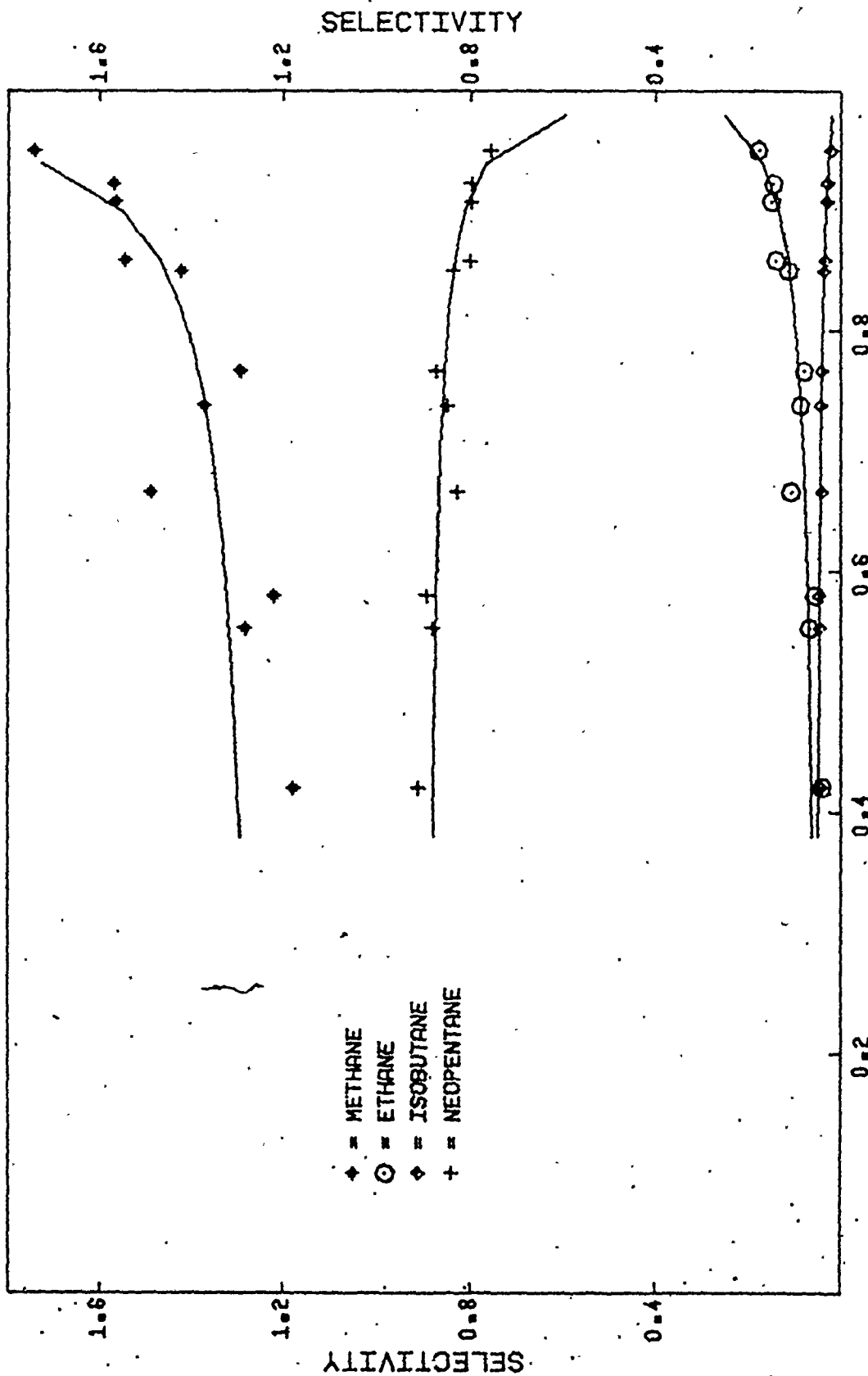
Figure 5-3 Product Distribution of Hydrogenolysis of 2,2-Dimethylbutane over
Ru/Al$_2$O$_3$ at 200°C and 1.2 atm.

At low conversion approximately equal amounts of methane and
neopentane are formed. Thus, almost all the reactions take
place at bond type I; neopentane has been shown to be very
stable over ruthenium (44, 47), the order of reactivity be-
ing much lower than that of other large hydrocarbons, about
equal to that of ethane. Once neopentane is formed, it will
not react further readily. With increasing conversion the
neopentane selectivity decreases, while the selectivities of
isobutane,ethane and especially methane increase. At $200^{\circ}C$,
the isobutane selectivity also decreases with increasing
conversion in agreement with the observation that the pro-
ducts of neopentane hydrogenolysis react faster than neopen-
tane itself (44).

The selectivity equations (5-1), (5-3), and (5-6)
were applied directly to the experimental data using nonli-
near least squares techniques (appendix B.2). First equation
(5-1) was used with the neopentane data, initial values for
the parameters being obtained from a plot of $1/S_{ne5}$ versus
$x/(1-x)$. Then equation (5-3) was fitted to the data for iso-
butane, using the predicted values of the neopentane selec-
tivities. Finally equation (5-6) was applied to the ethane
selectivities using the predicted values of the selectivities
for neopentane and isobutane. The predicted values of the
selectivities of isopentane, n-butane, and propane were always
zero since none of these were observed. The methane selecti-
vities were determined using equation (5-7) and the calcula-

ted values of the selectivities for the other products. The calculated selectivities, using the obtained parameters are shown in fig. 5-2 and fig. 5-3 as the solid lines. The estimated parameter values are in table 5-1 with their approximate 95% confidence intervals. The confidence limits are large for the smaller products as is explained in appendix B.2. The average deviation between the calculated and experimental selectivities is less than 3% for neopentane, but quite large for i-butane and ethane, due to the fact that they were present in only small amounts. In section 5.5 these values will be shown for all the experiments. The estimated value of ℓ is close to unity, confirming the observation that mainly bond I is attacked. The rate of desorption of the adsorbed species is greater than the rate of surface cracking, and the overall rates of hydrogenolysis of ethane and neopentane are of the same order and much smaller than that of 2,2-dimethylbutane.

5.2.3 2,2-Dimethylbutane over Nickel

Two nickel catalysts were used: NiMg/SiC and Ni/SiC. The experimental data expressed in terms of the selectivities of the products and the conversion of 2,2-dimethylbutane are tabulated in tables D-18 and D-15 for the two catalysts, respectively. The experiments were performed at 265°C with the promoted catalyst, at 290°C with the unpromoted one. Plots of the product distribution as a function of the conversion

Table 5-1

Analysis of Hydrogenolysis of 2,2-Dimethylbutane
over Ruthenium. Equations (5-1),(5-3),and (5-6)

Parameter	Estimated value	
	$185^{o}C$	$200^{o}C$
$\dfrac{k'_{ne5}\,\ell}{k'_{ne5}+k^{*}_{ne5}}$	0.93 ± 0.01	0.88 ± 0.03
k''_{ne5}/k''_6	0.01 ± 0.06	0.01 ± 0.01
$\dfrac{k'_{i4}}{k'_{i4}+k^{*}_{i4}}$	0.34 ± 0.10	0.43 ± 0.03
k''_{i4}/k''_6	0.005 ± 0.1	0.19 ± 0.04
$\dfrac{k'_2}{k'_2+k^{*}_2}$	0.86	0.99
ℓ	1.0	1.0
k''_2/k''_6	10^{-5}	0.01 ± 0.05

of 2,2-dimethylbutane are given in fig. 5-4 and fig. 5-5, the experimental points are described in the figures. On the promoted nickel catalyst, isopentane and in most cases n-butane were too small to be measured. The main products were neopentane and methane, but the amounts of ethane, propane, and i-butane obtained were larger than for ruthenium. With increasing conversion, the selectivity of neopentane decreases, that of methane increases, the others vary only slightly. On the unpromoted nickel catalyst, no i-pentane was observed, but the amount of n-butane was measurable and decreased with increasing conversion. There are more smaller products than on the promoted catalyst, especially methane and ethane, probably due to the higher temperature. The neopentane selectivity is consequently smaller and decreases with increasing conversion and the same is observed for the selectivity of isobutane. Ethane, and to a lesser extent propane, show a maximum in selectivity plots. Apparently nickel behaves basically like ruthenium in splitting primarily bonds of type I, but at higher temperature more extensive cracking takes place.

The selectivity equations (5-1) through (5-6) were applied to the data in the same way as for ruthenium; the resulting estimates of the parameters are in table 5-2. Initial guesses for equation (5-1) were again obtained from plots of $1/S_5$ versus $x/(1-x)$, and the predicted methane selectivities were obtained from the carbon balance of equation (5-7). The calculated selectivities are shown as the solid lines in

SELECTIVITY METHANE

SELECTIVITY

FRACTIONAL CONVERSION OF 2,2-DIMETHYLBUTANE
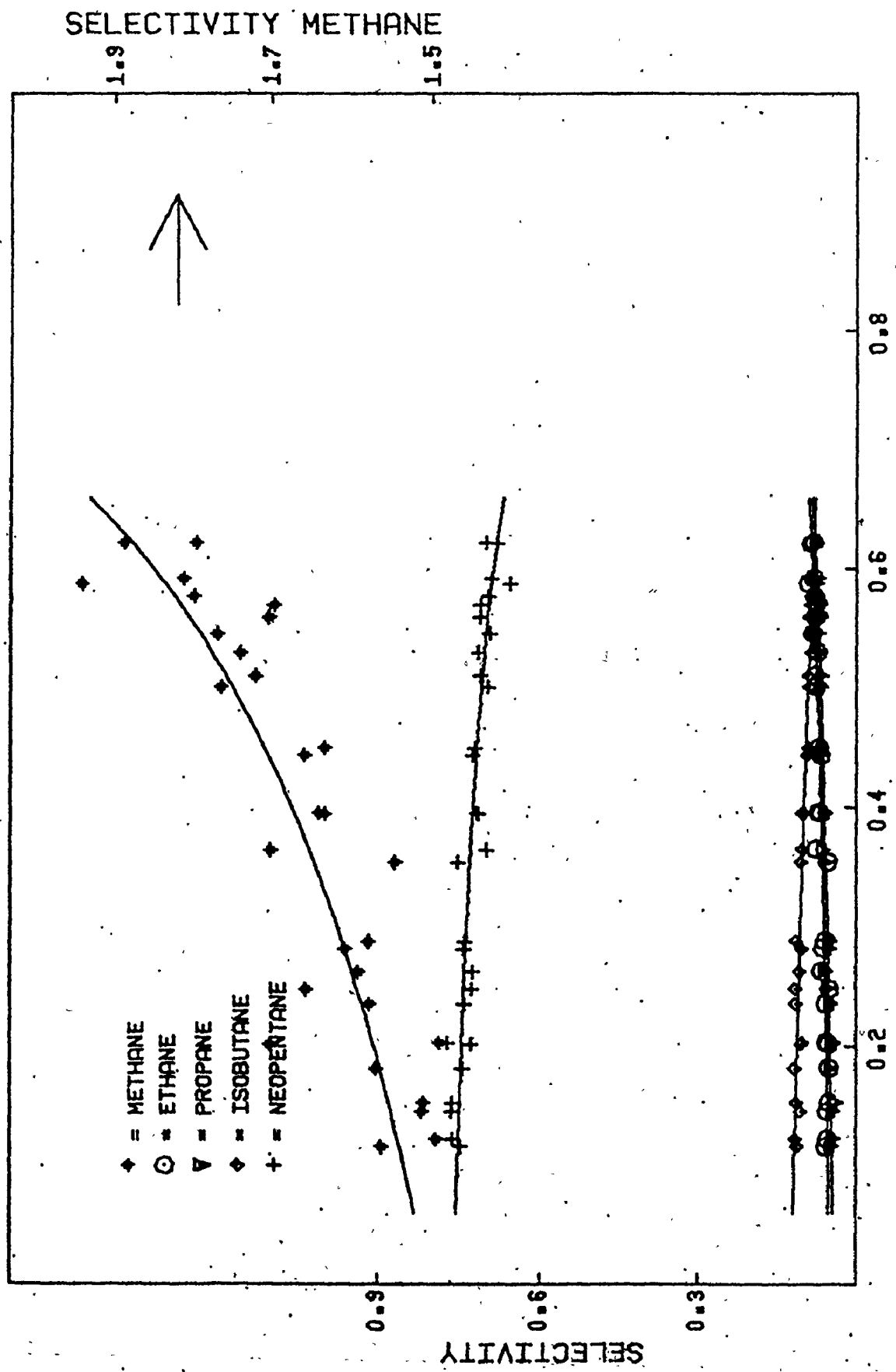
♦ = METHANE
⊙ = ETHANE
▽ = PROPANE
◆ = ISOBUTANE
+ = NEOPENTANE

Figure 5-4 Product Distribution of Hydrogenolysis of 2,2-Dimethylbutane over Ni-Mg/SiC at 265°C and 1.2 atm.
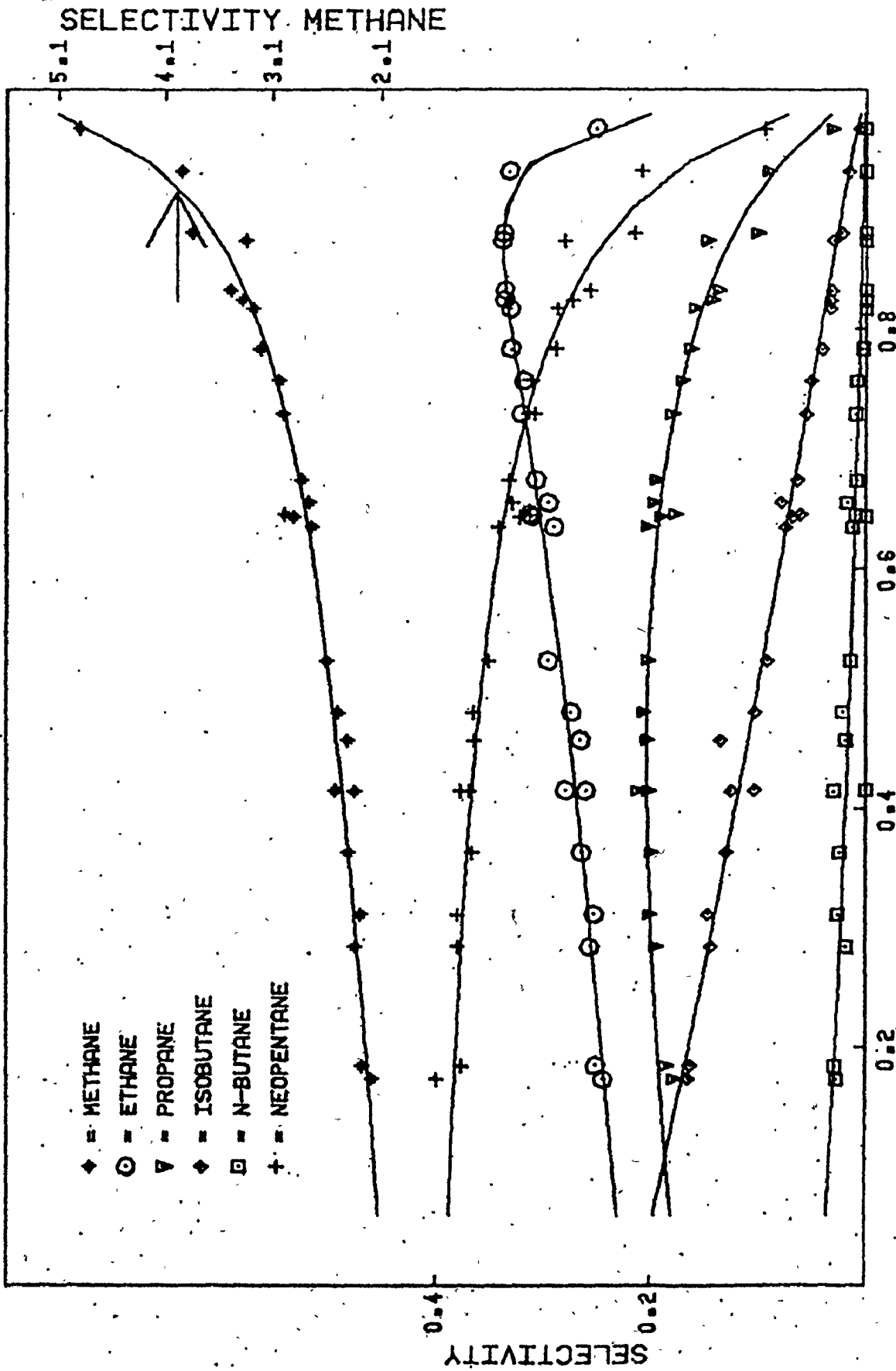
Figure 5-5 Product Distribution of Hydrogenolysis of 2,2-Dimethylbutane over Ni/SiC at 290°C and 1.2 atm.

Table 5-2

Analysis of Hydrogenolysis of 2,2-Dimethylbutane over Nickel

Equations (5-1) through (5-6)

Parameter	Estimated value	
	Ni-Mg/SiC(265°C)	Ni/SiC(290°C)
$\dfrac{k'_{ne5}\,\ell}{k'_{ne5}+k^{*}_{ne5}}$	0.76 ±0.01	0.39 ±0.01
k''_{ne5}/k''_6	0.07 ±0.02	0.09 ±0.01
$\dfrac{k'_{i4}}{k'_{i4}+k^{*}_{i4}}$	0.50 ±0.02	0.35 ±0.02
k''_{i4}/k''_6	0.62 ±0.07	1.2 ±0.2
$\dfrac{k'_{n4}\,\ell'\,f'}{k'_{n4}+k^{*}_{n4}}$	−	0.04 ±0.02
k''_{n4}/k''_6	−	1.7 ±1.3
$\dfrac{k'_3}{k'_3+k^{*}_3}$	0.35 ±0.02	0.48 ±0.02
k''_3/k''_6	0.04 ±0.05	0.25 ±0.03
$\dfrac{k'_2}{k'_2+k^{*}_2}$	0.52 ±0.08	0.49 ±0.05
ℓ	0.99 ±0.02	0.73 ±0.05
k''_2/k''_6	0.03	0.04 ±0.01

fig. 5-4 and fig. 5-5. The average deviation between experi-
mental and calculated selectivities never exceeds 8%, except
in the case of n-butane on Ni/SiC, because the experimental
values are very small. Again, neopentane reacts slower than
most of its products, but over these catalysts cracking is
not the slow step in the process; the rates of cracking and
desorption of the adsorbed species are about equal. A plot
of the experimental selectivities versus the calculated ones
is shown in fig. 5-6 for Ni/SiC, and it shows that the data
fit the selectivity equations quite well. Methane data are o-
mitted because their scale is very different. For NiMg/SiC,
the methane data instead of those of ethane were fitted to
equation (5-6) after substitution of equation (5-7), because
the data for ethane were small. The results were nearly iden-
tical than by fitting the ethane selectivities directly to
equation (5-6).

A few data were obtained at different temperatures
to compare the two nickel catalysts and to study the effect
of temperature on selectivities. The results are shown in
table 5-3. The promoted catalyst was more active than the un-
promoted preparation and the unpromoted catalyst produced
more ethane, propane and isobutane.

5.2.4 2,2-Dimethylbutane over Cobalt

The experimental data are expressed in terms of se-
lectivities of the products and the fractional conversion of
2,2-dimethylbutane, and are tabulated in table D-21.
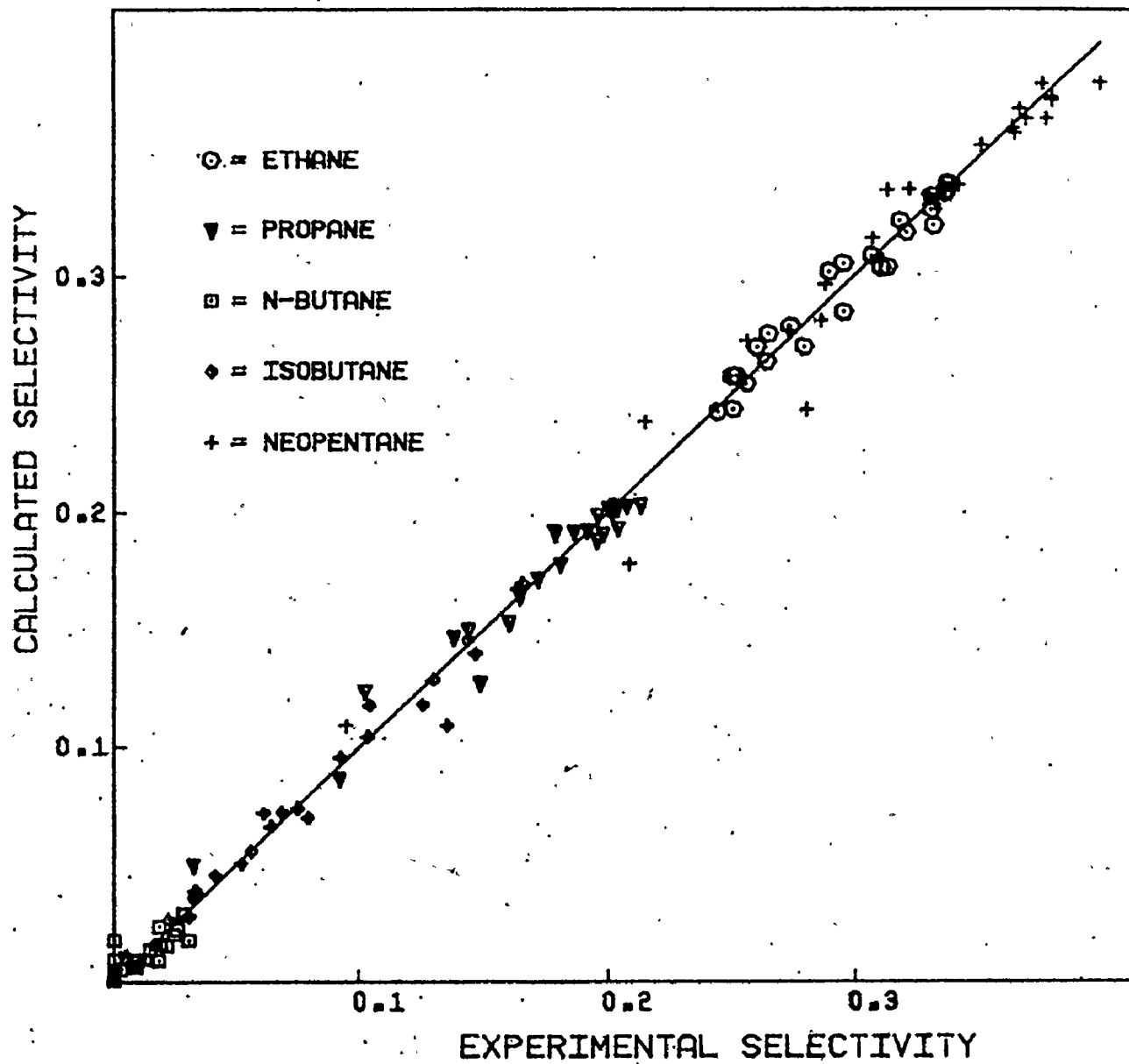
Figure 5-6   Experimental versus Calculated Selectivities
in the Hydrogenolysis of 2,2-Dimethylbutane over
Ni/SiC at 290°C and 1.2 atm.

Table 5-3

Product Distribution from Hydrogenolysis of 2,2-Dimethylbutane over Nickel at
other Temperatures

| Ni-Mg/SiC | | | | | | Temp. | Ni/SiC | | | | | |
S_1	S_2	S_3	S_{i4}	S_{ne5}	X	(°C)	X	S_{ne5}	S_{i4}	S_3	S_2	S_1
1.34	–	0.08	0.08	0.82	0.12	250	0.05	0.54	0.21	0.10	0.11	1.66
1.90	0.09	0.08	0.08	0.66	0.53	270	0.17	0.48	0.19	0.16	0.19	1.97
2.93	0.14	0.07	0.04	0.48	0.79	280	0.47	0.35	0.11	0.18	0.27	2.72
3.89	0.14	0.05	0.02	0.32	0.87	290	0.81	0.22	0.03	0.09	0.30	3.93
						300						

The experiments were carried out at 245°C. A plot of the product distribution as a function of conversion is shown in fig. 5-7 for the CoMg/SiC catalyst. The main products are neopentane and methane, suggesting that splitting of bond type I is again favoured. The amount of methane produced is larger than for the promoted nickel catalyst, but lower than for the unpromoted nickel catalyst, though the temperature is much lower for the cobalt catalyst. No isopentane and n-butane were observed. With increasing conversion, the selectivity of neopentane decreases, while that of methane increases. The amounts of other products remain small and nearly constant, indicating again that neopentane reacts slower than its products.

The data were fitted to the selectivity equations (5-1) through (5-6), and the results are shown in table 5-4; the solid curves in fig. 5-7 are the corresponding calculated selectivities. If the methane data were used in equations (5-6) and (5-7), instead of the data for ethane, the parameters obtained did not change. Over cobalt the rate of cracking of the adsorbed species is faster than the rate of desorption, which agrees with observations in the hydrogenolysis of propane:

5.3 2,3-Dimethylbutane

5.3.1 Introduction

2,3-Dimethylbutane has two different types of carbon-carbon bonds:
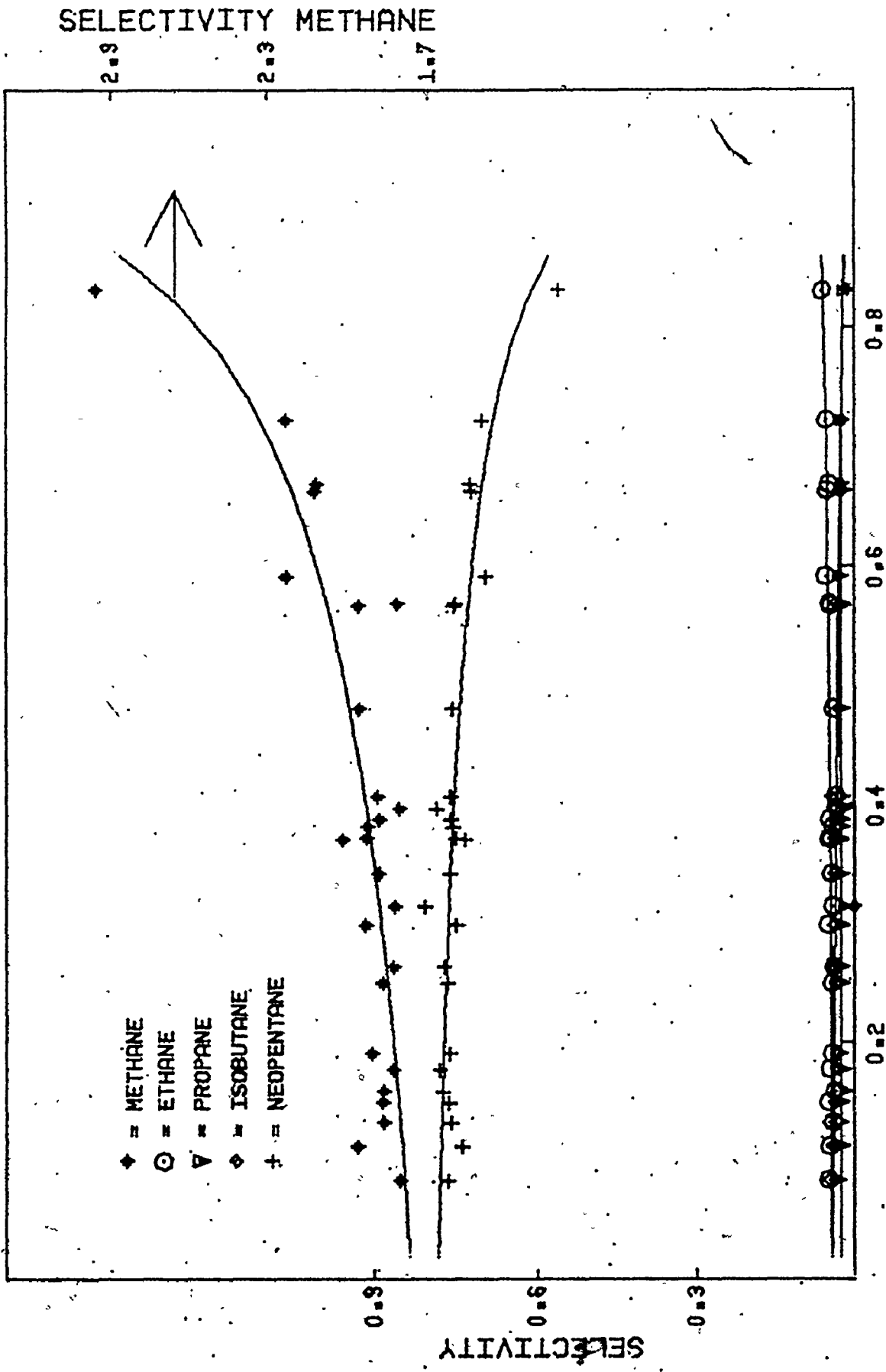
Figure 5-7 Product Distribution Of Hydrogenolysis of 2,2-Dimethylbutane over Co-Mg/SiC at 245°C and 1.2 atm.

Table 5-4

Analysis of Hydrogenolysis of 2,2-Dimethylbutane over Cobalt

Equations (5-1) through (5-6)

Parameter	Estimated value Co-Mg/SiC(245°C.)
$\dfrac{k'_{ne5}\ \ell}{k'_{ne5}+k^{*}_{ne5}}$	0.78 ±0.02
k''_{ne5}/k''_{6}	0.06 ±0.02
$\dfrac{k'_{i4}}{k'_{i4}+k^{*}_{i4}}$	0.19 ±0.03
k''_{i4}/k''_{6}	0.64 ±0.03
$\dfrac{k'_{3}}{k'_{3}+k^{*}_{3}}$	0.14 ±0.01
$k''_{3}\ /k''_{6}$	0.30 ±0.08
$\dfrac{k'_{2}}{k'_{2}+k^{*}_{2}}$	0.11 ±0.04
ℓ	0.8 ±0.1
$k''_{2}\ /k''_{6}$	0.02

$$\text{C} \underline{\quad} \text{C} \xrightarrow{\text{II}} \text{C} \xrightarrow{\text{I}} \text{C}$$

(with C groups below)
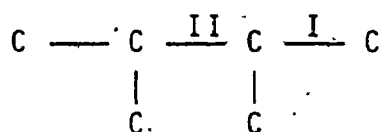
Cracking of bond II yields propane, which can crack further to ethane and methane.

Breaking of bond type I gives methane and isopentane. Isopentane has three different bond types itself and can yield n-butane and i-butane plus propane, ethane and methane. On ruthenium i-pentane gave mainly i-butane (47). 2,3-Dimethylbutane over nickel yielded i-pentane and methane only at low conversion (51), while on Pt substantial amounts of propane were also obtained and isomerisation to 2,2-dimethylbutane also occurred. Branched chain hydrocarbons were shown to be more reactive than the corresponding straight paraffins over nickel (55).

The proposed reaction scheme and the corresponding rate constants and splitting factors are shown in fig. 5-8; the derivation of the selectivity equations and the physical significance of the parameters are discussed in appendix C.3. The analytical results are:

$$S_{i5} = \frac{k'_{i5}\ell \; / \; (k'_{i5} + k^*_{i5})}{1 + (k''_{i5} \; / \; k''_6)\{ \; x/(1-x) \; \}} \tag{5-8}$$

$$S_{i4} = \frac{\{k'_{i4} \; / \; (k'_{i4} + k^*_{i4})\} \quad f(\ell - S_{i5})}{1 + (k''_{i4} \; / \; k''_6)\{ \; x/(1-x) \; \}} \tag{5-9}$$

$$S_{n4} = \frac{\{k'_{n4} / (k'_{n4} + k^*_{n4})\}\{ f' \, (\ell - S_{i5}) \}}{1 + \{k''_{n4} / k''_6\}\{ x/(1-x) \}} \qquad (5\text{-}10)$$

$$S_3 = \frac{\dfrac{k'_3}{(k'_3 + k^*_3)} \{ 2 - \ell (1 + mf') - S_{i4} - S_{n4}(1-m) - S_{i5}(1 - mf') \}}{1 + \{k''_3 / k''_6\}\{ x/(1-x) \}} \qquad (5\text{-}11)$$

$$S_2 = \frac{\dfrac{k'_2}{(k'_2 + k^*_2)} \{ 2 - \ell (f + f' - mf') - S_3 - S_{i4} - S_{n4}(1+m) - S_{i5} (2 + mf' - f - f') \}}{1 + \{k''_2 / k''_6\}\{ x/(1-x) \}} \qquad (5\text{-}12)$$

$$S_1 + 2S_2 + 3S_3 + 4(S_{n4} + S_{i4}) + 5S_{i5} = 6 \qquad (5\text{-}13)$$

where x = fractional conversion of 2,3-dimethylbutane

S_x = selectivity of product x

k = rate constants as defined in fig. 5-8

The maximum possible values for the selectivities are 1.0 for i-pentane and the butanes, 2.0 for propane and ethane, and 6.0 for methane. No products of isomerisation or chain growth reactions were observed during the experiments with 2,3-dimethylbutane.

$$C_6 \underset{k_6'}{\overset{k_6}{\rightleftarrows}} A_6 \qquad i\text{-}C_5 \underset{k_{i5}'}{\overset{k_{i5}}{\rightleftarrows}} i\text{-}A_5 \qquad i\text{-}C_4 \underset{k_{i4}'}{\overset{k_{i4}}{\rightleftarrows}} i\text{-}A_4$$

$$C_1 \underset{k_1'}{\overset{k_1}{\rightleftarrows}} A_1 \qquad C_2 \underset{k_2'}{\overset{k_2}{\rightleftarrows}} A_2 \qquad C_3 \underset{k_3'}{\overset{k_3}{\rightleftarrows}} A_3 \qquad n\text{-}C_4 \underset{k_{n4}'}{\overset{k_{n4}}{\rightleftarrows}} n\text{-}A_4$$

$$A_6 \xrightarrow{k_6^*} \begin{cases} \xrightarrow{\ell} & i\text{-}A_5 + A_1 \\ \xrightarrow{(1-\ell)} & 2\,A_3 \end{cases}$$

$$i\text{-}A_5 \xrightarrow{k_{i5}^*} \begin{cases} \xrightarrow{f} & i\text{-}A_4 + A_1 \\ \xrightarrow{f'} & n\text{-}A_4 + A_i \\ \xrightarrow{(1-f-f')} & A_3 + A_2 \end{cases}$$

$$i\text{-}A_4 \xrightarrow{k_{i4}^*} A_3 + A_1$$

$$n\text{-}A_4 \xrightarrow{k_{n4}^*} \begin{cases} \xrightarrow{m} & 2\,A_2 \\ \xrightarrow{(1-m)} & A_3 + A_1 \end{cases}$$

$$A_3 \xrightarrow{k_3^*} A_2 + A_1$$

$$A_2 \xrightarrow{k_2^*} 2\,A_1$$

C_x = gaseous hydrocarbon, carbon number x

A_x = adsorbed hydrocarbon species

k_x = adsorption rate constant k_x' = desorption rate constant

k_x^* = surface cracking rate constant $k_x'' = k_x\, k_x^* /(k_x' + k_x^*)$

Figure 5-8 Reaction Network for Hydrogenolysis of 2,3-DMB

The iron catalyst, FeMg/SiO$_2$, gave almost only methane, selectivities ranging from 4.3 to 5.8, no isopentane or butanes were observed at all, and only traces of propane and some ethane. The activity of the iron catalyst was nearly constant, but also rather small: the temperature required was 280-340°C. The large yield of methane indicates that the adsorbed species crack much faster than they desorb, this may be due partly to the high temperature.

5.3.2 2,3-Dimethylbutane over Ruthenium

The experimental data are expressed in terms of selectivities of the products and conversion of 2,3-dimethylbutane and are tabulated in table D-13. All experiments were performed at a total pressure of 1.20 atm and at 200°C. Plots of the product distribution as a function of conversion are shown in fig. 5-9. Only traces of n-butane were detected during the experiments with ruthenium, too small to be measured. These experiments agree with results of Kempling (44, 47) that isopentane cracks mainly to isobutane and only a small fraction forms n-butane. The ratio isobutane/n-butane appears to be even larger here. The main product was methane, increasing with increasing conversion. The selectivity for i-pentane decreases with increasing conversion as expected, those of i-butane and ethane increase. The i-butane selectivity levels off at high conversion and was expected to exhibit a maximum, but this occurred outside the range of the experimental conversions. The propane selectivity is remark-
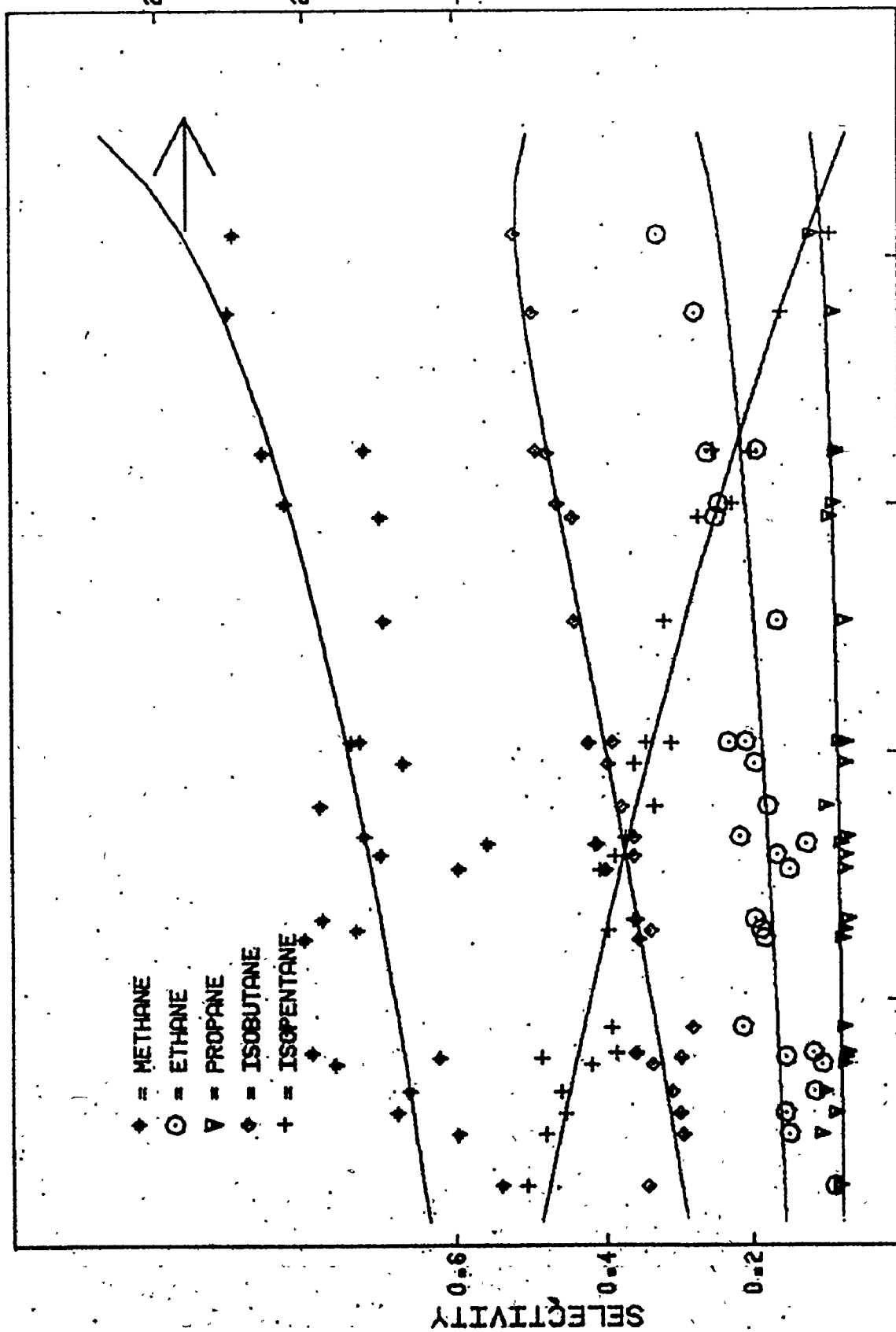
Figure 5-9 Product Distribution of Hydrogenolysis of 2,3-Dimethylbutane over Ru/Al$_2$O$_3$ at 200°C and 1.2 atm.

ably low, indicating that little, if any, cracking occurs at the centre bond (II). Selectivity equations (5-8) through (5-13) were applied to the experimental data using nonlinear regression techniques.

The selectivity data for pentane, butane, propane, and ethane were fitted consecutively to the equations using the predicted values of the selectivities of the larger molecules in the equations of the smaller ones. Initial values for the i-pentane equation were obtained from the plots of $1/S_{i5}$ versus $x/(1-x)$, in case of the other equations a grid search was used. The calculated selectivities are the solid lines in fig. 5-9, and the estimated parameters with their 95% confidence limits are shown in table 5-5. The goodness of fit is indicated in fig. 5-10, where the calculated and experimental selectivities are plotted. Methane was omitted because the scale is very different. As explained in appendix B.2, the confidence limits become large for the final equations: for S_3 and especially for S_2; the ethane data could not be fitted well as is also clear from fig. 5-10. The average deviations between calculated and experimental selectivities will be shown in section 5.5. Of the products, only isopentane reacts at a comparable rate with the feed hydrocarbon, the other products are much less reactive.

5.3.3 2,3-Dimethylbutane over Nickel

The experimental data are tabulated in tables D-19 and D-16 for the NiMg/SiC and Ni/SiC catalysts, respectively.

Table 5-5

Analysis of Hydrogenolysis of 2,3-Dimethylbutane over Ruthenium

Equations (5-8) through (5-13)

Parameter	Estimated value Ru/Al_2O_3 (200^{0}C)
$\dfrac{k'_{i5}\,\ell}{k'_{i5}+k^*_{i5}}$	0.49 ±0.03
k''_{i5}/k''_6	0.68 ±0.15
$\dfrac{k'_{i4}\,f}{k'_{i4}+k^*_{i4}}$	0.79 ±0.22
k''_{i4}/k''_6	0.03 ±0.03
ℓ	0.85 ±0.09
$\dfrac{k'_3}{k'_3+k^*_3}$	0.22 ±0.16
k''_3/k''_6	0.001±0.08
$\dfrac{k'_2}{k'_2+k^*_2}$	0.37
k''_2/k''_6	$3*10^{-5}$
$f+f'$	0.70
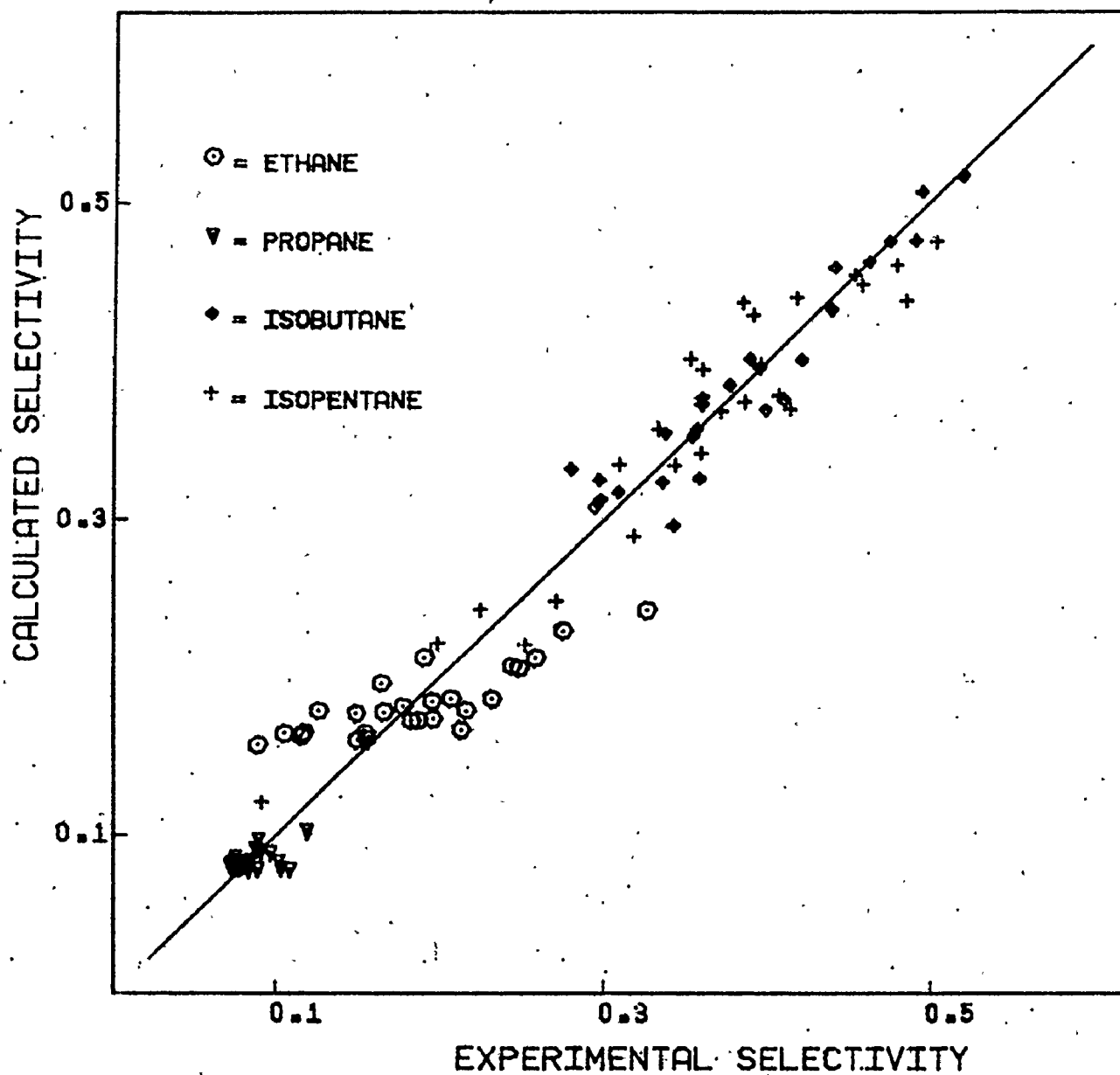
Figure 5-10   Experimental versus Calculated Selectivities
in the Hydrogenolysis of 2,3-Dimethylbutane over
Ru/Al_2O_3 at 200^OC and 1.2 atm.

The experiments were carried out at 245°C with the promoted catalyst, at 260°C with the unpromoted one. Fig. 5-11 and fig. 5-12 show the product distributions as a function of conversion of 2,3-dimethylbutane.

The data were fitted to the selectivity equations (5-8) through (5-13); the estimated parameter values are tabulated in table 5-6, and fig. 5-13 and fig. 5-14 show the goodness of fit in the form of plots of calculated versus experimental selectivities. The fit was much better than for ruthenium, the average deviation between calculated and experimental selectivities never exceeds 8%. Calculated selectivities are indicated in fig. 5-11 and fig. 5-12 as solid lines. The most remarkable observation is that there is a substantial amount of n-butane from both catalysts. The ratio n-butane/isobutane approaches unity at higher conversions on the promoted catalyst, while on the unpromoted one the amount of n-butane exceeds that of isobutane, the ratio varying from 4.0 to 7.0. The selectivity for n-butane passes through a maximum when plotted versus conversion, while that of isobutane is rather constant with conversion. The amount of methane produced is slightly larger on the unpromoted catalyst, and the amount of i-pentane is slightly lower; this may be due to the difference in temperature required. The selectivities for propane are also substantially larger than for the ruthenium catalyst. The values in table 5-6 indicate that the rates of surface cracking and desorption of the adsorbed surface spe-
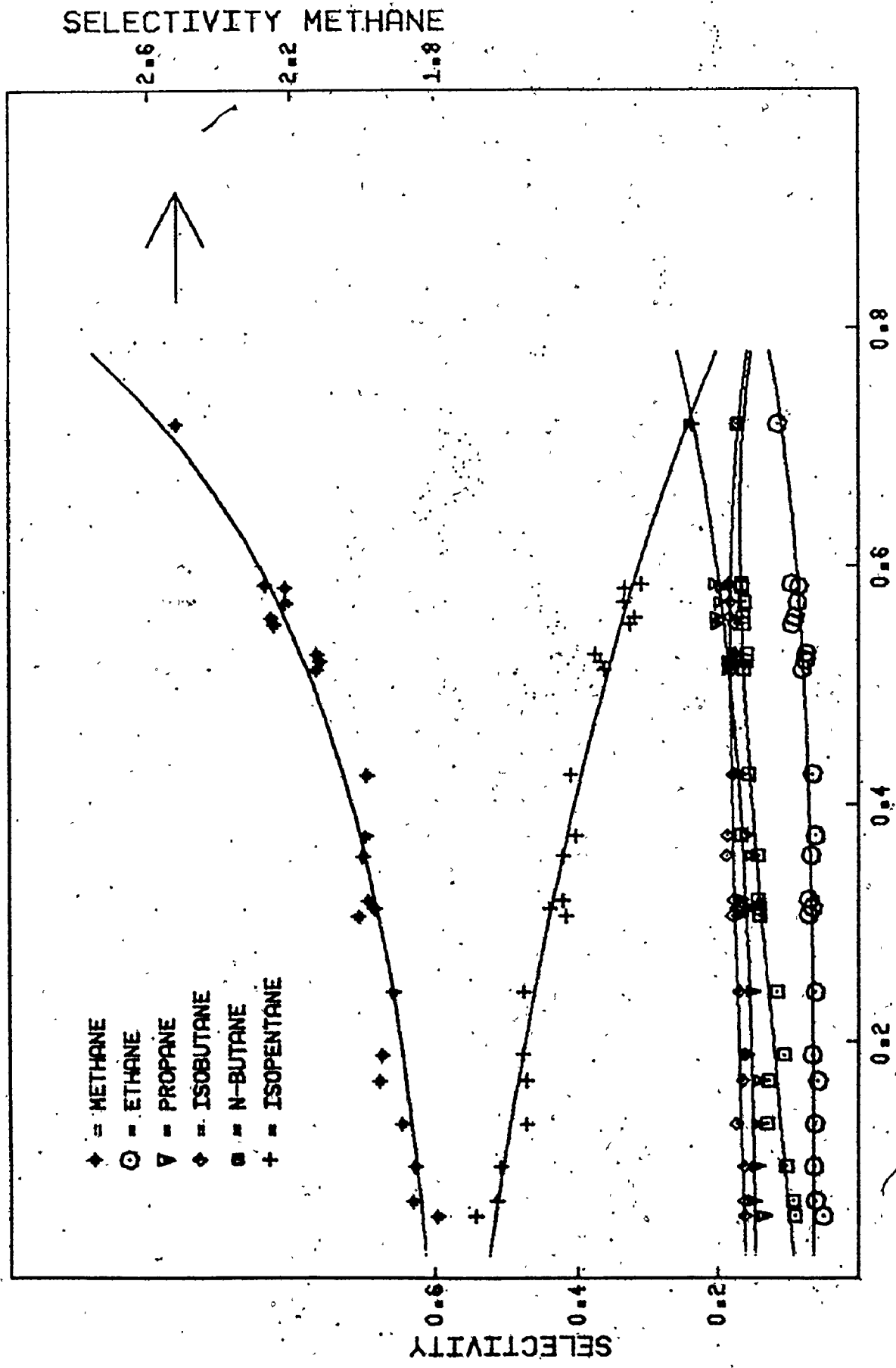
Figure 5-11. Product Distribution of Hydrogenolysis of 2,3-Dimethylbutane over Ni-Mg/SiC at 245°C and 1.2 atm.
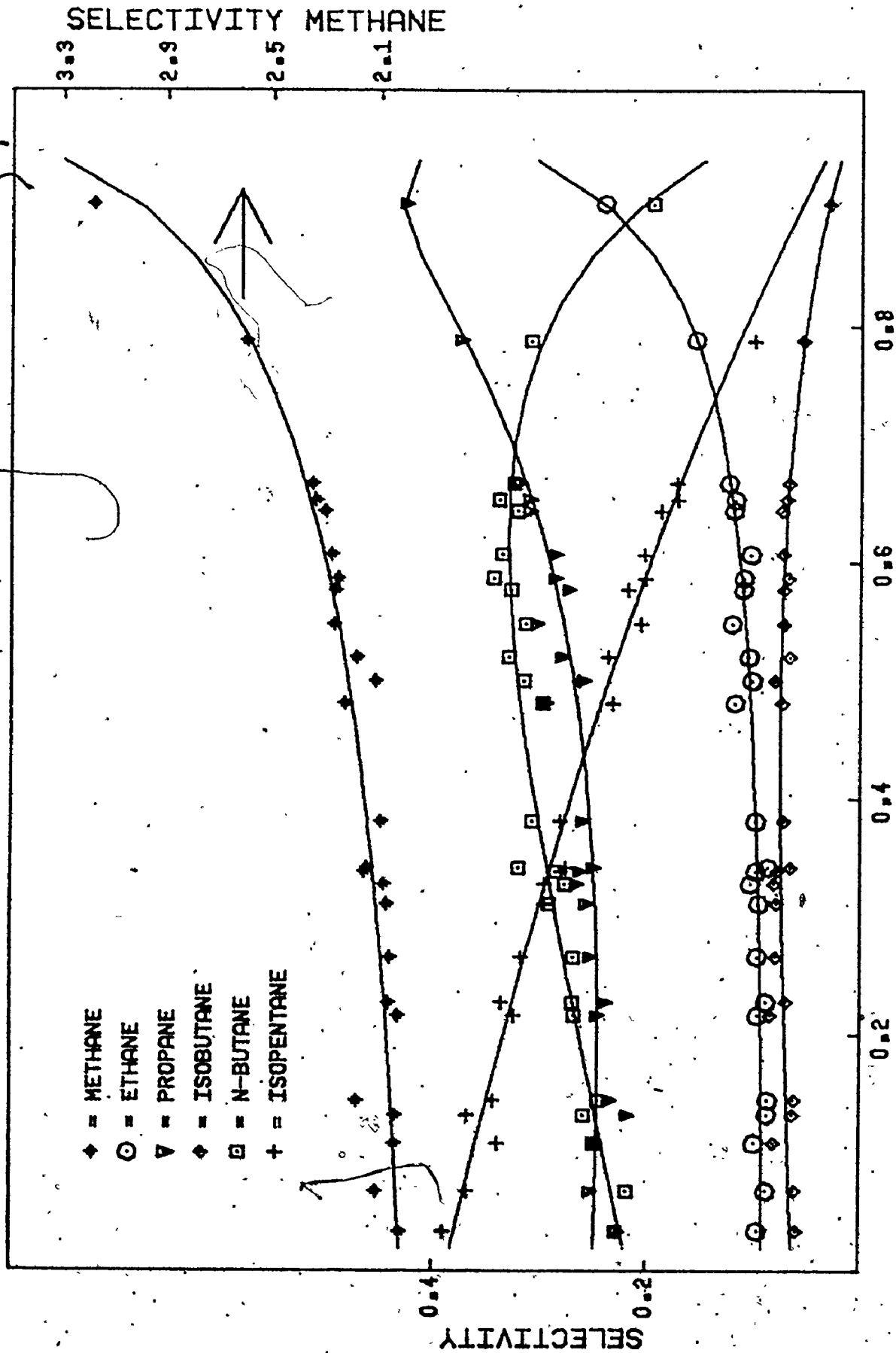
Figure 5-12 Product Distribution of Hydrogenolysis of 2,3-Dimethylbutane over
Ni/SiC at 260°C and 1.2 atm.

Table 5-6

Analysis of Hydrogenolysis of 2,3-Dimethylbutane over Nickel
Equations (5-8) through (5-13)

Parameter	Estimated value	
	Ni-Mg/SiC(245°C)	Ni/SiC(260°C)
$\dfrac{k'_{i5} \ell}{k'_{i5} + k^*_{i5}}$	0.53 ±0.02	0.39 ±0.01
k''_{i5}/k''_6	0.46 ±0.06	0.65 ±0.05
$\dfrac{k'_{n4} f'}{k'_{n4} + k^*_{n4}}$	0.79 ±0.32	0.50 ±0.02
k''_{n4}/k''_6	0.37 ±0.25	0.08 ±0.03
ℓ	0.64 ±0.06	0.9
$\dfrac{k'_{i4} f}{k'_{i4} + k^*_{i4}}$	0.39 ±0.18	0.13 ±0.01
k''_{i4}/k''_6	0.23 ±0.13	0.23 ±0.06
ℓ	0.93 ±0.2	
$k'_3/(k'_3 + k^*_3)$	0.5	0.55 ±0.11
k''_3/k''_6	0.03	0.01 ±0.01
$m f'$	0.	0. ±0.1
m	0.16 ±0.78	0.
$k'_2/(k'_2 + k^*_2)$	0.41 ±0.85	0.60 ±0.06
k''_2/k''_6	0.005	0.001±0.02
$f+f'$	0.99 ±1.25	0.98 ±0.05
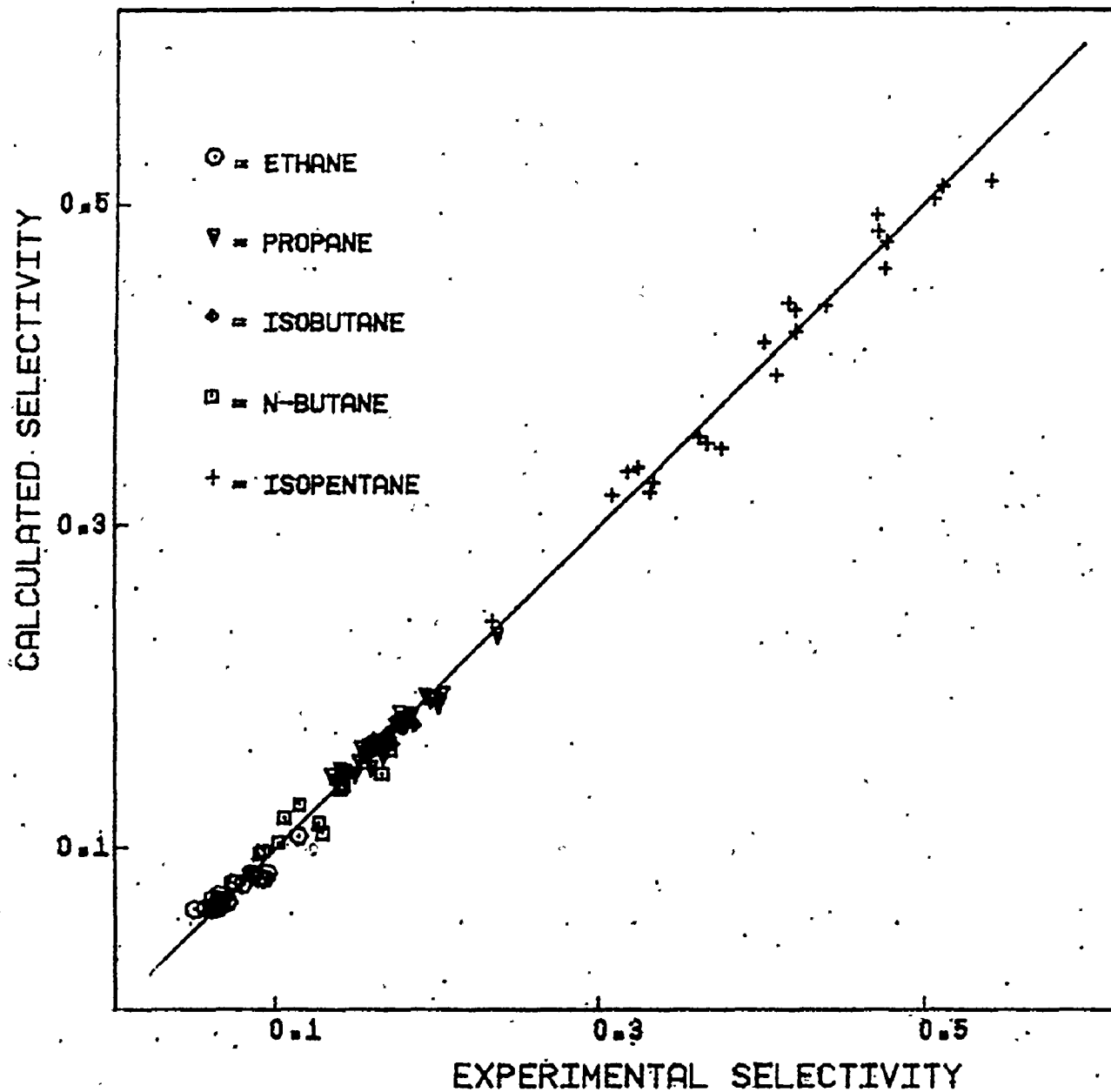
Figure 5-13   Calculated versus Experimental Selectivities
in the Hydrogenolysis of 2,3-Dimethylbutane over
Ni-Mg/SiC at 245°C and 1.2 atm.
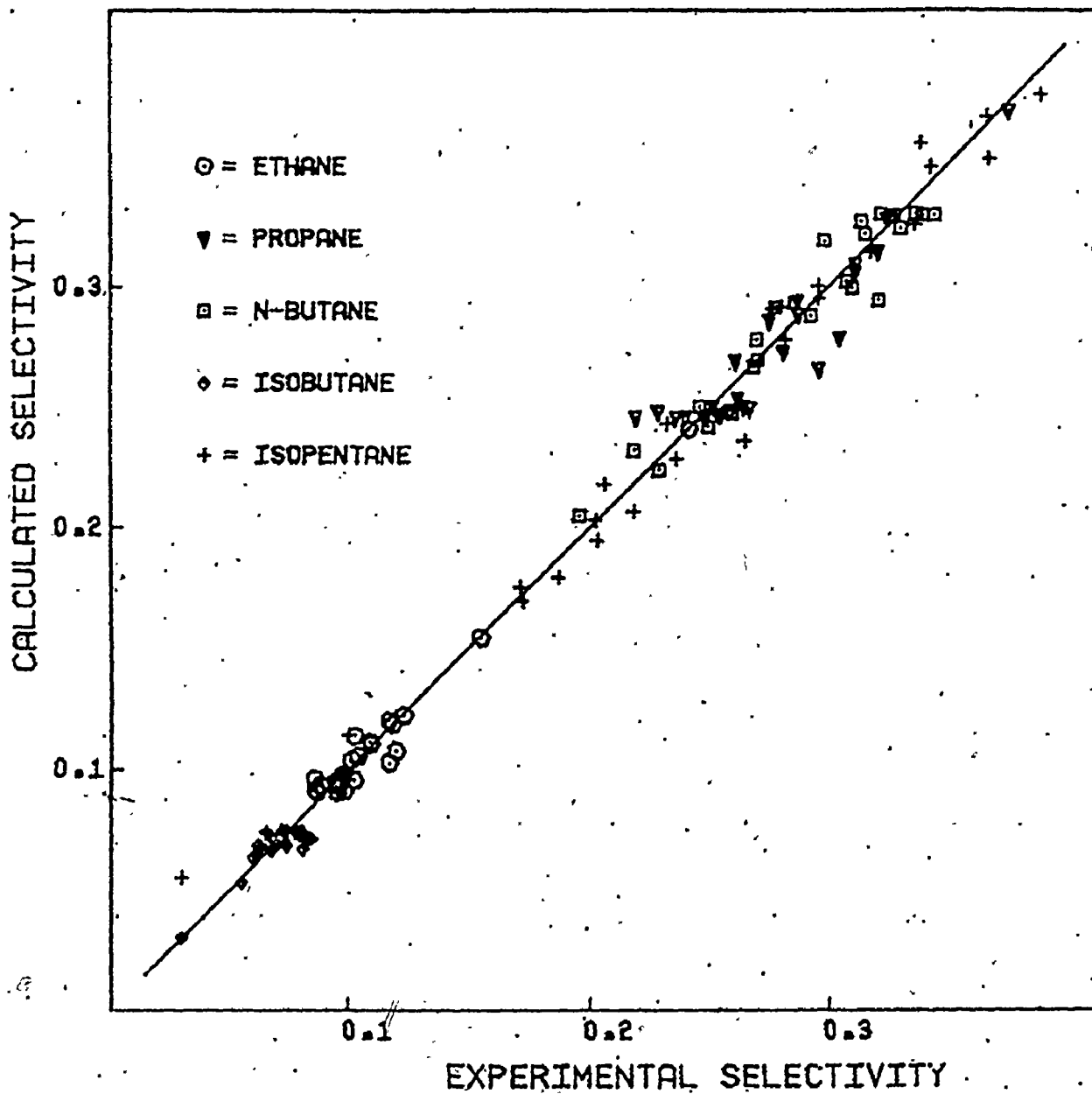
Figure 5-14: Calculated versus Experimental Selectivities in the Hydrogenolysis of 2,3-Dimethylbutane over Ni/SiC at 260°C and 1.2 atm.

cies are about equal.

The fact that the amount of n-butane equals or exceeds that of i-butane may be explained in two ways: a) i-pentane prefers to react to n-butane rather than to isobutane, i.e., the splitting factors are different; b) i-butane reacts faster than n-butane, leaving more n-butane in the products. It had been suggested (55) that branched chains are more reactive than the corresponding straight ones. The change of the selectivities as a function of conversion suggests that the second way may be the most important one in this case. In any case, these results are very different from the ones obtained with ruthenium in section 5.3.2 and with isopentane on ruthenium (44, 47).

A few experiments were performed at other temperatures as shown in table 5-7, in order to observe the effect of temperature on the product distribution for both catalysts. The promoted catalyst is more active than the unpromoted one. The ratio n-butane/isobutane increases with increasing temperature for both catalysts, but it is always higher for the unpromoted catalyst.

To compare the results with Kempling's work on isopentane over ruthenium, a few experiments were carried out over NiMg/SiC using isopentane, mainly at 248°C. The results are tabulated in table D-10. The product distribution as a function of conversion is shown in fig. 5-15, and a few selectivity curves at different temperatures in fig. 5-16.

Table 5-7

Product Distribution from Hydrogenolysis of 2,3-Dimethylbutane

over Nickel at other Temperatures

Ni-Mg /SiC							Temp.	Ni /SiC						
S_1	S_2	S_3	S_{i4}	S_{n4}	S_{i5}	x	$(^\circ C)$	x	S_{i5}	S_{n4}	S_{i4}	S_3	S_2	S_1
2.19	0.08	0.20	0.16	0.16	0.35	0.45	250	0.23	0.41	0.28	0.08	0.18	0.06	1.83
2.87	0.17	0.27	0.12	0.17	0.16	0.71	260	0.45	0.22	0.34	0.06	0.29	0.10	2.23
3.72	0.23	0.29	0.06	0.11	0.05	0.86	270	0.70	0.08	0.29	0.04	0.39	0.18	2.78
4.62	0.27	0.20	0.02	0.04	-	0.94	280	0.84	0.02	0.15	0.02	0.38	0.27	3.54

163
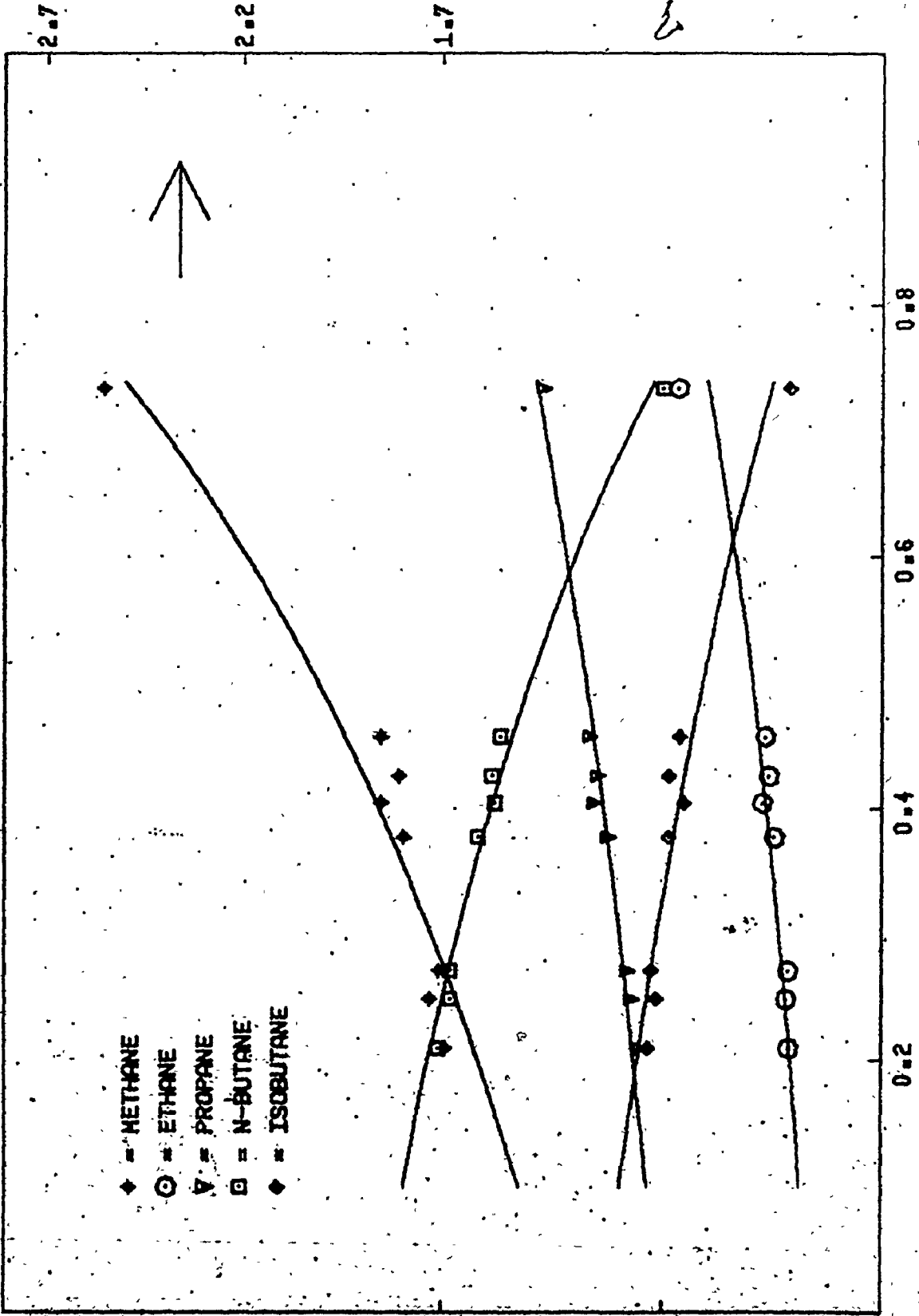
Figure 5-15 Product Distribution of Hydrogenolysis of Isopentane over Ni-Mg/SiC at 248°C and 1.2 atm.

165
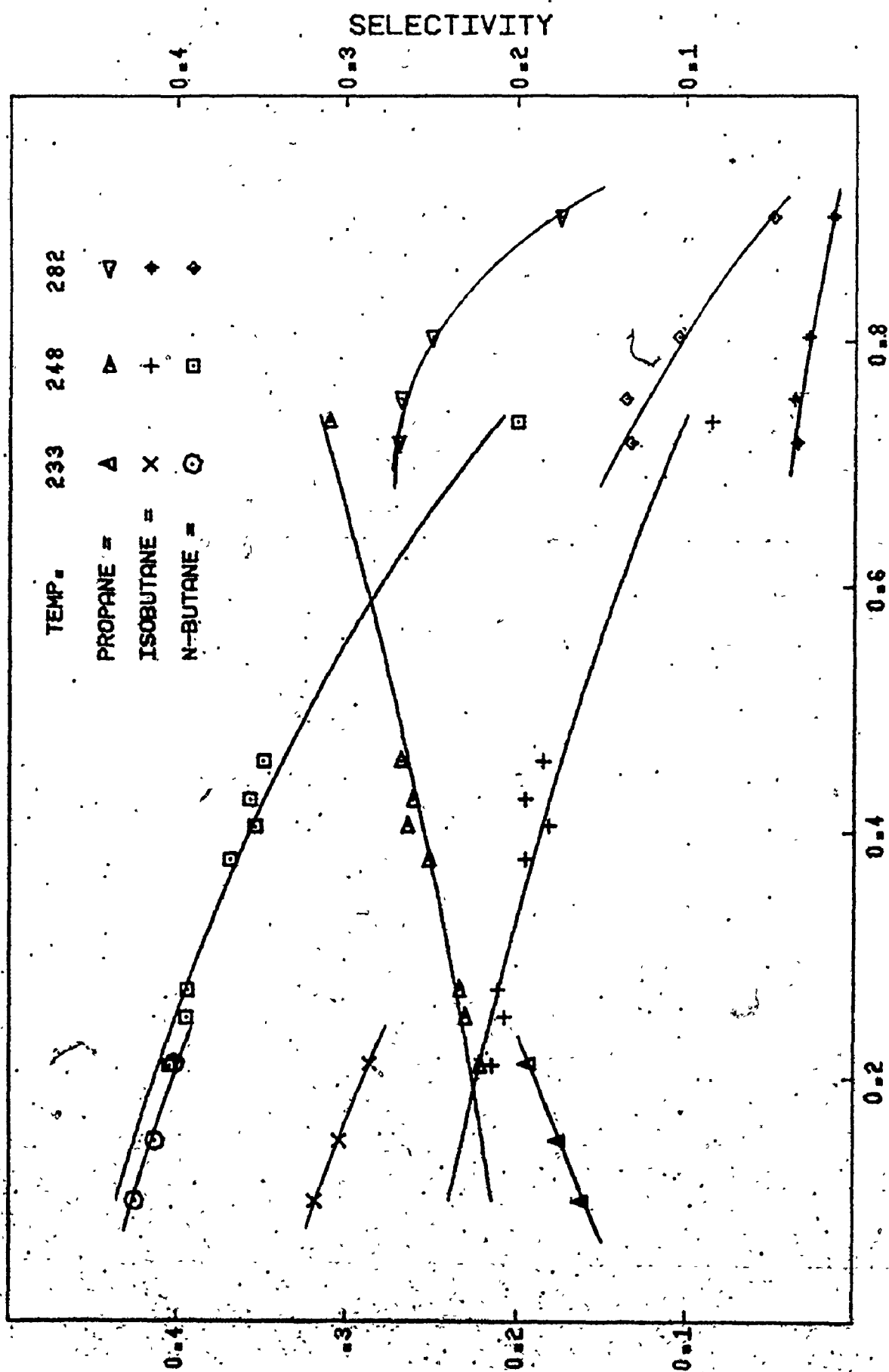
Figure 5-16. Product Distribution of Hydrogenolysis of Isopentane over Ni-Mg/SiC at other Temperatures and 1.2 atm.

Selectivity equations derived by Kempling (44), and similar
to the ones used in this chapter, were applied to the data at
248°C; the estimated parameter values are shown in table 5-8,
and the solid curves in fig. 5-15 are the calculated values
using the obtained parameters. The confidence limits for the
parameters from S_3 and S_2 were very large. The results in fig.
5-15 and fig. 5-16 agree with those of 2,3-dimethylbutane. The
selectivity of n-butane exceeds that of isobutane, and their
ratio seems to increase with increasing temperature. The a-
mount of propane obtained is also substantial. The fact that
the selectivities of both butanes change in about the same way
as conversion increases, suggests that splitting factors are
responsible for the large amount of n-butane produced.

5.3.4 2,3-Dimethylbutane over Cobalt

The experimental data are given in table D-22; the
experiments were carried out at 227°C. Fig. 5-17 is a plot of
the product distribution versus the conversion of 2,3-dime-
thylbutane. In agreement with the results for propane on co-
balt, the amount of small products is large: large amounts of
methane are produced and ethane is the second most abundant
product. The selectivity of isopentane is low compared to the
ruthenium and nickel catalysts. The amounts of n-butane and
isobutane are again approximately equal, the splitting fac-
tors for cobalt seem to be similar to those of nickel.

Equations (5-8) through (5-13) were applied to these

Table 5-8

Analysis of Hydrogenolysis of i-Pentane over Nickel

Equations from Kempling(44)

Parameter	Estimated value Ni-Mg/SiC(248°C)
$k'_{i4}\, f\, /(k'_{i4}+k^*_{i4})$	0.25 ± 0.03
$k''_{i4}\, /k''_{i5}$	0.55 ± 0.22
$k'_{n4}\, f'/(k'_{n4}+k^*_{n4})$	0.46 ± 0.02
$k''_{n4}\, /k''_{i5}$	0.42 ± 0.07

SELECTIVITY METHANE
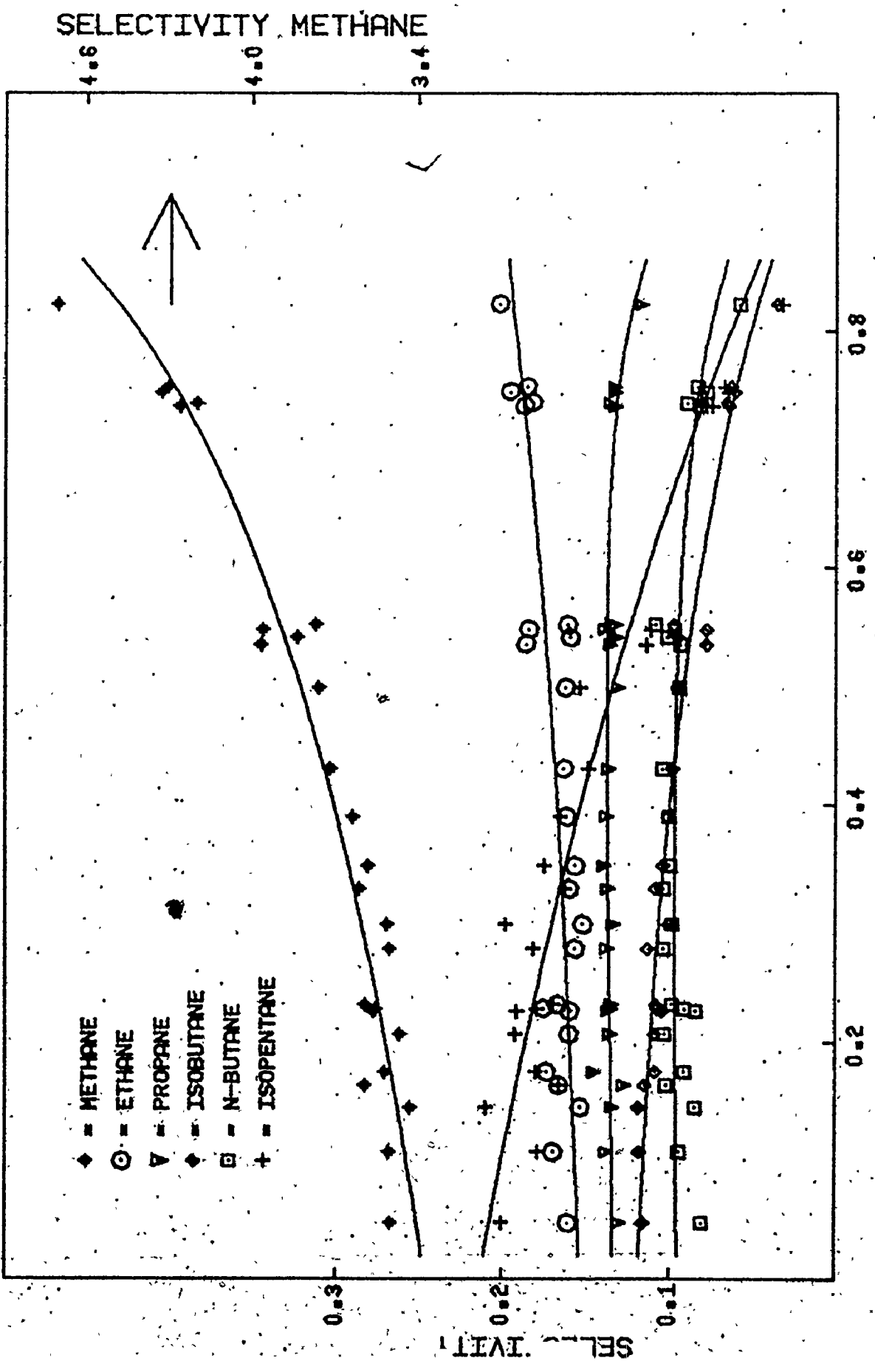
FRACTIONAL CONVERSION OF 2,3-DIMETHYLBUTANE

Figure 5-17 Product Distribution of Hydrogenolysis of 2,3-Dimethylbutane over
Co-Mg/SiC at 227°C and 1.2 atm.

Legend:
◆ = METHANE
⊙ = ETHANE
▽ = PROPANE
◆ = ISOBUTANE
⊡ = N-BUTANE
+ = ISOPENTANE

Table 5-9

Analysis of Hydrogenolysis of 2,3-Dimethylbutane over Cobalt

Equations (5-8) through (5-13)

Parameter	Estimated value Co-Mg/SiC(227°C)
$k'_{i5}\ \ell/(k'_{i5}+k^{*}_{i5})$	$0.21\ \pm0.01$
k''_{i5}/k''_{6}	$0.60\ \pm0.12$
$k'_{n4}\ f'/(k'_{n4}+k^{*}_{n4})$	$0.19\ \pm0.01$
k''_{n4}/k''_{6}	$0.16\ \pm0.03$
$k'_{i4}\ f\ /(k'_{i4}+k^{*}_{i4})$	$0.24\ \pm0.07$
k''_{i4}/k''_{6}	0.5
ℓ	$0.71\ \pm0.17$
$k'_{3}/(k'_{3}+k^{*}_{3})$	$0.15\ \pm0.01$
k''_{3}/k''_{6}	$0.09\ \pm0.01$
$m\ f'$	$0.$
$k'_{2}/(k'_{2}+k^{*}_{2})$	$0.21\ \pm0.01$
k''_{2}/k''_{6}	$0.02\ \pm0.01$

solid lines in fig. 5-17 are the calculated selectivities.
Fig. 5-18 is a plot of calculated versus experimental selec-
tivities; the agreement is good, average deviations not ex-
ceeding 10%. Values in table 5-9 show that the rates of
cracking of the adsorbed species are greater than the rates
of desorption; this situation was also observed for propane
on cobalt. A few experiments at other temperatures showed
that, similar to nickel, the ratio -n-butane/isobutane- in-
creases with increasing temperature. The selectivity for
both butanes decreases as the temperature is increased from
200°C to 240°C, but the i-butane selectivity decreases much
more rapidly.

5.4 n-Hexane

5.4.1 Introduction

n-Hexane has three different types of carbon-carbon
bonds:

$$C \rule{1em}{0.4pt} C \rule{1em}{0.4pt} C \underline{\;III\;} C \underline{\;II\;} C \underline{\;I\;} C$$

Cracking of bond type III yields propane which can crack
further to ethane and methane. Type II gives ethane and
n-butane, both of which can react further. Breaking of bond I
gives methane and n-pentane which can react further to give
all the products mentioned above. On nickel primarily succes-
sive demethylation takes place at terminal carbon-carbon
bonds to give methane and a hydrocarbon with one less car-
bon atom which will react further in the same way (α-scis-
sion).
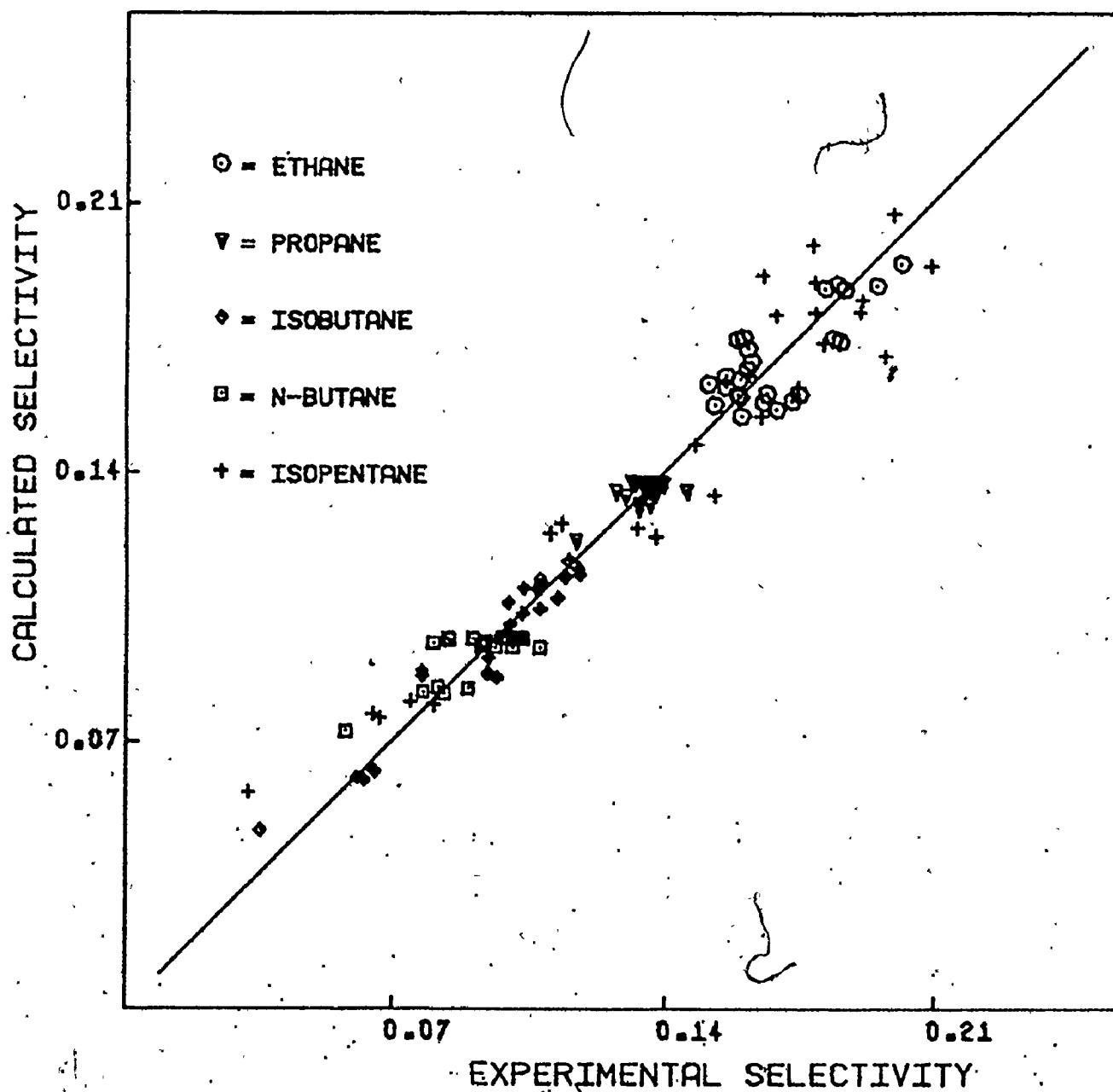
Figure 5-18: Calculated versus Experimental Selectivities in the Hydrogenolysis of 2,3-Dimethylbutane over Co-Mg/SiC at 227°C and 1.2 atm.

Such was the case with n-pentane (53, 54), n-hexane (51, 125), octane and decane (55). At high temperature and low hydrogen pressure, more extensive cracking took place to give smaller molecules (53). On most of the metals of the platinum group the bonds seemed to break almost statistically, and on Pt and Pd isomerisation and cyclisation took place as well. Cobalt and iron gave mainly methane as the product (54); the mechanism could not be deduced with certainty because desorption of products was slower than the cracking, but there were indications that successive terminal demethylation occurred on these metals as well. A similar pattern was observed for Pd and Rh with n-heptane (120); ruthenium was less selective.

The proposed reaction scheme and corresponding rate- and splitting constants are shown in fig. 5-19; the derivation of the selectivity equations is discussed in appendix C.5, the analytical results are:

$$S_{n5} = \frac{k'_{n5} \ell / (k'_{n5} + k^*_{n5})}{1 + (k^n_{n5} / k''_6)\{x/(1-x)\}} \qquad (5\text{-}14)$$

$$S_{n4} = \frac{\{k'_{n4} / (k'_{n4} + k^*_{n4})\}\{\ell' + f\ell - fS_{n5}\}}{1 + (k''_{n4} / k''_6)\{x/(1-x)\}} \qquad (5\text{-}15)$$

$$C_6 \underset{k_6'}{\overset{k_6}{\rightleftarrows}} A_6 \qquad n\text{-}C_5 \underset{k_{n5}'}{\overset{k_{n5}}{\rightleftarrows}} n\text{-}A_5 \qquad n\text{-}C_4 \underset{k_{n4}'}{\overset{k_{n4}}{\rightleftarrows}} n\text{-}A_4$$

$$C_1 \underset{k_1'}{\overset{k_1}{\rightleftarrows}} A_1 \qquad C_2 \underset{k_2'}{\overset{k_2}{\rightleftarrows}} A_2 \qquad C_3 \underset{k_3'}{\overset{k_3}{\rightleftarrows}} A_3$$

$$A_6 \xrightarrow{k_6^*} \begin{cases} \xrightarrow{\ell} & n\text{-}A_5 + A_1 \\ \xrightarrow{\ell'} & n\text{-}A_4 + A_2 \\ \xrightarrow{(1-\ell-\ell')} & 2\,A_3 \end{cases}$$

$$n\text{-}A_5 \xrightarrow{k_{n5}^*} \begin{cases} \xrightarrow{f} & n\text{-}A_4 + A_1 \\ \xrightarrow{(1-f)} & A_3 + A_2 \end{cases}$$

$$n\text{-}A_4 \xrightarrow{k_{n4}^*} \begin{cases} \xrightarrow{m} & 2\,A_2 \\ \xrightarrow{(1-m)} & A_3 + A_1 \end{cases}$$

$$A_3 \xrightarrow{k_3^*} A_2 + A_1$$

$$A_2 \xrightarrow{k_2^*} 2\,A_1$$

C_x = gaseous hydrocarbon, carbon number x

A_x = adsorbed hydrocarbon species

k_x = adsorption rate constant

k_x' = desorption rate constant

k_x^* = surface cracking rate constant

k_x'' = $k_x\, k_x^* /(k_x^* + k_x')$

Figure 5-19 <u>Reaction Network for Hydrogenolysis of n-C$_6$</u>

$$S_3 = \frac{\dfrac{k_3'}{(k_3' + k_3^*)} \{ 2 - \ell - \ell' - m\ell' - mf\ell - S_{n4}(1-m) - S_{n5}(1-mf) \}}{1 + (k_3''/k_6'')\{ x/(1-x) \}} \tag{5-16}$$

$$S_2 = \frac{\dfrac{k_2'}{(k_2' + k_2^*)} \{ 2 - f\ell + m\ell' + mf\ell - S_3 - S_{n4}(1+m) - S_{n5}(2+mf-f) \}}{1 + (k_2''/k_6'')\{ x/(1-x) \}} \tag{5-17}$$

$$S_1 + 2S_2 + 3S_3 + 4S_{n4} + 5S_{n5} = 6 \tag{5-18}$$

where x = conversion of n-hexane

S_x = selectivity of product x

k = rate constants as defined in fig. 5-19

Maximum possible values for the selectivities of n-pentane, n-butane, propane, ethane, and methane are 1.0, 1.0, 2.0, 3.0, and 6.0, respectively. No products of chain growth and isomerisation reactions were observed during the experiments with n-hexane.

The iron catalyst, FeMg/SiO$_2$, yielded almost exclusively methane, with small amounts of ethane and propane, traces of n-butane, but no n-pentane.

The catalyst activity was nearly constant and low, temperatures had to be at least 270°C to observe any reaction.

5.4.2   n-Hexane over Ruthenium

The experimental data, expressed in terms of selectivities of the products and conversion of n-hexane are tabulated in table D-14. The experiments were performed at 1.20 atm total pressure and at 149°C. Fig. 5-20 is a plot of the product distribution as a function of conversion of n-hexane. All the possible products are present, and it appears that the cracking of the different bonds is almost statistically: at low conversion the selectivity of all products is almost equal, except for methane. At higher conversion more of the smaller products are obtained: methane, ethane and propane. Selectivity equations (5-14) through (5-18) were applied to these data, the estimated parameters are tabulated in table 5-10, with their approximate 95% confidence limits; the solid curves in fig. 5-20 are the calculated values. Fig. 5-21 is a plot of the calculated versus the experimental selectivities and it indicates the goodness of fit. Average deviations do not exceed 4%. From the values in table 5-10 it appears that the rate of surface cracking of the adsorbed species is much lower than the rate of desorption, as is common on ruthenium in the other experiments. The rate of reaction decreases rapidly as the length of the carbon chain decreases.

A few experiments were carried out at other temperatures to check the dependence of the product distribution on
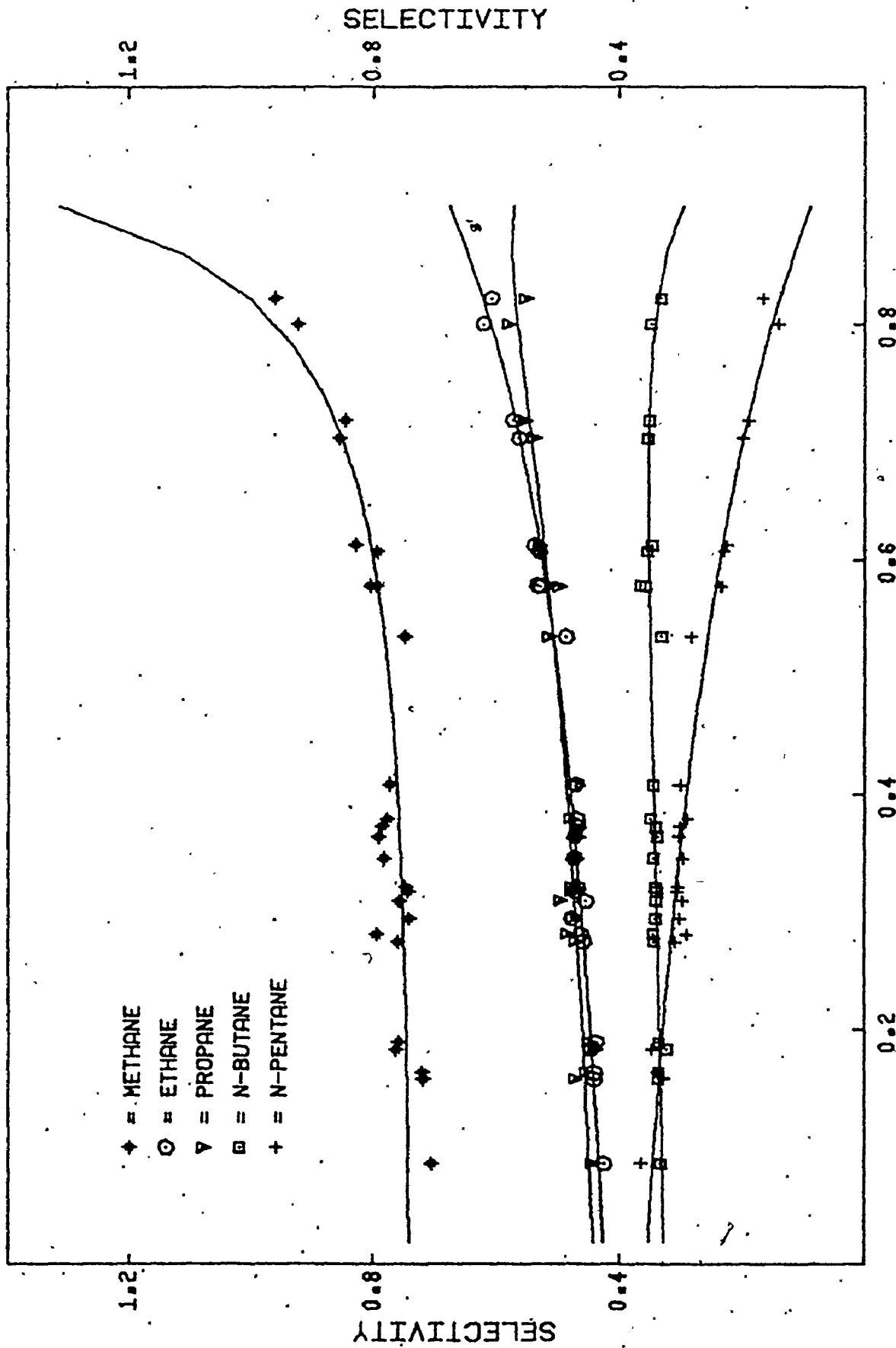
Figure 5-20 Product Distribution of Hydrogenolysis of n-Hexane over
Ru/Al$_2$O$_3$ at 149°C and 1.2 atm.

Table 5-10

Analysis of Hydrogenolysis of n-Hexane over Ruthenium

Equations (5-14) through (5-18)

Parameter	Estimated value Ru/Al$_2$O$_3$ (149°C)
$k'_{n5} \ell /(k'_{n5} + k^*_{n5})$	0.36 ±0.01
k''_{n5} / k''_6	0.34 ±0.04
$(\ell + f\ell)/f$	1.05 ±0.29
k''_{n4} / k''_6	0.06 ±0.03
$k'_{n4} f/(k'_{n4} + k^*_{n4})$	0:47 ±0.19
k''_3 / k''_6	0.03 ±0.09
$k'_3 /(k'_3 + k^*_3)$	0.97 ±1.1
$(1 + \ell' + m\ell' + mf\ell)$	1.00 ±0.02
m	0.42 ±1.7
k''_2 / k''_6	0.03 ±0.27
m	0:24 ±6.5
$k'_2 /(k'_2 + k^*_2)$	0.96 ±2.9
$(mf\ell + m\ell' - \ell f)$	0.002±0.9
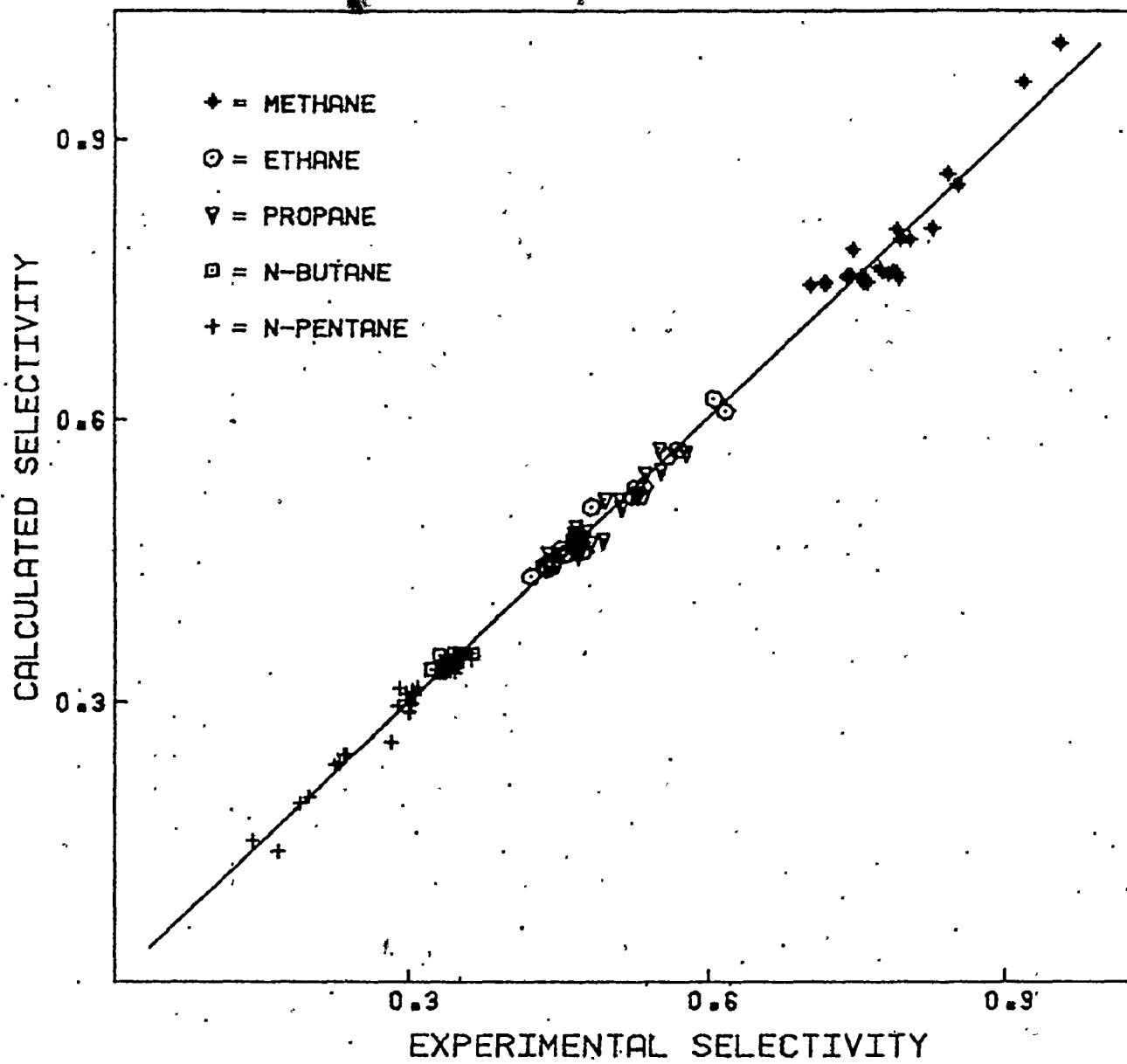
Figure 5-21: Calculated versus Experimental Selectivities in the Hydrogenolysis of n-Hexane over Ru/Al$_2$O$_3$ at 149°C and 1.2 atm.

temperature. The results in table 5-11,a) show that with increasing temperature the amount of smaller products increases as expected, Fig. 5-22 shows a few selected plots of selectivities at three different temperatures as a function of conversion; these plots agree with the observations of table 5-11, a). The data of fig. 5-22 are tabulated in table D-24, including the selectivities that are not shown in the figure. Values of k''_{n5}/k''_6 and $k'_{n5}\ell/(k'_{n5} + k^*_{n5})$ were obtained by plotting $1/S_{n5}$ versus $x/(1-x)$ at the different temperatures, the results are shown in table 5-11,b). The value of k''_{n5}/k''_6 increases with increasing temperature, indicating that the activation energy for the reaction of n-pentane is larger than that for n-hexane. The values of $k'_5\ell'/(k'_5 + k^*_5)$ do not change much. If random cracking is assumed, the value of ℓ is 0.4, so that the values of $k'_5/(k'_5 + k^*_5)$ are always close to unity; that is, the rate of cracking is slow compared to the rate of desorption.

5.4.3   n-Hexane over Nickel

The experimental data are tabulated in tables D-20 and D-17 for the promoted and the unpromoted nickel catalysts. The experiments were performed at 255°C and 285°C respectively. Plots of the product distributions as functions of the conversion of n-hexane are in fig. 5-23 and fig. 5-24. The data on NiMg/SiC seem to agree with the earlier observations that mainly successive demethylation takes place at the terminal carbon atoms: initially the main product is n-pentane,

Table 5-11

a) Product Distribution from n-Hexane over Ruthenium at other Temperatures (Ru/Al$_2$O$_3$)

Temp.	x	S_{n5}	S_{n4}	S_3	S_2	S_1
139°	0.24	0.32	0.36	0.49	0.44	0.63
149°	0.42	0.28	0.35	0.49	0.50	0.74
159°	0.61	0.21	0.33	0.50	0.59	0.99
170°	0.79	0.13	0.26	0.49	0.75	1.33
180°	0.89	0.04	0.16	0.44	0.98	1.85

b) Values of k''_{n5}/k''_6 and $k'_{n5}\ell/(k'_{n5}+k^*_{n5})$ obtained from plots of $1/S_{n5}$ versus $x/(1-x)$ at different temperatures

	139°	149°	163°
k''_{n5}/k''_6	0.16	0.34	0.50
$k'_{n5}\ell/(k'_{n5}+k^*_{n5})$	0.34	0.36	0.36
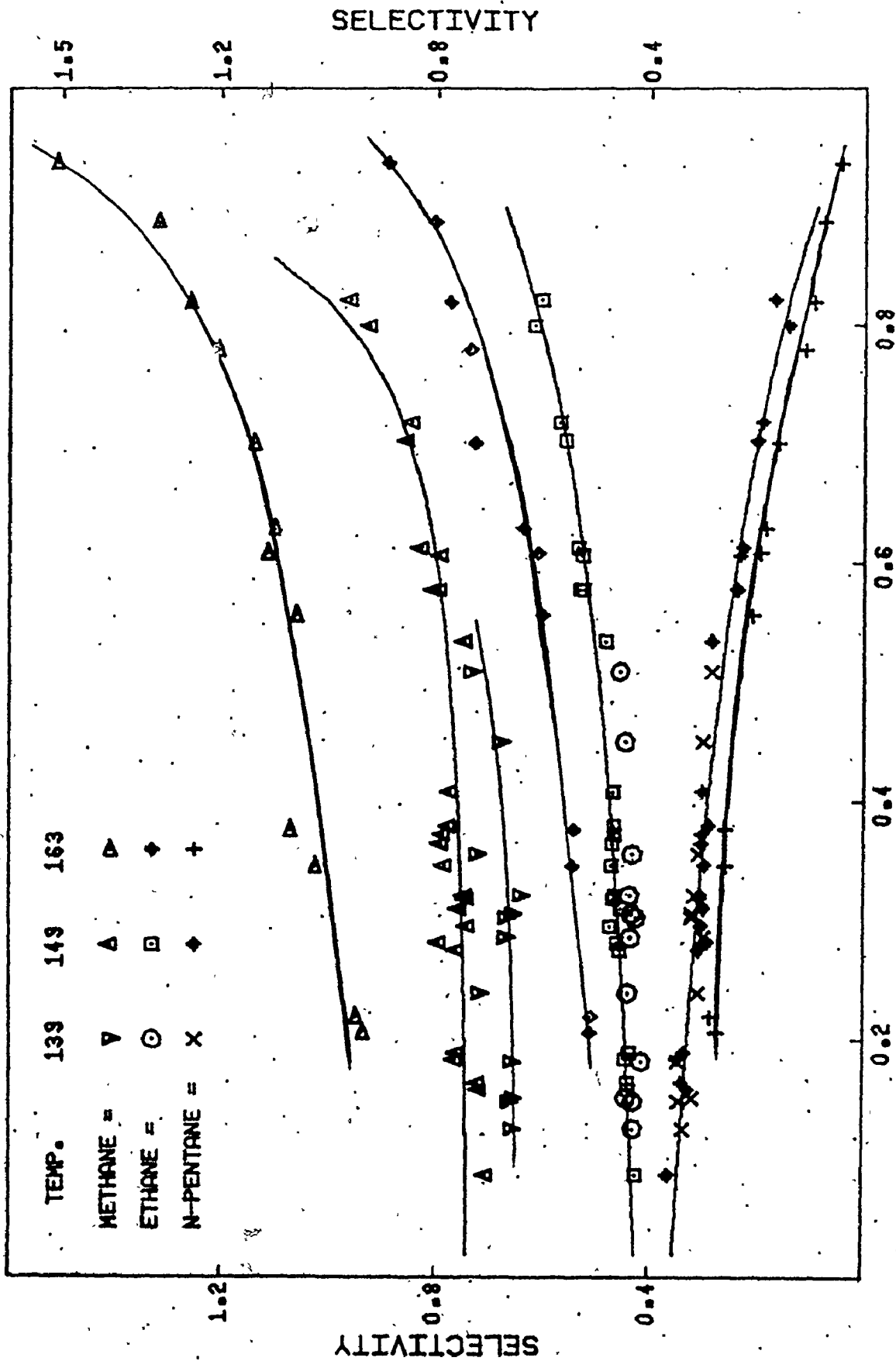
Figure 5-22 Product Distribution of Hydrogenolysis of n-Hexane over
Ru/Al$_2$O$_3$ at other Temperatures and 1.2 atm.
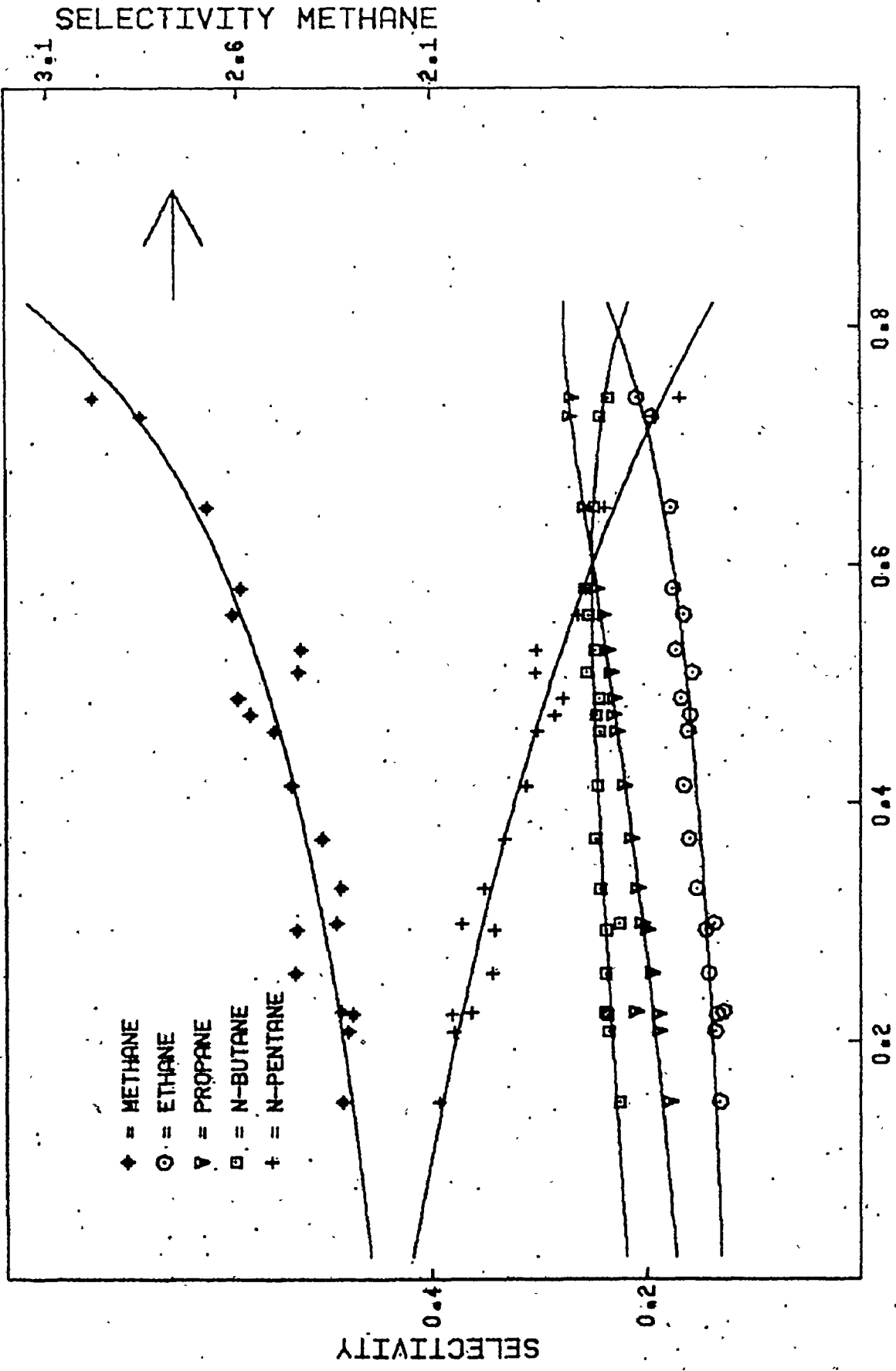
Figure 5-23 Product Distribution of Hydrogenolysis of n-Hexane over Ni-Mg/SiC at 255°C and 1.2 atm.
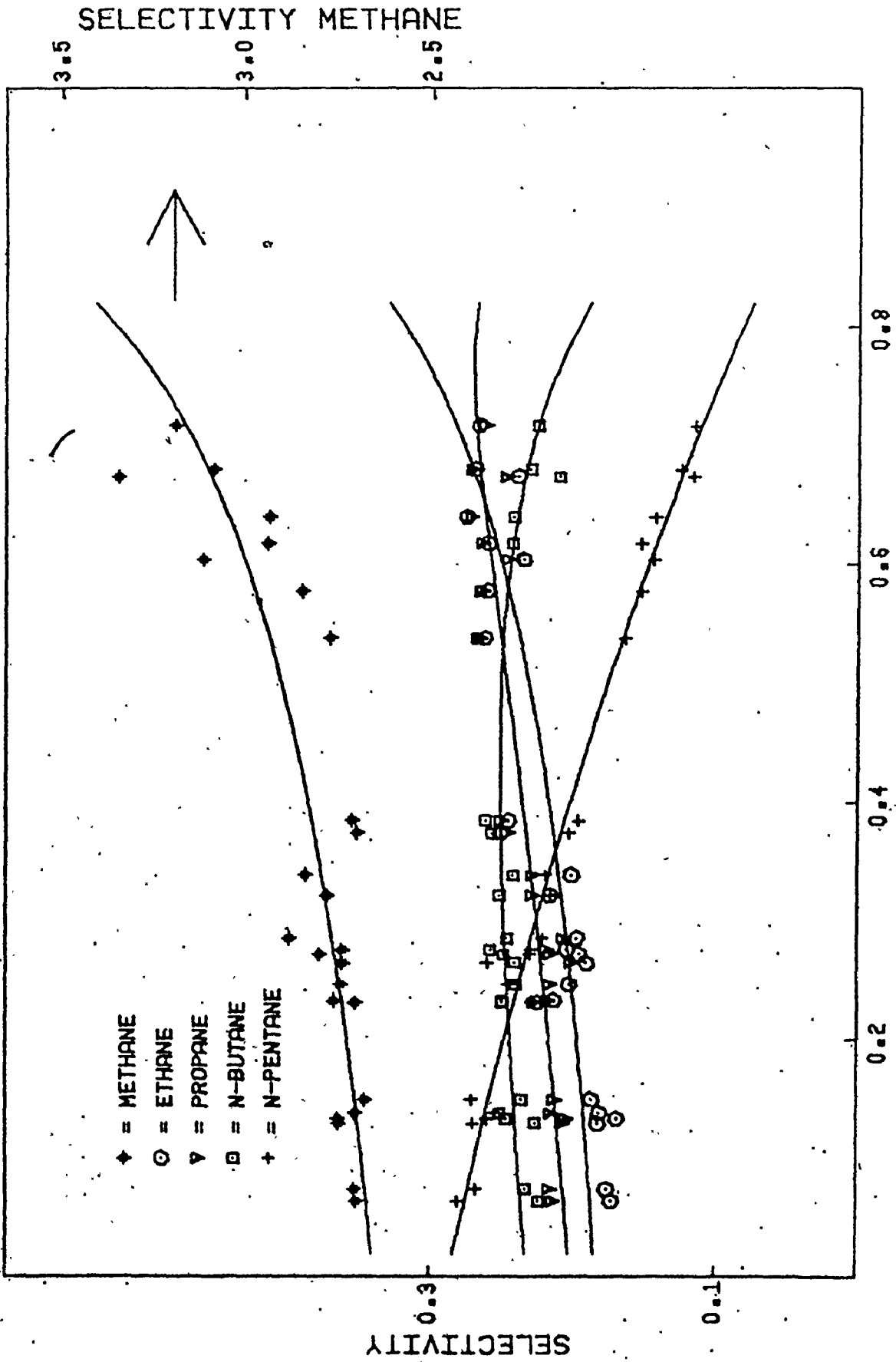
Figure 5-24 Product Distribution of Hydrogenolysis of n-Hexane over Ni/SiC at 285°C and 1.2 atm.

and the next most abundant products are in decreasing order
n-butane, propane and ethane. On the unpromoted catalyst more
of the smaller products are present, probably due to the
higher temperature required. The selectivity of n-butane ex-
hibits a maximum.

The data were fitted to selectivity equations (5-14)
through (5-18); the estimated parameter values are tabulated
in table 5-12, the solid lines in the figures are the calcu-
lated values. Fig. 5-25 is a plot of the calculated versus the
experimental selectivities for the promoted nickel catalyst.
The average deviation does not exceed 4%. The reactivity of
the hydrocarbons decreases rapidly with decreasing length of
the carbon chain. A few experiments were carried out at other
temperatures, the results are shown in table 5-13 for the two
nickel catalysts. The promoted catalyst is significantly more
active than the unpromoted one. At increasing temperature,
the selectivities of the smaller products increase as expect-
ed, especially that of methane.

5.4.4   n-Hexane over Cobalt

The experimental data are expressed as selectivities
of the products and conversion of n-hexane and are shown in
table D-23; they are also plotted in fig. 5-26. The data were
obtained at $219^{\circ}C$. In agreement with results from cobalt with
other feed molecules, more smaller molecules are obtained.
The selectivity of methane is high, if compared with the other
catalysts, and ethane is the second most abundant product.

Table 5-12

Analysis of Hydrogenolysis of n-Hexane over Nickel

Equations (5-14) through (5-18)

| Parameter	Estimated value	
	Ni-Mg/SiC(255°C)	Ni/SiC(285°C)
$k'_{n5}\, \ell/(k'_{n5}+k^*_{n5})$	0.42 ±0.02	0.28 ±0.01
k''_{n5}/k''_6	0.46 ±0.07	0.63 ±0.06
$(\ell'+f\ell)/f$	0.82 ±0.19	0.52 ±0.01
k''_{n4}/k''_6	0.16 ±0.08	0.32 ±0.03
$k'_{n4}\, f/(k'_{n4}+k^*_{n4})$	0.55 ±0.22	0.49
k''_3/k''_6	0.09	0.15 ±0.03
$k'_3/(k'_3+k^*_3)$	0.54 ±0.43	0.9
$(\ell+\ell')$	0.89 ±0.12	1.26 ±0.1
m	0.	0.
k''_2/k''_6	0.01	0.01
$k'_2/(k'_2+k^*_2)$	0.33	0.71 ±0.05
$(mf\ell+m\ell'-f\ell)$	-0.57	
$(1-f)$	0.58	
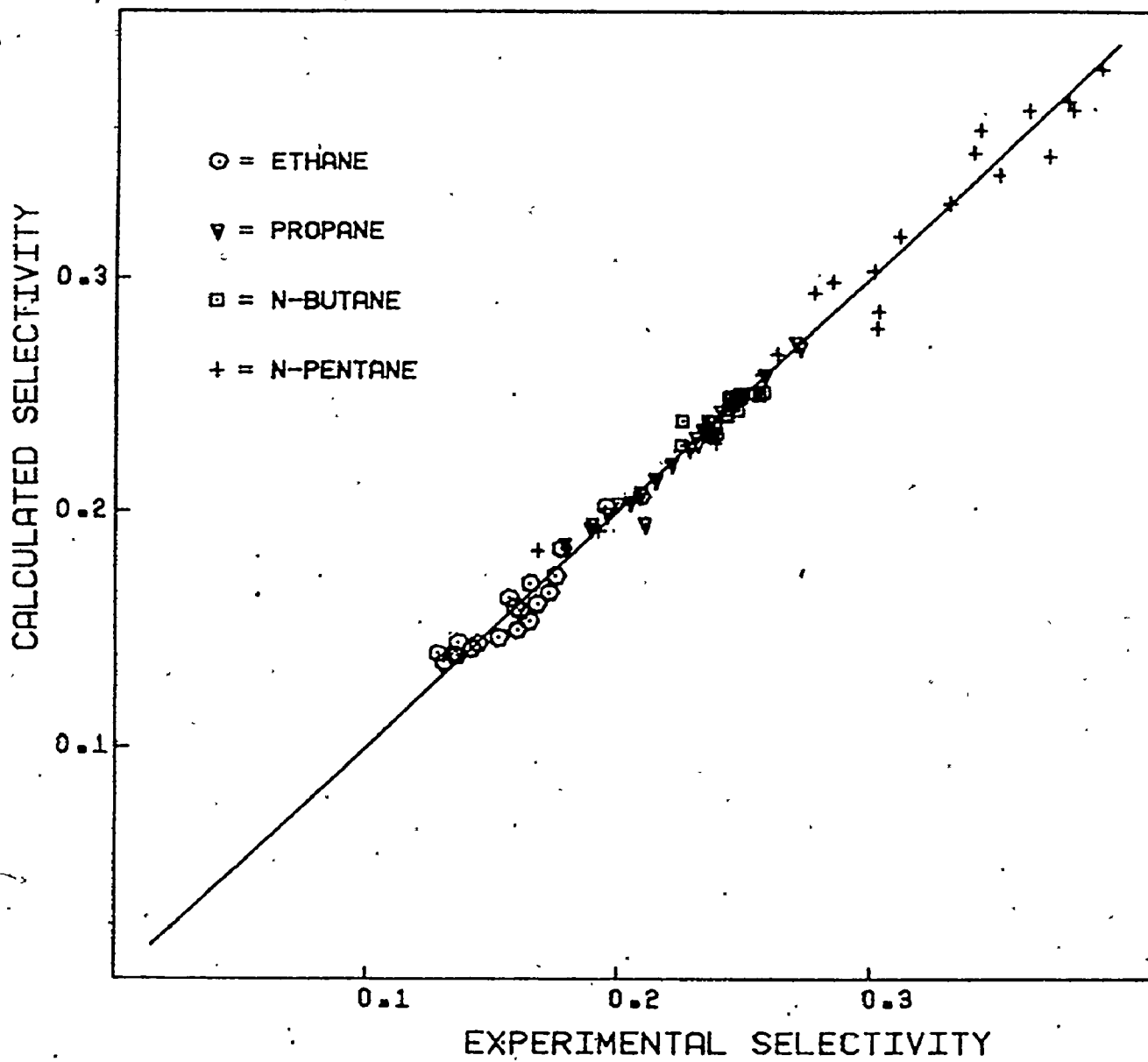
Figure 5-25: Calculated versus Experimental Selectivities in the
Hydrogenolysis of n-Hexane over Ni-Mg/SiC at 255°C
and 1.2 atm.

Table 5-13

Product Distribution from n-Hexane over Nickel at other Temperatures

Ni-Mg/SiC						Temp.(°C)	Ni/SiC					
S_1	S_2	S_3	S_{n4}	S_{n5}	x		x	S_{n5}	S_{n4}	S_3	S_2	S_1
1.21	0.05	0.58	0.17	0.45	0.10	230						
						240	0.03	0.54	0.20	0.16	0.11	1.80
1.83	0.12	0.34	0.22	0.40	0.27	245						
						250	0.06	0.51	0.23	0.15	0.15	1.76
2.73	0.18	0.30	0.22	0.23	0.57	260	0.10	0.41	0.31	0.18	0.17	1.82
						270	0.15	0.32	0.28	0.21	0.19	2.26
4.07	0.26	0.25	0.11	0.05	0.85	275						
						280	0.24	0.27	0.27	0.22	0.21	2.50
						290	0.38	0.18	0.24	0.23	0.24	2.99
						300	0.50	0.10	0.18	0.23	0.26	3.55
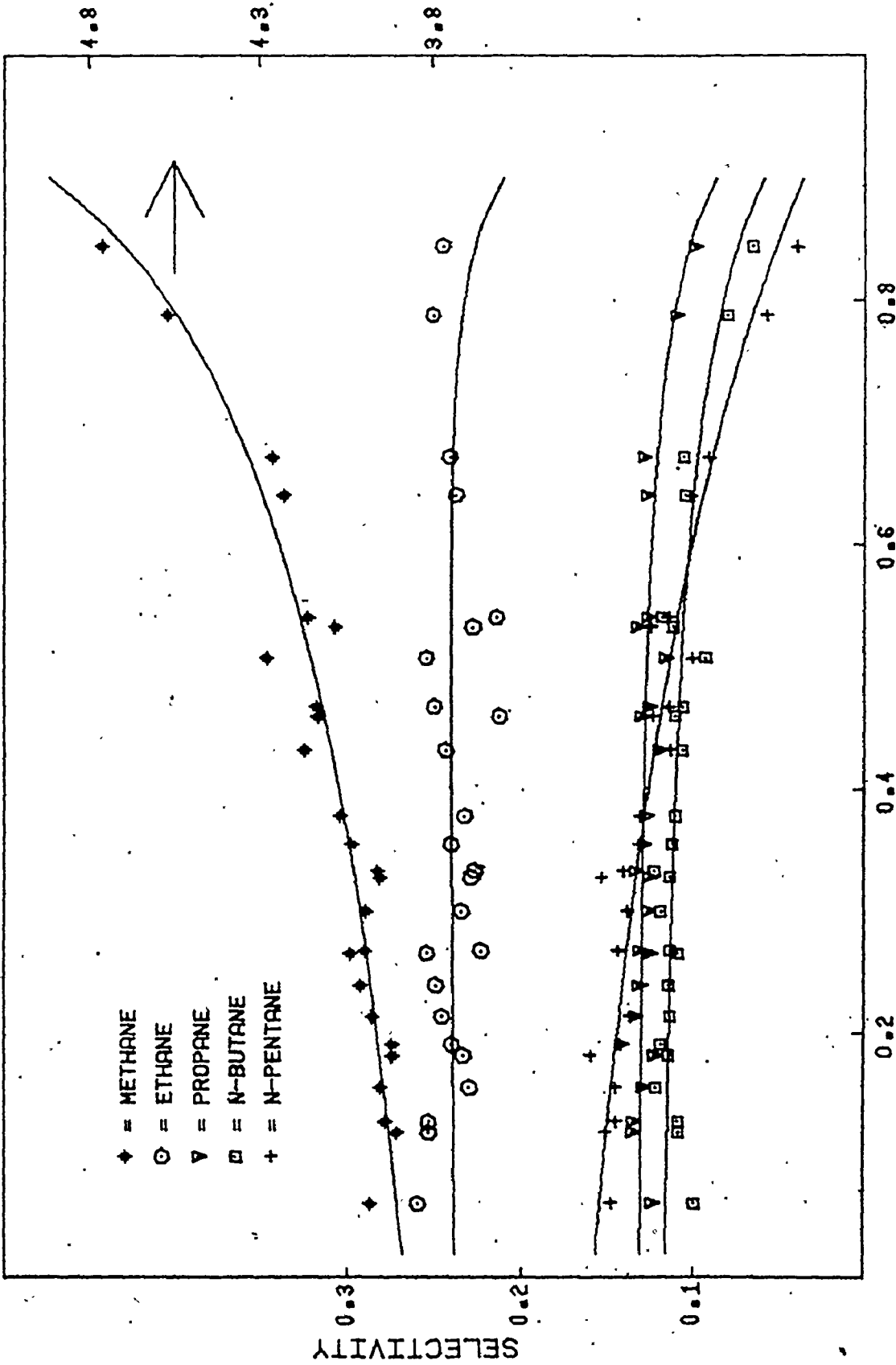
Figure 5-26 Product Distribution of Hydrogenolysis of n-Hexane over Co-Mg/SiC at 219°C and 1.2 atm.

This result suggests strongly adsorbed species that tend to crack further rather than desorb.

The data were fitted to the selectivity equations (5-14) through (5-18), using nonlinear least squares. The resulting estimated parameters are shown in table 5-14, the solid lines in fig. 5-26 are the calculated values. The average deviations between the calculated and experimental values do not exceed 7%. The parameter estimates confirm that the desorption step is slower than the cracking step on cobalt for the adsorbed species involved here. The reactivity of the hydrocarbons decreases rapidly with decreasing length of the carbon chain.

5.5 Discussion

The hydrogenolysis of the three hexanes was studied over the same four metals that were used in the experiments with propane. The catalysts supported on the low area supports were used (except ruthenium), because they caused less pressure drop and were less likely to cause diffusional problems. The effect of a structural promoter was studied by using the magnesium-promoted and the unpromoted nickel catalysts. Kinetic experiments were not made since the catalysts lost activity too rapidly in most cases. Some kinetic results were obtained nevertheless. Logarithmic plots of rate versus partial pressure of hexane give an estimate of the order of the reaction with respect to the hexane, because the experiments were isothermal and the hydrogen partial pressure did not vary

Table 5-14

Analysis of Hydrogenolysis of n-Hexane over Cobalt

Equations (5-14) through (5-18)

Parameter	Estimated value Co-Mg/SiC(219°C)
$k'_{n5} \; \ell/(k'_{n5} + k^{*}_{n5})$	0.16 ± 0.01
k''_{n5} / k''_{6}	0.39 ± 0.07
$(\ell' + f\ell)/f$	1.
k''_{n4} / k''_{6}	0.14 ± 0.04
$k'_{n4} \; f/(k'_{n4} + k^{*}_{n4})$	0.14 ± 0.01
k''_{3} / k''_{6}	0.09
$k'_{3} / (k'_{3} + k^{*}_{3})$	0.14 ± 0.06
$(\ell + \ell^{i})$	0.79 ± 0.47
m	0.
k''_{2} / k''_{6}	0.04
$k'_{2} / (k'_{2} + k^{*}_{2})$	0.21 ± 0.12
$(1 - f\ell)$	0.51 ± 0.67

much (excess of hydrogen). These plots were always nearly
linear and gave values of the exponent varying from 0.6 to
1.1. The hydrogen exponent could not be determined in the
same way because the partial pressure of the hexane varied
over a much wider range, and the plots were not linear. It
was observed though that the order with respect to hydrogen
was again negative for these reactions.

The data of the experiments with isopentane over
NiMg/SiC were fitted to the power rate law; no deactivation
of the catalyst occurred in this case. The orders of reaction
with respect to hydrogen and isopentane were (-1.6) and 0.8
respectively, and the activation energy 43.3 kcal/mol (181
kJ/mol), a much lower value than that for propane on the
same catalyst. From the values of these exponents, a value of
"a", the degree of unsaturation of the surface complex, was
calculated similarly as in chapter 4. The value is 2.0, i.e.,
the adsorbed species is missing 4 hydrogen atoms, suggesting,
1,2-diadsorption at the tertiary carbon atom and a terminal
carbon atom, which would explain the large amount of n-butane
obtained in the products. On ruthenium (44), the value of "a"
was found to be 2.5, and the mechanism was explained as 1,2-
diadsorption at the opposite end of the chain from the terti-
ary carbon atom. The main product was isobutane.

The deactivation process had little or no effect on
the selectities of the reactions; therefore the attention was
focused on the product distributions.

Experiments were carried out at constant temperature and total pressure, and as wide a range of conversion as possible. For practical reasons, the conversions were not greater than 90% or much smaller than 10%. The product distributions were applied to the reaction networks, derived in appendix C. The selectivity equations were derived assuming no specific rate limiting step; adsorption and desorption were assumed to be reversible for all hydrocarbons, and rupture of the carbon-carbon bonds irreversible. All the reactions were assumed to be first order in the hydrocarbon involved, and the effects of hydrogen partial pressure were incorporated in the rate constants. The data fitted the equations very well, as is shown by the plots of calculated versus experimental selectivities (figures 5-6, 5-10, 5-13, 5-14, 5-18, 5-21, 5-25). A measure of the goodness of fit was defined as in chapter 4, equation (4-2), using the residual sum of squares after fitting the selectivity data. A summary of these results is given in table 5-15. The fits are satisfactory; they are only poor if the experimental selectivities are small. The values obtained for the parameters were in most cases acceptable and agreed with observations on the product distributions as functions of conversion. These two factors combined suggest that the proposed reaction networks are a satisfactory way of representing the complex sequence of reactions in the hydrogenolysis of these molecules.

Table 5-15

Average Deviations between Calculated and Experimental Selectivities

Expressed in %, using equation (4-2)

2,2-Dimethylbutane

	Ru/Al_2O_3 (185°C)	Ru/Al_2O_3 (200°C)	Ni/SiC	Ni-Mg/ SiC	Co-Mg/ SiC
S_{ne5}	2	3	4	2	5
S_{i4}	40	5	8	4	27
S_{n4}	–	–	52	–	–
S_3	–	–	5	5	10
S_2	34	15	2	7	10

2,3-Dimethylbutane

	Ru/Al_2O_3	Ni/SiC	Ni-Mg/SiC	Co-Mg/SiC
S_{i5}	8	5	5	10
S_{i4}	5	8	3	6
S_{n4}	–	4	6	8
S_3	13	4	4	3
S_2	21	5	8	6

n-Hexane

	Ru/Al_2O_3	Ni/SiC	Ni-Mg/SiC	Co-Mg/SiC
S_{n5}	4	4	4	7
S_{n4}	2	4	2	6
S_3	2	4	2	4
S_2	2	3	4	6

The iron catalyst produced almost only methane, as was found in the experiments with propane. Apparently the hydrocarbon species are adsorbed very strongly on iron. The only experiments that showed appreciable amounts of other products were those with 2,2-dimethylbutane, neopentane being obtained in relatively large amounts. Neopentane is clearly not very reactive, so that it has a good change to desorb instead of reacting further. This result was observed on the other catalysts as well, the selectivity for neopentane was always large, near unity, especially at low conversions. The one exception was the unpromoted nickel catalyst, but the temperature for this catalyst was much higher, almost as high as that used for the iron catalyst.

Using 2,3-dimethylbutane as feed hydrocarbon, no n-butane was obtained over ruthenium, in agreement with earlier results (44, 47). Over nickel and cobalt, however, the amount of n-butane usually exceeded that of isobutane, and their ratio increased with increasing temperature. This was confirmed by using isopentane as feed over the nickel catalyst. Clearly a different mechanism is operable in the adsorption and/or rupture over nickel compared to ruthenium. Indications are that on nickel adsorption is principally at the tertiary carbon atom and a terminal carbon atom; this type of adsorption should yield n-butane. This also agrees with observations that branched hydrocarbons are more reactive than straight ones over nickel (55).

On ruthenium, branched hydrocarbons are less reactive (44), and the adsorption of isopentane was suggested to be primarily at the straight section of the chain. Cobalt behaves like nickel, but produces more smaller products. The adsorption on cobalt is stronger, but not as strong as on iron. The results with n-hexane indicate that there is close to random splitting over ruthenium, while on nickel and cobalt the splitting is preferentially at the terminal carbon-carbon bonds.

Three types of parameters were obtained from the selectivity equations. The parameters had good confidence limits for the equations of S_5 and S_4, and sometimes for S_3, but the equations for the smaller products, S_2 and usually S_3, gave values with large confidence limits because of an increased number of parameters and large correlations between them. The first type of parameters are the groups $k_x' / (k_x' + k_x^*)$, where k_x' and k_x^* are the rate constants for desorption and cracking of the adsorbed species of hydrocarbon x, respectively. Because both reactions were assumed to be first order in the concentration of adsorbed hydrocarbon, the rates of desorption and cracking vary directly with the values of these rate constants. This type of parameter must have a value between zero and unity. In hydrogenolysis reactions the rupture of the carbon-carbon bond has often been shown to be the slowest step (24, 44, 53), and the parameter $k_x' / (k_x' + k_x^*)$ will then have a value close to unity. A summary of the values of this parameter, obtained from the different cata-

lysts and using all three feed hydrocarbons, is shown in table 5-16. In some cases the parameter could not be separated from other parameters. Only for ruthenium are the values close to unity in most cases, indicating that desorption is faster than cracking; with 2,3-dimethylbutane though, this is not so because of the higher temperature used in the experiments. On the nickel catalysts, the rates of desorption and cracking are about equal, and on cobalt the rate of cracking is usually greater than that of desorption. These results agree with observations that in the sequence, ruthenium-nickel-cobalt-iron, the amount of smaller molecules in the product increases; in this sequence the strength of adsorption of the hydrocarbon species increases. The parameter for neopentane is large on all catalysts, which agrees with the fact that neopentane is not very reactive, and k^*_{ne5} is relatively small.

The second type of parameter obtained are splitting factors, representing the probability that a particular bond will break in a molecule with different types of carbon-carbon bonds. These parameters must also be between zero and unity, because the cracking is assumed to be irreversible. For 2,2-dimethylbutane, the value of "ℓ" was close to unity for all catalysts; thus most of the reaction took place in the ethyl end of the molecule and produced neopentane. Quaternary carbon atoms appear to be very stable. For 2,3-dimethylbutane, the value of "ℓ" was also close to unity for all catalysts, indicating that the central bond is not likely to break; the

Table 5-16
Summary of Desorption-Cracking Parameters

2,2-Dimethylbutane

	Ru/Al$_2$O$_3$ (185°C)	(200°C)	Ni/SiC (290°C)	Ni-Mg/SiC (265°C)	Co-Mg/SiC (245°C)
$k'_{ne5}/(k'_{ne5}+k^*_{ne5})$	0.93	0.88	0.53	0.77	0.98
$k'_{i4}/(k'_{i4}+k^*_{i4})$	0.34	0.43	0.35	0.50	0.19
$k'_3/(k'_3+k^*_3)$	-	-	0.48	0.35	0.14
$k'_2/(k'_2+k^*_2)$	0.86	0.99	0.49	0.52	0.11

2,3-Dimethylbutane

	Ru/Al$_2$O$_3$ (200°C)	Ni/SiC (260°C)	Ni-Mg/SiC (245°C)	Co-Mg/SiC (227°C)
$k'_{i5}/(k'_{i5}+k^*_{i5})$	0.58	0.43	0.57	0.30
$k'_3/(k'_3+k^*_3)$	0.22	0.55	0.50	0.15
$k'_2/(k'_2+k^*_2)$	0.37	0.60	0.41	0.21

n-Hexane

	Ru/Al$_2$O$_3$ (149°C)	Ni/SiC (285°C)	Ni-Mg/SiC (255°C)	Co-Mg/SiC (219°C)
$k'_3/(k'_3+k^*_3)$	0.97	0.90	0.54	0.14
$k'_2/(k'_2+k^*_2)$	0.96	0.71	0.33	0.21

Propane

	Ru/Al$_2$O$_3$ (180°)	(150°)	Ni/SiC (277°)	(292°)	(305°)	Ni-Mg/SiC (251°)	(266°)	(281°)
$k'_2/(k'_2+k^*_2)$	0.98	0.99	0.71	0.56	0.45	0.77	0.67	0.50

initial reaction is most likely the removal of a methyl group.
The splitting factors of isopentane could not be separated
from the data of 2,3-dimethylbutane, but the product distri-
butions suggest that on ruthenium most of the cracking is in
the straight section of the molecule to yield isobutane. On
nickel and cobalt the methyl groups at the tertiary carbon
atom are removed as rapidly as the methyls at the other end
of the molecule. For n-hexane, the splitting factors could
only be separated for ruthenium, values of "ℓ" (0.35) and of
"ℓ'" (0.43),for the splitting factors of n-hexane, indicated
that splitting of the different bonds was almost at random;
the expected values in that case are 0.4 for both parameters.
The estimated value of "f", the splitting factor of n-pentane,
is 0.62, again close to the expected value for statistical
splitting, 0.5. Two estimates of "m" were obtained, the split-
ting factor in n-butane. In case of random splitting this pa-
rameter should have the value 0.33, the estimates were 0.24
and 0.42. The product distribution on nickel suggests that on
this metal the splitting is preferentially at the terminal
carbon-carbon bonds, as has been shown in several previous
studies (51, 53, 54, 55). The same pattern appears to
hold for cobalt, but the results are less obvious because the
adsorbed products are likely to react further rather than to
desorb.

The final type of parameter obtained are the groups
k_x'' / k_6'', representing the ratio of overall rates of hydrogen-

olysis of product x and the feed hydrocarbon. This is again
so because the elementary steps in the reactions were assumed
to be first order in the hydrocarbon species involved. The
estimated parameter values are summarized in table 5-17. In
general the rates of hydrogenolysis decrease rapidly as the
number of carbon atoms of the molecule decreases, with the
exception of neopentane which reacts slower than its products.
With one exception the feed hydrocarbon is always more reac-
tive than any of its products. On ruthenium the decrease of
reactivity with carbon number is largest, over nickel and
cobalt it is more gradual. If this parameter becomes very
small, the value can not be estimated accurately because of
the nature of the selectivity equations. The equations are
not sensitive to this parameter if it has small values, unless
the conversion of the feed hydrocarbon is very large.

For ruthenium the hydrogenolysis reactions were fast-
er for normal hydrocarbons than for branched isomers of the
same carbon number (44, 47), while on nickel the opposite was
found (55), for hydrocarbons with tertiary carbon atoms. The
present data confirm this observation: the temperature re-
quired for n-hexane was much lower than that for the branched
hexanes over the ruthenium catalyst. On the nickel catalysts
this was not the case, and the rates of hydrogenolysis of
isobutane and n-butane also were about the same. The sequence
of activity of the catalysts can roughly be estimated from
the temperatures required for the reactions. The promoted

Table 5-17

Summary of the estimated values of the ratios of overall rates of hydrogenolysis of products and feed

2,2-Dimethylbutane

	Ru/Al_2O_3		Ni/SiC	$Ni\text{-}Mg/SiC$	$Co\text{-}Mg/SiC$
	($185°C$)	($200°C$)	($290°C$)	($265°C$)	($245°C$)
k''_{ne5}/k''_6	0.01	0.01	0.09	0.07	0.06
k''_{i4}/k''_6	0.01	0.19	1.2	0.62	0.64
k''_{n4}/k''_6	-	-	1.7	-	-
k''_3/k''_6	-	-	0.25	0.04	0.30
k''_2/k''_6	10^{-5}	0.01	0.04	0.03	0.02

2,3-Dimethylbutane

	Ru/Al_2O_3	Ni/SiC	$Ni\text{-}Mg/SiC$	$Co\text{-}Mg/SiC$
	($200°C$)	($260°C$)	($245°C$)	($227°C$)
k''_{i5}/k''_6	0.68	0.65	0.46	0.60
k''_{i4}/k''_6	0.03	0.23	0.23	0.50
k''_{n4}/k''_6	-	0.08	0.37	0.16
k''_3/k''_6	0.001	0.01	0.03	0.09
k''_2/k''_6	10^{-5}	0.001	0.005	0.02

n-Hexane

	Ru/Al_2O_3	Ni/SiC	$Ni\text{-}Mg/SiC$	$Co\text{-}Mg/SiC$
	($149°C$)	($285°C$)	($255°C$)	($219°C$)
k''_{n5}/k''_6	0.34	0.63	0.46	0.39
k''_{n4}/k''_6	0.06	0.32	0.16	0.14
k''_3/k''_6	0.03	0.15	0.09	0.09
k''_2/k''_6	0.03	0.01	0.01	0.04

nickel catalyst was always more active than the unpromoted one. The sequence of activity of the different metals was the same for all the hydrocarbons used: Ru > Co > Ni > Fe, and 'this sequence was also found for propane in chapter 4. The sequence of reactivity of the feed hydrocarbons depended on the metal used. On ruthenium n-hexane was most reactive, 2,2-dimethylbutane, 2,3-dimethylbutane, and propane were about equally reactive. Over nickel 2,3-dimethylbutane was most reactive, n-hexane and 2,2-dimethylbutane were about equally reactive, and propane had the lowest activity. Over cobalt n-hexane was slightly more reactive than 2,3-dimethylbutane followed by 2,2-dimethylbutane and propane. On iron n-hexane was much more reactive than the other three molecules, which had about equal reactivity.

Some of the selectivity equations simplify as the conversion approaches zero; for instance a value for the group of parameters $\{ k_5' \ell /(k_5' + k_5^*) \}$ in the selectivity equations for pentane (like equation (5-14)) can be obtained directly from the initial product distribution. With 2,2-dimethylbutane, parameters for isobutane and propane can be obtained directly from the initial distribution also. All the parameters obtained in this way agreed very closely to those obtained from the nonlinear regression programs. This is an indication of the validity of the technique used.

A few parameters can be obtained from different sources and the different estimates can then be compared.

Unfortunately, the only parameters that can be considered are those of ethane and propane, and these have the largest degrees of uncertainties as has been mentioned before. Table 5-18 tabulates three parameters that were determined from several different sources. k_2^* /k_2' and k_3^* /k_3' are the relative rates of cracking and desorption of an adsorbed C_2 and C_3 species and are determined from the values of $k_x' /(k_x' + k_x^*)$. Values of k_2'' /k_3'' indicate the relative rates of hydrogenolysis of ethane and propane; these values from hexane tests are determined by dividing k_2'' /k_6'' by k_3'' /k_6''. The temperatures at which the experiments were performed are included in the table, and differences in temperature should be considered in comparing the parameters. With a few exceptions, the parameters from different sources are self-consistent. Values of k_2^*/ k_2' are very small for ruthenium, around unity for nickel and larger for cobalt. Values of k_2'' /k_3'' also were very small for ruthenium, and somewhat larger for the nickel and cobalt catalysts. It has been known that hydrogenolysis of ethane is much slower than that of propane over a number of metals. The parameter values were not accurate enough for evaluation of the temperature dependences quantitatively.

Table 5-18

Comparison of Parameters from different sources

A k_2^* / k_2'

Source (feed hydrocarbon)	Ru (T,^{o}C)	Ni (T,^{o}C)	Ni-Mg (T,^{o}C)	Co-Mg (T,^{o}C)
Propane	0.01(150)	0.4(277)	0.3(251)	4.0(245)
	0.02(180)	0.8(292)	0.5(266)	4.2(255)
		1.2(305)	1.0(281)	4.2(265)
n-Hexane	0.04(149)	0.4(285)	2.0(255)	3.8(219)
2,3-Dimethylbutane	1.7 (200)	0.7(260)	1.4(245)	3.8(227)
2,2-Dimethylbutane	0.1 (185)	1.0(290)	0.9(265)	8.1(245)
	0.01(200)			

B k_3^* / k_3'

Source (feed hydrocarbon)	Ru (T,^{o}C)	Ni (T,^{o}C)	Ni-Mg (T,^{o}C)	Co-Mg (T,^{o}C)
n-Hexane	0.03(149)	0.1(285)	0.9(255)	6.1(219)
2,3-Dimethylbutane	3.6 (200)	0.8(260)	1.0(245)	5.7(227)
2,2-Dimethylbutane		1.1(290)	1.9(265)	6.1(245)

Table 5-18

(continued)

<u>C</u>. k_2'' / k_3''

Source (feed hydrocarbon)	Ru (T, $^{\circ}$C)	Ni (T, $^{\circ}$C)	Ni-Mg (T, $^{\circ}$C)	Co-Mg (T, $^{\circ}$C)
Propane	0.03(150)	1.4(277)	0.1(251)	0.7(245)
	0.01(180)	0.3(292)	0.6(266)	0.3(255)
		0.2(305)	0.3(281)	0.6(265)
n-Hexane	1.0 (149)	0.1(285)	0.1(255)	0.4(219)
2,3-Dimethylbutane	0.02(200)	0.1(260)	0.2(245)	0.2(227)
2,2-Dimethylbutane		0.2(290)	0.7(265)	0.1(245)

Chapter 6

CONCLUSIONS

The hydrogenolysis reactions of propane, n-hexane, 2,3-dimethylbutane, and 2,2-dimethylbutane were studied over catalysts of ruthenium, nickel, cobalt, and iron. The metals were impregnated on both low-area supports and high-area supports, and some of the nickel, cobalt, and iron catalysts contained magnesiumoxide as a structural promoter. The metal loading varied from 0.5 to 20. weight percent. The catalysts and the supports were examined using nitrogen adsorption at 78 K, hydrogen adsorption at room temperature, X-ray line broadening, and electron microscopy, to determine their physical properties. The total surface area and the metal surface area were measured, and in one case the pore distribution and the metal particle size distribution.

A recycle-type differential reactor provided close to ideal mixing, and physical transport limitations were shown to be negligible under the reaction conditions. A gas chromatographic system was able to separate and measure all the reactants and products. No products of isomerisation- and chain growth reactions were observed. The unpromoted iron catalysts lost their activity very quickly and could not be

reactivated. The promoted iron catalyst had nearly constant but low activity. The promoted catalysts of cobalt and nickel were more active than similar unpromoted ones, in fact the promoted catalysts on the low area supports were as active as the catalysts on the high area supports, but they contained about three times as much metal. The different supports used did not seem to influence the activity of the catalysts. The sequence of activity of the metals was ruthenium > cobalt > nickel > iron. For the hydrogenolysis of propane, the reaction order in the hydrocarbon was unity or slightly smaller over all the catalysts. The hydrogen order varied from small positive for iron to large negative for nickel, and the activation energies varied from 93 to 217 kJ/mol. A compensation effect appears to be operable. In all cases it was noticed that with increasing temperature the hydrogen exponent increased. The number of hydrogen atoms lost on adsorption of the hydrocarbon was calculated according to the mechanism of Sinfelt; 1,2-diadsorbed species were suggested. The hydrocarbon orders in the reactions with the hexanes were also close to unity and the hydrogen pressure had again a negative effect on the reaction rate, but this could not be determined quantitatively. The order of reactivity of the four feed molecules depended on the metals, but in general n-hexane was most reactive and propane was least reactive.

The product distributions of the reactions were ana-

lyzed using selectivity equations that were based on reversible adsorption and desorption of all hydrocarbons and irreversible rupture of the carbon-carbon bonds; no rate limiting step was assumed. The amounts of smaller molecules in the products increased in the sequence - ruthenium, nickel, cobalt, iron -, and also with increasing temperature and conversion. On ruthenium the surface splitting reaction was much slower than the desorption, on nickel the two rates were about equal, and on cobalt the desorption was slower. This probably is due to different modes of adsorption on the different metals. The rate of hydrogenolysis decreased as the carbon number decreased, and this was most noticable over ruthenium. Ruthenium preferred to attack the straight section of the chains, and in straight chains the splitting of different carbon-carbon bonds was almost statistically. Nickel and cobalt preferentially attacked the terminal carbon-carbon bonds of the molecules, and there was no preference for splitting methyl-groups attached to secondary or tertiary carbon atoms. Quaternary carbon atoms were very stable over all catalysts, while tertiary ones were relatively stable on ruthenium, but not on nickel and cobalt. The parameters obtained from the selectivity equations were consistent with other observations and with previous work. The fit of the data to these equations was good.

REFERENCES

1. Bond, G.C., "Catalysis by Metals", Academic Press, New York (1962).

2. Sinfelt, J.H., Ind. Eng. Chem., 58, 18 (1966).

3. Germain, J.E.,"Catalytic Conversion of Hydrocarbons", Academic Press, New York (1969).

4. Pauling, L., Proc. Roy. Soc., Ser. A, 196, 343 (1949).

5. Morikawa, K., Benedict, W.J., Taylor, H.S., J. Amer. Chem. Soc., 58, 1795 (1936).

6. Taylor, E.H., Taylor, H.S., J. Amer. Chem.Soc., 61, 503 (1939).

7. Cimino, A., Boudart, M., Taylor, H.S., J. Phys. Chem., 58, 796 (1954).

8. Kemball, C., Taylor, H.S., J. Amer. Chem. Soc., 70, 345 (1948).

9. Sheppard, F.E., J. Catal., 14, 148 (1969).

10. Sinfelt, J.H., Taylor, W.F., Yates, D.J.C., J. Phys. Chem., 69, 95 (1965).

11. Sinfelt, J.H., Yates, D.J.C., J. Catal., 8, 82 (1967).

12. Sinfelt, J.H., Yates, D.J.C., J. Catal., 10, 362 (1968).

13. Sinfelt, J.H., J. Phys. Chem., 68, 344 (1964).

14. Taylor, W.F., Sinfelt, J.H., Yates, D.J.C., J. Phys. Chem., 69, 3857 (1965).

15. Yates, D.J.C., Sinfelt, J.H., Taylor, W.F., Trans. Faraday Soc., 61, 2044 (1965).

16. Yates, D.J.C., Taylor, W.F., Sinfelt, J.H., J. Amer. Chem., Soc., 86, 2996 (1964).

17. Taylor, W.F., Yates, D.J.C., Sinfelt, J.H., J. Phys. Chem., 68, 2962 (1964).

18. Yates, D.J.C., Sinfelt, J.H., J. Catal.; 8, 348 (1967).

19. Carter, J.L., Cusumano, J.A., Sinfelt, J.H., J. Phys.Chem., 70, 2256 (1966).

20. Yates, D.J.C., Sinfelt, J.H., J. Catal., 14, 182 (1969).

21. Sinfelt, J.H., Nature Phys. Sci., 229, 27 (1971).

22. Cotton, F.A., Wilkinson, G., "Advanced Inorganic Chemistry", Interscience, New York (1962).

23. Thomas, J.M. & Thomas, W.J., "Introduction to the Principles of Heterogeneous Catalysis", Academic Press (1967).

24. Sinfelt, J.H., Cat. Reviews, 3, 175 (1969).

25. Sinfelt, J.H., A.I.Ch.E.J., 19, 673 (1973).

26. Anderson, J.R., Kemball, C., Proc. Roy. Soc., Ser.A, 223, 361 (1954).

27. Sinfelt, J.H., Taylor, W.F., Trans. Faraday Soc., 64, 3086 (1968).

28. Kemball, C., Disc. Faraday Soc., 41, 190 (1966).

29. Sinfelt, J.H., J. Catal., 27, 468 (1972).

30. Guczi, L., Gudkov, B.S., Tétényi, P., J.Catal., 24, 187 (1972).

31. Tajbl, D.G., Ind. Eng. Chem., Process Des. Develop., 8, 364 (1969).

32. Anderson, J.R., Baker, B.G., Proc.Roy.Soc., Ser.A, 271, 402 (1963).

33. Tsjeng, P.K., M. Eng. Thesis, McMaster University (1973).

34. Semenov, N.N., "Some Problems of Chemical Kinetics and Reactivity", volume I, Pergamon Press (1958).

35. Anderson, J.R., Avery, N.R., J. Catal., 5, 446 (1966).

36. Anderson, J.R., Avery, N.R., J. Catal., 7, 315 (1967).

37. Kemball, C., Cat. Reviews, 5, 33 (1971).

38. Anderson, J.R., Avery, N.R., J. Catal., 2, 542 (1963).

39. Dowie, R., Whan, D., Kemball, C., Chem. Soc. J., Faraday Trans. I, 68, 2150 (1972).

40. Boudart, M., Aldag, A., Ptak, L., Benson, J., J. Catal., 11, 35 (1968).

41. Boudart, M., Ptak, L., J. Catal. 16, 90 (1970).

42. Kemball, C., Kempling, J.C., Proc. Roy. Soc., Ser.A, 329, 391 (1972).

43. Dowie, R., Kemball, C., Kempling, J.C., Whan, D., Proc. Roy. Soc., Ser.A, 327, 491 (1972).

44. Kempling, J.C., Ph D thesis, McMaster University (1971).

45. Kempling, J.C., Anderson, R.B., Ind. Eng. Chem., Process Des. Develop., 9, 116 (1970).

46. Kempling, J.C., Anderson, R.B., Ind. Eng. Chem., Process Des. Develop., 11, 46 (1972).

47. Kempling, J.C., Anderson, R.B., "Catalysis", ed. J.W. Hightower, Elsevier, 1973, vol. 2, 1099.

48. Haensel, V., Ipatieff,V., J. Amer. Chem. Soc., 68, 345 (1946).

49. Haensel, V., Ipatieff,V., Ind. Eng. Chem., 39, 853 (1947).

50. Anderson, J.R., Baker, B., Nature, 68, 937 (1960).

51. Matsumoto, H., Saito, Y., Yoriedo, Y., J. Catal., 19, 101 (1970).

52. Barron, Y., Maire, G., Muller, J., Gault, F., J. Catal., 5, 428 (1966).

53. Kikuchi, E., Morita, Y., J. Catal., 15, 217 (1969).

54. Kikuchi, E., Tsumuri, M., Morita, Y., J. Catal., 22, 226 (1971).

55. Kochloefl, K., Bazant, B., J. Catal., 10, 140 (1968).

56. Taylor, W., Yates, D., Sinfelt, J., J. Catal., 4, 374 (1965).

57. Sinfelt, J., Yates, D., Taylor, W., J. Phys. Chem., <u>69</u>, 1877 (1965).

58. Maire, G., Plonidy, G., Prudhomme, Gault, F., J. Catal., <u>4</u>, 556 (1965).

59. Corroleur, C., Tomanova, D., Gault, F., J. Catal., <u>24</u>, 401 (1972).

60. Kochloefl, K., Bazant, V., J. Catal., <u>8</u>, 250 (1967).

61. Sinfelt, J., Carter, J., Yates, D., J. Catal., <u>24</u>, 283 (1972).

62. Beelen, J., Ponec, V., Sachtler, W., J. Catal., <u>28</u>, 376 (1973).

63. Roberti, A., Ponec, V., Sachtler, W., J. Catal., <u>28</u>, 381 (1973).

64. Sinfelt, J., J. Catal., <u>29</u>, 308 (1973).

65. Whyte, J.R., Cat. Reviews, <u>8</u>, 117 (1973).

66. Storch, H., Golumbic, N., Anderson, R.B., "The Fischer-Tropsch and Related Syntheses", John Wiley & Sons, New York (1951).

67. Carter, J.L., Sinfelt, J.H., J. Catal., <u>10</u>, 134 (1968).

68. Carter, J.L., Sinfelt, J.H., J. Phys. Chem., <u>70</u>, 3003 (1966).

69. Anderson, R.B., "Experimental Methods in Catalytic Research", chapter I, Academic Press, New York (1968).

70. Brunauer, S., Emmett, P.H., Teller, E., J. Amer. Chem. Soc., <u>60</u>, 309 (1938).

71. Emmett, P.H., "Catalysis", vol. I, Reinhold Publ. Corp., New York (1954).

72. Hagen, D.I., Somorjai, G.A., J. Catal., <u>41</u>, 466 (1976).

73. Reman, W.G., Ali, A.H., Schuit, G.C.A., J. Catal., <u>20</u>, 374 (1971).

74. Mears, D.E., J. Catal., <u>30</u>, 283 (1973).

75. Satterfield, C.N., "Mass Transfer in Heterogeneous Catalysis", MIT Press (1970).

76. Satterfield, C.N., Sherwood, T., "The Role of Diffusion in Catalysis", Addison-Wesley publ. Corp., Mass.(1963).

77. Hougen, O.A., Watson, K.M., Ind. Eng. Chem., 35, 529 (1943).

78. Reilly, P.M., Can. J. Chem. Eng., 48, 168 (1970).

79. Himmelblau, D.M., "Process Analysis by Statistical Methods", John Wiley & Sons, New York (1968).

80. Draper, N.R., Smith, H., "Applied Regression Analysis", John Wiley & Sons, New York (1966).

81. Box, G., Draper, N., Biometrika, 52, 355 (1965).

82. Matsumoto, H., Saito, Y., Yoneda, Y., J. Catal., 22, 182 (1971).

83. Dixon, L.T., Borth, R., Kokes, R.J., Gryder, J.W., J. Catal., 37, 376 (1975).

84. Brooks, C.S., Christopher, G.L.M., J. Catal., 10, 211 (1968).

85. Flynn, P.C., Wanke, S.E., J. Catal., 37, 432 (1975).

86. Flynn, P.C., Wanke, S.E., J. Catal., 33, 233 (1974).

87. Robertson, S.D., Anderson, R.B., J. Catal., 23, 286 (1971).

88. Selwood, P., "Chemisorption and Magnetisation", Academic Press (1975).

89. Nelsen, F.M., Eggertsen, F.T., Anal. Chem., 30, 1387 (1958).

90. Ettre, Z., Z. Phys. Chem., bd 219, 17 (1962).

91. Emmett, P.H., "Catalysis", vol. III, Reinhold Publ.Corp., New York (1955).

92. Anderson, R.B., Hofer, L.J.E., Ind. Eng. Chem., 39, 1618 (1947).

93. Anderson, R.B., Hofer, L.J.E., J. Amer. Chem. Soc., 73, 944 (1951).

94. Sadek, H., Taylor, H., J. Amer. Chem. Soc., 72, 1168 (1950).

95. Brunauer, S., "The Adsorption of Gases and Vapours-Physical Adsorption", Princeton (1942).

96. Boudart, M., Advan. Catal., 20, 153 (1969).

97. Boudart, M., A.I.Ch.E.J., 18, 465 (1972).

98. Boudart, M., "Kinetics of Chemical Processes", Prentice Hall, N.J. (1968).

99. Carberry, J., "Chemical and Catalytic Reaction Engineering", McGraw-Hill, New York (1976).

100. Ollis, D.F., Taheri, H.T., A.I.Ch.E.J., 22, 1112 (1976).

101. Tsjeng, P., Anderson, R.B., Can. J. Chem. Eng., 54, 101 (1976).

102. Dowie, R.S., Kemball, C., Whan, D.A., J. Phys. Chem., 80, 2900 (1976).

103. Dietz, W.A., J. Gas Chromatogr., Feb., 68 (1967).

104. Purcell, J., Ettre, L., J. Gas Chromatogr., 3, 69 (1965).

105. Schmauch, Anal. Chem., 32, 343 (1960).

106. Leva, M., Grummer, M., Chem. Eng. Progr., 43, 633 (1947).

107. Leva, M., Chem. Eng. Progr., 43, 549 (1947).

108. Brownell, L.E., Katz, D.C., Chem. Eng. Progr., 43, 537 (1947).

109. Levenspiel, O., "Chemical Reaction Engineering", John Wiley & Sons, New York (1962).

110. Berty, J.M., Chem Eng. Progr., 70, 78 (1974).

111. Bennet, C.O., Cutlip, M.B., Yang, C.C., Chem. Eng. Sci., 27, 2255 (1972).

112. Mears, D.E., Ind. Eng. Chem., Process Des. Develop., 10, 541 (1971).

113. De Acetis, J., Thodos, G., Ind. Eng. Chem., 52, 1003 (1960).

114. Bird, R.B., Stewart, W.E., Lightfoot, E.N., "Transport Phenomena", John Wiley & Sons, New York (1960).

115. Smith, J.H., Van Ness, H.C., "Introduction to Chemical Engineering Thermodynamics", McGraw-Hill Book Co., Inc. (1959).

116. Anderson, R.B., Lee, C.B., Machiels, C.J., Can. J. Chem. Eng., 54, 590 (1976).

117. Tajbl, D.G., Can.J. Chem. Eng., 47, 154 (1969).

118. Yermakov, Y.I., Kutznetsov, B..N., Ryndin, Y.A., J. Catal., 42, 72 (1976).

119. Frennet, A., Degols, L., Lienard, G., Crucq, A., J. Catal., 35, 18 (1974).

120. Carter, J.L., Cusumano, J.A., Sinfelt, J.H., J.Catal., 20, 223 (1971).

121. Pitzer, K.S., Brewer, L., revision of Lewis,G.N. and Randall, M., "Thermodynamics", McGraw-Hill, New York, (1961), appendix 7.

122. Martin, G.A., Imelik, B., Surface Science, 42, 157 (1974).

123. Anderson, J.R., Shimoyama, "Catalysis", ed. J.W. Hightower, Elsevier, 1973, vol.I, 695.

124. Morikawa, K., Shirasaki, T., Okada, M., Advan. Catal., 20, 97 (1969).

125. Anderson, J.R., Macdonald, R.J., Shimoyama, Y., J. Catal., 20, 147 (1971).

126. Sargent, C.M., Embury, J.D., "Experimental Methods in Catalytic Research", ed. R.B. Anderson, P.T.Dawson, vol. II, chapter IV, Academic Press, New York, (1976).

127. Brunelle, J., Sugier, A., Le Page, J., J. Catal., 43, 273 (1976).

128. Webb, A.N., J. Catal., 39, 485 (1975).

129. Huang, Y.Y., Anderson, J.R., J. Catal., 40, 143 (1975).

130. Ragaini, V., Forni,L.,J. Catal., 37, 339 (1975).

131. Weller, S.W., A.I.Ch.E.J., 2, 59 (1956).

132. Schuit, G.C.A., van Reyen, L.L., Advan. Catal., 10, 242 (1958).

133. Weller, S.W., "Reviews of Chemical Reaction Engineering", Evanston, Ill., Aug. 1974, Advan. Chem. Series.

134. Moss, R.L.,"Experimental Methods in Catalytic Research", ed. R.B. Anderson, P.T. Dawson, vol. II, chapter II, Academic Press, New York (1976).

135. Anderson, J.R., Advan. Catal., 23, 1 (1973).

136. Sinfelt, J.H., Advan. Catal., 23, 91 (1973).

137. Stull, D.R., Westrum, E.F., Sinke, G.C., "The Chemical Thermodynamics of Organic Compounds", John Wiley & Sons, New York (1969).

138. Guczi, L., Sarkany, A., Tétényi, P., "Catalysis", ed. J.W. Hightower, Elsevier, 1973, vol. 2, 1111.

139. Boudart, M., Delbouille, A., Dumesic, J., Khammouma, S., Topsoe, H., J. Catal., 37, 486 (1975).

140. Box, G., Hunter, W., MacGregor, J., Erjavec, Technometrics, 15, 33 (1973).

141. Box, G.E.P., Cox, D.R., J.Roy. Stat. Soc., B, 211 (1973).

142. Anscombe, F.J., Tukey, J.W., Technometrics, 5, 141 (1963).

143. Meeter, D.A., Gaushaus, vol. IV, Rev. B.,Sec 3.22 (1966), University of Wisconsin Computing Center.

144. Box, G.E.P., Hill, W.J., Technometrics, 16, 385 (1974).

145. Johnson, R.A., Standall, N.A., Ind. Eng. Chem. Fundam., 7, 181 (1968).

146. Leclercq, G., Leclercq, L., Maurel, R., J. Catal., 44, 68 (1976).

147. Leclercq, G., Leclercq, L., Maurel, R., Bull. Soc. Chim. Fr., 455, 2329 (1974).

148. Maurel, R., Leclercq, G., Bull. Soc. Chim. Fr., 208, 1234 (1971),

149. Kittrell, J.R., Mezaki, R., Watson, C.C., Ind. Eng. Chem., 57, 18 (1965).

150. Dumesic, J.A., Topsoe, H., Advan. Catal., 26, 122 (1977).

151. Galwey, A.K., Advan. Catal., 26, 247 (1977).

152. Planck, C., Nace, D., Ind. Eng. Chem. 47, 2347 (1955).

153. Prater, C.D., Lago, R.M., Advan. Catal., 8, 293. (1956).

154. Ponec, V., Sachtler, W., "Catalysis", ed. J.W. Hightower, Elsevier, 1973, vol.I, 645.

A P P E N D I X   A

ANALYSIS BY GAS CHROMATOGRAPHY

During the first part of the experiments with propane, one chromatograph was used to separate hydrogen, methane, ethane, and propane. This unit was a Varian 1520 B Temperature Programmable chromatograph with helium (high purity, Matheson) as carrier gas and a 2m Poropak Q (50-80 mesh, Waters Associates Inc.) column. Poropak Q is a porous polymer from ethylvinylbenzenes and styrene, surface area 500-600 m^2/g, pore volume .34 g/cc. It does not have strong adsorptive sites which usually cause tailing, and no liquid phase bleeding is possible. Poropak Q is stable up to 250°C. A six-way linear gas sampling valve from Varian Aerograph, with a sample loop of 0.2 cc was used. One of the problems with this setup was that the thermal response of hydrogen in helium is not a linear function of the concentration (104, 105), the thermal conductivity of helium-hydrogen mixtures exhibits a minimum at 8% hydrogen and 92% helium. Very small sample loops had to be used, to avoid splitting the hydrogen peaks into three parts (104), and this limitation decreased the sensitivity for the other components, which were present

in the mixture in smaller amounts. The sensitivity of hydrogen in helium is also very low, because the difference in thermal conductivities is small. The calibration for hydrogen was not satisfactory, the calibration curve not being linear. Deviations from linearity were especially large if the effluent stream contained more than 90% hydrogen, which was often the case.

To avoid problems of this type, the analysis system was changed for the experiments with the hexanes and the propane experiments with the low area catalysts. In the new setup, two Varian 90-P gaschromatographs were used with isothermal columns. The first column was a 2m (0.64 cm O.D.) coconut charcoal column(80-100 mesh), and argon (high purity, Union Carbide) was used as a carrier gas. The sampling valve had a sample loop of 0.6 cc. This column separated hydrogen from all the hydrocarbons, which had very long retention times. The response of hydrogen in argon was found to be linear with concentration, and the sensitivity was large. After the hydrogen peak was recorded, the integrator was switched to the second chromatograph, which contained a 2m Poropak Q column (O.D. 0.64 cm), a sample loop of 0.7 cc; hydrogen (prepurified, Matheson) was used as a carrier gas. Both carrier gases were dried with 4A molecular sieves.

A second sample was taken here from the effluent stream at the same time of the first sample, and an empty column of 4m (O.D. 0.64 cm), before the Poropak Q column, retained the gases for about two minutes, until the hydrogen peak had been integrated and the system was switched to the second chromatograph. Because hydrogen was the carrier gas, the hydrogen in the sample did not disturb the second part of the chromatogram. The Poropak column could separate all the products that were possible in these experiments: methane, ethane, propane, iso- and n-butane, neo- iso- and n-pentane, 2,2-dimethylbutane, 2,3-dimethylbutane and n-hexane; all within 28 minutes. Calibrations of all the hydrocarbons were checked with literature values of thermal response factors (103), and were found to agree well, usually within 3%. To check for the linear response of the different components, binary mixtures were analyzed, of hydrogen, methane, ethane propane, and isobutane, covering a wide range of compositions. The agreement with the response factors obtained from the pure components was always good, less than 1% deviation. The response factors for the liquid hydrocarbons were obtained from a range of mixtures of the hydrocarbons with hydrogen and propane. The thermal responses were all linear with concentration, and the calibrations were checked regularly.

Table A-1 shows the conditions of operation of the two gas chromatographs, table A-2 the retention times and

Table A-1

Operating Conditions of Gas Chromatographs

G.L.C.I(hydrogen)		G.L.C.II(hydrocarbons)
Varian 90-P		Varian 90-P
2 m charcoal	Column	4 m empty 2 m Poropak Q
79°C	Column temp.	166°C
123°C	Detector temp.	193°C
80°C	Injector temp.	122°C
100 mA	Filament current	200 mA
Argon	Carrier gas	Hydrogen
50 psi	Pressure	50 psi
67 cm^3/min	Flow rate	76 cm^3/min
25 cm^3/min	Flow rate Ref.	29 cm^3/min
1	Attenuation	1

Table A-2

Retention Times and Thermal Responses of the Components

Component	Retention time (min)	M.W.	Boiling point (^{o}C)	Thermal[a] conductivity $*10^6$ (cal/s,cm,^{o}C)	Thermal Response Factor[b,c]
Hydrogen	0.65	2		471.	0.169
Methane	2.25	16	-162.	89.3	0.278
Ethane	2.7	30	- 87.	58.3	0.202
Propane	3.8	44	- 45.	48.3	0.161
Isobutane	5.7	58	- 12.	44.2	0.138
n-Butane	6.4	58	- 0.5	43.2	0.133
Neopentane	8.9	72	10.		0.117
Isopentane	11.2	72	28.		0.115
n-Pentane	12.4	72	36.		0.113
2,2-Dimethyl- butane	19.6	86	50.		0.104
2,3-Dimethyl- butane	22.6	86	58.		0.106
n-Hexane	25.5	86	68.		0.101

(a) at 48.9^{o}C

(b) ±3%

(c) defined as the inverse of the response of the pure component, $* 10^5$

the response factors of all the components, and fig. A-1
is an example of a chromatogram with all the products pre-
sent. This chromatogram is plotted using a logarithmic scale.
The chromatograms were analyzed with a Hewlett-Packard
Integrator (3380 A), which was programmed to identify each
possible component, based on retention time, and also con-
tained the calibration factors. The integrator then calcu-
lated and printed the normalized composition of the gas
sample. This printout is shown in fig. A-1, as well as the
settings of the integrator. To avoid effects of gas flow
through the sample loops, the effluent gas was switched to
bypass the loops just before the samples were taken, so that
the samples were always at atmospheric pressure. The tubing
in the complete system, including the effluent lines and the
sample loops, were heated with heating tape to avoid conden-
sation; the temperatures of the loops were about $80^{\circ}C$.

Sensitivity and accuracy in gas chromatography are
largest if the thermal conductivity of the carrier gas and
the component to be measured are as far apart as possible,
and if the thermal conductivity of the mixture is linear
with composition. A number of values of thermal conductivi-
ties are given in table A-2, and if they are compared with
the values at the same temperature of argon (45.7) and
hydrogen (471), it is evident that the present system com-
bines a maximum sensitivity with the ability to separate all
the components very well.
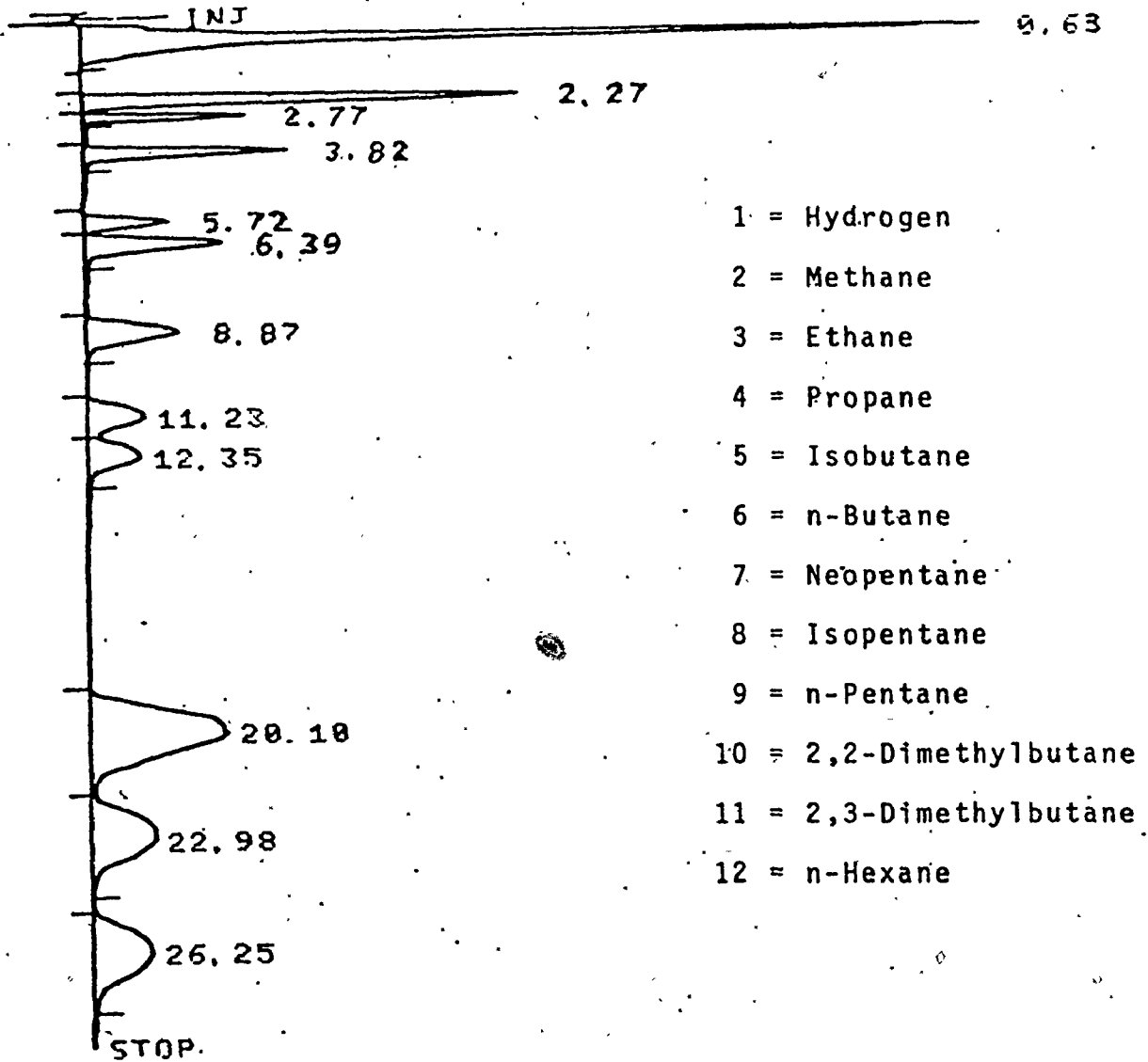
INJ   0.63

2.27

2.77

3.82

5.72
6.39

8.87

11.23
12.35

20.10

22.98

26.25

STOP

1 = Hydrogen
2 = Methane
3 = Ethane
4 = Propane
5 = Isobutane
6 = n-Butane
7 = Neopentane
8 = Isopentane
9 = n-Pentane
10 = 2,2-Dimethylbutane
11 = 2,3-Dimethylbutane
12 = n-Hexane

RT	TYPE	AREA	NORM. ID#	AMT
63		532106	1	86.29
2 27		29492	2	8.297
2 77	M	2511	3	507 7
3 82		4377	4	705 4
5 72		1793	5	247 6
6 39	M	3856	6	514 7
8 87		3236	7	279
11 23		2317	8	266 8
12 35	M	2271	9	256 9
20 10		14481	10	1.508
22 98	M	6494	11	689 1
26 25		5339	12	411 5

TOTAL 99.983 7

XF 1

Figure A-1 Chromatogram with all Components present.

A P P E N D I X B

CALCULATION PROCEDURES AND KINETIC MODELS

B.1 Calculation of Conversion, Selectivity and Rate of Reaction

The composition of the effluent gas was representative for the composition of the gas in the reactor once steady state was reached, since the reactor was a differential one. All the reactions are equimolar, so that the effluent flow rate also represented the feed flow rate and that through the reactor. Other measured variables, except for effluent flow rate and composition, were reactor temperature and pressure. In calculating the partial pressures of the components, ideal gas behaviour was assumed. The fractional conversion, X_n, of the feed hydrocarbon was defined as the ratio of the moles of feed hydrocarbon reacted and the moles of feed hydrocarbon supplied to the reactor; the following generalized equation was used:

$$X_n = \sum_{j=1}^{N} n_j Y_j \Big/ \sum_{j=1}^{M} n_j Y_j \qquad (B-1)$$

where X_n = fractional conversion

          j = series of integer numbers representing the different products in the effluent

          Y_j = mole fraction of hydrocarbon j in effluent

          n_j = carbon number of hydrocarbon j

          N = total number of hydrocarbon products

          M = (N+1), includes the feed hydrocarbon

Only hydrogenolysis reactions were considered, and it was assumed that no significant amounts of carbon were deposited on the catalyst, so that a carbon balance over the reactor was valid. The selectivity S_i, for a reaction product i, was defined as the moles of that product formed per mole of feed hydrocarbon consumed, and was calculated from

$$S_i = n \, Y_i \bigg/ \sum_{j=1}^{N} n_j \, Y_j \qquad\qquad \text{(B-2)}$$

where n = number of carbon atoms of feed hydrocarbon

The rate of reaction, r, of a feed hydrocarbon was calculated in moles per second-gram of catalyst:

$$r = \frac{F}{W} \sum_{j=1}^{N} n_j \, Y_j \, / \, n \qquad\qquad \text{(B-3)}$$

where F = effluent flow rate (mol/s)

          W = weight of catalyst (g)

The rate data can easily be converted to other units, such as per weight of metal or per metal surface area, using the results of chapter 2.

B.2 Parameter Estimations

Parameters in the power rate law (equation (4-1)) and in several mechanistic rate equations (described in appendix B.3) were estimated from the kinetic data, while the selectivity data were used to calculate parameters in selectivity equations for ethane in the case of propane hydrogenolysis, and for ethane through pentane in the hexane hydrogenolysis reactions. The best estimates of the parameters were taken to be those that minimized the sum of squares of the differences between the experimental and calculated values of the rate or selectivity. Nonlinear least squares analysis was used in all of these parameter estimations. In some cases parameters were also obtained by using linear least squares and a linearized form of the rate- or selectivity equation, or by plotting a linearized form; these results were always very close to those obtained by the nonlinear program.

A general nonlinear equation can be represented by (79, 80)

$$\underline{y} = f(\underline{X}, \underline{\theta}) + \underline{\varepsilon} \tag{B-4}$$

where $\underline{y}$ = vector of observations (dependent variables)

$\underline{X}$ = matrix of independent variables (temperature, pressure, etc.)

$\underline{\theta}$ = vector of parameters

$\underline{\varepsilon}$ = vector of errors

and $\partial f / \partial \theta_i = F(\underline{\theta})$ for a nonlinear model.

The vector of errors includes:

1) measurement and sampling errors

2) incorrect form of the model

3) errors in the independent variables

4) effect of any independent variables not included in the model

The assumptions in least squares analysis are:

  i) the independent variables have fixed and known values

 ii) the model is adequate: $E(\underline{y}) = f(\underline{X}, \underline{\theta})$

iii) the errors are independent and normally distributed with constant variance σ^2

If the assumptions are valid, the parameter values which minimize the residual sum of squares will also be the maximum-likelihood estimates (80):

$$RSS = \Sigma \{ \underline{y} - f(\underline{X}, \underline{\theta}) \}^2 \text{ is the residual sum of}$$

squares which is minimized.

The adequacy of a model can be checked by plotting the residuals versus the independent variables (142, 145) or by an analysis of variance (79, 80). If the assumptions are not satisfied, weighted least squares can be used (144, 145), or a transformation of the dependent variable which does satisfy the assumptions (141).

Plotting of residuals was used to check whether the errors were normally distributed with constant variance.

The approximate individual 95% confidence intervals of the parameters, based on a linear approximation in the region of $\hat{\underline{\theta}}$ (= vector of best parameter estimates), is obtained using the values of the "Student's t" distribution corresponding to the appropriate number of degrees of freedom:

$$\underline{\theta} = \hat{\underline{\theta}} \pm t^n_{0.95} \{ (\underline{X}'\underline{X})^{-1} \sigma^2 \}^{\frac{1}{2}} \tag{B-5}$$

where s^2, an estimate of σ^2, can be obtained from replicate experiments. Individual confidence intervals can be misleading if there is a large correlation between the parameters.

$$\rho_{\hat{\theta}_1 \hat{\theta}_2} = \frac{\text{cov} (\hat{\theta}_1, \hat{\theta}_2)}{\{ \text{var}(\hat{\theta}_1) \text{var}(\hat{\theta}_2) \}^{\frac{1}{2}}} \tag{B-6}$$

Large correlations can cause a compensating effect where both parameters can be changed substantially without changing RSS very much. This can be reduced by using weighted least squares (144, 145), or by reparameterizing the equation (for instance around a mean temperature if an Arrhenius type expression is used). Reparameterizing was tried in some cases with the power rate law, but the results remained the same. Large correlations occurred also in some of the selectivity equations, but reparameterizing was not possible in those cases. There are several methods to obtain the parameters:

a) a simple grid·search

b) minimization routines like steepest descent or Simplex
   methods

c) Gauss' linearization method, where the model is expanded
   as a Taylor series.

This gives good results if the starting values of the para-
meters are good.

In the present work, Marquardt's compromise was used,
which is a combination of the method of steepest descent
and a linearization method, with more emphasis on the latter
as the program converges. The initial values of the para-
meters were obtained by linearization of the equation or by
a grid search technique. Other techniques can be used (149).
These initial guesses are very important in determining the
number of iterations required and whether a minimum is local
or global. A description of the Gaushaus program can be
found in reference (143). A main program supplied the vari-
ables, the model to be fitted and initial guesses for the
parameters. Criteria of convergence were if either the RSS
or all the parameters did not change more than 0.1% between
two iterations. The program provided the parameter values
and their approximate individual 95% confidence limits, the
correlations between all the parameters, the final calculat-
ed function values, the residuals and the approximate con-
fidence limits for each function value. It was verified that
the experimental values always were within these confidence

limits. The confidence limits of the parameters are only very approximate in these experiments because the assumptions of least squares are not necessarily satisfied (rates and selectivities are not the true independent variables).

In the selectivity experiments with the hexanes, we are dealing with a multiresponse problem since both the conversion and the selectivity for all the products are dependent variables (81, 140). In multiresponse situations, the errors are again asssumed to be normally distributed and observational errors are correlated in the same run, but uncorrelated in separate runs. The standard procedure, in which the sum of squares is minimized for all dependent variables, causes problems since the number of parameters involved was very large. Instead, the problem was solved by consecutive fitting of the data to the selectivity equations, starting with C_5 products, and moving down to ethane. In the equations for C_2-C_4 (appendix C), the selectivity of the products with higher carbon numbers were regarded as independent variables, and their calculated values were used as such. This worked well, except for the selectivity of ethane, and sometimes of propane, where correlations and confidence intervals now became a serious problem.

B.3 Kinetic Models in the Hydrogenolysis of Propane

Several mechanistic rate equations based on Langmuir-Hinshelwood reaction models were tried. The models usually involved one or more adsorption steps, and the cracking step was supposed to be the rate determining one in most cases; this step could involve adsorbed hydrogen.

gaseous hydrogen, or just the adsorbed hydrocarbon species. In the derivation of the rate equations from the reaction mechanisms standard procedures were followed (77, 99). The power rate law as given in equations (1-8) or (1-12), is in fact a simplification of a mechanistic rate equation. Some of the rate equations examined are shown in table B-1.

Equation (1) was derived by Sinfelt (29). No adsorption equilibrium was assumed and in principle this equation can account for hydrogen exponents that change with temperature. Equation (2) was proposed in references (146, 147); "a", as usual, stands for the number of hydrogen molecules released in the dissociative adsorption step, λ is an adsorption equilibrium constant for propane. The cracking reaction is the slowest step and involves a reaction with gaseous hydrogen. This equation, like most others, can be linearized, and plots of P_{H_2} / r versus $P_{H_2}^a$ / $P_{C_3H_8}$ for different acceptable values of "a" (0.5, 1.0, 1.5, through 4.0) may determine which value of "a" is best, and allows determination of the other parameters from the slope and the intercept (146, 147). Linear plots were frequently used to obtain initial parameter estimates for the least squares programs. Equation (5) was found by Tsjeng (33) to provide the best fit for the reaction of propane over ruthenium over a wide range of pressures. In the derivation of equations (6) through (10), it was assumed that the hydrocarbon species as well as the adsorbed hydrogen were absorbed on pairs of sites.

Table B-1

Mechanistic rate equations for the Hydrogenolysis of Propane

1 $\qquad r = \dfrac{k\, P_{C3H8}}{1 + b\, P_{H_2}^a} \qquad\qquad b = f(T)$

2 $\qquad r = \dfrac{k\, \lambda\, P_{C3H8}\, P_{H2}}{P_{H2}^a + \lambda\, P_{C3H8}}$

3 $\qquad r = \dfrac{k\, P_{H2}\, P_{C3H8}}{1 + k'\, P_{H2}^a}$

4 $\qquad r = \dfrac{k\, P_{C3H8}/P_{H2}^2}{1 + k'\, P_{C3H8}/P_{H2}^a}$

5 $\qquad r = \dfrac{k\, P_{C3H8}\,/\,P_{H2}^2}{\left(1 + k' P_{H2}^{\frac{1}{2}} + k'' P_{C3H8}/P_{H2}^{\frac{1}{2}}\right)^2}$

6 $\qquad r = \dfrac{k\, P_{C3H8}\,/\,P_{H2}^{a+1}}{\left(1 + k'(P_{C3H8}/P_{H2})\right)\left(1 + k''/P_{H2}^a\right)}$

7 $\qquad r = \dfrac{k\, P_{C3H8}\,/\,P_{H2}^a}{\left(1 + k'(P_{C3H8}/P_{H2})(1 + k''/P_{H2}^a) + k''''P_{H2}\right)^2}$

Table B-1

(continued)

$\underline{8}$ $\qquad r = \dfrac{k\ P_{C3H8}}{\left(1 + k'P_{C3H8}/P_{H2} + k''P_{H2}\right)^2}$

$\underline{9}$ $\qquad r = \dfrac{k\ P_{C3H8}}{1 + k'P_{C3H8}/P_{H2}}$

$\underline{10}$ $\qquad r = \dfrac{k\ P_{C3H8}/\left(P_{H2} + k'P_{H2}^{a+1}\right)}{1 + k''\ P_{C3H8}/P_{H2}}$

$\underline{11}$ $\qquad r = \dfrac{k\ P_{C3H8}}{1 + K_{H2}P_{H2} + K_1 P_{CH4}/P_{H2}^{c}} \qquad\qquad c = 0., 0.5, \cdots, 2.0$

As in Sinfelt's mechanism, two types of adsorbed hydrocarbon
species are assumed, the first being in equilibrium with the
gaseous hydrocarbon, the second is the dehydrogenated species.
The cracking step is irreversible. Equations (6) through (10)
were also extended by assuming interaction of gaseous or
adsorbed hydrogen and/or competition for sites by hydrogen;
the equations become more complicated in these cases. All
these equations were a result of a balance for the dehydro-
genated species. Model 11 was derived on the assumption of
slow and strong adsorption of all hydrocarbons. The surface
splitting reactions are irreversible, but they are fast compared to
adsorption, so that most of the surface will be covered by
adsorbed C_1 species. This mechanism might explain the high
selectivity of methane on the iron catalysts. The value of
c is the number of hydrogen molecules needed in the desorp-
tion of the C_1 species. Of all the models tried with the
propane data, only model 2 gave consistently reasonable
results; the fit was usually about as good as that to the
power rate law while the parameters had acceptable values,
although at increasing temperature values for "a" tended to
decrease here also, and the rate-and adsorption constants
usually could not be fitted to an Arrhenius type equation.
This mechanism was based (146) on the assumption of a single
catalytic site, a preponderance of the most dehydrogenated
species, and adsorption-desorption equilibrium.

A P P E N D I X C

THE DERIVATION OF THE SELECTIVITY EQUATIONS

C.1 Introduction

The selectivity for a particular hydrocarbon was de-
fined as the moles of that product formed per mole of feed
hydrocarbon consumed. The product distributions depend very
much on the catalyst used, and on the temperature, but not
very much on the total pressure (44). As the temperature
increases, the product distributions shift more toward pro-
ducts with lower carbon numbers, and the same change in se-
lectivity occurs in going from ruthenium to nickel, to co-
balt, to iron. The product distribution also depends on the
conversion of the feed hydrocarbon, because every product,
except methane, can crack further to give still smaller
products. Any reaction network proposed to explain the pro-
duct distributions, must take these consecutive reactions
into account, and must also allow for the parallel hydroge-
nolysis in case of hydrocarbons with more than one type of
carbon-carbon bond. Since the reaction schemes are too
complex for exact solutions, some simplifying assumptions
are made, but the resulting equations are still very gene-
ral, since no rate-limiting step is assumed and all the

possible reactions are considered.

The assumptions are:

1. Isomerisation reactions do not occur, since no isomer-
   isation products were observed in the experiments.

2. All hydrocarbons are assumed to adsorb and desorb revers-
   ibly, to form surface intermediates; this is according to
   the schemes developed by Cimino et al (7) and Sinfelt (29),
   and in contrast to the scheme proposed by Boudart (97).
   This assumption agrees also with deuterium exchange ex-
   periments (26, 42, 43). Iron may be different in this
   respect (102).

3. The surface intermediates react irreversibly via the
   rupture of one single carbon-carbon bond to produce
   smaller adsorbed species. Multiple bond breaking does not
   occur, and the reverse reaction of chain growth also is
   not considered because the hydrogenolysis reaction is
   highly favoured thermodynamically.

4. If the feed hydrocarbon and/ or one of the products con-
   tain more than one type of carbon-carbon bond, a fraction-
   al split factor is assigned to each bond type, defined as
   the probability that hydrogenolysis will occur at that
   bond type. These split factors are assumed to be constant
   with conversion.

5. All the surface reactions are assumed to be first order
   in the hydrocarbon species involved, which is reasonable,
   since hydrogenolysis reactions always have been reported

to be nearly first order with respect to the hydrocarbon (24, 44).

6. Hydrogen may take part in the surface cracking reaction either in an adsorbed form or from the gas phase. The effects of hydrogen are assumed to be nearly constant, and incorporated into the rate constants. This is reasonable because the parameters in the selectivity equations always occur as ratios of rate constants, thus any errors of incorporating hydrogen pressure effects into a rate constant are minimized by dividing by another rate constant with similar errors.

7. No rate limiting step is assumed, but overall balances are used in the derivations.

8. Time is eliminated as a variable, and only ratios of rate constants are obtained. On this basis the first order kinetics can be justified, as common terms cancel, e.g. the denominator in Langmuir-Hinshelwood equations.

9. A consequence of the features of the selectivity equations as described in 8. is that the equations may be valid, in some cases, for catalysts with changing activity.

C.2 Propane

The proposed reaction network for the hydrogenolysis of propane is shown in fig. C-1 with the corresponding rate constants. This reaction network can be solved by using the steady state approximation for the adsorbed species, (98, 99).

Figure C-1

Propane Hydrogenolysis Reaction Network
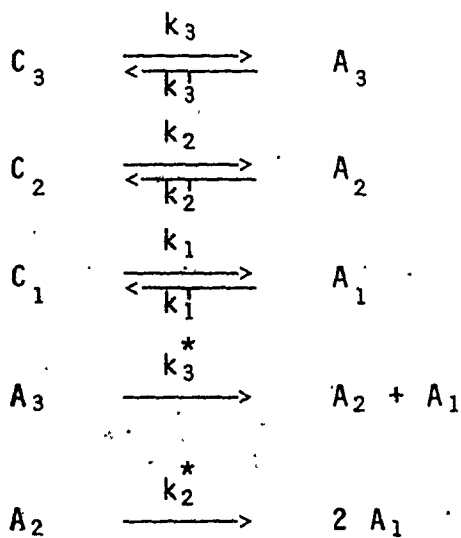
$$C_3 \quad \underset{k_3'}{\overset{k_3}{\rightleftharpoons}} \quad A_3$$

$$C_2 \quad \underset{k_2'}{\overset{k_2}{\rightleftharpoons}} \quad A_2$$

$$C_1 \quad \underset{k_1'}{\overset{k_1}{\rightleftharpoons}} \quad A_1$$

$$A_3 \quad \xrightarrow{k_3^*} \quad A_2 + A_1$$

$$A_2 \quad \xrightarrow{k_2^*} \quad 2\,A_1$$

C_x = gaseous hydrocarbon, carbon number x

A_x = adsorbed hydrocarbon species

k_x = adsorption rate constant

k_x' = desorption rate constant

k_x^* = surface cracking rate constant

$k_x'' = k_x\, k_x^* / (k_x' + k_x^*)$

The overall rate of propane formation, R_3, is:

$$R_3 = -k_3 C_3 + k_3' A_3 \qquad \text{(C-1)}$$

$$R_3 = -k_3^* A_3 \qquad \text{(C-2)}$$

where C_3 and A_3 are the concentration of gaseous propane and the fractional coverage of the catalyst surface by the ad-sorbed C_3 species.

Combination of (C-1) and (C-2) gives:

$$-R_3 = k_3'' C_3 \qquad \text{(C-3)}$$

where $\quad k_x'' = k_x k_x^* / (k_x' + k_x^*)$ $\qquad$ (C-3a)

The hydrogenolysis reactions are equimolar, so there are no changes in volume and in flow rate between inlet and outlet, and a propane mass balance over the reactor gives:

$$F C_3^o = F C_3 + V k_3'' C_3 \qquad \text{(C-4)}$$

$$C_3^o = C_3 + \tau k_3'' C_3 \qquad \text{(C-5)}$$

where $\quad C_3^o$ = concentration of propane in inlet

$\qquad\quad C_3$ = concentration of propane in effluent

$\qquad\quad F$ = total flow rate in moles/ unit time

$\qquad\quad V$ = reactor volume

$\qquad\quad \tau$ = reactor residence time (V/F)

Using the definition of the conversion of propane, X_3:

$$X_3 = (C_3^O - C_3) / C_3^O \tag{C-6}$$

one obtains

$$X_3 = \tau k_3'' / (1 + \tau k_3'') \tag{C-7}$$

or $\qquad \tau = X_3 / \{ k_3'' (1-X_3) \} \tag{C-8}$

The overall rate of ethane formation, R_2, is similarly.

$$R_2 = -k_2 C_2 + k_2' A_2 \tag{C-9}$$

$$R_2 = -k_2^* A_2 + k_3^* A_3 \tag{C-10}$$

Substitution of (C-2) and (C-3) yields

$$-R_2 = k_2'' C_2 - \frac{k_3'' k_2'}{k_2^* + k_2'} C_3 \tag{C-11}$$

A mass balance of ethane, using (C-11), gives.

$$0 = C_2 + \tau \left(k_2'' C_2 - \frac{k_2' k_3''}{k_2' + k_2^*} C_3 \right) \tag{C-12}$$

and substitution of (C-6) and (C-8)

$$\frac{C_2}{C_3^o} = \frac{\dfrac{k_2'}{k_2'+k_2^*}\, X_3}{1 + \dfrac{k_2''}{k_3''}\cdot\dfrac{X_3}{1-X_3}} \qquad \text{(C-13)}$$

The selectivity of ethane, S_2, is defined as

$$S_2 = C_2 /(C_3^o X_3) \qquad \text{(C-14)}$$

So that, S_2

$$S_2 = \frac{k_2' /(k_2'+k_2^*)}{1 + \dfrac{k_2''}{k_3''}\cdot\dfrac{X_3}{1-X_3}} \qquad \text{(C-15)}$$

The parameter $k_2' /(k_2'+k_2^*)$ corresponds to the relative rates of desorption and cracking of the adsorbed C_2 species, while k_2'' / k_3'' is the ratio of the overall rates for ethane and propane hydrogenolysis, since all reactions are assumed to be first order in the hydrocarbon involved. Similar ratios k_x'' / k_6'' and $k_x' /(k_x'+k_x^*)$ will appear in the selectivity equations for the hexanes. If desorption of the adsorbed hydrocarbon species is much faster than cracking, as is often assumed in the hydrogenolysis of ethane (surface cracking rate-limiting step), the parameter $k_2' /(k_2'+k_2^*)$ should approach

unity. The methane selectivity, S_1, is fixed by a carbon balance according to

$$S_1 + 2S_2 = 3 \qquad (C-16)$$

C.3 2,3-Dimethylbutane

The reaction network for hydrogenolysis of 2,3-dimethylbutane is given in fig. C-2. The assumptions and the definitions of the rate constants are identical as for propane, and splitting factors are assigned were necessary. A slightly different approach is followed to derive the selectivity equations. The overall rate of formation of hexane (in this case 2,3-dimethylbutane) is given by:

$$R_6 = -k_6 C_6 + k_6' A_6 \qquad (C-17)$$

$$R_6 = -k_6^* A_6 \qquad (C-18)$$

or, by combining these two

$$(-R_6) = k_6'' C_6 \qquad (C-19)$$

where k_6'' is defined as in (C-3a).

Some groups of constants and variables are defined as follows, in order to make derivations easier.

$$j_x = \frac{k_x'}{k_x + k_x^*} \qquad (C-20)$$

Figure C-2

Reaction Network for the Hydrogenolysis of 2,3-DMB

Constants are defined in Figure C-1

$$C_6 \xrightleftharpoons[k_6']{k_6} A_6 \qquad i\text{-}C_5 \xrightleftharpoons[k_{i5}']{k_{i5}} i\text{-}A_5 \qquad i\text{-}C_4 \xrightleftharpoons[k_{i4}']{k_{i4}} i\text{-}A_4$$

$$C_1 \xrightleftharpoons[k_1']{k_1} A_1 \qquad C_2 \xrightleftharpoons[k_2']{k_2} A_2 \qquad C_3 \xrightleftharpoons[k_3']{k_3} A_3 \qquad n\text{-}C_4 \xrightleftharpoons[k_{n4}']{k_{n4}} n\text{-}A_4$$

$$A_6 \xrightarrow{k_6^*} \begin{cases} \xrightarrow{\ell} & i\text{-}A_5 + A_1 \\ \xrightarrow{(1-\ell)} & 2\,A_3 \end{cases}$$

$$i\text{-}A_5 \xrightarrow{k_{i5}^*} \begin{cases} \xrightarrow{f} & i\text{-}A_4 + A_1 \\ \xrightarrow{f'} & n\text{-}A_4 + A_1 \\ \xrightarrow{(1-f-f')} & A_3 + A_2 \end{cases}$$

$$i\text{-}A_4 \xrightarrow{k_{i4}^*} A_3 + A_1$$

$$n\text{-}A_4 \xrightarrow{k_{n4}^*} \begin{cases} \xrightarrow{m} & 2\,A_2 \\ \xrightarrow{(1-m)} & A_3 + A_1 \end{cases}$$

$$A_3 \xrightarrow{k_3^*} A_2 + A_1$$

$$A_2 \xrightarrow{k_2^*} 2\,A_1$$
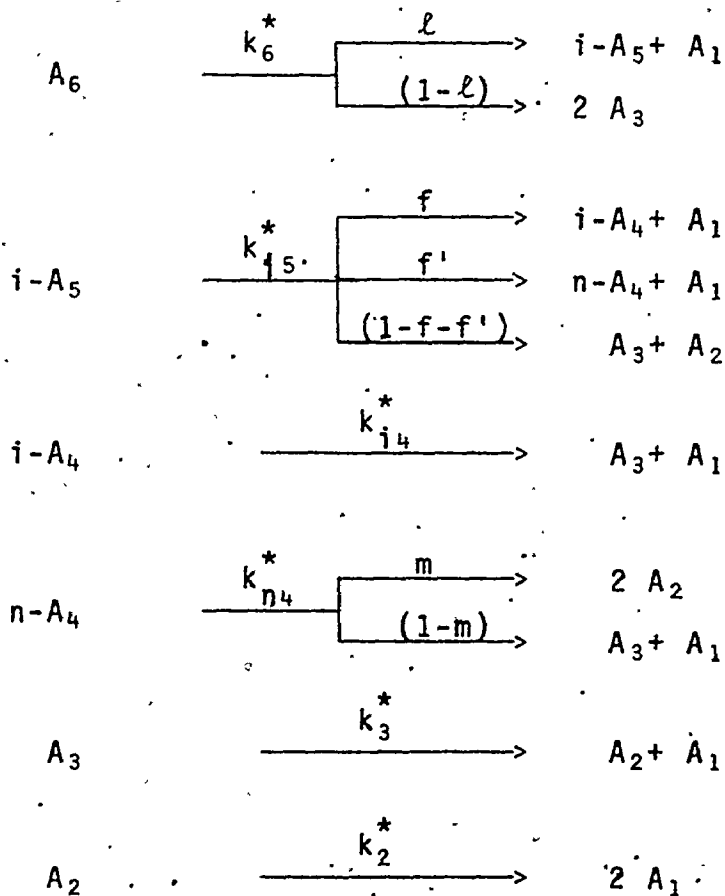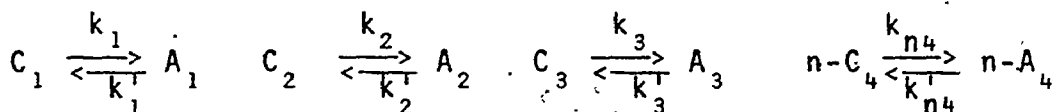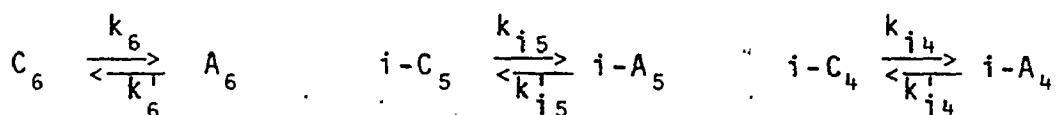
or $(1-j_x) = \dfrac{k_x^*}{k_x' + k_x^*}$ (C-21)

$Y_6 = X_6 / (1-X_6)$ (C-22)

$Z_x = 1 + \dfrac{k_x''}{k_6''} \cdot Y_6$ (C-23)

From equations like (C-17), it can be observed that for a component x,

$$A_x = \dfrac{R_x + k_x C_x}{k_x'} = \dfrac{R_x}{k_x'} + \dfrac{k_x}{k_x'} C_x$$ (C-24)

and finally, the selectivity for product x can be written as

$$S_x = \dfrac{R_x}{(-R_6)}$$ (C-25)

or $\quad S_x = \dfrac{C_x}{C_6^0 X_6} = \dfrac{C_x}{C_6 X_6 / (1-X_6)}$ (C-25a)

Starting from (C-24), the following general path can be

followed.

$$\frac{A_x}{-R_6} = \frac{S_x}{k_x'} - \frac{k_x C_x}{k_x' R_6} \qquad \text{(with (C-25))}$$

$$= \frac{S_x}{k_x'} + \frac{k_x}{k_x'} \frac{C_x}{k_6'' C_6} \qquad \text{(with (C-19))}$$

$$= \frac{S_x}{k_x'} + \frac{k_x}{k_x'} \frac{S_x Y_6}{k_6''} \qquad \text{(with (C-25a))}$$

$$= \frac{S_x}{k_x'} \left(1 + \frac{k_x}{k_6''} Y_6\right)$$

now,

$$\frac{k_x^* A_x}{-R_6} = S_x \left\{ \frac{k_x^*}{k_x'} + \frac{k_x k_x^*}{k_x' k_6''} Y_6 \frac{k_x' + k_x^*}{k_x' + k_x^*} \right\}$$

$$= S_x \left\{ \frac{k_x^*}{k_x'} + Z_x \frac{k_x' + k_x^*}{k_x'} - \frac{k_x' + k_x^*}{k_x'} \right\}$$

$$= S_x \left\{ \frac{Z_x}{j_x} - 1 \right\} \qquad \text{(C-26)}$$

The overall rate of formation of isopentane is given by

$$R_{i5} = -k^*_{15}A_{i5} + \ell\, k^*_6 A_6 \tag{C-27}$$

$$S_{i5} = \left(\frac{R_{15}}{-R_6}\right) = -\left(\frac{k^*_{15}A_{i5}}{-R_6}\right) + \frac{\ell\, k^*_6 A_6}{(-R_6)} \tag{C-28}$$

and with (C-26)

$$S_{i5} = -\frac{S_{i5}Z_{i5}}{j_{i5}} + S_{i5} + \ell$$

working this out, and substituting the appropriate para-
meters gives

$$S_{i5} = \frac{\ell j_{i5}}{Z_{i5}} = \frac{\left(\dfrac{k'_{15}}{k'_{15}+k^*_{15}}\right)\ell}{\left\{\,1 + \dfrac{k''_{15}}{k''_6}\left(\dfrac{X_6}{1-X_6}\right)\right\}} \tag{C-29}$$

and

$$\frac{S_{i5}Z_{i5}}{j_{i5}} = \ell \tag{C-29a}$$

The selectivities of other products are determined in exact-
ly the same way.

For isobutane, $R_{i4} = -k^*_{14}A_{i4} + fk^*_{15}A_{i5}$ (C-30)

$$S_{i4} = \frac{R_{i4}}{-R_6} = -\frac{S_{i4}Z_{i4}}{j_{i4}} + S_{i4} + fS_{i5}(\frac{Z_{i5}}{j_{i5}} - 1)$$

using (C-29a) this gives

$$\frac{S_{i4}Z_{i4}}{j_{i4}} = f\ell - fS_{i5}, \text{ and with the necessary}$$

substitutions,

$$S_{i4} = \frac{\{\frac{k'_{i4}}{k'_{i4}+k^*_{i4}}\} f(\ell S_{i5})}{\{1 + \frac{k''_{i4}}{k''_6}(\frac{X_6}{1-X_6})\}} \qquad (C-31)$$

and $\quad \frac{S_{i4}Z_{i4}}{j_{i4}} = f(\ell-S_{i5}) \qquad (C-31a)$

Similarly for n-butane

$$S_{n4} = \frac{\{\frac{k'_{n4}}{k'_{n4}+k^*_{n4}}\} f'(\ell-S_{i5})}{\{1 + \frac{k''_{n4}}{k''_6}(\frac{X_6}{1-X_6})\}} \qquad (C-32)$$

and $\quad \frac{S_{n4}Z_{n4}}{j_{n4}} = f'(\ell-S_{i5}) \qquad (C-32a)$

for propane

$$R_3 = -k_3^* A_3 + 2(1-\ell) k_6^* A_6 + (1-f-f') k_{i5}^* A_{i5} + k_{i4}^* A_{i4}$$
$$+ (1-m) k_{n4}^* A_{n4} \qquad (C-33)$$

$S_3 = (R_3 / -R_6)$, with the appropriate substitutions gives

$$S_3 = \frac{\{\dfrac{k_3'}{k_3'+k_3^*}\} (2 - \ell(1+mf') - S_{i4} - S_{n4}(1-m) - S_{i5}(1-mf'))}{\{ 1 + \dfrac{k_3''}{k_6''} (\dfrac{X_6}{1-X_6})\}} \qquad (C-34)$$

for ethane

$$R_2 = -k_2^* A_2 + k_3^* A_3 + 2m k_{n4}^* A_{n4} + (1-f-f') k_{i5}^* A_{i5}$$

and

$$S_2 = \frac{\{\dfrac{k_2'}{k_2'+k_2^*}\} (2 - \ell(f+f'-mf') - S_3 - S_{i4} - S_{n4}(1+m) - S_{i5}(2+mf'-f-f'))}{\{ 1 + \dfrac{k_2''}{k_6''} (\dfrac{X_6}{1-X_6})\}} \qquad (C-35)$$

The selectivity for methane can be obtained by a simple carbon balance: $S_1 + 2S_2 + 3S_3 + 4(S_{i4}+S_{n4}) + 5S_{i5} = 6$ which can be verified by deriving S_1, in the same way as the other selectivities, starting from the overall rate of

formation of methane:

$$R_1 = 2k_2^* A_2 + k_3^* A_3 + (1-m) k_{n4}^* A_4 + k_{i4}^* A_{i4} + (f+f') k_{i5}^* A_{i5}$$
$$+ \ell k_6^* A_6.$$

Equations (C-29), (C-31), (C-32), (C-34), and (C-35) are relations between the selectivities of the products and the conversion of 2,3-dimethylbutane, and these equations can be applied directly to the experimental data to find the parameters. If one or more of the products are never present on a certain catalyst, the equations simplify accordingly. It is not always possible to separate all the groups of para-meters. The value for k_x''/k_6'' is the ratio of the rates of hydrogenolysis of product x and the feed hydrocarbon. Values for $k_x'/(k_x' + k_x^*)$ can give the relative rates of desorption and surface cracking for component x, and are an indication of which steps in the network may be rate-limiting.

C.4 2,2-Dimethylbutane

The reaction network for the hydrogenolysis of 2,2-dimethylbutane is given in fig. C-3. In the derivation of the selectivity equations, the same approach is used as before: starting from an expression of the overall rate of formation of the product and using equation (C-26). The summarized results are as follows.

for neopentane,

$$R_{ne5} = -k_{ne5}^* A_{ne5} + \ell k_6^* A_6$$

Figure C-3

Reaction Network for the Hydrogenolysis of 2,2-DMB

$$C_6 \underset{k_6'}{\overset{k_6}{\rightleftarrows}} A_6 \qquad ne\text{-}C_5 \underset{k_{ne5}'}{\overset{k_{ne5}}{\rightleftarrows}} ne\text{-}A_5 \qquad i\text{-}C_5 \underset{k_{i5}'}{\overset{k_{i5}}{\rightleftarrows}} i\text{-}A_5 \qquad i\text{-}C_4 \underset{k_{i4}'}{\overset{k_{i4}}{\rightleftarrows}} i\text{-}A_4$$

$$C_1 \underset{k_1'}{\overset{k_1}{\rightleftarrows}} A_1 \qquad C_2 \underset{k_2'}{\overset{k_2}{\rightleftarrows}} A_2 \qquad C_3 \underset{k_3'}{\overset{k_3}{\rightleftarrows}} A_3 \qquad n\text{-}C_4 \underset{k_{n4}'}{\overset{k_{n4}}{\rightleftarrows}} n\text{-}A_4$$

Constants are defined in Figure C-1

$$A_6 \xrightarrow{k_6^*} \begin{cases} \overset{\ell}{\longrightarrow} & ne\text{-}A_5 + A_1 \\ \overset{\ell'}{\longrightarrow} & i\text{-}A_5 + A_1 \\ \overset{(1-\ell-\ell')}{\longrightarrow} & i\text{-}A_4 + A_1 \end{cases}$$

$$i\text{-}A_5 \xrightarrow{k_{i5}^*} \begin{cases} \overset{f}{\longrightarrow} & i\text{-}A_4 + A_1 \\ \overset{f'}{\longrightarrow} & n\text{-}A_4 + A_1 \\ \overset{(1-f-f')}{\longrightarrow} & A_3 + A_2 \end{cases}$$

$$ne\text{-}A_5 \xrightarrow{k_{ne5}^*} i\text{-}A_4 + A_1$$

$$i\text{-}A_4 \xrightarrow{k_{i4}^*} A_3 + A_1$$

$$n\text{-}A_4 \xrightarrow{k_{n4}^*} \begin{cases} \overset{m}{\longrightarrow} & 2\,A_2 \\ \overset{(1-m)}{\longrightarrow} & A_3 + A_1 \end{cases}$$

$$A_3 \xrightarrow{k_3^*} A_2 + A_1$$
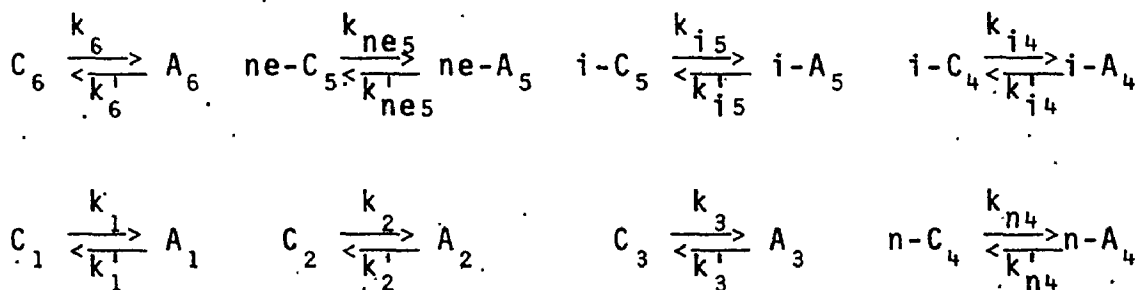
$$A_2 \xrightarrow{k_2^*} 2\,A_1$$
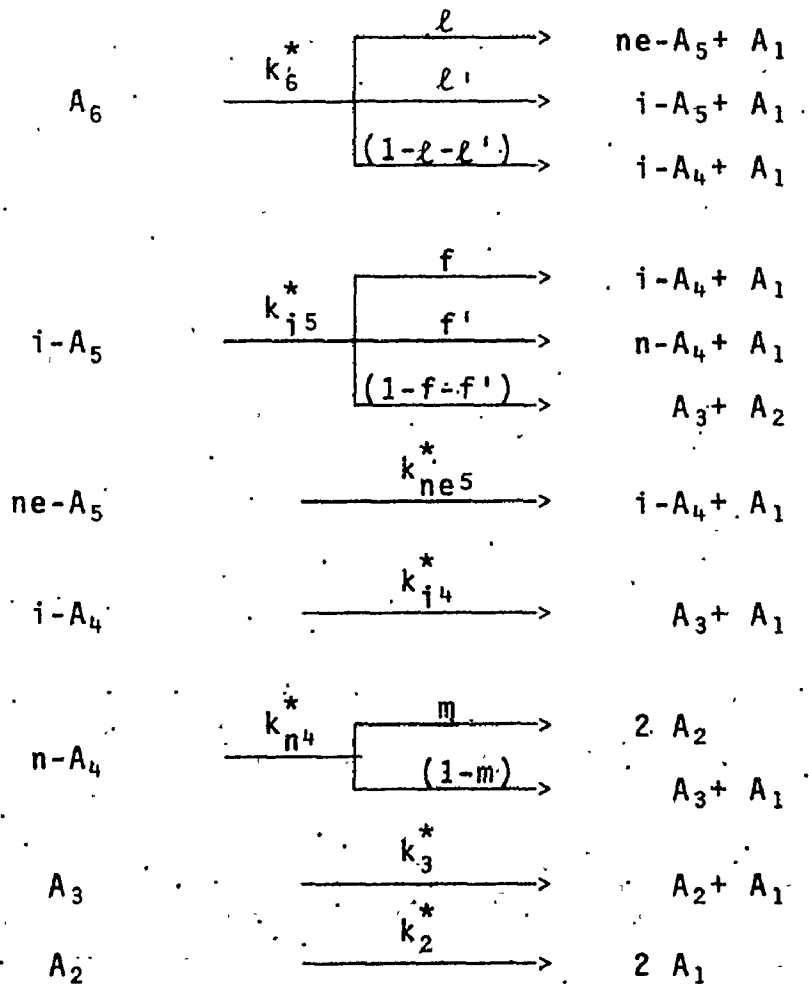
and
$$S_{ne5} = \frac{\{\dfrac{k'_{ne5}}{k'_{ne5}+k^*_{ne5}}\}\, \ell}{\{1 + \dfrac{k''_{ne5}}{k''_6}\,(\dfrac{X_6}{1-X_6})\}} \qquad (C-36)$$

for isopentane,

$$S_{i5} = \frac{\{\dfrac{k'_{i5}}{k'_{i5}+k^*_{i5}}\}\, \ell'}{\{1 + \dfrac{k''_{i5}}{k''_6}\,(\dfrac{X_6}{1-X_6})\}} \qquad (C-37)$$

for isobutane

$$R_{i4} = -k^*_{i4}A_{i4} + (1-\ell-\ell')\,k^*_6 A_6 + k^*_{ne5}A_{ne5} + fk^*_{i5}A_{i5}$$

and
$$S_{i4} = \frac{\{\dfrac{k'_{i4}}{k'_{i4}+k^*_{i4}}\}\,(1-\ell(1-f)-S_{ne5}-fS_{i5})}{\{1 + \dfrac{k''_{i4}}{k''_6}\,(\dfrac{X_6}{1-X_6})\}} \qquad (C-38)$$

for n-butane

$$S_{n4} = \frac{\{\dfrac{k'_{n4}}{k'_{n4}+k^*_{n4}}\}\, f'(\ell'-S_{i5})}{\{1 + \dfrac{k''_{n4}}{k''_6}\,(\dfrac{X_6}{1-X_6})\}} \qquad (C-39)$$

for propane,

$$R_3 = -k_3^* A_3 + (1-m) k_{n4}^* A_{n4} + k_{i4}^* A_{i4} + (1-f-f') k_{i5}^* A_{i5}$$

and

$$S_3 = \frac{\{ \frac{k_3'}{k_3'+k_3^*} \} (1-mf'\ell' -S_{n4}(1-m) -S_{i4} -S_{ne5} -S_{i5}(1-mf'))}{\{1 + \frac{k_3''}{k_6''} (\frac{X_6}{1-X_6})\}} \qquad \text{(C-40)}$$

for ethane,

$$S_2 = \frac{\{ \frac{k_2'}{k_2'+k_2^*} \} (2-\ell-f\ell'-f'\ell'+mf'\ell' -S_3 -S_{n4}(1+m)-S_{i4} -S_{ne5} -S_{i5}(2-f-f'+mf'))}{\{1 + \frac{k_2''}{k_6''} (\frac{X_6}{1-X_6})\}} \qquad \text{(C-41)}$$

the methane selectivity follows from the carbon balance:

$$S_1 + 2S_2 + 3S_3 + 4(S_{n4} + S_{i4}) + 5(S_{ne5} + S_{i5}) = 6 \qquad \text{(C-42)}$$

C.5 n-Hexane

The reaction network for hydrogenolysis of n-hexane is in fig. C-4. The derivation of the selectivity equations is as before, and the results are as follows.

for n-pentane,

Figure C-4

Reaction Network for the Hydrogenolysis of n-Hexane

Constants are defined in Figure C-1

$$C_6 \; \underset{k_6'}{\overset{k_6}{\rightleftharpoons}} \; A_6 \qquad\qquad n\text{-}C_5 \; \underset{k_{n5}'}{\overset{k_{n5}}{\rightleftharpoons}} \; n\text{-}A_5 \qquad n\text{-}C_4 \underset{k_{n4}'}{\overset{k_{n4}}{\rightleftharpoons}} n\text{-}A_4$$

$$C_1 \; \underset{k_1'}{\overset{k_1}{\rightleftharpoons}} \; A_1 \qquad\qquad C_2 \underset{k_2'}{\overset{k_2}{\rightleftharpoons}} A_2 \qquad\qquad C_3 \underset{k_3'}{\overset{k_3}{\rightleftharpoons}} A_3$$

$$A_6 \xrightarrow{k_6^*}
\begin{cases}
\xrightarrow{\ell} & n\text{-}A_5 + A_1 \\
\xrightarrow{\ell'} & n\text{-}A_4 + A_2 \\
\xrightarrow{(1-\ell-\ell')} & 2\,A_3
\end{cases}$$

$$n\text{-}A_5 \xrightarrow{k_{n5}^*}
\begin{cases}
\xrightarrow{f} & n\text{-}A_4 + A_1 \\
\xrightarrow{(1-f)} & A_3 + A_2
\end{cases}$$

$$n\text{-}A_4 \xrightarrow{k_{n4}^*}
\begin{cases}
\xrightarrow{m} & 2\,A_2 \\
\xrightarrow{(1-m)} & A_3 + A_1
\end{cases}$$

$$A_3 \xrightarrow{k_3^*} A_2 + A_1$$

$$A_2 \xrightarrow{k_2^*} 2\,A_1$$
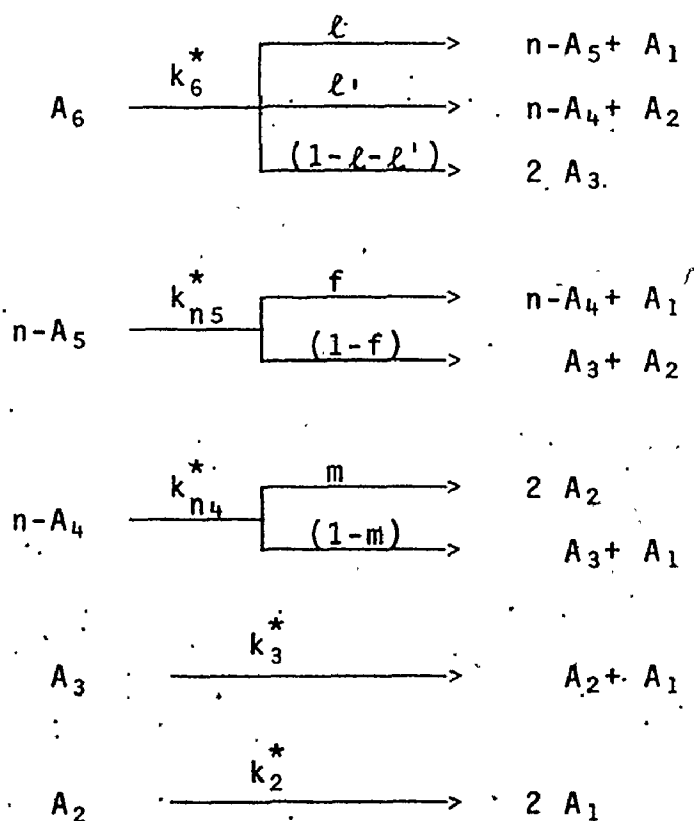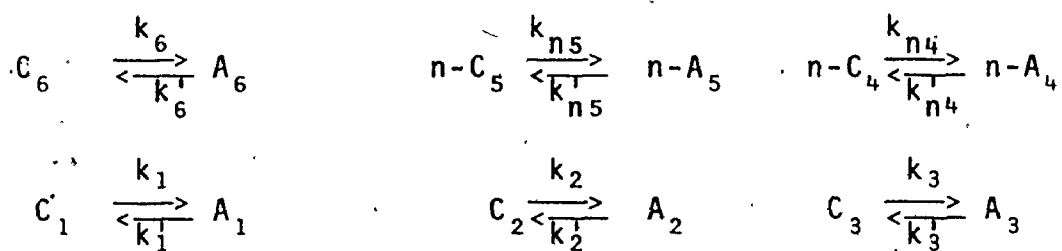
$$S_{n5} = \frac{\{\dfrac{k'_{n5}}{k'_{n5}+k^*_{n5}}\}\; \ell}{\{1 + \dfrac{k''_{n5}}{k''_6}\; (\dfrac{X_6}{1-X_6})\}} \tag{C-43}$$

for n-butane,

$$S_{n4} = \frac{\{\dfrac{k'_{n4}}{k'_{n4}+k^*_{n4}}\}(\ell' + f\ell - fS_{n5})}{\{1 + \dfrac{k''_{n4}}{k''_6}\; (\dfrac{X_6}{1-X_6})\}} \tag{C-44}$$

for propane,

$$S_3 = \frac{\{\dfrac{k'_3}{k'_3+k^*_3}\}(2-\ell-\ell'-m\ell'-mf\ell\; -S_{n4}(1-m) +S_{n5}(mf-1))}{\{1 + \dfrac{k''_3}{k''_6}\; (\dfrac{X_6}{1-X_6})\}} \tag{C-45}$$

for ethane,

$$S_2 = \frac{\{\dfrac{k'_2}{k'_2+k^*_2}\}(2-f\ell+m\ell'+mf\ell\; -S_3\; -S_{n4}(1+m) -S_{n5}(2+mf-f))}{\{1 + \dfrac{k''_2}{k''_6}\; (\dfrac{X_6}{1-X_6})\}} \tag{C-46}$$

for methane,

$$S_1 = 6 - 5S_{n5} - 4S_{n4} - 3S_3 - 2S_2 \qquad \text{(C-47)}$$

A P P E N D I X D

TABLES OF EXPERIMENTAL DATA

Rate Data for the Hydrogenolysis of Propane over Ruthenium on Alumina

Temp (°C)	Total Pressure (atm)	% Hydrogen in feed	Conversion	Rate $\left[\frac{\mu\,mol}{s\cdot g\ cat.}\right]$	Selectivity Methane	Ethane
150.2	1.31	69.85	0.125	1.034	1.03	0.99
150.3	1.30	73.08	0.122	0.859	1.03	0.99
150.3	1.30	84.25	0.116	0.410	1.03	0.99
150.3	1.30	81.21	0.143	0.505	1.03	0.99
150.2	1.30	75.81	0.195	0.692	1.03	0.98
150.2	1.29	89.32	0.179	0.238	1.03	0.99
150.2	1.29	93.19	0.113	0.148	1.03	0.99
150.5	1.95	77.44	0.037	0.332	1.01	1.00
150.1	1.95	82.96	0.034	0.210	1.01	1.00
150.5	1.94	92.29	0.032	0.081	1.02	0.99
150.1	1.95	82.99	0.062	0.155	1.01	1.00
149.5	1.95	70.97	0.068	0.336	1.01	0.99
149.7	1.95	77.95	0.044	0.221	1.01	1.00
149.9	1.94	85.47	0.025	0.130	1.02	0.99
178.6	1.95	87.88	0.183	1.864	1.05	0.97
178.8	1.94	92.27	0.192	1.174	1.05	0.97
178.8	1.93	97.03	0.206	0.461	1.06	0.97
179.2	1.93	95.29	0.297	0.665	1.05	0.97
178.8	1.94	91.96	0.434	0.981	1.05	0.97

TABLE D-1 (continued)

Temp (°C)	Total Pressure (atm)	% Hydrogen in feed	Conversion	Rate $\left[\dfrac{\mu\ mol}{(s \cdot g\ cat.)}\right]$	Selectivity Methane	Ethane
178.2	1.95	80.01	0.538	2.852	1.07	0.96
178.7	1.95	86.54	0.380	2.019	1.05	0.97
178.3	1.95	78.22	0.395	3.767	1.06	0.97
178.9	1.30	93.33	0.490	1.390	1.09	0.96
179.0	1.31	80.22	0.421	5.117	1.10	0.95
178.7	1.31	85.03	0.335	4.026	1.08	0.96
178.8	1.30	93.02	0.355	1.813	1.08	0.96
178.8	1.29	94.79	0.504	1.079	1.08	0.96
178.8	1.30	95.27	0.573	0.778	1.08	0.96
178.5	1.30	82.47	0.392	4.269	1.09	0.95

TABLE D-2

Rate Data for the Hydrogenolysis of Propane over Nickel on Silica

Temp (°C)	Total Pressure (atm)	% Hydrogen in feed	Conversion	Rate $\left[\dfrac{\mu\,mol}{s \cdot g\,cat.}\right]$	Selectivity Methane	Ethane
254.6	2.07	89.30	0.157	0.374	1.61	0.70
254.2	2.08	82.12	0.181	0.765	1.64	0.68
254.8	2.10	71.35	0.320	2.448	1.86	0.57
254.4	2.10	72.92	0.260	2.022	1.80	0.60
254.8	2.08	81.31	0.118	0.935	1.66	0.67
254.4	2.09	76.83	0.134	1.386	1.69	0.66
254.5	2.08	79.14	0.131	1.186	1.67	0.67
254.7	2.08	85.13	0.100	0.604	1.61	0.69
254.8	2.05	92.30	0.087	0.253	1.67	0.67
254.6	2.09	75.69	0.128	1.432	1.68	0.66
254.4	2.10	72.61	0.143	1.873	1.72	0.64
254.4	2.09	77.41	0.094	1.234	1.66	0.67
253.9	2.10	73.01	0.108	1.793	1.70	0.65
254.4	1.67	81.63	0.336	1.067	1.85	0.58
254.1	1.68	77.64	0.201	1.513	1.84	0.58
254.1	1.67	84.05	0.172	0.860	1.78	0.61
254.4	1.65	90.41	0.173	0.478	1.76	0.61
254.5	1.64	93.64	0.152	0.273	1.73	0.64
254.5	1.67	84.63	0.170	0.807	1.77	0.61
254.2	1.67	80.20	0.186	1.207	1.80	0.60

TABLE D-2 (continued)

Temp (°C)	Total Pressure (atm)	% Hydrogen in feed	Conversion	Rate $\left[\frac{\mu \text{mol}}{\text{s} \cdot \text{g cat.}}\right]$	Selectivity Methane	Ethane
254.3	1.67	78.39	0.212	1.409	1.83	0.59
254.4	1.66	83.86	0.139	0.912	1.76	0.62
254.6	1.65	91.92	0.124	0.373	1.72	0.64
254.5	1.64	93.66	0.127	0.292	1.78	0.61
254.0	1.68	73.99	0.174	2.068	1.85	0.58
255.7	1.15	83.69	0.567	1.406	2.18	0.41
254.4	1.15	88.71	0.359	0.851	2.00	0.50
254.6	1.15	91.86	0.341	0.558	1.98	0.51
254.0	1.17	77.78	0.474	2.474	2.17	0.42
254.2	1.16	80.89	0.444	1.896	2.14	0.43
254.2	1.15	85.96	0.379	1.127	2.04	0.48
254.2	1.15	88.90	0.291	0.846	1.99	0.51
254.2	1.14	93.39	0.266	0.440	1.95	0.53
253.9	1.15	85.65	0.300	1.178	2.00	0.50
254.2	1.16	82.35	0.332	1.659	2.05	0.48
254.2	1.17	79.63	0.360	2.143	2.09	0.46
254.0	1.17	76.77	0.395	2.790	2.14	0.43
255.2	1.17	78.31	0.416	2.811	2.16	0.42
277.8	2.08	89.53	0.121	1.804	1.98	0.51
277.8	2.08	87.67	0.121	2.111	1.96	0.52

TABLE D-2 (continued)

Temp (°C)	Total Pressure (atm)	% Hydrogen in feed	Conversion	Rate $\left[\dfrac{\mu \text{ mol}}{s \cdot g \text{ cat.}}\right]$	Selectivity Methane	Ethane
279.0	2.08	89.50	0.424	1.682	2.05	0.47
278.2	2.10	81.27	0.185	5.200	2.01	0.50
278.2	2.08	81.67	0.179	4.847	1.99	0.51
278.0	2.08	85.00	0.163	3.508	1.95	0.53
278.2	2.08	88.43	0.160	2.551	1.93	0.53
278.5	2.06	91.20	0.154	1.803	1.93	0.53
278.7	2.03	97.74	0.159	0.463	2.04	0.48
278.2	2.04	94.67	0.305	0.835	1.97	0.52
278.0	2.08	85.51	0.383	3.088	2.04	0.48
278.0	2.09	81.48	0.435	4.638	2.11	0.45
278.2	2.06	92.60	0.152	1.555	1.93	0.54
278.5	1.68	81.70	0.223	7.051	2.12	0.44
278.4	1.67	87.60	0.214	4.301	2.08	0.46
278.5	1.66	91.22	0.208	2.843	2.07	0.47
278.6	1.64	95.01	0.205	1.569	2.06	0.47
278.7	1.63	98.58	0.218	0.460	2.13	0.43
278.3	1.63	99.28	0.222	0.232	2.19	0.40
279.1	1.65	92.62	0.571	1.513	2.19	0.40
278.5	1.67	84.15	0.668	4.092	2.33	0.33
278.1	1.68	80.42	0.733	5.765	2.44	0.28

Temp (°C)	Total Pressure (atm)	% Hydrogen in feed	Conversion	Rate $\left[\dfrac{\mu\,mol}{s \cdot g\ cat.}\right]$	Selectivity Methane	Ethane
278.2	1.65	94.88	0.540	0.967	2.16	0.42
277.9	1.66	90.54	0.345	2.680	2.10	0.45
278.5	1.16	89.92	0.459	4.180	2.33	0.34
278.6	1.15	95.10	0.447	1.906	2.31	0.35
278.4	1.14	98.18	0.442	0.676	2.27	0.36
278.5	1.16	90.00	0.468	4.305	2.34	0.33
278.4	1.17	87.75	0.473	5.414	2.34	0.33
278.4	1.17	86.00	0.488	6.538	2.37	0.32
278.6	1.18	78.98	0.525	11.417	2.43	0.28
278.5	1.14	94.06	0.776	1.250	2.49	0.26
278.6	1.16	87.48	0.820	2.980	2.58	0.21
279.2	2.08	91.43	0.545	1.589	2.10	0.45
279.1	2.07	91.35	0.535	1.616	2.09	0.45
279.1	2.07	91.26	0.522	1.669	2.08	0.46
279.5	2.07	90.15	0.550	2.108	2.12	0.44
279.2	2.07	90.47	0.525	1.897	2.08	0.46
279.0	2.07	90.99	0.537	1.723	2.08	0.46
278.8	2.08	89.79	0.534	1.961	2.07	0.46
279.0	2.06	90.94	0.561	1.884	2.10	0.45
279.6	2.06	91.10	0.636	2.058	2.15	0.43

Temp (°C)	Total Pressure (atm)	% Hydrogen in feed	Conversion	Rate $\left[\frac{\mu\,mol}{s \cdot g\,cat.}\right]$	Selectivity Methane	Ethane
279.4	2.06	90.96	0.565	1.911	2.10	0.45
279.2	2.06	89.25	0.470	2.623	2.04	0.48
279.3	2.06	90.02	0.569	2.106	2.10	0.45
304.1	2.07	91.19	0.791	6.147	2.51	0.25
304.2	2.06	93.92	0.667	5.476	2.38	0.31
303.9	2.07	88.80	0.705	11.138	2.44	0.28
303.5	2.08	85.72	0.731	15.271	2.49	0.26
303.9	2.07	86.35	0.614	17.608	2.40	0.30
303.2	2.06	89.48	0.592	12.683	2.37	0.32
303.2	2.06	88.79	0.594	13.694	2.37	0.31
303.9	2.06	91.17	0.580	10.202	2.35	0.33
303.9	2.05	92.48	0.576	8.537	2.34	0.33
303.9	2.03	93.38	0.572	7.394	2.34	0.33
303.9	2.03	94.11	0.540	6.984	2.31	0.34
304.6	1.65	89.68	0.887	6.753	2.71	0.15
304.1	1.64	93.06	0.782	6.282	2.56	0.22
303.7	1.65	90.10	0.789	9.371	2.58	0.21
303.7	1.66	89.44	0.791	10.350	2.59	0.20
303.6	1.66	87.68	0.801	12.078	2.60	0.20
303.4	1.66	87.25	0.798	12.527	2.61	0.20

Temp (°C)	Total Pressure (atm)	% Hydrogen in feed	Conversion	Rate $\left[\dfrac{\mu \text{ mol}}{\text{s} \cdot \text{g cat.}}\right]$	Selectivity Methane	Ethane
303.5	1.67	85.33	0.713	19.248	2.55	0.23
303.5	1.66	85.92	0.713	18.300	2.54	0.23
303.3	1.66	88.18	0.700	14.805	2.52	0.24
303.4	1.65	90.24	0.695	11.694	2.51	0.25
303.4	1.64	95.80	0.695	4.783	2.49	0.25
304.6	1.16	89.77	0.937	5.736	2.85	0.08
304.0	1.15	93.02	0.869	6.111	2.74	0.13
303.6	1.15	95.03	0.796	5.982	2.67	0.17
303.8	1.16	90.52	0.784	11.785	2.67	0.16
303.2	1.16	88.19	0.765	14.802	2.66	0.17
303.2	1.17	86.41	0.770	17.423	2.68	0.16
303.1	1.17	87.77	0.731	17.101	2.65	0.18
303.8	1.16	89.91	0.759	14.368	2.67	0.17
303.7	1.16	91.66	0.773	11.982	2.67	0.16
303.6	1.15	94.69	0.693	9.348	2.62	0.19
303.8	1.16	91.90	0.662	13.991	2.60	0.20
303.8	1.16	90.04	0.637	16.788	2.59	0.20
281.5	20.7	90.82	0.633	2.037	2.17	0.42
309.2	2.07	91.18	0.845	6.579	2.61	0.20

Rate Data for the Hydrogenolysis of Propane over Nickel on Siliconcarbide

Temp (°C)	Total Pressure (atm)	% Hydrogen in feed	Conversion	Rate $\frac{\mu \text{ mol}}{(s \cdot g \text{ cat.})}$	Selectivity Methane	Ethane
277.2	1.14	87.50	0.171	0.323	2.08	0.46
277.1	1.14	90.14	0.125	0.236	2.06	0.47
277.0	1.14	77.53	0.161	0.806	2.15	0.43
277.5	1.14	82.41	0.107	0.545	2.11	0.45
277.1	1.14	92.26	0.360	0.149	2.13	0.43
277.1	1.14	97.02	0.181	0.059	2.05	0.48
277.1	1.14	99.00	0.178	0.019	2.02	0.49
276.9	1.14	89.67	0.198	0.242	2.08	0.46
277.2	1.14	78.32	0.282	0.827	2.20	0.40
277.4	1.14	83.92	0.176	0.500	2.11	0.44
277.1	1.14	97.68	0.132	0.047	2.04	0.48
276.8	1.14	85.52	0.102	0.406	2.08	0.46
277.2	1.99	93.61	0.088	0.037	1.74	0.63
276.8	1.99	80.11	0.119	0.185	1.83	0.59
277.4	1.99	93.20	0.029	0.049	1.69	0.66
277.0	1.99	84.45	0.031	0.135	1.67	0.67
277.4	1.99	76.02	0.108	0.273	1.88	0.56
277.0	1.99	94.16	0.067	0.089	1.70	0.65
277.4	1.99	86.10	0.083	0.109	1.77	0.62
276.9	1.99	75.46	0.095	0.256	1.83	0.58

Temp (°C)	Total Pressure (atm)	% Hydrogen in feed	Conversion	Rate $\left(\frac{\mu\,mol}{s\cdot g\,cat.}\right)$	Selectivity Methane	Ethane
277.2	1.99	83.16	0.052	0.143	1.80	0.60
277.3	1.99	88.39	0.065	0.082	1.75	0.62
277.0	1.99	82.33	0.112	0.140	1.82	0.59
277.4	1.99	88.30	0.052	0.086	1.74	0.63
293.4	1.14	94.55	0.687	0.267	2.41	0.30
291.6	1.14	97.01	0.307	0.203	2.22	0.39
291.4	1.14	89.54	0.770	0.389	2.48	0.26
291.4	1.14	94.50	0.502	0.303	2.30	0.35
291.5	1.14	96.16	0.397	0.234	2.24	0.38
291.6	1.14	96.64	0.316	0.229	2.22	0.39
291.7	1.14	97.12	0.265	0.212	2.23	0.39
291.5	1.14	95.46	0.259	0.333	2.19	0.40
291.4	1.14	93.27	0.396	0.445	2.27	0.37
291.4	1.14	91.54	0.480	0.524	2.31	0.35
291.5	1.14	84.01	0.278	1.609	2.31	0.35
291.4	1.14	76.04	0.293	3.108	2.38	0.31
291.4	1.99	84.96	0.159	0.546	2.01	0.50
291.9	1.99	88.49	0.120	0.409	1.99	0.51
291.6	1.99	99.62	0.104	0.010	1.92	0.54
291.3	1.99	97.22	0.096	0.072	1.89	0.56

Temp (°C)	Total Pressure (atm)	% Hydrogen in feed	Conversion	Rate $\left[\dfrac{\mu\ mol}{s \cdot g\ cat.}\right]$	Selectivity Methane	Ethane
291.3	1.99	78.96	0.131	0.930	2.04	0.48
291.4	1.99	84.37	0.080	0.573	2.00	0.50
291.5	1.99	96.80	0.067	0.086	1.88	0.56
291.4	1.99	96.27	0.291	0.072	1.96	0.52
291.2	1.99	91.83	0.252	0.193	1.97	0.51
291.4	1.99	95.92	0.128	0.101	1.86	0.57
290.7	1.99	83.04	0.149	0.564	1.94	0.53
291.1	1.99	87.81	0.048	0.387	1.90	0.55
305.9	1.14	98.38	0.696	0.175	2.50	0.25
305.4	1.14	99.44	0.558	0.079	2.41	0.30
305.1	1.14	93.08	0.568	1.063	2.49	0.26
305.0	1.14	86.37	0.628	2.485	2.58	0.21
305.0	1.14	97.92	0.441	0.378	2.41	0.30
305.0	1.14	91.16	0.454	1.810	2.47	0.27
305.1	1.14	85.43	0.484	3.372	2.53	0.24
306.0	1.14	92.44	0.284	1.890	2.44	0.28
305.1	1.14	86.14	0.287	3.689	2.48	0.26
305.4	1.14	96.22	0.275	0.881	2.43	0.29
304.7	1.14	97.52	0.203	0.544	2.38	0.31
305.0	1.14	86.29	0.597	2.432	2.58	0.21

Temp (°C)	Total Pressure (atm)	% Hydrogen in feed	Conversion	Rate $\frac{\mu mol}{s \cdot g\ cat.}$	Selectivity Methane	Ethane
305.5	1.99	87.92	0.554	0.925	2.24	0.38
305.6	1.99	93.12	0.291	0.588	2.10	0.45
305.4	1.99	87.11	0.326	1.313	2.15	0.42
305.1	1.99	81.85	0.366	2.213	2.21	0.39
305.4	1.99	86.51	0.237	1.529	2.14	0.43
305.9	1.99	94.90	0.553	0.277	2.18	0.41
304.9	1.99	86.38	0.400	1.340	2.19	0.41
306.0	1.99	95.88	0.345	0.310	2.10	0.45
305.9	1.99	96.70	0.190	0.265	2.13	0.44
305.6	1.99	91.89	0.209	0.750	2.09	0.45
305.4	1.99	84.74	0.236	1.748	2.14	0.43
306.2	1.99	97.30	0.205	0.234	2.08	0.46

TABLE D-4

Rate Data for the Hydrogenolysis of Propane over Nickel-Magnesium on Siliconcarbide

Temp (°C)	Total Pressure (atm)	% Hydrogen in feed	Conversion	Rate $\left[\frac{\mu \text{ mol}}{\text{s} \cdot \text{g cat.}}\right]$	Selectivity Methane	Ethane
250.6	1.14	91.82	0.354	0.173	2.01	0.50
250.8	1.14	96.72	0.156	0.078	1.88	0.56
251.1	1.14	87.15	0.537	0.273	2.14	0.43
250.9	1.14	96.38	0.163	0.086	1.90	0.55
250.6	1.14	88.07	0.175	0.331	1.96	0.52
250.5	1.14	78.20	0.228	0.890	2.05	0.48
250.3	1.14	84.43	0.417	0.446	2.10	0.45
250.4	1.14	99.23	0.155	0.026	1.99	0.51
250.5	1.14	95.45	0.109	0.114	1.90	0.55
250.1	1.14	87.10	0.125	0.405	1.93	0.53
250.1	1.14	79.06	0.152	0.886	2.02	0.49
250.1	1.14	75.26	0.167	1.212	2.05	0.47
250.9	1.99	91.96	0.103	0.077	1.61	0.69
250.6	1.99	86.94	0.177	0.133	1.67	0.66
250.2	1.99	82.01	0.192	0.211	1.70	0.65
250.7	1.99	98.02	0.049	0.021	1.46	0.77
250.4	1.99	88.95	0.049	0.128	1.59	0.71
250.1	1.99	85.43	0.053	0.189	1.58	0.71
250.0	1.99	72.81	0.061	0.465	1.70	0.65
250.5	1.99	93.84	0.137	0.059	1.60	0.70

Temp (°C)	Total Pressure (atm)	% Hydrogen in feed	Conversion	Rate $\frac{\mu mol}{s \cdot g\ cat.}$	Selectivity Methane	Ethane
250.2	1.99	68.83	0.227	0.671	1.84	0.58
250.6	1.99	73.38	0.163	0.491	1.76	0.62
250.7	1.99	78.70	0.110	0.342	1.70	0.65
251.2	1.99	93.18	0.096	0.081	1.61	0.69
266.5	1.14	87.73	0.317	1.510	2.22	0.39
266.5	1.14	83.47	0.480	2.212	2.33	0.33
266.6	1.14	97.71	0.359	0.195	2.17	0.41
266.8	1.14	96.01	0.511	0.270	2.24	0.38
266.4	1.14	86.63	0.615	1.206	2.37	0.31
266.8	1.14	98.55	0.288	0.140	2.03	0.49
266.8	1.14	97.46	0.279	0.241	2.12	0.44
266.5	1.14	91.41	0.295	0.924	2.20	0.40
266.4	1.14	87.24	0.329	1.609	2.23	0.39
266.5	1.14	77.04	0.347	3.241	2.34	0.33
266.5	1.14	75.25	0.356	5.260	2.35	0.33
266.7	1.14	93.89	0.239	0.701	2.16	0.42
266.0	1.99	84.66	0.232	0.64	1.95	0.52
266.2	1.99	89.53	0.151	0.417	1.85	0.58
266.2	1.99	78.49	0.437	1.206	2.12	0.44
266.4	1.99	96.12	0.285	0.115	1.89	0.56

Temp (°C)	Total Pressure (atm)	% Hydrogen in feed	Conversion	Rate $\left[\dfrac{\mu\text{ mol}}{\text{s} \cdot \text{g cat.}}\right]$	Selectivity	
					Methane	Ethane
266.4	1.99	89.30	0.301	0.361	1.93	0.54
266.5	1.99	92.92	0.200	0.236	1.86	0.57
266.3	1.99	91.26	0.354	0.269	1.92	0.54
266.6	1.99	96.46	0.157	0.124	1.74	0.63
266.2	1.99	90.40	0.163	0.373	1.84	0.58
266.1	1.99	85.69	0.175	0.631	1.87	0.57
266.6	1.99	78.10	0.219	1.328	1.97	0.51
266.6	1.99	88.03	0.098	0.574	1.84	0.58
281.0	1.14	98.88	0.638	0.249	2.44	0.28
281.0	1.14	94.99	0.658	1.188	2.46	0.27
281.0	1.14	89.94	0.711	2.709	2.53	0.23
281.0	1.14	85.06	0.781	4.744	2.63	0.19
281.0	1.14	78.82	0.866	7.898	2.78	0.11
280.9	1.14	86.69	0.629	5.845	2.51	0.24
281.2	1.14	92.06	0.541	2.817	2.43	0.29
281.1	1.14	95.71	0.511	1.383	2.40	0.30
281.2	1.14	99.17	0.492	0.245	2.39	0.31
281.1	1.14	99.42	0.402	0.205	2.30	0.35
280.6	1.14	95.99	0.364	1.342	2.33	0.33
288.9	1.14	91.17	0.408	3.515	2.37	0.32

Temp (°C)	Total Pressure (atm)	% Hydrogen in feed	Conversion	Rate $\left[\dfrac{\mu \text{mol}}{\text{s} \cdot \text{g cat.}}\right]$	Selectivity Methane	Ethane
280.8	1.99	80.97	0.167	2.738	2.13	0.44
280.9	1.99	87.74	0.161	1.563	2.08	0.46
281.1	1.99	93.17	0.152	0.767	2.03	0.49
281.1	1.99	94.26	0.179	0.650	2.05	0.48
281.1	1.99	93.14	0.233	0.790	2.07	0.47
281.5	1.99	96.76	0.222	0.332	2.06	0.47
280.8	1.99	87.35	0.265	1.707	2.11	0.44
280.8	1.99	99.23	0.231	0.071	2.11	0.45
281.0	1.99	88.02	0.297	1.616	2.13	0.44
280.7	1.99	79.92	0.615	3.300	2.38	0.31
280.8	1.99	88.66	0.469	1.279	2.19	0.41
280.2	1.99	84.91	0.637	1.713	2.33	0.33

TABLE D-5

Rate Data for the Hydrogenolysis of Propane
over Cobalt on Silica

Temp (°C)	Total Pressure (atm)	Pressure Hydrogen (atm)	Conversion	Rate $\left(\dfrac{\mu \text{ mol}}{\text{s} \cdot \text{g cat.}}\right)$	Selectivity Methane	Ethane
228.8	1.16	1.139	0.032	0.065	3.00	0.00
228.9	1.17	1.025	0.183	0.211	2.56	0.22
228.7	1.16	1.109	0.079	0.093	2.46	0.27
228.7	1.17	1.062	0.079	0.191	2.51	0.25
228.5	1.18	0.956	0.081	0.447	2.53	0.23
228.3	1.21	0.826	0.082	0.890	2.55	0.23
228.8	1.21	0.706	0.118	1.293	2.60	0.20
229.1	1.18	0.982	0.111	0.364	2.55	0.23
228.5	1.18	0.901	0.152	0.495	2.57	0.22
228.6	1.18	1.001	0.033	0.374	2.49	0.26
229.4	2.14	1.943	0.040	0.129	2.15	0.42
229.0	2.17	1.852	0.056	0.178	2.19	0.41
229.0	2.13	2.019	0.018	0.058	2.03	0.49
227.8	2.18	1.752	0.080	0.198	2.16	0.42
228.2	2.20	1.752	0.020	0.267	1.97	0.52
229.0	2.14	1.959	0.060	0.081	2.10	0.45
229.3	2.13	2.037	0.034	0.046	1.95	0.53
228.5	2.17	1.888	0.031	0.135	2.04	0.48
248.8	1.18	1.052	0.062	1.154	2.66	0.17
248.6	1.18	0.962	0.096	1.828	2.72	0.14

TABLE D-5 (continued)

Temp (°C)	Total Pressure (atm)	Pressure Hydrogen (atm)	Conversion	Rate $\left[\dfrac{\mu\,mol}{s \cdot g\,cat.}\right]$	Selectivity	
					Methane	Ethane
248.6	1.24	0.908	0.090	2.664	2.72	0.14
248.9	1.18	1.044	0.093	1.028	2.71	0.15
248.5	1.18	1.090	0.092	0.617	2.70	0.15
248.5	1.18	1.039	0.133	0.874	2.71	0.15
248.5	1.17	0.939	0.562	0.554	2.80	0.10
248.5	1.16	1.089	0.304	0.303	2.74	0.13
248.5	1.18	0.920	0.313	1.211	2.76	0.12
248.3	1.20	0.755	0.322	2.404	2.79	0.11
248.3	2.16	1.632	0.409	0.763	2.59	0.21
249.2	2.13	2.006	0.155	0.315	2.49	0.25
248.8	2.14	1.895	0.145	0.626	2.49	0.25
248.4	2.16	1.767	0.153	1.075	2.49	0.25
249.0	2.13	2.082	0.089	0.142	2.41	0.29
248.7	2.14	2.042	0.092	0.264	2.43	0.29
248.6	2.14	1.945	0.094	0.580	2.47	0.26
249.0	2.13	2.045	0.190	0.181	2.51	0.25
248.0	2.16	1.759	0.086	1.279	2.51	0.25
248.3	2.15	1.898	0.055	0.829	2.47	0.27
267.7	1.20	1.129	0.120	0.710	2.78	0.11
267.9	1.20	1.084	0.121	1.248	2.77	0.12

TABLE D-5 (continued)

Temp (°C)	Total Pressure (atm)	Pressure Hydrogen (atm)	Conversion	Rate $\left[\dfrac{\mu \ mol}{s \cdot g \ cat.}\right]$	Selectivity Methane	Ethane
267.9	1.20	1.061	0.119	1.586	2.78	0.11
267.9	1.21	1.000	0.116	2.374	2.78	0.11
267.7	1.22	0.927	0.109	3.429	2.79	0.11
267.9	1.20	1.055	0.199	1.449	2.78	0.11
267.9	1.21	0.976	0.274	2.009	2.80	0.10
267.6	1.23	0.808	0.239	3.791	2.82	0.09
268.2	1.18	1.135	0.296	0.397	2.77	0.12
268.3	1.18	1.098	0.421	0.517	2.79	0.10
268.2	1.22	0.864	0.411	2.457	2.83	0.09
268.0	1.24	0.740	0.388	3.635	2.85	0.08
267.8	2.18	1.690	0.314	2.882	2.68	0.16
268.0	2.18	1.856	0.229	2.115	2.66	0.17
268.0	2.16	1.952	0.163	1.507	2.64	0.18
267.9	2.14	2.002	0.118	1.103	2.63	0.19
268.0	2.12	2.063	0.127	0.441	2.57	0.22
267.4	2.18	1.830	0.110	2.744	2.63	0.19
268.1	2.15	1.954	0.139	1.041	2.57	0.22
267.7	2.18	1.843	0.130	1.738	2.59	0.21
267.2	2.20	1.633	0.127	3.226	2.62	0.19

TABLE D-6

Rate Data for the Hydrogenolysis of Propane
over Cobalt-Magnesium on Siliconcarbide

Temp (°C)	Total Pressure (atm)	% Hydrogen in feed	Conversion	Rate $\left[\frac{\mu \text{mol}}{\text{s} \cdot \text{g cat.}}\right]$	Selectivity Methane	Ethane
245.1	1.21	97.92	0.189	0.075	2.67	0.16
245.3	1.21	88.91	0.156	0.359	2.62	0.19
245.5	1.21	91.05	0.411	0.278	2.69	0.16
245.3	1.21	90.15	0.100	0.324	2.59	0.21
245.3	1.21	88.28	0.071	0.414	2.58	0.21
245.6	1.21	86.45	0.256	0.400	2.65	0.18
245.0	1.21	97.04	0.240	0.094	2.67	0.17
245.2	1.22	68.88	0.125	1.052	2.69	0.15
245.4	1.22	76.21	0.091	0.777	2.65	0.17
245.4	1.22	80.59	0.073	0.626	2.63	0.19
245.3	1.21	83.29	0.075	0.539	2.63	0.19
245.4	1.22	69.65	0.168	1.198	2.67	0.16
245.5	1.22	57.93	0.508	2.787	2.89	0.06
245.4	1.22	72.99	0.247	1.026	2.70	0.15
245.7	1.21	87.79	0.239	0.394	2.66	0.17
255.6	1.21	97.25	0.286	0.136	2.66	0.17
255.5	1.21	98.54	0.289	0.072	2.67	0.16
255.7	1.21	98.15	0.326	0.088	2.60	0.20
255.6	1.21	97.29	0.319	0.128	2.65	0.18
255.8	1.21	91.92	0.333	0.417	2.66	0.17

TABLE D-6 (continued)

Temp (°C)	Total Pressure (atm)	% Hydrogen in feed	Conversion	Rate $\frac{\mu \text{mol}}{(s \cdot g \text{ cat.})}$	Selectivity Methane	Ethane
255.5	1.21	79.72	0.359	1.298	2.72	0.14
255.3	1.21	84.10	0.274	1.031	2.68	0.16
255.3	1.21	96.79	0.280	0.187	2.65	0.18
255.2	1.21	88.40	0.267	0.707	2.66	0.18
255.7	1.21	91.89	0.204	0.543	2.66	0.17
255.7	1.21	98.29	0.201	0.106	2.66	0.17
255.8	1.21	84.62	0.212	1.141	2.66	0.17
255.4	1.21	78.00	0.215	1.819	2.67	0.17
255.6	1.22	83.16	0.163	1.378	2.64	0.18
255.5	1.21	86.04	0.134	1.138	2.62	0.19
255.4	1.22	77.67	0.134	2.006	2.64	0.18
265.3	1.22	79.46	0.589	2.241	2.81	0.10
265.4	1.21	83.51	0.488	1.892	2.76	0.12
265.4	1.21	94.40	0.470	0.546	2.72	0.14
265.3	1.22	72.03	0.564	4.285	2.84	0.08
265.2	1.22	78.95	0.406	3.108	2.75	0.12
265.3	1.21	98.08	0.401	0.225	2.73	0.13
265.3	1.21	88.48	0.387	1.445	2.71	0.15
265.5	1.21	91.16	0.316	1.203	2.69	0.16
265.6	1.21	97.40	0.312	0.328	2.70	0.15

TABLE D-6 (continued)

Temp (°C)	Total Pressure (atm)	% Hydrogen in feed	Conversion	Rate $\frac{\mu\,mol}{(s \cdot g\ cat.)}$	Selectivity Methane	Ethane
265.6	1.22	83.57	0.332	2.554	2.71	0.14
265.6	1.21	86.69	0.273	2.122	2.69	0.16
265.0	1.21	97.00	0.264	0.412	2.68	0.16
265.6	1.21	92.76	0.275	1.082	2.68	0.16
265.1	1.22	82.43	0.278	3.015	2.69	0.15
265.0	1.21	88.16	0.347	1.671	2.70	0.15

TABLE D-7

Rate Data for the Hydrogenolysis of Propane over Iron-Magnesium on Silica

Temp (°C)	Total Pressure (atm)	% Hydrogen in feed	Conversion	Rate $\left[\frac{\mu mol}{s \cdot g\ cat.}\right]$	Selectivity Methane	Ethane
314.6	1.14	95.92	0.055	0.068	2.78	0.11
314.6	1.14	93.23	0.060	0.073	2.83	0.09
314.3	1.14	95.14	0.086	0.048	2.88	0.06
314.3	1.14	93.15	0.102	0.056	2.90	0.05
314.1	1.14	85.70	0.073	0.091	2.86	0.07
314.2	1.14	87.58	0.078	0.105	2.93	0.04
314.2	1.14	90.51	0.056	0.073	2.89	0.05
314.4	1.14	97.90	0.078	0.021	3.00	0.00
314.1	1.14	73.32	0.031	0.141	2.86	0.07
314.5	1.14	86.22	0.113	0.070	2.94	0.03
314.7	1.14	94.66	0.068	0.043	3.00	0.00
314.4	1.14	75.69	0.034	0.123	2.88	0.06
314.0	1.98	85.34	0.073	0.056	2.83	0.09
314.2	1.99	86.93	0.070	0.096	2.85	0.08
314.0	1.99	95.01	0.042	0.058	3.00	0.00
314.1	1.99	78.00	0.018	0.133	2.73	0.13
314.0	1.99	71.00	0.013	0.136	2.69	0.16
315.0	1.99	96.14	0.088	0.041	2.90	0.05
314.8	1.99	97.19	0.070	0.032	3.00	0.00
313.5	1.99	73.68	0.059	0.106	2.81	0.09

TABLE D-7 (continued)

Temp (°C)	Total Pressure (atm)	% Hydrogen in feed	Conversion	Rate $\left[\dfrac{\mu\,mol}{s\cdot g\ cat.}\right]$	Selectivity Methane	Ethane
314.2	1.99	86.13	0.051	0.094	2.82	0.09
314.5	1.99	89.30	0.049	0.092	2.76	0.12
313.7	1.99	77.70	0.027	0.119	2.78	0.11
314.9	1.99	96.42	0.063	0.036	3.00	0.00
334.1	1.13	97.99	0.141	0.056	3.00	0.00
333.6	1.14	84.99	0.076	0.260	2.95	0.03
333.8	1.14	95.06	0.119	0.120	3.00	0.00
333.6	1.14	93.70	0.137	0.135	3.00	0.00
333.4	1.14	76.67	0.069	0.309	2.96	0.02
333.2	1.14	70.73	0.072	0.321	2.94	0.03
333.2	1.14	83.15	0.103	0.226	2.95	0.02
333.5	1.14	96.09	0.166	0.073	3.00	0.00
334.5	1.14	92.19	0.243	0.101	2.95	0.03
334.3	1.14	96.95	0.170	0.074	2.90	0.05
333.5	1.14	91.86	0.124	0.152	2.92	0.04
334.0	1.14	96.01	0.100	0.120	3.00	0.00
333.6	1.99	84.08	0.102	0.379	2.93	0.04
333.8	1.99	89.18	0.131	0.310	2.95	0.02
333.6	1.99	85.50	0.141	0.330	2.95	0.03
334.1	1.99	89.98	0.244	0.239	2.95	0.03

TABLE D-7 (continued)

Temp (°C)	Total Pressure (atm)	% Hydrogen in feed	Conversion	Rate $\left[\dfrac{\mu mol}{s \cdot g \ cat.}\right]$	Selectivity Methane	Ethane
333.4	1.99	96.45	0.150	0.154	3.00	0.00
333.8	1.99	90.31	0.256	0.249	2.94	0.03
333.3	1.99	81.22	0.162	0.338	2.92	0.04
333.3	1.99	89.21	0.138	0.290	2.92	0.04
333.4	1.99	97.42	0.212	0.096	3.00	0.00
333.4	1.99	98.21	0.182	0.081	3.00	0.00
333.1	1.99	88.45	0.103	0.333	2.92	0.04
333.4	1.99	84.70	0.086	0.385	2.92	0.04
352.9	1.14	75.56	0.147	0.538	2.95	0.03
353.5	1.14	83.91	0.139	0.516	2.96	0.02
353.5	1.14	76.95	0.116	0.675	2.95	0.03
353.2	1.14	78.54	0.179	0.324	2.94	0.03
353.4	1.14	89.96	0.150	0.274	2.95	0.02
353.1	1.14	79.40	0.100	0.422	2.94	0.03
353.0	1.14	79.27	0.258	0.273	2.93	0.04
353.2	1.14	85.55	0.245	0.259	2.95	0.03
353.6	1.14	94.33	0.170	0.184	2.95	0.02
353.4	1.14	83.22	0.113	0.414	2.92	0.04
353.8	1.14	97.94	0.185	0.101	3.00	0.00
353.3	1.14	78.52	0.077	0.551	2.92	0.04

TABLE D-7 (continued)

Temp (°C)	Total Pressure (atm)	% Hydrogen in feed	Conversion	Rate $\left[\dfrac{\mu \text{ mol}}{\text{s} \cdot \text{g cat.}}\right]$	Selectivity Methane	Ethane
353.8	1.99	88.52	0.356	0.554	2.96	0.02
353.7	1.99	92.60	0.313	0.496	2.96	0.02
353.7	1.99	94.17	0.289	0.458	2.96	-0.02
353.7	1.99	95.17	0.266	0.426	2.96	0.02
353.4	1.99	96.08	0.248	0.397	2.95	0.03
353.4	1.99	98.01	0.285	0.227	3.00	0.00
353.3	1.99	93.44	0.207	0.570	2.96	0.02
353.1	1.99	90.92	0.179	0.686	2.95	0.02
352.8	1.99	87.26	0.196	0.764	2.96	0.02
353.5	1.99	90.94	0.238	0.628	2.97	0.02
353.8	1.99	97.60	0.391	0.188	3.00	0.00
353.8	1.99	84.19	0.208	0.774	2.96	0.02

TABLE D-8

Rate Data for the Hydrogenolysis of Propane over Promoted Ammonia Synthesis Catalyst

Temp ($^{\circ}$C)	Total Pressure (atm)	% Hydrogen in feed	Conversion	Rate $\left[\dfrac{\mu mol}{s \cdot g\ cat.}\right]$	Selectivity Methane	Ethane
287.8	1.64	74.94	0.023	0.053	2.79	0.11
287.9	1.61	93.41	0.009	0.022	3.00	0.00
287.5	1.62	85.58	0.015	0.035	2.79	0.11
287.8	1.63	79.82	0.010	0.050	2.74	0.13
287.8	1.64	75.29	0.009	0.061	2.69	0.16
287.6	1.64	78.36	0.008	0.059	2.68	0.16
288.4	1.63	76.65	0.028	0.050	2.85	0.07
287.8	1.13	85.95	0.045	0.016	2.84	0.08
288.1	1.13	95.39	0.017	0.008	3.00	0.00
288.0	1.13	83.09	0.016	0.030	2.76	0.12
287.7	1.13	73.72	0.015	0.048	2.68	0.16
287.5	1.14	66.92	0.010	0.055	2.56	0.22
310.9	2.03	89.28	0.090	0.130	2.95	0.03
311.1	2.03	89.36	0.061	0.141	3.00	0.00
311.6	2.03	89.19	0.185	0.112	2.95	0.03
310.8	2.04	80.82	0.041	0.329	2.89	0.06
310.8	2.04	86.61	0.038	0.292	2.89	0.06
311.2	2.04	86.73	0.043	0.333	2.90	0.05
311.2	2.03	85.65	0.110	0.316	2.94	0.03
311.1	2.04	77.41	0.146	0.357	2.93	0.04

TABLE D-8 (continued)

Temp (°C)	Total Pressure (atm)	% Hydrogen in feed	Conversion	Rate $\left[\frac{\mu \text{ mol}}{\text{s} \cdot \text{g cat.}}\right]$	Selectivity Methane	Ethane
311.1	2.04	74.81	0.163	0.387	2.93	0.03
310.5	2.03	86.00	0.181	0.210	2.94	0.03
310.7	2.04	77.46	0.243	0.276	2.93	0.03
310.8	2.04	77.55	0.234	0.266	2.93	0.04
311.0	2.02	95.52	0.093	0.108	3.00	0.00
310.2	1.61	83.17	0.269	0.115	2.93	0.04
310.5	1.61	81.38	0.090	0.217	2.92	0.04
310.8	1.60	89.11	0.068	0.161	2.92	0.04
309.4	1.12	65.22	0.109	0.062	2.76	0.12
310.3	1.12	67.39	0.147	0.077	2.79	0.11
311.0	1.12	89.52	0.082	0.050	2.89	0.05
310.8	1.11	89.66	0.185	0.026	2.87	0.07
310.6	1.11	89.68	0.137	0.032	2.88	0.06
330.4	1.99	89.55	0.114	0.541	2.96	0.02
330.5	1.99	89.50	0.099	0.551	3.00	0.00
330.4	1.99	89.34	0.081	0.636	2.72	0.14
330.4	1.99	89.46	0.139	0.517	2.98	0.01
330.3	1.98	89.44	0.180	0.480	2.98	0.01
329.9	1.98	89.41	0.223	0.432	2.97	0.02
330.2	1.98	89.34	0.329	0.361	2.97	0.02

TABLE D-8 (continued)

Temp (°C)	Total Pressure (atm)	% Hydrogen in feed	Conversion	Rate $\left[\dfrac{\mu\text{ mol}}{s \cdot g \text{ cat.}}\right]$	Selectivity Methane	Ethane
329.9	1.98	89.39	0.482	0.249	2.98	0.01
331.8	2.00	75.50	0.073	1.284	2.92	0.04
330.5	2.00	64.57	0.089	0.807	2.90	0.05
329.5	2.01	54.68	0.085	0.759	2.87	0.07
330.0	2.00	61.48	0.088	0.579	2.89	0.06
330.9	1.98	90.66	0.132	0.308	2.97	0.01
330.4	1.61	92.74	0.075	0.145	3.00	0.00
330.4	1.61	89.54	0.100	0.189	2.96	0.02
330.4	1.60	98.26	0.120	0.035	3.00	0.00
330.0	1.61	80.25	0.119	0.252	2.93	0.04
329.9	1.62	73.17	0.138	0.297	2.92	0.04
330.4	1.62	59.86	0.164	0.341	2.88	0.06
330.4	1.61	90.67	0.082	0.177	2.92	0.04
330.3	1.60	93.48	0.079	0.155	2.92	0.04
329.7	1.61	85.86	0.078	0.212	2.94	0.03
330.1	1.60	90.97	0.068	0.161	2.94	0.03
330.2	1.11	87.41	0.036	0.132	3.00	0.00
330.0	1.11	83.59	0.035	0.131	2.91	0.04
339.2	2.03	88.67	0.073	0.495	3.00	0.00
339.2	2.03	88.61	0.062	0.598	2.64	0.18

TABLE D-8(continued)

Temp (°C)	Total Pressure (atm)	% Hydrogen in feed	Conversion	Rate $\frac{\mu \text{mol}}{(s \cdot g \text{ cat.})}$	Selectivity Methane	Ethane
316.1	2.03	88.64	0.021	0.202	2.92	0.04
316.1	2.03	88.69	0.041	0.181	3.00	0.00
290.4	1.13	86.65	0.050	0.017	2.84	0.08
316.2	2.03	89.36	0.116	0.169	2.94	0.03
317.9	2.01	89.37	0.134	0.175	2.95	0.03
308.9	2.04	80.86	0.032	0.259	2.85	0.08
313.2	2.04	77.23	0.157	0.387	2.94	0.03
315.2	1.61	82.84	0.352	0.151	2.95	0.03
316.1	1.60	98.13	0.384	0.017	3.00	0.00
313.5	1.59	98.43	0.514	0.006	3.00	0.00
313.8	1.12	88.47	0.086	0.069	2.91	0.04
312.5	1.11	89.51	0.205	0.032	2.89	0.06
318.1	2.02	89.72	0.134	0.221	2.96	0.02
316.4	2.03	89.86	0.146	0.209	2.95	0.02
316.1	2.02	89.84	0.139	0.200	2.95	0.02
335.4	2.01	89.84	0.158	0.659	2.98	0.01

TABLE D-9

Rate Data for the Hydrogenolysis of Propane over Extracted Ammonia Synthesis Catalyst

Temp ($^\circ$C)	Total Pressure (atm)	% Hydrogen in feed	Conversion	Rate $\dfrac{\mu \text{mol}}{(\text{s} \cdot \text{g cat.})}$	Selectivity Methane	Ethane
269.8	2.04	69.80	0.020	0.057	2.59	0.20
270.6	2.05	63.02	0.019	0.071	2.59	0.21
269.5	2.04	71.08	0.015	0.054	2.60	0.20
270.1	2.04	76.79	0.014	0.052	2.50	0.25
270.4	2.05	69.90	0.013	0.067	2.43	0.29
270.1	1.63	69.00	0.010	0.050	2.65	0.18
269.7	1.64	62.79	0.025	0.055	2.56	0.22
270.1	1.13	79.29	0.017	0.035	2.66	0.17
297.0	2.03	89.51	0.031	0.106	3.00	0.00
296.9	2.03	89.45	0.021	0.114	3.00	0.00
297.1	1.62	89.46	0.026	0.110	3.00	0.00
297.4	1.10	89.45	0.034	0.091	3.00	0.00
297.6	1.10	89.39	0.049	0.087	3.00	0.00
296.8	1.10	89.49	0.095	0.073	2.94	0.03
297.4	2.04	79.86	0.074	0.316	2.89	0.06
297.4	2.04	74.05	0.086	0.365	2.90	0.05
297.2	2.04	80.00	0.092	0.279	2.90	0.05
297.8	2.04	75.52	0.105	0.315	2.90	0.05
296.9	2.04	86.83	0.070	0.213	2.90	0.05
297.3	2.04	90.97	0.059	0.183	2.89	0.06

TABLE D-9 (continued)

Temp (°C)	Total Pressure (atm)	% Hydrogen in feed	Conversion	Rate $\left[\dfrac{\mu\ mol}{s \cdot g\ cat.}\right]$	Selectivity Methane	Ethane
297.7	1.62	91.04	0.054	0.186	2.91	0.05
297.4	1.62	87.03	0.070	0.238	2.91	0.05
297.3	1.62	81.42	0.081	0.284	2.91	0.05
297.9	1.61	89.43	0.090	0.163	2.90	0.05
297.6	1.62	85.14	0.101	0.181	2.90	0.05
296.1	1.62	81.98	0.097	0.172	2.92	0.04
297.8	1.63	77.32	0.109	0.191	2.91	0.05
297.3	1.13	89.99	0.046	0.088	2.89	0.06
296.9	1.13	86.10	0.050	0.100	2.90	0.05
297.1	1.13	95.05	0.156	0.053	3.00	0.00
298.0	1.13	82.93	0.126	0.170	2.95	0.03
297.4	1.13	88.91	0.091	0.120	2.94	0.03
297.0	1.13	75.88	0.070	0.235	2.91	0.04
296.0	2.02	89.51	0.088	0.095	2.92	0.04
318.6	2.02	89.25	0.077	0.279	2.94	0.03
318.4	2.02	89.09	0.061	0.295	3.00	0.00
318.8	2.02	89.08	0.093	0.300	2.95	0.03
318.6	2.02	89.24	0.113	0.288	2.95	0.03
318.0	1.61	89.17	0.092	0.264	3.00	0.00
318.7	1.61	89.38	0.122	0.257	2.97	0.01

TABLE D-9 (continued).

Temp (°C)	Total Pressure (atm)	% Hydrogen in feed	Conversion	Rate $\left[\dfrac{\mu\,mol}{(s\cdot g\ cat.)}\right]$	Selectivity Methane	Ethane
318.7	1.61	89.18	0.059	0.300	3.00	0.00
318.5	1.61	89.10	0.187	0.245	2.96	0.02
319.4	1.12	89.10	0.147	0.209	2.96	0.02
318.6	1.12	89.21	0.105	0.222	3.00	0.00
317.9	1.12	89.21	0.065	0.224	3.00	0.00
318.9	2.04	78.32	0.162	0.904	2.95	0.03
318.5	2.05	74.90	0.144	0.977	2.94	0.03
318.3	2.04	71.65	0.126	1.025	2.94	0.03
318.8	2.04	75.72	0.115	0.932	2.93	0.04
318.6	2.04	80.05	0.102	0.861	2.94	0.03
319.5	2.04	84.28	0.095	0.783	2.94	0.03
318.4	2.04	60.51	0.328	1.024	2.90	0.05
318.0	1.61	82.41	0.150	0.509	2.95	0.03
318.2	1.60	85.95	0.173	0.452	2.95	0.02
319.0	1.60	90.72	0.149	0.387	2.96	0.02
318.6	1.62	74.37	0.106	0.934	2.93	0.03
317.9	1.62	72.94	0.207	0.670	2.93	0.03
318.1	1.62	77.14	0.166	0.550	2.93	0.03
318.1	1.62	81.83	0.110	0.372	2.92	0.04
319.1	1.60	92.45	0.073	0.254	3.00	0.00

TABLE D-9 (continued)

Temp (°C)	Total Pressure (atm)	% Hydrogen in feed	Conversion	Rate $\left[\frac{\mu\,mol}{s\cdot g\,cat.}\right]$	Selectivity Methane	Ethane
318.9	1.13	90.19	0.064	0.230	3.00	0.00
318.9	1.13	86.96	0.068	0.247	2.94	0.03
318.0	1.13	88.14	0.073	0.222	2.94	0.03
337.9	2.03	89.58	0.220	0.663	2.97	0.01
337.9	2.03	89.61	0.372	0.510	2.98	0.01
337.9	2.03	89.79	0.203	0.750	2.98	0.01
337.4	1.62	89.67	0.208	0.606	2.98	0.01
337.6	1.62	89.66	0.169	0.686	2.98	0.01
337.9	1.62	89.67	0.149	0.745	2.98	0.01
337.8	1.13	89.68	0.116	0.630	3.00	0.00
337.8	1.13	89.68	0.182	0.558	3.00	0.00
337.6	1.13	89.60	0.277	0.477	2.98	0.01
337.8	1.14	67.54	0.278	1.523	2.93	0.03
338.4	1.13	84.88	0.211	1.122	2.97	0.02
337.8	1.13	89.82	0.245	0.821	2.97	0.02
337.6	1.13	72.77	0.443	1.313	2.97	0.02
336.9	1.14	57.64	0.429	1.325	2.91	0.04
337.3	1.13	68.67	0.421	0.800	2.94	0.03
337.6	1.63	72.75	0.409	0.841	2.93	0.04
338.1	1.61	81.10	0.329	0.691	2.93	0.03

TABLE D-9 (continued)

Temp (°C)	Total Pressure (atm)	% Hydrogen in feed	Conversion	Rate $\left[\dfrac{\mu \text{ mol}}{\text{s} \cdot \text{g cat.}}\right]$	Selectivity	
					Methane	Ethane
337.9	1.62	78.79	0.285	1.098	2.95	0.03
338.5	1.61	84.46	0.274	1.061	2.97	0.02
338.5	1.61	86.69	0.266	1.033	2.97	0.01
338.7	1.63	72.66	0.455	1.113	2.94	0.03
337.8	1.62	76.54	0.424	1.047	2.95	0.02
338.4	1.61	94.32	0.254	0.621	3.00	0.00
337.6	2.02	94.17	0.316	0.714	2.98	0.01
337.6	2.04	84.92	0.170	1.080	2.95	0.02
337.5	2.03	90.66	0.134	0.847	2.95	0.03
337.2	2.03	86.74	0.267	0.639	2.95	0.03
337.5	2.02	91.15	0.243	0.575	2.97	0.02
295.1	2.05	66.68	0.027	0.317	2.84	0.08
299.5	1.13	95.83	0.171	0.050	3.00	0.00
320.8	2.04	85.49	0.201	0.695	2.95	0.03
346.5	1.13	77.98	0.402	1.298	2.96	0.02
334.7	1.63	72.25	0.434	0.914	2.94	0.03
339.5	2.02	94.22	0.358	0.809	2.98	0.01

TABLE D-10

Rate Data and Selectivities for the Hydrogenolysis of Isopentane over Nickel-Magnesium on Siliconcarbide

Temp (°C)	Total Pressure (atm)	% Hydrogen in feed	Conversion	Rate $\left[\dfrac{\mu\ mol}{s\cdot g\cdot cat.}\right]$	Selectivity				
					$n-C_4$	$1-C_4$	Propane	Ethane	Methane
233.2	1.29	88.43	0.212	0.219	0.40	0.29	0.19	0.07	1.55
233.2	1.29	91.90	0.149	0.163	0.41	0.30	0.18	0.06	1.49
233.1	1.29	95.27	0.099	0.104	0.42	0.32	0.16	0.05	1.45
262.9	1.29	88.44	0.789	0.937	0.18	0.07	0.32	0.20	2.64
263.0	1.29	94.99	0.661	0.714	0.25	0.10	0.31	0.17	2.33
263.0	1.29	88.61	0.651	1.632	0.24	0.09	0.31	0.18	2.42
282.2	1.29	81.97	0.902	2.212	0.05	0.01	0.17	0.25	3.73
282.2	1.29	91.13	0.804	2.037	0.10	0.03	0.25	0.24	3.25
282.5	1.29	94.67	0.718	1.777	0.13	0.03	0.27	0.22	3.08
282.7	1.29	97.35	0.753	0.880	0.14	0.04	0.27	0.22	3.07
247.7	1.29	91.47	0.459	0.489	0.35	0.18	0.27	0.11	1.86

TABLE D -10 (continued)

Temp (°C)	Total Pressure (atm)	% Hydrogen in feed	Conversion	Rate $\left[\dfrac{\mu\text{ mol}}{s \cdot g\ \text{cat.}}\right]$	Selectivity				
					n-C4	1-C4	Propane	Ethane	Methane
248.0	1.29	94.69	0.379	0.378	0.37	0.19	0.25	0.10	1.80
247.7	1.29	96.14	0.272	0.325	0.39	0.21	0.23	0.09	1.71
249.6	1.29	97.42	0.250	0.256	0.39	0.21	0.23	0.09	1.73
248.3	1.29	95.02	0.211	0.442	0.40	0.21	0.22	0.09	1.70
248.2	1.29	85.16	0.406	0.926	0.35	0.18	0.26	0.11	1.86
248.5	1.30	64.53	0.735	1.685	0.20	0.08	0.31	0.19	2.56
247.3	1.29	92.00	0.428	0.454	0.36	0.19	0.26	0.10	1.81

TABLE D-11

Product Distribution for the Hydrogenolysis of 2,2-Dimethylbutane

over Ruthenium on Alumina

Temperature: 185.0 °C

Total Pressure: 1.20 atm

Conversion of 2,2-Dimethylbutane	Selectivities				
	Neopentane	Isopentane	Propane	Ethane	Methane
0.049	0.96	0.00	0.00	0.00	1.21
0.093	0.97	0.00	0.00	0.00	1.16
0.117	0.96	0.00	0.00	0.00	1.19
0.211	0.93	0.03	0.00	0.02	1.22
0.225	0.91	0.03	0.00	0.02	1.28
0.317	0.92	0.03	0.00	0.04	1.23
0.323	0.90	0.03	0.00	0.02	1.35
0.333	0.93	0.03	0.00	0.03	1.16
0.345	0.92	0.03	0.00	0.02	1.22

TABLE D-1.1 (continued)

Conversion of 2,2-Dimethylbutane	Neopentane	Selectivities Isopentane	Propane	Ethane	Methane
0.350	0.92	0.03	0.00	0.04	1.18
0.402	0.90	0.04	0.00	0.02	1.29
0.485	0.93	0.03	0.01	0.03	1.17
0.537	0.92	0.03	0.01	0.04	1.18
0.605	0.92	0.04	0.01	0.04	1.19
0.625	0.92	0.03	0.00	0.04	1.16
0.770	0.90	0.03	0.01	0.06	1.22
0.788	0.89	0.04	0.01	0.07	1.25
0.821	0.89	0.03	0.01	0.07	1.23
0.828	0.90	0.03	0.01	0.06	1.23

296

TABLE D-12

Product Distribution for the Hydrogenolysis of 2,2-Dimethylbutane

over Ruthenium on Alumina

Temperature: 200.0 °C

Total Pressure: 1.20 atm.

Conversion of 2,2-Dimethylbutane	Neopentane	Isopentane	Propane	Ethane	Methane
			Selectivities		
0.421	0.91	0.04	0.01	0.04	1.18
0.554	0.88	0.04	0.01	0.07	1.28
0.581	0.89	0.05	0.01	0.06	1.22
0.667	0.83	0.04	0.00	0.11	1.49
0.739	0.85	0.04	0.01	0.09	1.37
0.767	0.87	0.04	0.01	0.08	1.29
0.851	0.84	0.03	0.01	0.11	1.42
0.859	0.80	0.03	0.01	0.14	1.54
0.908	0.80	0.03	0.01	0.15	1.56
0.923	0.80	0.03	0.01	0.14	1.56
0.950	0.76	0.02	0.01	0.18	1.74

TABLE D-13

Product Distribution for the Hydrogenolysis of 2,3-Dimethylbutane

over Ruthenium on Alumina

Temperature: 200.0 °C

Total Pressure: 1.20 atm.

Conversion of 2,3-Dimethylbutane	Isopentane	Selectivities Isobutane	Propane	Ethane	Methane
0.049	0.50	0.34	0.08	0.09	1.68
0.091	0.48	0.29	0.11	0.15	1.79
0.108	0.45	0.30	0.09	0.16	1.96
0.126	0.46	0.31	0.10	0.12	1.92
0.148	0.42	0.34	0.08	0.11	2.12
0.153	0.49	0.30	0.07	0.16	1.84
0.157	0.39	0.36	0.07	0.12	2.19
0.178	0.39	0.28	0.08	0.21	2.26
0.249	0.35	0.35	0.08	0.18	2.21
0.256	0.40	0.34	0.08	0.19	2.06

TABLE D-13 (continued)

Conversion of 2,3-Dimethylbutane	Isopentane	Isobutane	Selectivities Propane	Ethane	Methane
0.265	0.36	0.36	0.07	0.20	2.16
0.306	0.41	0.40	0.08	0.15	1.79
0.316	0.39	0.36	0.08	0.17	2.00
0.326	0.41	0.41	0.08	0.13	1.72
0.331	0.37	0.36	0.07	0.22	2.05
0.357	0.33	0.38	0.10	0.18	2.16
0.391	0.36	0.40	0.07	0.20	1.94
0.408	0.31	0.42	0.07	0.23	2.08
0.409	0.34	0.39	0.08	0.21	2.06
0.506	0.32	0.44	0.08	0.17	1.99
0.590	0.27	0.44	0.10	0.25	2.00
0.600	0.23	0.46	0.09	0.24	2.26
0.642	0.20	0.48	0.09	0.26	2.32
0.644	0.25	0.49	0.09	0.19	2.04
0.755	0.16	0.50	0.09	0.28	2.41
0.819	0.09	0.52	0.12	0.33	2.39

TABLE D-14

Product Distribution for the Hydrogenolysis of n-Hexane

over Ruthenium on Alumina

Temperature: 149.0 °C

Total Pressure: 1.20 atm.

Conversion of n-Hexane	Selectivities				
	n-Pentane	n-Butane	Propane	Ethane	Methane
0.086	0.36	0.33	0.44	0.42	0.71
0.158	0.33	0.34	0.47	0.44	0.72
0.164	0.34	0.34	0.45	0.44	0.72
0.184	0.35	0.32	0.44	0.44	0.76
0.190	0.34	0.34	0.45	0.44	0.76
0.276	0.31	0.34	0.47	0.46	0.76
0.282	0.29	0.34	0.48	0.46	0.79
0.296	0.30	0.34	0.48	0.48	0.74
0.311	0.30	0.34	0.50	0.45	0.76
0.319	0.31	0.34	0.48	0.47	0.74
0.322	0.30	0.34	0.48	0.47	0.75
0.347	0.30	0.34	0.47	0.47	0.78
0.365	0.30	0.34	0.47	0.47	0.79
0.373	0.30	0.34	0.47	0.47	0.79
0.380	0.29	0.35	0.48	0.47	0.78

TABLE D-14 (continued)

Conversion of n-Hexane	n-Pentane	n-Butane	Selectivities Propane	Ethane	Methane
0.409	0.30	0.34	0.47	0.47	0.77
0.535	0.28	0.33	0.51	0.48	0.75
0.578	0.24	0.37	0.50	0.53	0.81
0.578	0.23	0.36	0.51	0.53	0.80
0.607	0.23	0.35	0.53	0.53	0.79
0.613	0.22	0.35	0.53	0.54	0.83
0.703	0.20	0.35	0.54	0.56	0.85
0.719	0.19	0.35	0.55	0.57	0.84
0.800	0.14	0.35	0.58	0.62	0.92
0.822	0.17	0.33	0.55	0.61	0.96

TABLE D-15

Product Distribution of the Hydrogenolysis of 2,2-Dimethylbutane

over Nickel on Siliconcarbide

Temperature: 290.0 °C

Total Pressure: 1.20 atm.

Conversion of 2,2-Dimethylbutane	Neopentane	n-Butane	Isobutane	Propane	Ethane	Methane
			Selectivities			
0.173	0.40	0.03	0.17	0.18	0.24	2.20
0.184	0.38	0.03	0.16	0.19	0.25	2.28
0.284	0.38	0.02	0.14	0.20	0.26	2.35
0.310	0.38	0.03	0.15	0.20	0.25	2.30
0.362	0.37	0.02	0.13	0.20	0.26	2.42
0.414	0.38	0.03	0.13	0.20	0.26	2.35
0.414	0.37	0.00	0.10	0.21	0.28	2.53
0.456	0.36	0.02	0.14	0.20	0.27	2.42
0.480	0.37	0.02	0.10	0.21	0.27	2.50
0.523	0.35	0.01	0.09	0.20	0.30	2.61
0.634	0.34	0.01	0.07	0.20	0.29	2.75

TABLE D-15(continued)

Conversion of 2,2-Dimethylbutane	Neopentane	n-Butane	Selectivities Isobutane	Propane	Ethane	Methane
0.634	0.32	0.00	0.07	0.19	0.31	2.91
0.644	0.31	0.01	0.06	0.18	0.31	2.99
0.654	0.33	0.02	0.08	0.20	0.30	2.77
0.673	0.33	0.01	0.06	0.20	0.31	2.84
0.729	0.31	0.01	0.06	0.18	0.32	3.01
0.756	0.31	0.01	0.05	0.17	0.32	3.05
0.783	0.29	0.00	0.04	0.16	0.33	3.22
0.816	0.29	0.00	0.03	0.16	0.33	3.29
0.824	0.27	0.00	0.03	0.14	0.34	3.39
0.832	0.26	0.00	0.03	0.14	0.34	3.50
0.874	0.28	0.00	0.03	0.15	0.34	3.35
0.880	0.22	0.00	0.02	0.10	0.34	3.85
0.932	0.21	0.00	0.02	0.09	0.33	3.95
0.967	0.09	0.00	0.01	0.03	0.25	4.90

TABLE D-16

Product Distribution for the Hydrogenolysis of 2,3-Dimethylbutane

over Nickel on Siliconcarbide

Temperature: 260.0 °C

Total Pressure: 1.20 atm

Conversion of 2,3-Dimethylbutane	Selectivities					
	Isopentane	n-Butane	Isobutane	Propane	Ethane	Methane
0.033	0.39	0.23	0.06	0.23	0.10	2.02
0.067	0.37	0.22	0.06	0.25	0.09	2.11
0.108	0.34	0.25	0.08	0.25	0.10	2.04
0.132	0.37	0.26	0.06	0.22	0.09	2.04
0.144	0.34	0.25	0.06	0.24	0.09	2.18
0.216	0.33	0.27	0.08	0.25	0.10	2.03
0.227	0.34	0.27	0.07	0.24	0.09	2.06
0.266	0.32	0.27	0.08	0.25	0.10	2.06
0.311	0.30	0.29	0.08	0.26	0.09	2.07
0.327	0.30	0.28	0.08	0.27	0.10	2.08
0.338	0.28	0.29	0.08	0.26	0.10	2.16

TABLE D-16 (continued)

Conversion of 2,3-Dimethylbutane	Selectivities					
	Isopentane	n-Butane	Isobutane	Propane	Ethane	Methane
0.341	0.28	0.32	0.07	0.25	0.09	2.15
0.380	0.28	0.31	0.07	0.26	0.10	2.10
0.481	0.23	0.30	0.07	0.30	0.12	2.23
0.499	0.26	0.32	0.08	0.26	0.10	2.11
0.520	0.24	0.33	0.07	0.28	0.10	2.18
0.547	0.21	0.31	0.07	0.30	0.12	2.27
0.576	0.22	0.33	0.07	0.27	0.11	2.27
0.586	0.20	0.35	0.07	0.29	0.11	2.26
0.606	0.20	0.34	0.07	0.29	0.10	2.28
0.643	0.19	0.32	0.07	0.31	0.12	2.31
0.652	0.17	0.34	0.07	0.31	0.12	2.34
0.666	0.17	0.33	0.07	0.32	0.12	2.35
0.788	0.10	0.31	0.05	0.38	0.16	2.60
0.903	0.03	0.20	0.03	0.43	0.24	3.18

TABLE D-17

Product Distribution for the Hydrogenolysis of n-Hexane

over Nickel on Siliconcarbide

Temperature: 285.0 °C

Total Pressure: 1.20 atm

Conversion of n-Hexane	Selectivities				
	n-Pentane	n-Butane	Propane	Ethane	Methane
0.064	0.28	0.22	0.22	0.17	2.70
0.074	0.27	0.23	0.22	0.18	2.71
0.130	0.27	0.23	0.21	0.18	2.75
0.133	0.26	0.25	0.21	0.17	2.75
0.138	0.26	0.25	0.22	0.18	2.70
0.149	0.27	0.24	0.21	0.19	2.68
0.231	0.23	0.25	0.23	0.23	2.71
0.233	0.23	0.25	0.22	0.21	2.76
0.246	0.25	0.24	0.22	0.20	2.74
0.265	0.26	0.24	0.20	0.19	2.74
0.272	0.23	0.25	0.22	0.20	2.80
0.276	0.23	0.26	0.22	0.21	2.74
0.285	0.22	0.25	0.21	0.20	2.88
0.321	0.22	0.25	0.23	0.22	2.78
0.339	0.22	0.24	0.23	0.20	2.84
0.374	0.20	0.26	0.25	0.25	2.70
0.385	0.20	0.26	0.25	0.25	2.72

TABLE D-17 (continued)

Conversion of n-Hexane	Selectivities				
	n-Pentane	n-Butane	Propane	Ethane	Methane
0.537	0.16	0.27	0.27	0.26	2.77
0.577	0.15	0.27	0.27	0.26	2.85
0.603	0.14	0.24	0.25	0.24	3.12
0.617	0.15	0.24	0.27	0.26	2.94
0.639	0.14	0.24	0.27	0.28	2.94
0.673	0.12	0.21	0.25	0.24	3.35
0.679	0.13	0.23	0.27	0.27	3.09
0.716	0.12	0.23	0.26	0.27	3.19

TABLE D-18

Product Distribution for the Hydrogenolysis of 2,2-Dimethyl-butane over Nickel-Magnesium on Siliconcarbide

Temperature: 265.0 °C

Total Pressure: 1.20 atm

Conversion of 2,2-Dimethylbutane	Neopentane	Selectivities Isobutane	Propane	Ethane	Methane
0.115	0.75	0.11	0.05	0.06	1.56
0.122	0.76	0.12	0.04	0.05	1.49
0.145	0.76	0.11	0.05	0.06	1.51
0.152	0.76	0.11	0.04	0.05	1.51
0.182	0.74	0.12	0.05	0.05	1.57
0.202	0.73	0.10	0.05	0.05	1.70
0.203	0.77	0.10	0.05	0.06	1.49
0.235	0.74	0.11	0.05	0.06	1.58
0.248	0.73	0.11	0.05	0.05	1.66
0.262	0.72	0.11	0.06	0.07	1.59
0.282	0.74	0.10	0.05	0.06	1.61
0.288	0.74	0.11	0.05	0.06	1.58
0.355	0.75	0.10	0.06	0.05	1.55
0.365	0.70	0.10	0.06	0.08	1.70
0.395	0.71	0.10	0.06	0.07	1.63
0.395	0.72	0.10	0.06	0.07	1.64
0.444	0.72	0.09	0.07	0.07	1.66

TABLE D-18 (continued)

Conversion of 2,2-Dimethylbutane	Neopentane	Selectivities Isobutane	Propane	Ethane	Methane
0.450	0.72	0.09	0.07	0.07	1.63
0.501	0.69	0.09	0.07	0.07	1.76
0.510	0.71	0.09	0.07	0.08	1.72
0.530	0.71	0.08	0.07	0.07	1.74
0.546	0.69	0.08	0.07	0.08	1.77
0.560	0.71	0.09	0.07	0.07	1.70
0.570	0.71	0.09	0.07	0.07	1.70
0.577	0.70	0.08	0.08	0.08	1.80
0.588	0.66	0.08	0.08	0.09	1.94
0.592	0.69	0.08	0.07	0.08	1.81
0.622	0.68	0.07	0.08	0.09	1.89
0.623	0.70	0.08	0.08	0.08	1.80

TABLE D-19

Product Distribution for the Hydrogenolysis of 2,3-Dimethylbutane over Nickel-Magnesium on Siliconcarbide

Temperature: 245.0 °C

Total Pressure: 1.20 atm

Conversion of 2,3-Dimethylbutane	Selectivities					
	Isopentane	n-Butane	Isobutane	Propane	Ethane	Methane
0.052	0.54	0.09	0.16	0.13	0.05	1.79
0.064	0.51	0.09	0.16	0.15	0.06	1.86
0.094	0.51	0.10	0.16	0.14	0.06	1.86
0.130	0.47	0.13	0.17	0.14	0.06	1.89
0.166	0.47	0.13	0.16	0.14	0.06	1.95
0.188	0.48	0.10	0.16	0.16	0.06	1.95
0.241	0.48	0.11	0.17	0.15	0.06	1.92
0.306	0.42	0.14	0.18	0.17	0.07	2.01
0.312	0.44	0.14	0.17	0.16	0.06	1.96
0.319	0.42	0.14	0.18	0.17	0.07	1.98

TABLE D-19 (continued)

Conversion of 2,3-Dimethylbutane	Selectivities					
	Isopentane	n-Butane	Isobutane	Propane	Ethane	Methane
0.356	0.42	0.14	0.19	0.15	0.07	2.00
0.373	0.40	0.17	0.19	0.16	0.06	1.99
0.425	0.41	0.16	0.18	0.17	0.06	1.99
0.512	0.36	0.16	0.18	0.18	0.08	2.13
0.520	0.37	0.16	0.18	0.18	0.07	2.12
0.526	0.37	0.16	0.18	0.18	0.07	2.12
0.551	0.32	0.16	0.17	0.20	0.09	2.25
0.556	0.32	0.16	0.18	0.20	0.09	2.25
0.569	0.33	0.16	0.18	0.20	0.09	2.21
0.582	0.33	0.16	0.18	0.19	0.08	2.21
0.584	0.31	0.16	0.18	0.20	0.09	2.27
0.719	0.23	0.17	0.17	0.24	0.11	2.52

TABLE D-20

Product Distribution for the Hydrogenolysis of n-Hexane

over Nickel-Magnesium on Siliconcarbide

Temperature: 255.0 °C

Total Pressure: 1.20 atm

Conversion of n-Hexane	Selectivities				
	n-Pentane	n-Butane	Propane	Ethane	Methane
0.150	0.39	0.22	0.18	0.13	2.33
0.209	0.38	0.24	0.19	0.14	2.32
0.224	0.38	0.24	0.19	0.13	2.31
0.226	0.36	0.24	0.21	0.13	2.34
0.258	0.34	0.24	0.20	0.14	2.46
0.294	0.34	0.24	0.20	0.14	2.45
0.300	0.37	0.23	0.21	0.14	2.35
0.329	0.35	0.24	0.21	0.15	2.34
0.371	0.33	0.25	0.21	0.16	2.39
0.415	0.31	0.25	0.22	0.17	2.46
0.461	0.30	0.24	0.23	0.16	2.51
0.474	0.29	0.25	0.23	0.16	2.57
0.488	0.28	0.24	0.23	0.17	2.60
0.510	0.30	0.26	0.23	0.16	2.45
0.529	0.30	0.25	0.24	0.17	2.44
0.558	0.26	0.25	0.24	0.17	2.62
0.580	0.26	0.26	0.25	0.18	2.60
0.648	0.24	0.25	0.26	0.18	2.68
0.725	0.19	0.24	0.27	0.20	2.86
0.740	0.17	0.24	0.27	0.21	2.98

TABLE D-21

Product Distribution for the Hydrogenolysis of 2,2-Dimethyl-butane over Cobalt-Magnesium on Siliconcarbide

Temperature: 245.0 °C

Total Pressure: 1.20 atm

Conversion of 2,2-Dimethylbutane	Selectivities				
	Neopentane	Isobutane	Propane	Ethane	Methane
0.083	0.76	0.05	0.03	0.05	1.81
0.112	0.74	0.04	0.03	0.05	1.97
0.132	0.76	0.05	0.03	0.04	1.87
0.149	0.76	0.04	0.03	0.05	1.87
0.158	0.77	0.03	0.02	0.04	1.86
0.177	0.78	0.03	0.02	0.05	1.83
0.190	0.76	0.03	0.03	0.04	1.91
0.249	0.76	0.04	0.02	0.04	1.87
0.263	0.77	0.04	0.02	0.04	1.83
0.298	0.75	0.04	0.03	0.05	1.93
0.314	0.81	0.00	0.02	0.04	1.83
0.341	0.76	0.04	0.03	0.04	1.89
0.370	0.73	0.03	0.03	0.05	2.02
0.371	0.75	0.04	0.03	0.04	1.93
0.381	0.75	0.04	0.03	0.04	1.93
0.387	0.76	0.04	0.03	0.05	1.88
0.396	0.78	0.04	0.02	0.03	1.81

TABLE D-21 (continued)

Conversion of 2,2-Dimethylbutane	Selectivities				
	Neopentane	Isobutane	Propane	Ethane	Methane
0.407	0.76	0.04	0.02	0.04	1.89
0.480	0.76	0.03	0.02	0.04	1.96
0.566	0.75	0.03	0.02	0.04	1.96
0.568	0.75	0.04	0.02	0.05	1.82
0.591	0.69	0.03	0.03	0.05	2.23
0.663	0.72	0.02	0.02	0.05	2.12
0.668	0.72	0.02	0.02	0.05	2.12
0.722	0.70	0.02	0.02	0.05	2.23
0.831	0.56	0.01	0.02	0.06	2.96

TABLE D-22

Product Distribution for the Hydrogenolysis of 2,3-Dimethylbutane over Cobalt-Magnesium on Siliconcarbide

Temperature: 227.0 °C

Total Pressure: 1.20 atm

Conversion of 2,3-Dimethylbutane	Selectivities					
	Isopentane	n-Butane	Isobutane	Propane	Ethane	Methane
0.047	0.20	0.08	0.12	0.13	0.16	3.50
0.107	0.18	0.09	0.12	0.14	0.17	3.51
0.164	0.17	0.10	0.11	0.13	0.17	3.59
0.175	0.18	0.09	0.11	0.15	0.17	3.52
0.207	0.19	0.10	0.11	0.14	0.16	3.47
0.226	0.19	0.08	0.10	0.14	0.16	3.56
0.229	0.18	0.09	0.11	0.14	0.17	3.56
0.232	0.17	0.10	0.11	0.14	0.17	3.59
0.279	0.18	0.10	0.11	0.14	0.14	3.50

TABLE D-22 (continued)

| Conversion of 2,3-Dimethylbutane | Selectivities | | | | | |
	Isopentane	n-Butane	Isobutane	Propane	Ethane	Methane
0.299	0.20	0.10	0.10	0.13	0.15	3.51
0.329	0.16	0.10	0.11	0.14	0.16	3.61
0.349	0.17	0.10	0.10	0.14	0.16	3.58
0.390	0.17	0.10	0.10	0.14	0.16	3.64
0.430	0.15	0.10	0.10	0.14	0.16	3.72
0.499	0.15	0.09	0.09	0.13	0.16	3.76
0.535	0.11	0.09	0.08	0.14	0.19	3.97
0.541	0.13	0.10	0.09	0.13	0.16	3.84
0.548	0.11	0.10	0.08	0.14	0.18	3.96
0.552	0.14	0.11	0.10	0.13	0.16	3.77
0.736	0.07	0.08	0.06	0.13	0.19	4.27
0.739	0.08	0.09	0.07	0.14	0.18	4.20
0.748	0.06	0.08	0.06	0.13	0.20	4.33
0.753	0.07	0.08	0.06	0.13	0.19	4.31
0.823	0.03	0.06	0.04	0.12	0.20	4.71

TABLE D-23

Product Distribution for the Hydrogenolysis of n-Hexane

over Cobalt-Magnesium on Siliconcarbide

Temperature: 219.0 °C

Total Pressure: 1.20 atm

Conversion of n-Hexane	Selectivities				
	n-Pentane	n-Butane	Propane	Ethane	Methane
0.061	0.15	0.10	0.12	0.26	3.98
0.119	0.15	0.11	0.14	0.25	3.91
0.128	0.14	0.11	0.13	0.25	3.94
0.156	0.14	0.12	0.13	0.23	3.95
0.182	0.16	0.11	0.12	0.23	3.92
0.191	0.14	0.12	0.14	0.24	3.92
0.214	0.14	0.11	0.13	0.24	3.98
0.240	0.13	0.11	0.13	0.25	4.01
0.266	0.13	0.11	0.13	0.25	4.04
0.268	0.14	0.11	0.13	0.22	4.00
0.301	0.14	0.12	0.13	0.23	3.99
0.328	0.15	0.11	0.13	0.23	3.95
0.334	0.14	0.12	0.13	0.23	3.96
0.355	0.13	0.11	0.13	0.24	4.03
0.379	0.13	0.11	0.13	0.23	4.07
0.432	0.11	0.11	0.12	0.24	4.17
0.460	0.12	0.11	0.13	0.21	4.13

TABLE D-23(continued)

Conversion of n-Hexane	n-Pentane	Selectivities n-Butane	Propane	Ethane	Methane
0.468	0.11	0.11	0.13	0.25	4.14
0.508	0.10	0.09	0.12	0.25	4.28
0.533	0.12	0.11	0.13	0.23	4.08
0.541	0.11	0.12	0.13	0.21	4.16
0.641	0.10	0.10	0.13	0.24	4.23
0.672	0.09	0.10	0.13	0.24	4.26
0.788	0.06	0.08	0.11	0.25	4.57
0.844	0.04	0.06	0.10	0.24	4.76

TABLE D-24

Product Distribution for the Hydrogenolysis of n-Hexane
over Ruthenium on Alumina

Temperature: Other temperatures

Total Pressure: 1.20 atm

Temp (°C)	Conversion of n-Hexane	n-Pentane	n-Butane	Selectivities Propane	Ethane	Methane
139.0	0.12	0.34	0.34	0.47	0.43	0.66
139.0	0.15	0.34	0.34	0.47	0.43	0.66
139.0	0.15	0.32	0.36	0.46	0.44	0.66
139.0	0.18	0.35	0.34	0.47	0.42	0.66
139.0	0.24	0.31	0.33	0.51	0.44	0.72
139.0	0.29	0.30	0.36	0.50	0.44	0.67
139.0	0.30	0.32	0.35	0.50	0.42	0.67
139.0	0.31	0.32	0.35	0.49	0.43	0.66
139.0	0.32	0.32	0.35	0.50	0.44	0.64
139.0	0.36	0.31	0.35	0.49	0.43	0.73
139.0	0.45	0.30	0.36	0.50	0.45	0.68
139.0	0.51	0.28	0.36	0.50	0.46	0.74
163.0	0.21	0.27	0.35	0.42	0.51	0.93
163.0	0.22	0.29	0.34	0.41	0.51	0.95
163.0	0.35	0.26	0.32	0.44	0.55	1.02
163.0	0.38	0.26	0.31	0.44	0.54	1.07

TABLE D-24 (continued)

Temp (°C)	Conversion of n-Hexane	n-Pentane	n-Butane	Selectivities Propane	Ethane	Methane
163.0	0.56	0.21	0.32	0.47	0.60	1.06
163.0	0.61	0.19	0.31	0.49	0.61	1.11
163.0	0.63	0.18	0.31	0.49	0.64	1.10
163.0	0.70	0.16	0.30	0.47	0.73	1.14
163.0	0.78	0.11	0.28	0.54	0.74	1.21
163.0	0.82	0.10	0.27	0.55	0.78	1.26
163.0	0.89	0.08	0.25	0.56	0.81	1.32
163.0	0.94	0.05	0.21	0.55	0.89	1.51